New results on the stability of large antagonistic systems on complex networks a random matrix approach

Mambuca, Andrea Marcello

Awarding institution:
King's College London

King's College London

Faculty of Natural & Mathematical Sciences

Department of Mathematics

New results on the stability of large antagonistic systems on complex networks: a random matrix approach

This thesis is submitted for the degree of
Doctor of Philosophy in Applied Mathematics

Supervisors:
Dr Izaak NERI
Dr Chiara CAMMAROTA

Candidate:
Andrea Marcello MAMBUCA

Academic Year 2020/2021

A Nonna Flora

Abstract

New results on the stability of large antagonistic systems on complex networks: a random matrix approach

Andrea Marcello Mambuca
King's College London

We study the local stability of dynamical systems on complex networks with a random matrix approach. In this approach the Jacobian of the linearised dynamics at the fixed points is described by a sparse random matrix. Inspired by the ecological food webs, we consider degrees of freedom that have pairwise correlated interactions that can be predator-prey, competitive, or mutualistic. Matrices where all interactions are of the predator-prey type define the antagonistic ensemble, while matrices with all the three kinds of interactions define the mixture ensemble. We develop an exact theory to evaluate the spectral properties of infinitely large sparse random matrices with pairwise correlated interactions, and use this theory to infer the system stability. This theory shows that the kind of the interactions plays a major role for the stability of sparse systems. In particular, we find that the leading eigenvalue of infinitely large antagonistic matrices is finite, while the leading eigenvalue of mixture ones is not. This implies that the fixed points of infinitely large antagonistic matrices can be stable, while mixture ones are unstable. In addition, it emerges that degree fluctuations in the network topology typically provide further stabilising effects for infinitely large antagonistic systems. Finally, we find a peculiar behaviour in the spectra of antagonistic matrices at small values of the mean degree, which we denominate the reentrance effect. The leading eigenvalue is imaginary in this case and consequently, as illustrated, the dynamical recovery to a fixed point of the corresponding antagonistic system is typically oscillatory. The reentrance effect characterises a continuous phase transition from a region where the recovery is oscillatory for small enough mean degrees to a phase with a monotonic response for larger connectivities, as instead the leading eigenvalue is real.

Declaration of Originality

This thesis describes work I have carried out between October 2016 and December 2020.

This thesis contains material appearing in the following article:

- Dynamical systems on large networks with predator-prey interactions are stable and exhibit oscillations, https://arxiv.org/abs/2009.11211,
  AMM, Cammarota C., Neri I., September 2020;

In addition to the above, I have contributed to the following online article during the course of my PhD:

- "How To Measure The Proximity To A Market Crash: Introducing System Resilience Indicators (SRI)", http://www.fasanara.com/cookie-06112018,
  AMM, Balata A., Lamperti M., Filia F., November 2018.

This thesis is my own work and contains only original material. It has not been submitted in whole or in part for any degree or diploma at this or any other university.

Andrea Marcello Mambuca
May 2021

Acknowledgements

This thesis tells the story of a beautiful journey, both at the scientific and personal levels, that I made during the years of my PhD. I feel lucky for having shared this journey with a rich network of interesting and smart people. I would like to explicitly thank here some of these people.

I feel grateful to my supervisors Izaak and Chiara, for having participated with much dedication in the study of the topics of this thesis, which have revealed a rich ground of unexpected, surprising and exciting phenomena. For having shared with me your views in science and a strategic approach to the research. For having been much supportive and for having taught me many things.

I want to thank the examiners of my PhD, Prof Jean-Philippe Bouchaud and Prof Tobias Galla, for the time spent in carefully reading my thesis and the excitement that they showed on my work and on the results obtained, as well as for the useful feedback that they provided.

I also want to thank all the other staff members in the Mathematics Department, in particular in the Disordered Systems Group at King's, especially Reimer, Alessia, Pierpaolo, Yan, all my PhD colleagues met at King's and outside, who became also friends, for interesting scientific discussions, the people and the new friends met at schools and conferences, in particular at Beg Rohu in 2017 and at Como in 2019, for sharing views and current fascinating research in complex systems. Finally all the swimmers of KCL Swimming and Waterpolo Society, for always make me feel in a great community at King's.

On a personal note, I would like to thank the most significant people that are very significant to me and have been in this PhD journey. All my lifelong friends in Bergamo, Trento, Trieste and the new ones in London. My girlfriend Gaia, whom in the last two years has become such important and central in my life, with whom I hope to share and enjoy life also in the years to come. Last, but not least, a huge thank to my entire family, especially grandmas Maria, Flora, mum Lidia, dad Sergio, sister Arianna, whose unconditional love has always given me the extra power to face everything, and for the support in letting me have the privilege to get to study at such an advanced level, and for having stimulated my infinite curiosity that pushes me constantly to understand more and more of this fascinating and complex world.

Contents

List of Figures

List of Tables

Chapter 1

Introduction and Motivations

Real-world systems in many areas can be described as complex systems, characterised by a large number of degrees of freedom interacting with each other. A central question is to understand which conditions keep a complex system stable in one configuration, allowing the coexistence of its different components. In order to address this question, among others, an active area of study is modelling complex systems as networks of interacting nodes [Dorogovtsev and Mendes, 2013; Easley and Kleinberg, 2010]. For example, in theoretical ecology it is important, for the coexistence of species, to understand how the architecture of a food web affects the dynamics of an ecosystem [Allesina et al., 2015; Allesina and Pascual, 2008; Coyte et al., 2015; Dunne et al., 2002b; Haas et al., 2020]. In the context of neural networks, it is interesting to study how the network of neural connections is related to the patterns of brain activity [Bimbard et al., 2016; Brunel, 2000; Bullmore and Sporns, 2009; Kadmon and Sompolinsky, 2015; Sporns, 2010]. After the Global Financial Crisis of 2007-2008, a strong interest has been devoted to understand what keep financial systems stable: for example, by modelling them in terms of networks and studying the systemic risk [Bardoscia et al., 2017; Battiston et al., 2016, 2012; Caccioli et al., 2018; Haldane and May, 2011; Mambuca et al., 2018; May, 2013; Sandhu et al., 2016].

This thesis studies how network topology affects the stability of complex systems, exploring the interplay between the network structure and the kinds of interactions. In this chapter we motivate and introduce the scientific paradigm on which this thesis builds upon. Section 1.1 presents the mathematical approach that we adopted to address these question, which is to consider the linearisation of the dynamics of complex systems around fixed points. This linearisation allows to establish stability criteria that open up to the mathematical paradigm of random matrix theory (see Sec. 1.2). Section 1.3 summarises briefly the main results of random matrix theory related to the area of research of this thesis, i.e., to the spectral distribution, in terms of universal laws. In Sec. 1.4 we present the main concepts of complex networks, that take into account the network structure which we consider in this thesis. Section 1.5 introduces and discusses sparse random matrices, which are useful to connect complex networks and random

matrices, and which are the class of random matrices we consider for the model of this thesis. In Sec. 1.6 we review some models from the literature on random matrices with pairwise correlated interactions, and discuss them in light of the universal laws of previous sections. Finally, Sec. 1.7 discusses the ideas, developed along this chapter, that highlight the interest in studying the models of this thesis, that will be defined in detail in Ch. 2.

1.1 Linearised dynamics and stability criteria of complex systems

We start with the general mathematical model that describes the dynamics of complex systems of N degrees of freedom. We consider a set of first-order and non-linear autonomous differential equations, i.e.,

$$\partial_t \vec{x} = \vec{f}(\vec{x}), \tag{1.1}$$

where $\vec{x} = \vec{x}(t) := (x_1(t), \ldots, x_N(t))^{\mathrm{T}} \in \mathbb{R}^N$ is a column vector that represents the state of the system at a time t, and where the vector field $\vec{f} : \mathbb{R}^N \to \mathbb{R}^N$ maps the state of the system $\vec{x}$ into a column vector $\vec{f}(\vec{x}) := (f_1(\vec{x}), \ldots, f_N(\vec{x}))^{\mathrm{T}}$ that couples the degrees of freedom $\{x_i\}$ in a non-linear way. One example is a generalised Lotka-Volterra model within theoretical ecology (see for example Ref. [Hofbauer and Sigmund, 1998; May, 1973]), which describes the dynamics of N biological species, represented by their numbers $x_i \geq 0$, where the components of dynamical vector field $\vec{f}$ are given by

$$f_i(\{x_i\}) = x_i(J_{ii} + \sum_{j=1, j\neq i}^{N} J_{ij} x_j). \tag{1.2}$$

Here the diagonal parameters $\{J_{ii}\} < 0$ account for self-regulation mechanisms in the absence of interactions. In the general Lotka-Volterra model the diagonal contributions can be non linear in x_i: for example the logistic growth model includes a negative quadratic term to account for a limited carrying capacity (see for example [Galla, 2018]). The couplings $\{J_{ij}\}$ assemble into a $N \times N$ matrix, named in this context as the community matrix in the generalised Lotka-Volterra model, where $J_{i\neq j}$ model the effect of species j on the growth in size of species i. In a general ecosystem, $J_{i\neq j}$ can be of any sign: a competitive (cooperative) dynamics between species $i \neq j$ would have $J_{ij}, J_{ji} < 0$ ($J_{ij}, J_{ji} > 0$), where species i is disadvantaged (favoured) to grow in the presence of species j; the predator-prey interaction between species $i \neq j$ would have instead $J_{ij}J_{ji} < 0$, modelling the fact that if one species is favoured by the presence of another one, then the other is disadvantaged. In this example it is important to observe that the effect of species i on j may be dependent on the effect of species j on i; for example, in the predator-prey dynamics, opposite entries are constrained to have opposite signs.

In general complex systems with non-linear dynamics are not analytically solvable.

Then one typically considers a linear stability analysis. This consists first in determining the fixed (stationary) points of the (global) dynamics, i.e., all the zeroes $\vec{x}^*$ of $\vec{f}(\vec{x})$, as follows

$$\vec{f}(\vec{x}^*) = \vec{0}. \tag{1.3}$$

Second, in evaluating the Taylor expansion of each component $f_k(\vec{x})$ in the neighbourhood of each of the fixed points, i.e.,

$$\forall k = 1, \ldots, N \quad f_k(\vec{x}) = f_k(\vec{x}^*) + \sum_{j=1}^{N} \frac{\partial f_k(\vec{x}^*)}{\partial x_j}(x_j - x_j^*) + \mathcal{O}((x_j - x_j^*)^2). \tag{1.4}$$

Third, in replacing the non-linear dynamical function close to the stationary points with their first order, i.e., linear, approximations. At this point the Hartman-Grobman theorem guarantees that the local stability of a fixed point is governed by the linear approximation of the dynamics in the proximity of the fixed point itself [Grobman, 1959; Hartman, 1960; Place and Arrowsmit, 1992]. Accordingly, we first conveniently express the elements of Jacobian matrix of $\vec{f}$ at the fixed point as the sum of a diagonal matrix $\mathbf{d}$, with diagonal elements d_j, and an interaction matrix $\mathbf{A}$ with elements A_{kj}, so that $A_{jj} = 0$ for all j, i.e.,

$$-\, d_j\, \delta_{j,k} + A_{kj} := \frac{\partial f_k(\vec{x}^*)}{\partial x_j}, \tag{1.5}$$

where we have used $\delta_{j,k}$ for the Kronecker delta function and the parameters d_j are positive. The magnitude of d_j sets the time-scale for the exponential relaxation to the stable fixed point: given an initial fluctuation from $\vec{x}^*$, the species described by x_j returns back in a typical relaxation time given by d_j^{-1} in the absence of interactions. We note that in Eq. (1.5) there is an implicit dependence on the fixed point $\vec{x}^*$.

The linearised dynamics of Eq. (1.1) from Eq. (1.5) reads

$$\partial_t \vec{y} = -\mathbf{d}\, \vec{y} + \mathbf{A}\vec{y}, \tag{1.6}$$

where the column vector in $\mathbb{R}^N$

$$\vec{y} = \vec{y}(t) := \vec{x} - \vec{x}^* \tag{1.7}$$

denotes the deviation from the fixed point $\vec{x}^*$ at time t, which, for example in the ecological context, measures the variations in the population density of species i at time t. Equations of the form (1.6) are used to model, for example, the dynamics of ecosystems [Allesina and Tang, 2012; Gibbs et al., 2018; Grilli et al., 2016] and neural networks [Ahmadian et al., 2015; Amir et al., 2016; Kadmon and Sompolinsky, 2015; Sompolinsky et al., 1988] in the vicinity of some fixed point $\vec{x}^*$. In the case of ecosystems $\mathbf{A}$ is the

community[1] matrix, for the linearised dynamics, that measure the per capita effect of species j on species k at $\vec{x}^*$, equivalently to the interaction matrix J of the generalised Lotka-Volterra model in Eq. (1.2). In the context of neural networks the entries A_{kj} denote the strength of the synaptic connections between neurons represented by j, k.

As a first qualitative argument, one has that if the interactions A_{kj} are small enough, then the fixed point $\vec{x}^*$ is stable since

$$\lim_{t\to\infty} |\vec{y}(t)| = 0, \tag{1.8}$$

for all initial states $\vec{y}(0)$, where $|\cdot|$ is the norm of a vector. On the other hand, large interactions A_{kj} can destabilise the fixed point giving

$$\lim_{t\to\infty} |\vec{y}(t)| = \infty, \tag{1.9}$$

for all initial states $\vec{y}(0)$.

For general interactions A_{kj}, given an initial fluctuation $\vec{y}(0)$, the time dependence of the solution of Eq. (1.6) can be written as

$$\vec{y}(t) = e^{(-\mathbf{d}+\mathbf{A})t}\vec{y}(0), \tag{1.10}$$

the stability of which is governed by the spectrum of the matrix $\mathbf{A}$, which is defined as the set of its eigenvalues

$$\sigma(\mathbf{A}) := \{\lambda \in \mathbb{C} : \det(\mathbf{A} - \lambda \mathbf{1}_N) = 0\}, \tag{1.11}$$

where $\mathbf{1}_N$ is an identity matrix of rank N. Specifically, as shown in Appendix A.1, the long time dynamics[2] of Eq. (1.10) is governed by the leading eigenvalue $\lambda_1(\mathbf{A})$ of the matrix $\mathbf{A}$, defined as the eigenvalue that has the largest real part, i.e.,

$$\Re(\lambda_1(\mathbf{A})) \geq \Re(\lambda_2(\mathbf{A})) \geq \ldots \geq \Re(\lambda_N(\mathbf{A})), \tag{1.12}$$

where if there exists more than one eigenvalue with the same real part, for example because $\lambda_1(\mathbf{A})$ has a non-zero imaginary part, then we choose $\lambda_1(\mathbf{A})$ to be the eigenvalue with the largest imaginary part. The Hartman-Grobman theorem mentioned above assures that the local stability of the fixed point $\vec{x}^*$, associated to a zero fluctuation $\vec{y} = \vec{0}$, can be expressed in terms of simple stability criteria on $\lambda_1(\mathbf{A})$. Under the assumption that $d_j = d$ for all j, if the real part $\Re(\lambda_1(\mathbf{A}))$ of the leading eigenvalue

[1] according to the context of study, the community matrix in ecology can refer to the interaction matrix of the non-linearised dynamics or to the interaction matrix within the linearised approach

[2] in non-symmetric community matrices, the fluctuation around a stable fixed point within linear dynamics as in Eq. (1.6), may experience a transient dynamical behaviour characterised by a growth of the initial fluctuation[Grela, 2017]

satisfies

$$\Re(\lambda_1(\mathbf{A})) < d, \tag{1.13}$$

then the fixed point $\vec{y} = 0$ is stable, while if

$$\Re(\lambda_1(\mathbf{A})) > d, \tag{1.14}$$

then the fixed point is unstable, as we discuss in Appendix A.1.

In order to infer the stability properties of fixed points in the limit of infinitely large systems, it is important to know the dependence of the leading eigenvalue $\lambda_1(\mathbf{A})$ on N. In particular, what matters is whether $\lambda_1(\mathbf{A})$ diverges or stays finite when $N \to \infty$. For example, only a finite leading eigenvalue guarantees that the fixed point $\vec{x}^*$ remains stable, for a fixed and finite value of d. On the other side, if $\lambda_1(\mathbf{A})$ diverges with N, there not exists a fixed and finite value of d that would keep the system stable.

Besides the stability criteria, the leading eigenvalue is central also in establishing how large dynamical systems respond to external perturbations. As we discuss in Appendix A.1, if

$$\Im(\lambda_1(\mathbf{A})) = 0, \tag{1.15}$$

then the response of $\vec{y}$ is nonoscillatory, while if

$$\Im(\lambda_1(\mathbf{A})) > 0, \tag{1.16}$$

then the response is oscillatory. In particular, the imaginary part of λ_1 determines the frequency of oscillations of the slowest mode when the system is stable, and of the fastest destabilising mode when the system is unstable.

1.2 Random matrix approach to the linearised dynamics

We discuss now a remarkable classical result on the stability of complex systems within the linearised dynamics approach of Sec. 1.1, first shown in Refs. [Gardner and Ashby, 1970; May, 1972]. They considered a simple model of complex systems, based on the assumption that all the entries A_{ij} can be approximated by independent and identically distributed (i.i.d.) random variables drawn from a distribution with zero mean and variance σ^2. Accordingly, almost surely (with probability one[3]) if [May, 1972]

$$\sigma\sqrt{N} < 1, \tag{1.17}$$

then the fixed point $\vec{y} = 0$ is stable (for example, if $\sigma = N^{-1/2-\alpha}$, with $\alpha > 0$), while if

$$\sigma\sqrt{N} > 1, \tag{1.18}$$

[3]i.e., the probability $P(\sigma, N) \to 1$ for $N \to \infty$, where $\sigma = \sigma(N)$

it is unstable. These stability criteria are examples of Eqs. (1.13)-(1.14) with $d = 1$, based on the fact the leading eigenvalue for the random matrix considered above is typically equal to $\sigma\sqrt{N}$ [Ginibre, 1965]. The key point of these stability criteria is that the system described in Eq. (1.6) almost surely becomes unstable for N large enough, for a fixed value of σ, given that $\Re(\lambda_1)$ diverges in the limit $N \to \infty$. In the context of ecology, this result was in contrast with the diffused idea that more diversity in ecosystems helps to re-absorb the fluctuations around equilibrium, increasing the stability [Fortuna et al., 2010; Haydon, 2000; Hooper et al., 2005; Kirk et al., 2015; Roberts, 1974]) Accordingly, and in light of more ecological aspects, the instability criteria in Eqs. (1.17)-(1.18) became part of the diversity-stability debate that has been investigated in the following decades, questioning on how natural systems might violate the assumptions of complexity leading to stabilising or destabilising features (see for example Refs. [Kondoh, 2003; Mccann, 2000; Moore and Hunt, 1988; Pimm, 1984]).

The classical result above is based on the idea of replacing the complex structure of the Jacobian at the fixed point with a random matrix of i.i.d. entries. Indeed, the true dynamics of large systems with high complexity is generally inaccessible, i.e., the analytical expression of the components $f_k(\vec{x})$ in Eq. (1.1) — from which one should evaluate the Jacobian matrix in Eq. (1.5) at one fixed point $\vec{x}^*$ to solve the linearised dynamics in Eq. (1.6) — is typically unknown. On the other side, often in statistical physics in the limit of large systems some observables may become universal, despite being characterised by different microscopic details. In this case, a few shared structural properties of the dynamical functions $f_k(\vec{x})$ define universality classes of systems. One successful and very fascinating example of this methodological approach is Random Matrix Theory (which we name RMT from now on): it manages to describe in a single conceptual framework many properties of systems of very different nature [Akemann et al., 2011]. The simple idea of RMT is to infer properties of large matrices with entries drawn from specific random distributions: since the first work in the field by Wigner [Wigner, 1958] to study the energy levels of heavy nuclei, RMT has become one of the fastest growing area of mathematics [Bai and Silverstein, 2010]. This fact offers a great interest for many real systems, spanning from biology, neuroscience to finance, where the complexity is present with large size systems and inherently random features. In the ecological context, the diversity-stability debate has been considered in the light of RMT (see Ref. [Allesina and Tang, 2015] and references therein); recently, in establishing stability criteria for complex ecosystems [Allesina and Tang, 2012], a non-linear generalisation of the classical linearised approach [Fyodorov and Khoruzhenko, 2016], and in studying destabilising effects due to dispersal in space [Baron and Galla, 2020]. Finally, the RMT approach on the stability of fixed points of complex systems has become a paradigm in complex systems science: for example, it has been used to understand the behaviour of financial ecosystems [Farmer and Skouras, 2013; Haldane and May, 2011], and recently the resilience of large economies to perturbations [Moran

and Bouchaud, 2019], as well as in the study of randomly assembled communities of highly diverse species, which is an active field of research [Fried et al., 2016].

In the next section we briefly present the main results in RMT, namely the universal laws for the spectral distribution, that allow ultimately to establish stability criteria as in Eqs. (1.17)-(1.18).

1.3 Universal laws in RMT: dense and dilute random matrices

We summarise here the main results of RMT (see Appendix A.2 for more details), on which this thesis builds upon and further extends. We focus first on the cases of dense random matrices. We focus first on dense matrices as those random matrices $\mathbf{A}$ where all the entries are non-zero with probability one, in contraposition with sparse matrices presented in Sec. 1.5. The ensemble considered in the model by [May, 1972], discussed in the previous section, is an example of a dense matrix. The RMT result on which the result above is based is an example of universal law in RMT.

The spectrum (defined in Eq. (1.11)) of a random matrix $\mathbf{A}$ can be conveniently encoded in the empirical spectral density that is defined as a sum of δ-distributions in $\mathbb{C}$, i.e.,

$$\rho_{\mathbf{A}}(z) := \frac{1}{N}\sum_{j=1}^{N}\delta(z-\lambda_j(\mathbf{A})), \quad \text{with} \quad z\in\mathbb{C}, \tag{1.19}$$

where the delta distribution in Eq. (1.19) is the bi-dimensional distribution that sometimes is denoted with $\delta^{(2)}$: for $z\in\mathbb{C}, \delta^{(2)}(z)=\delta(x)\delta(y)$, with $x:=\Re(z)$ and $y:=\Im(z)$, that we will simply denote as $\delta(z)$.

The fundamental object in RMT is, if it exists, the limiting spectral distribution ρ of the empirical spectral density in Eq. (1.19), for $N\to\infty$. In this case $\rho_{\mathbf{A}}(z)$ is self-averaging. Self-averaging quantities in disordered systems are those for which the limit $N\to\infty$ exists and it is deterministic. In general, it is not easy to show whether $\rho_{\mathbf{A}}(z)$ is self-averaging. However, there are important theorems in RMT (see Appendix A.2) that establish the convergence of the empirical spectral measure associated to $\rho_{\mathbf{A}}(z)$ for dense matrices, and hence establish that $\rho_{\mathbf{A}}(z)$ is self-averaging. Moreover, these theorems for dense matrices express the limiting distribution ρ as universal laws: the universality principle [Tao and Vu, 2010; Wood, 2012] for dense matrices in RMT predicts that the limiting distribution ρ should not depend on the specific distribution of the entries. In the following we summarise the universal laws for three classes of random matrices: Hermitian, the non-Hermitian with i.i.d. entries and the non-Hermitian with i.i.d. pairs of entries random matrices, and the associated universal laws laws known as semi-circular law (also Wigner's law), circular law (also Girko's law) and the elliptic law (also generalised Girko's law), respectively (see Appendix A.2 for the corresponding theorems).

First, we consider non-Hermitian random matrices $\mathbf{A}$ with i.i.d. entries on and above

the diagonal, with mean zero and variance one. As first shown by Wigner [Wigner, 1958] the limiting distribution of the empirical spectral density on the real axis of $\mathbf{A}/\sqrt{N}$ is given by

$$\rho = \rho^{(\mathrm{sc})}(x) = \begin{cases} \frac{1}{2\pi}\sqrt{4-x^2}, & \text{if } |x| \leq 2; \\ 0, & \text{otherwise}, \end{cases} \tag{1.20}$$

with $x \in \mathbb{R}$. The result in Eq. (1.20) is known in the literature as semi-circular law; the corresponding Theorem 1 by [Bai, 1999] is stated in Appendix A.2.

Let us now consider non-Hermitian matrices $\mathbf{A}$ with independent and identical distributed (i.i.d.) entries A_{ij}. As originally shown by [Mehta, 1967], by using the joint probability density of the eigenvalues of $\mathbf{A}/\sqrt{N}$ in the Gaussian ensemble, derived by [Ginibre, 1965], the density of the empirical spectral measure converges to

$$\rho = \rho^{(\mathrm{c})}(z) = \begin{cases} \frac{1}{\pi}, & \text{if } |z| \leq 1; \\ 0, & \text{otherwise}, \end{cases} \tag{1.21}$$

with $z \in \mathbb{C}$.

In the 1980s, Girko originally started to study (and continued for thirty years) more general matrices which combine Hermitian and non-Hermitian models (see for example [Girko, 2006] and references therein), where mainly the hypothesis of i.i.d. in non-Hermitian has been relaxed to include correlations between the off-diagonal elements of $\{(A_{ij}A_{ji})\}$, with arrange in i.i.d. pairs. Also in this case there exist an universal law. Namely, under the assumptions (see for more detailed hypotheses the condition in Def. A.2.1) that all the entries A_{ij} have mean zero and variance one, and that $\langle A_{ij}A_{ji}\rangle = \tau$, where $\langle\rangle$ denotes the expectation value with the given probability distribution, the limiting spectral distribution of $\mathbf{A}/\sqrt{N}$ satisfies the elliptic law

$$\rho = \rho^{(\mathrm{e})}(z) = \begin{cases} \frac{1}{\pi(1-\tau^2)}, & \text{if } z \in E_\tau; \\ 0, & \text{otherwise}, \end{cases} \tag{1.22}$$

where the elliptic support is defined through

$$E_\tau := \left\{ z \in \mathbb{C} : \left(\frac{\Re(z)}{1+\tau}\right)^2 + \left(\frac{\Im(z)}{1-\tau}\right)^2 \leq 1 \right\}, \tag{1.23}$$

which is an ellipse of horizontal semiaxis $1+\tau$ and vertical semiaxis $1-\tau$. In the case of $\tau = 0$, the elliptic law correctly recovers the circular law.

An important observation about the elliptic Theorem 3 (and similarly for the semi-circular and circular Theorems) is that it rules the convergence for $N \to \infty$. However, in some contexts, by neglecting the convergence problem to a compact support for $N \to \infty$, where N is large but finite, an elliptic law in Eq. (1.22) and Eq. (1.23) (and similarly for

the semicircular and circular laws) can be considered without rescaling the matrix $\mathbf{A}$ by $1/\sqrt{N}$, for which one simply finds the rescaled semiaxes $\sqrt{N}(1 \pm \tau)$, while the density remains uniform but rescaled to be normalised. This scenario is the one in the model by [May, 1972] in Sec. 1.2, where the matrix entries A_{ij} are assumed to be independent of N, hence the mean and the variance as well. Accordingly, in all the dense ensembles of this section the leading eigenvalue diverges in the limit $N \to \infty$, a fact that in these cases is guaranteed by the universal laws. This translates into the fact that for N large enough the fixed points of the systems represented by these ensembles, within the linearised dynamics approach, are almost surely unstable. Moreover, we note that while in the hypotheses of the theorems for the universal laws the variance of the entries A_{ij} is assumed to be unitary, one can have a finite variance σ^2 for and the supports rescaled by $\sqrt{\sigma}$; for example, the elliptic support have rescaled semiaxes $\sigma(1 \pm \tau/\sigma^2)$.

An important extension of the three universal laws presented here for dense matrices can be obtained when the entries of the corresponding matrices $\mathbf{A}$ are non-zero with a probability that depends on the matrix size N. Indeed, when A_{ij} is non-zero with probability of order $\mathcal{O}(N^{\alpha-1})$, with $0 < \alpha \leq 1$, then the empirical spectral density of the matrix $\mathbf{A}/\sqrt{N^\alpha}$ converges to the Eqs. (1.20)-(1.22) [Basak and Rudelson, 2017; Dumitriu and Pal, 2012; Mirlin and Fyodorov, 1991; Tran et al., 2010; Wood, 2012] (see Theorem 4 for the non-Hermitian case with i.i.d. entries). A remarkable exception that does not satisfy the universal laws is when $\alpha = 0$: we discuss more in detail this case in Sec. 1.5.

The random matrix ensembles discussed above can be described, from a network perspective, in terms of dense or dilute graphs. However, the constituents of real-world systems interact through specific preferential interaction whose structure is better described by large, complex networks where nodes are not all linked with all the others. It is therefore interesting to understand the stability of dynamical systems defined on infinitely large, sparse, random graphs with edges that are characterised by random weights with zero mean and finite second moment. Under these assumptions, interactions can still be approximated by random variables, within RMT approach, but it can be studied how the non trivial graph structure may affect system stability.

In the next section, we introduce complex networks, and the main concepts of networks that are used in this thesis.

1.4 Complex networks

Here we first introduce the notion of a graph, second we develop the concept of random graphs [Albert and Barabási, 2002; Bollobás, 2001; Dorogovtsev and Mendes, 2013; Newman, 2010].

Some authors use the word “networks” to denote the physical objects in the real world, and “graphs” for their mathematical description. In this thesis we will not make this distinction.

1.4.1 Graph theory elements

A graph $\mathcal{G}$ is defined as a pair of a set of nodes (or vertices) $V = 1, \ldots, N$ and a set of edges (or links) $E \subset V \times V$ which connect the nodes. A subgraph $\mathcal{G}'$ of $\mathcal{G}$ is a graph with nodes V' and links E' such that $V' \subseteq V$ and $E' \subseteq E$.

A first useful distinction is between undirected and directed graphs. The first are those in which $\forall (i,j) \in E \ : (j,i) \in E$; the second are those where this last condition is not met, i.e., $\exists (i,j) \in E \ : (j,i) \notin E$. This symmetry in undirected graph allows to disregard the order in the pairs (i,j) if dealing with only undirected graphs, so that in undirected graphs E can be considered as a set of unordered pairs of vertices which are connected by a (bidirectional or undirected) link. Simple graphs are those graphs where self loops (or self links) are excluded, i.e., $\forall i \in V \ (i,i) \notin E$.

The possible number of links in a given graph of N nodes is a combinatorial problem: it is straightforward to see that for undirected simple graphs there are $\binom{N}{2}$ possible edges, which are the possible unordered pairs of N vertices. Similarly, for directed simple graphs there are a double number of possible (directed) links, i.e., $2\binom{N}{2}$. A very useful object that bijectively determines a generic graph is its adjacency matrix. Given a graph $\mathcal{G}$ of N vertices, its adjacency matrix $\mathbf{C}$ of size N has entries C_{ij} defined as

$$C_{ij} = \begin{cases} 1 & \text{if } (i,j) \in E; \\ 0, & \text{otherwise,} \end{cases} \tag{1.24}$$

i.e., C_{ij} is a binary logical variable which is non-zero when there is a link between nodes j and i, where $i, j = 1, \ldots, N$. A property of undirected graphs is that their adjacency matrices are symmetric. From now on we leave understood that the number of vertices of a graph and the size of its adjacency matrix is denoted by N.

The adjacency matrix allows to define many graph properties in a simple way. We mention now the ones that will be used in this thesis. Given a node j, the neighbourhood ∂_j is the defined as the set of neighbours of node j, i.e.,

$$\partial_j = \{i : \ i \neq j, C_{ij} = 1\}. \tag{1.25}$$

A path of length k is an ordered sequence of k nodes $\{i_\ell\}$ such that the nodes i_ℓ and $i_{\ell+1}$ are connected, i.e., in terms of the adjacency matrix

$$\prod_{\ell=1}^{k-1} C_{i_\ell i_{\ell+1}} = 1 \quad \text{if the graph contains the path } i_k \to i_{k-1} \to \cdots \to i_1. \tag{1.26}$$

From the definition of paths one can introduce cycles, which we refer many times, which are defined as paths of length larger than two where the only repeated indices are the first and the last, i.e., $i_k = i_1$[4].

[4]This definition of cycles excludes the paths made by moving along an existing path and returning

Other important objects in a graph $\mathcal{G}$ that can be defined in terms of path are the connected components, which are the largest subgraphs of $\mathcal{G}$ such that for each subgraph there exists a path between all vertices within the subgraphs. In a connected graph there is only one connected component that coincides with the graph.

Now we can define one kind of graph, the tree graph or simply tree, that is very important for this thesis (see Ch. 3). Trees are connected graphs without any cycles. Trees can be either directed or undirected, although we will consider undirected ones.

The adjacency matrix can be used to define other graph properties, such as the degree of a node i — for simplicity we consider undirected graphs —: it is the number of nodes connected to the vertex i, or and is given simply by

$$k_i(\mathbf{C}) := \sum_{j=1}^{N} C_{ij}, \tag{1.27}$$

while ordering all the node degrees one has the degree sequence

$$\mathbf{k}(\mathbf{C}) := (k_1(\mathbf{C}), \ldots, k_N(\mathbf{C})), \tag{1.28}$$

From the node degrees (and hence from the original adjacency matrix itself) one can also evaluate useful scalars, such as the average degree of the graph

$$\bar{k}(\mathbf{C}) := \frac{1}{N}\sum_{i=1}^{N} k_i(\mathbf{C}) = \frac{1}{N}\sum_{i,j=1}^{N} C_{ij}, \tag{1.29}$$

and the degree distribution

$$p_{\deg}(k|\mathbf{C}) := \frac{1}{N}\sum_{i=1}^{N} \delta_{k_i(\mathbf{C}),k},\ \forall k \in \mathbb{N}. \tag{1.30}$$

1.4.2 Random graphs

A random graph is a graph where the edges occur at random, according to an assigned rule which defines the random graph ensemble. A first example of random graph is given by Erdös and Rényi, who introduced the random graph model $\Gamma_{M,N}$ [Erdös and Rényi, 1959] characterised by a number M of edges and N nodes: the $\binom{\binom{N}{2}}{M}$ graphs in this ensemble have the same fixed number of edges and these graphs are all equally likely. The prototypical random graph $G(N,p)$ introduced by Gilbert [Gilbert, 1959] [5] assigns to each possible edge in E the same probability p to exist. This specific ensemble is characterised by its corresponding (random) adjacency matrix $\mathbf{C}$ which in this case can

to the first node through the inverse path, which is always possible in undirected graphs, as well as it excludes self-loops

[5] same year but independently from Erdös and Rényi [Erdös and Rényi, 1959]

be easily defined by the following joint factorising probability density

$$P(\mathbf{C}) = \prod_{i<j} \left[p\delta_{C_{ij},1} + (1-p)\delta_{C_{ij},0} \right] \delta_{C_{ij},C_{ji}}, \tag{1.31}$$

where $p \in [0,1]$ denotes the probability of a single link to be present, independently from any other edge, while the $\delta_{C_{ij},C_{ji}}$ forces $\mathbf{C}$ to be a symmetric matrix (which corresponds to an undirected simple graph). While in the model introduced originally by Erdös and Rényi [Erdös and Rényi, 1959] the number M of edges is fixed among the realisations of the random graph, in the Gilbert model the number M of edges fluctuates, while the probability p of a single edge independently from the other edges is fixed. One year later Erdös and Rényi studied further the model $G(N,p)$ and explored the behaviour for $N \to \infty$ limit [Erdös and Rényi, 1960]; their results became a reference point for random graphs studies and the $G(N,p)$ is nowadays generally referred to as the Erdös-Rényi model, also for its simplicity.

We would like now to explore briefly the large N limit in the random graphs, mainly for two reasons: first, real world networks are usually very large and, second, mathematical results in terms of universal laws can be obtained in this limit, similarly to the dense case in Sec. 1.3. For simplicity, we consider now the $G(N,p)$ random graph model, with joint probability density of its adjacency matrix as in Eq. (1.31), but the following reason is valid in general. The expected mean degree in Eq. (1.29) with respect to the joint probability density in Eq. (1.31) can be easily evaluated and it reads

$$\langle \bar{k}(\mathbf{C}) \rangle_P = p \times (N-1). \tag{1.32}$$

The dependence of p in Eq. (1.31) on N is relevant in the $N \to \infty$ limit, as it can be seen already at the level of the mean degree in Eq. (1.32). With this respect, we make explicit its dependence on N by defining

$$p := \frac{c}{(N-1)^{1-\alpha}}, \tag{1.33}$$

where c is independent of N and finite, while $0 \leq \alpha \leq 1$. Accordingly, the expected average degree in Eq. (1.32) reads

$$\langle \bar{k}(\mathbf{C}) \rangle_P = c \times (N-1)^{\alpha}. \tag{1.34}$$

While for $0 < \alpha \leq 1$ the expected average degree in Eq. (1.34) diverges in the $N \to \infty$ limit, it stays finite (and equal to c independently of N) when $\alpha = 0$. This last case is special for the random graphs point of view, because it allows to model very large complex networks with a finite number of connections per single node, hence $\alpha = 0$ is called the finite connectivity regime in the Erdös-Rényi model. Graphs with $0 < \alpha \leq 1$ are considered as dilute graphs. Also at the level of the expected degree distribution —

which is the ensemble average of Eq. (1.30) such as Eq. (1.32) is the ensemble average of Eq. (1.29) — one can show that $\alpha = 0$ is peculiar. Indeed, in the Erdös-Rényi model with p as in Eq. (1.33) one can evaluate the degree probability distribution by the expected degree sequence

$$p_{\text{deg}}(k|N) := \langle p_{\text{deg}}(k|\mathbf{C})\rangle_P = \binom{N-1}{k}\left(1 - \frac{c}{(N-1)^{1-\alpha}}\right)^{N-1-k}(\frac{c}{(N-1)^{1-\alpha}})^k, \quad (1.35)$$

i.e., it is a binomial distribution with $N-1$ independent Bernoulli trials with probability of success $p = c/(N-1)^{1-\alpha}$. Eq. (1.35) admits the following limit for $N \to \infty$ if $\alpha = 0$:

$$p_{\text{deg}}(k) := \lim_{N\to\infty} \langle p_{\text{deg}}(k|\mathbf{C})\rangle_P^{(\alpha=0)} = e^{-c}\frac{c^k}{k!}, \quad (1.36)$$

i.e., it is a poissonian degree distribution with mean degree c.

Finally, an important question for random graphs is to determine the criteria for the existence of a largest connected (or giant) component. Indeed, a graph from a general random graph ensemble typically decomposes into a giant component and a large number of small clusters. For example, a remarkable first result on the $G(N,p)$ in the finite connectivity regime is that a giant component exists for $c > 1$, and $c = 1$ is the percolation transition [Erdös and Rényi, 1960]. We revise briefly percolation theory in Appendix A.8, where we also apply it to determine the criteria for the existence of a largest connected component for the random graphs models considered in this thesis.

1.4.2.1 Random graphs with prescribed degree distribution

For general degree distributions, for example the ones built from the graph as in the degree distribution in Eq. (1.30) it is necessary to take the ensemble average to evaluate the expected degree distributions, as in the left hand side of Eq. (1.35). Another approach is to assign a prescribed degree distribution a priori, as an input and independently from a single realisation of a random graph, and then the random graph is determined as a consequence. We define here the random graph ensemble in terms of prescribed degree distributions $p_{\text{deg}}(k|N)$ (we do not change notation from above, i.e., we denote prescribed degree distributions with the notation p_{deg}), which is the approach that we use in this thesis. Fixed a prescribed degree distributions $p_{\text{deg}}(k|N)$,

1. generate a degree sequence with the degrees i.i.d. random variables drawn from

$$\mathbf{k} := (k_1, \ldots, k_N), \quad \text{with} \quad k_i \sim p_{\text{deg}}(k|N); \quad (1.37)$$

2. given this degree sequence in 1) vertices are uniformly and randomly connected, as in the configurational model [Bollobás, 2001; Dorogovtsev and Mendes, 2013; Newman, 2018].

For example, in the Erdős-Rényi graph above, within the prescribed degree distribution approach, one would assign a priori the binomial distribution in the right hand side of Eq. (1.35) to $p_{\rm deg}(k|\mathbf{C}) = p_{\rm deg}(k|N)$. In the limit $N \to \infty$, the prescribed degree distribution may converge to a distribution that is independent of N, i.e.,

$$\lim_{N\to\infty} p_{\rm deg}(k|N) = p_{\rm deg}(k), \tag{1.38}$$

which is an example of a self-averaging object in disordered systems. For example, in the Erdős-Rényi graph above, the limit $N \to \infty$ gives the poissonian degree distribution when $\alpha = 0$. Other examples of finite-connectivity ensembles with a prescribed degree distribution are the regular ensemble, for which $p_{\rm deg}(k) = \delta_{k,c}$, and the exponential random graph ensemble, for which $p_{\rm deg}(k) = [c/(c+1)]^k (c+1)^{-1}$.

1.4.2.2 Locally treelike random graphs

Locally treelike graphs [Bordenave and Lelarge, 2010; Dembo et al., 2010; Metz et al., 2019] are defined as a sequence of sparse random graph for which any finite neighbourhood of a randomly chosen vertex is connected like a tree graph almost surely (i.e., with probability one when $N \to \infty$). In other words, in locally treelike graphs cycles of a given finite length (i.e., small cycles) are rare, although there exists still a finite number of them in the $N \to \infty$ limit [Bollobás, 2001; Neri and Metz, 2020]. As shown in [Dembo et al., 2010], random graphs with a prescribed degree distribution $p_{\rm deg}$ (see Sec. 1.4.2.1) that converges for $N \to \infty$ as in Eq. (1.38) are an example of locally treelike graphs.

Note that the locally treelikeness is a local property, since it does not exclude the presence of cycles of divergent length, which indeed are present typically in a divergent number with the system size [Bianconi and Marsili, 2005]. We refer to these cycles as long cycles, to distinguish them from the short ones discussed above. Note also that the locally treelikeness is an asymptotic property, hence one typically considers the $N \to \infty$ limit in order to exploit this property.

1.5 Sparse random graphs and sparse random matrices

1.5.1 The leading eigenvalue of random graphs

From a random matrix perspective, it is very interesting to investigate on the spectral properties of the adjacency matrix of a random graph. In particular, one important spectral quantity is the leading eigenvalue λ_1 since it governs the stability properties of complex systems as discussed in Sec. 1.1. When we refer to the leading eigenvalue λ_1 of a graph, we mean the leading eigenvalue λ_1 of its associated adjacency matrix. the From a graph perspective, we can significantly extend the classical results on the leading eigenvalue of dense matrices, which are equivalent to dense graphs, to dilute graphs, for example in the $G(N,p)$ model above when $0 < \alpha \leq 1$, and to sparse graphs characterised

by a finite mean connectivity, for instance $\alpha = 0$ in the $G(N,p)$ model. In the following, we consider the regimes above the percolation threshold, i.e., when a giant component in the graph exists. In particular, in the $G(N,p)$ model almost surely for $N \gg 1$ the leading eigenvalue λ_1 of the adjacency matrix in Eq. (1.31), with p in Eq. (1.33) is given by [Krivelevich and Sudakov, 2003]

$$\lambda_1 = \begin{cases} \max\{\sqrt{k_{\max}}, cN^{\alpha}\}, & \text{if} \quad 0 < \alpha \leq 1; \\ \sqrt{\dfrac{\log N}{\log(\log N)}}, & \text{if} \quad \alpha = 0; \end{cases} \tag{1.39}$$

where $k_{\max}$ is the maximal degree of the graph $G(N,p)$. This exact result translates into the fact that the leading eigenvalue λ_1 diverges in the $G(N,p)$ model, since $k_{\max}$ diverges. In general, random undirected graph ensembles defined on prescribed degree distribution p_{deg} the leading eigenvalue has a lower bound, i.e., $\lambda_1 \geq \sqrt{k_{\max}}$ [Chung et al., 2004]. More specifically, there are two regimes where almost surely for $N \gg 1$ the leading eigenvalue is given by

$$\lambda_1 = \begin{cases} K_{p_{\text{deg}}}, & \text{if} \quad K_{p_{\text{deg}}} > \sqrt{k_{\max}} \log N; \\ \sqrt{k_{\max}}, & \text{if} \quad K_{p_{\text{deg}}} < \dfrac{\sqrt{k_{\max}}}{\log^2 N}; \end{cases} \qquad \text{where} \quad K_{p_{\text{deg}}} := \frac{\langle k^2 \rangle_{p_{\text{deg}}}}{\langle k \rangle_{p_{\text{deg}}}}. \tag{1.40}$$

Accordingly, for infinitely large and undirected random graphs defined with prescribed degree distribution the leading eigenvalue diverges when the degree distribution has unbounded support (hence $k_{\max}$ diverges). This fact has implications in the stability of fixed points of complex systems modelled on such graphs with symmetric interactions (see Sec. 1.5), since their leading eigenvalue behaves as in the underlying undirected graph, hence in the limit $N \to \infty$ λ_1 diverges. Recently, studies on random directed graphs [Neri and Metz, 2016, 2020; Tarnowski et al., 2020] show significant distinctions with respect to undirected graph. In particular, for adjacency matrices of directed random graphs on prescribed joint degree distribution $p^{\text{d}}_{\text{deg}}(k_{\text{in}}, k_{\text{out}})$ of indegrees k_{in} and outdegrees k_{out}, the leading eigenvalue is given by

$$\lambda_1 = \tilde{c}(\tilde{\rho} + 1), \quad \text{with } \tilde{\rho} := \frac{\langle k_{\text{in}} k_{\text{out}} \rangle_{p^{\text{d}}_{\text{deg}}} - \tilde{c}^2}{\tilde{c}^2}, \tag{1.41}$$

where $\tilde{c} := \langle k_{\text{in}} \rangle_{p^{\text{d}}_{\text{deg}}} = \langle k_{\text{out}} \rangle_{p^{\text{d}}_{\text{deg}}}$ is the mean outdegree. The quantity $\tilde{c}(\tilde{\rho}+1)$, that we name effective mean degree, characterises the effective number of degrees of freedom each node in the network interacts with. Hence, in the limit $N \to \infty$, the leading eigenvalue of random, directed graphs is finite as soon as the effective mean degree is finite. As discussed above, this implies that complex systems defined on these graphs can be stable in the limit $N \to \infty$.

The results discussed above gives a first example on how interactions between single components play a major role on the stability property of the system granting the sta-

bility of many directed graphs with same structure and statistical properties as unstable undirected ones. Symmetric and unidirectional interactions are often not realistic types of interactions for modelling real world systems, such as, ecosystems [Allesina and Tang, 2012; Barbier et al., 2018] and neural networks [Martí et al., 2018]. In general, interactions between the constituents of complex systems are bidirectional and non-symmetric, and this fact motivates this thesis in studying complex systems on networks where the interactions are bidirectional and non-symmetric. In the next section we discuss sparse random matrices from a complex network perspective, where the universal laws in Sec. 1.3 stop to be valid.

1.5.2 Sparse random matrices from a network perspective

Sparse matrices can be defined as those random matrices that contain "many" zeros such that the universal laws in Eqs. (1.20)-(1.22) (and the corresponding Theorems 1, 2 and 3) stop to be valid. The adjacency matrix in Eq. (1.31) is an example of a sparse matrix, and the associated graph with $\alpha = 0$ in Eq. (1.33), i.e., in the finite connectivity regime, an example of sparse random graph. In this section, we summarise the results in the study of the spectra of sparse matrices, to show how they distinguish from the dense and dilute matrices at the level of the spectral distribution.

While the adjacency matrices entries are $0, 1$ only, one typically consider sparse random matrices which have non-zero entries distributed according to a given distribution. This can be reached with the following parametrisation of a sparse random matrix $\mathbf{A} = \{A_{ij}\}$ with entries

$$A_{ij} = C_{ij} J_{ij}, \qquad i, j \in \{1, \dots, N\}\,, \tag{1.42}$$

where $\mathbf{C} = \{C_{ij}\}$ is an adjacency matrix of a given random graph ensemble which takes into account the sparsity, while $\mathbf{J} = \{J_{ij}\}$ is a random matrix with a given joint distribution of its entries, that can be a Hermitian or non-Hermitian matrix, such as in Sec. 1.3. Equivalently, one can see the random matrix $\mathbf{A}$ as a weighted random graph, where the $\{J_{ij}\}$ are the weights of the links between nodes i, j when they are connected with a link, i.e., when $C_{ij} = 1$. We consider here the adjacency matrix of the Gilbert model in Eq. (1.31), with p as in Eq. (1.33) with $\alpha = 0$, i.e., random graphs in the finite connectivity regime, when $N \to \infty$. The corresponding adjacency matrix displays a finite number of non-zero elements per row and a non-zero probability of having all-zeroes rows; the probability of a row to be filled by all zeroes converges to a constant for $N \to \infty$, and thus with probability one a constant fraction of the rows contain all zeroes for $N \to \infty$. In the following we explore the random matrix theory results for matrices such as Eq. (1.42), for Hermitian and non-Hermitian matrices $\mathbf{J} = \{J_{ij}\}$. We note that the symmetry properties of $\mathbf{J}$ are the same than $\mathbf{A}$, whereas $\mathbf{C}$ encodes only the sparse network structure.

Let us now consider the case of symmetric sparse matrices. In the sparse regime, the graph associated to the matrix typically decomposes into a giant component and a large number of small clusters, mostly trees. The isolated finite clusters are typically associated to localised eigenstates which contribute to the point spectrum. In particular, the spectral distribution is typically characterised by spikes [Bauer and Golinelli, 2001a; Duras et al., 1997; Kühn, 2008; Mirlin and Fyodorov, 1991; Nagao and Tanaka, 2007; Rodgers and Bray, 1988; Rogers et al., 2008; Sato and Kobayashi, 1976; Semerjian and Cugliandolo, 2002; Sodin, 2009], and extended tails on the real line, i.e., Lifshitz tails [Bapst and Semerjian, 2011; Bauer and Golinelli, 2001b; Khorunzhiy et al., 2006; Krivelevich and Sudakov, 2003; Slanina, 2011, 2012]. In particular, when entries J_{ij} can be ± 1 the tails are characterised by the scaling of the spectral distribution as

$$\rho(x) = \mathcal{O}(x^{-2x^2}), \quad \text{for } x^2 \to \infty, \tag{1.43}$$

and its support extends to the entire real line. Accordingly, the leading eigenvalue diverges. The tails in the spectrum can be related to the fact that the leading eigenvalue of the associated adjacency matrix diverges with the system size, as discussed in Sec. 1.4. These facts confirm that the case $\alpha = 0$ is excluded from the universal law in Eq. (1.20) and the hypotheses of Theorem 1.

The spectral distribution on non-Hemitian and sparse random matrices has been much less studied in the mathematical literature than its symmetric counterpart. For example, it has been investigated with the cavity method for non-Hermitian random matrices [Neri and Metz, 2012; Rogers and Pérez Castillo, 2009], which will be presented in Ch. 3. A numerical investigation for sparse non-Hermitian matrices has been made when violating the Hypothesis (ii) in the condition in Def. A.2.1, where the pairs of opposite matrix entries are independent but not-identically distributed; accordingly, the support of the empirical spectral density deviates from the ellipse in the complex plane [Cicuta and Molinari, 2016] (see the next Sec. 1.6 for more details). In the case of directed random graphs on prescribed joint degree distribution $p^{\mathrm{d}}_{\mathrm{deg}}$ and with i.i.d. $J_{ij} \sim p(J)$, [Neri and Metz, 2020] provided an exact formula for the typical value of the leading eigenvalue, i.e.,

$$\lambda_1^* = \begin{cases} \tilde{c}(\tilde{\rho}+1)\left\langle J\right\rangle_p, & \text{if} \quad \left\langle J\right\rangle_p > \sqrt{\dfrac{\left\langle J^2\right\rangle_p}{\tilde{c}(\tilde{\rho}+1)}}; \\ \sqrt{\tilde{c}(\tilde{\rho}+1)\left\langle J^2\right\rangle_p}, & \text{if} \quad \left\langle J\right\rangle_p \leq \sqrt{\dfrac{\left\langle J^2\right\rangle_p}{\tilde{c}(\tilde{\rho}+1)}}; \end{cases} \tag{1.44}$$

where $\tilde{c}$ and $\tilde{\rho}$ are as in Eq. (1.41). Similarly to the leading eigenvalue in Eq. (1.41), the leading eigenvalue is finite as the effective mean degree $\tilde{c}(\tilde{\rho}+1)$ is finite, and this property guarantees the stability of the fixed point in the limit $N \to \infty$.

Finally, we show in Table 1.1 a schematic summary of the results for the spectra of dense, dilute and sparse matrices presented in this chapter to collocate them in light of the universal laws in RMT.

Table 1.1: Picture of the most recent and relevant results known in the literature of RMT in the infinite size limit.

SPARSITY ↓	HERMITIAN	NON-HERMITIAN	
		i.i.d. A_{ij}	i.i.d. $(A_{ij}, A_{ji})_{i \neq j}$
DENSE	Theorem 1: [Bai, 1999]	Theorem 2: [Tao and Vu, 2010]; May model: [May, 1972]	Theorem 3: [Nguyen and O'Rourke, 2015], [Götze et al., 2015]
DILUTE $0 < \alpha \leq 1$	[Mirlin and Fyodorov, 1991]	Theorem 4: [Wood, 2012]; May model ($\alpha = 1$): [May, 1972]	[Allesina and Tang, 2012], [Tang et al., 2014], (both $\alpha = 1$)
SPARSE $\alpha = 0$	[Rodgers and Bray, 1988] (replica), [Mirlin and Fyodorov, 1991] (susy), [Semerjian and Cugliandolo, 2002], [Kühn, 2008] (replica), [Rogers et al., 2008] (cavity), and main text	[Rogers and Pérez Castillo, 2009] (cavity), [Metz et al., 2019] (cavity)	[Rogers and Pérez Castillo, 2009] (cavity), [Neri and Metz, 2012] (cavity); Directed graphs: [Neri and Metz, 2016], [Tarnowski et al., 2020], [Neri and Metz, 2020]

Legend. Different colours refer to the following universal laws in RMT: (i) Semi-circular law in Eq. (1.20), (light-blue); (ii) Circular law in Eq. (1.21), (amber); (iii) Elliptic law in Eq. (1.22), (green). The columns refer to Hermitian and non-Hermitian complex matrices $\mathbf{A}$ (the real matrices are included); as for the non-Hermitian, both cases of i.i.d. entries and i.i.d. pairs of opposite entries are listed. The rows refer to sparsity in $\mathbf{A}$, ranging from non-sparse (dense) to the sparse ensembles as defined in Eq. (1.42) with the matrix $\mathbf{C}$ as in Eq. (1.31) with p depending on α as in Eq. (1.33), with the special case of sparse ($\alpha = 0$), for which the universal laws (i-iii) are violated.

1.6 Antagonistic random matrices in previous works

Now we discuss briefly the models of complex systems in literature that can be classified with the non-Hermitian random matrices with pairwise correlation between off-diagonal elements, with a special focus on antagonistic matrices.

Recently, [Cicuta and Molinari, 2016] suggested to consider as a model for the ecological community matrix in Eq.(1.6), within the linearised approach, a matrix belonging to the random antagonistic ensemble $\mathcal{A}$, as generalisation of anti-symmetric matrices. Antagonistic matrices $\mathbf{A}$ in the work by Cicuta [Cicuta and Molinari, 2016] are defined by having zero diagonal terms, while off-diagonal opposite terms ($i \neq j$) are either zero $A_{ij} = A_{ji} = 0$ or with opposite signs $A_{ij}A_{ji} < 0$. These are sparse matrices, in a broad sense, with some of the entries being equal to zero, modelling large ecosystems where the different interacting species in the couples have a predator-prey interaction.

The idea of focusing on predator-prey interaction follows essentially from [Allesina and Pascual, 2008; Allesina and Tang, 2012; Tang et al., 2014], which show that such sign correlated interactions between different species have strong stabilising effects: among the all kinds of community matrices $\mathbf{A}$, i.e., cooperative, competitive, predator-prey, mixture or random, the predator-prey matrices are the most likely to be stable at fixed finite N, while the mixture matrices are the least likely to be stable. Another feature highlighted in [Allesina and Tang, 2012] is that the probability of stability for predator-prey systems decreases if there is a large preponderance of weak interaction [Emmerson and Yearsley, 2004; Mccann et al., 1998]. The models considered by [Allesina and Tang, 2012] and [Tang et al., 2014] included the probability C — independent of N — for a couple to be interacting, while with probability $1 - C$ a couple is not interacting. The parameter C is known as the connectance in ecological context [Gardner and Ashby, 1970], and reflects the fact that each species do not interact with every other species, but with only a fraction C of them. Although this inclusion is not introduced via modelling a network structure, as for example it would be within Eq. (1.42), Allesina's antagonistic matrices can be obtained via Eq. (1.42): one would have $\alpha = 1$ in Eq. (1.33), i.e., $p = c = C$ and the expected average degree in Eq. (1.34) is $C \times (N - 1)$. This approach of reducing the fully connected structure via the connectance C, was also considered in May's model within symmetric matrices [May, 1972], where in that context it resulted to a simple rescaling of the circular law, compatible with an all-to-all model of interactions.

Some of the definitions of antagonistic matrices in [Cicuta and Molinari, 2016] and the models considered in [Allesina and Tang, 2012] are related to the mathematical framework and hypotheses introduced for the elliptic Theorem 3 [Götze et al., 2015; Nguyen and O'Rourke, 2015]; for example, the matrices introduced in [Allesina and Tang, 2012] satisfy these hypotheses — in particular the condition (ii) in Def. A.2.1 — and so the elliptic law is obtained. This turns out, for example, to establish the stability criteria in [Allesina and Tang, 2012], where the leading eigenvalue λ_1 — which governs the stability — of the matrices considered is on real axis and is on the boundary of the

rescaled ellipse. More specifically, in terms of the elliptic law in Eq. (1.22) and Eq. (1.23), one has that stability is controlled by the value of the horizontal semiaxis of the elliptic law, which in this case reads

$$\lambda_1 = \sigma\sqrt{NC}(1 + \tau/\sigma^2), \tag{1.45}$$

with variance σ and covariance τ. It is important to observe that in this elliptic regime the leading eigenvalue diverges in the infinite size limit, independently of the kind of interactions considered.

[Allesina and Tang, 2012] considered also the interplay between the kinds of interactions (predator-prey or others) and their weakness, which give stabilising and destabilising effects, in providing stability criteria for systems of large but finite sizes. It is unknown, however, and this is the main question of this thesis, how including a sparse network structure influences the stability.

We show now in Table 1.2 a scheme of the current study on sparse matrices with pairwise correlated interactions $(J_{ij}, J_{ji})_{i\neq j}$, where we mention that the model for the matrices will be presented in Ch. 2.

Table 1.2: Picture of the investigations known in the literature of RMT on random antagonistic matrices with i.i.d. pairs of opposite entries.

SPARSITY ↓	SPARSE MATRICES with i.i.d. $(A_{ij}, A_{ji})_{i\neq j}$ $A_{ij}A_{ji} \leq 0$, $i \neq j$
DENSE	Theorem 3: [Nguyen and O'Rourke, 2015], [Götze et al., 2015]; [Cicuta and Molinari, 2016].
DILUTE $0 < \alpha \leq 1$	[Allesina and Tang, 2012], [Tang et al., 2014], (both $\alpha = 1$)
SPARSE $\alpha = 0$	This thesis (see Ch. 2)

Legend. The rows refer to sparsity in **A**, ranging from non-sparse (dense) to the sparse ensembles with the special case of $\alpha = 0$, for which the elliptic law in Eq. (1.22) is violated. In green the Elliptic law in Eq. (1.22) and the cases where it is valid. In this table, we present also where our results would be collocated, i.e. the sparse regime where the underlying graph is in the finite connectivity regime.

One example in the literature [Cicuta and Molinari, 2016] of antagonistic matrices which violates the hypotheses of the elliptic Theorem 3 has been to consider pairs of opposite entries $(A_{i\neq j}, A_{j\neq i})$ to be independent but not identically distributed — i.e., hypothesis (ii) in condition in Def. A.2.1 is relaxed —, where the pairs of opposite

entries $(A_{i\neq j}, A_{j\neq i})$ are distributed as

$$p_{ij}(u,l) = \begin{cases} (2\gamma_{ij})^{-1}, & \text{if } u \in (1, 1+\gamma_{i,j}) \text{ and } l \in (-1-\gamma_{i,j}, -1); \\ (2\gamma_{ij})^{-1}, & \text{if } l \in (1, 1+\gamma_{i,j}) \text{ and } u \in (-1-\gamma_{i,j}, -1); \\ 0, & \text{otherwise,} \end{cases} \tag{1.46}$$

with

$$\gamma_{i,j} = \frac{c}{1+(j-i)^p},$$

for different values of c, p. As the size N of the antagonistic matrix $\mathbf{A}$ increases, the pair of entries far from the diagonal are increasingly similar to an antisymmetric matrix. All the eigenvalues $\lambda_i(\mathbf{A})$ are in a strip $|\Re(\lambda_i(\mathbf{A}))| < a$ where the width a of the strip does not increase with N; actually it slightly decreases, as one can see from Fig. 1.1.

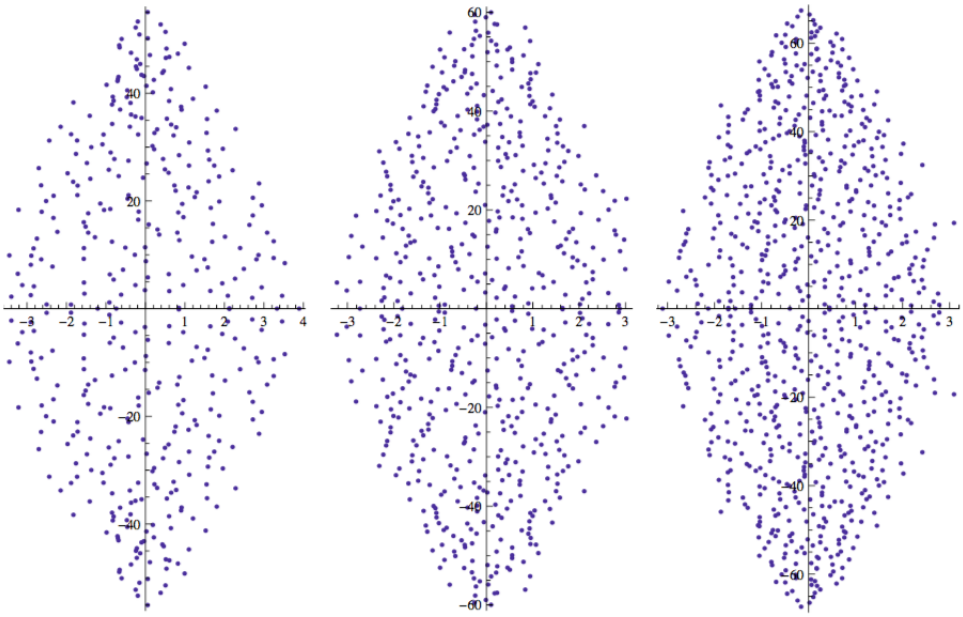

Figure 1.1: [Cicuta and Molinari, 2016]: Eigenvalues of a random antagonistic matrix with independent but *not* identically distributed pairs of opposite entries as in Eq. (1.46), and parameters $c = 50$, $p = 8$, $N = 400, 600, 800$.

1.7 Sparse random matrices with antagonistic interactions

In this thesis we are interested in generalising the antagonistic matrices $\mathbf{A}$ of previous works as in Sec. 1.6, which model the dynamics of species with predator-prey interactions, by studying the effect of including a sparse network structure. As discussed in Sec. 1.5, sparse networks have been considered with symmetric, i.i.d. non-symmetric, or directed interactions; however, by definition, these models do not allow for sign constrained pair interactions, like predator-prey ones. The sparse network structure reproduces the realistic feature that in a given ecosystem each species does not interact really with everyone,

neither with a fraction of them C which is independent of the number of species N, but only with a few of them. In this direction and in light of the summary on sparse random graphs presented in Sec. 1.5, we consider in this thesis sparse matrices in the regime $\alpha = 0$ (while the constant C is equivalent to $\alpha = 1$, as discussed in Sec.. 1.6). The underlying random network is in the finite connectivity regime, i.e., the expected average degree in Eq. (1.34) is equal to c, which is finite, also known as the mean degree (or connectivity) of the graph. This regime corresponds to real world systems where the degrees of freedom are interacting with a finite number of other degrees of freedom; in particular, when some species are added to the ecosystem, the expected average degree in the ecosystem remains roughly constant. This property does not hold only for ecosystems, but also for general complex systems, for example social networks [Backstrom et al., 2011], and so it is very interesting, under a general perspective, to study the properties of these sparse interacting systems. As also pointed out by Allesina [Allesina et al., 2015], developing a model for complex systems which includes this sparsity property, as well an interaction structure (predator-prey), would make a big step forward in understanding realistic food webs, as well as many real world systems.

The stability criteria based on the leading eigenvalue in Eqs. (1.13)-(1.14) highlight also the importance to study the infinite size limit, to establish whether the associated fixed point can be stable or not. As discussed in Sec. 1.5 the regime $\alpha = 0$ is very interesting also from the mathematical point of view, since it violates the hypotheses of the theorems for the universal laws and, in particular for antagonistic matrices, of the elliptic Theorem 3 in its weakest versions [Götze et al., 2015; Nguyen and O'Rourke, 2015]. Accordingly, studying these ensembles from a random matrix point of view is a further extension of the current literature on sparse non-Hermitian random matrices [Metz et al., 2019; Rogers and Pérez Castillo, 2009].

Finally, sparse antagonistic random matrices as in this thesis can be a good model — i.e., with a realistic progress with respect to existing models — for the Jacobian matrix $\mathbf{A}$ at a given fixed point $\vec{x}^*$ in Eq. (1.6), which is the linearised (local) dynamics in the vicinity of $\vec{x}^*$ of the global global dynamics in Eq. (1.1) (which is generally unknown). Accordingly, with the characterisation of sparse antagonistic random matrices we can provide useful insights into the generic qualitative features of such systems. The interest on potential applications goes far beyond the mathematical ecology context: e.g., games strategies [Galla and Farmer, 2013] or financial ecosystems [Farmer and Skouras, 2013; Haldane and May, 2011]. Moreover, the interplay between network structure and interactions among the degrees of freedom of a system is of relevance as applications of systems of many coupled nonlinear ODEs (e.g., complex gene regulatory networks [de Jong, 2002], neural networks [Sompolinsky et al., 1988; Wainrib and Touboul, 2012] and [Amir et al., 2016], or random catalytic reaction networks [Stadler et al., 1993]).

1.8 Thesis outline

The rest of the thesis is organised as follows. In Ch. 2 we introduce the general model of this thesis, i.e., sparse random matrices with pairwise correlated interactions, in particular the antagonistic and mixture ensembles that we study in detail in this thesis. Chapter 3 presents the cavity method for determining spectral properties of sparse non-Hermitian random matrices. In Ch. 4 we extend the theory of Ch. 3 to study the general model introduced in Ch. 2. Chapter 5 shows the numerical solutions of the theory developed in Ch. 4 and compare them with the spectra of the models presented in Ch. 2. Chapter 6 presents a detailed study on the leading eigenvalue of the models presented in Ch. 2 which is central to determine stability properties of the fixed points of complex systems, as discussed in this chapter. Finally, in Ch. 7 we discuss the conclusions of this thesis, where we highlight the novel results and the extension in the current literature of sparse random matrices, and further challenges that can build upon or results or generalise them. We end this thesis with Appendices, where we present the main nontrivial mathematical methods that have been used to derive the results of this thesis discussed in the main chapters.

Chapter 2

The model

In this chapter we define the models of complex systems that we consider in this thesis, motivated from the discussion in Ch. 1, and for which we present results in Chs. 4-6.

This chapter is structured as follows. Section 2.1 defines the general random matrix ensemble on sparse networks with pairwise correlated interactions. In Sec. 2.1.1 we recover, from the general model, the symmetric, the i.i.d. non-symmetric and the oriented sparse matrices. Then, Sec. 2.1.2 focuses on random matrix models that represent sparse systems with predator-prey interactions only, and in Sec. 2.1.3 we consider a mixture of predator-prey, mutualistic and competitive interactions. We refer to the former as the antagonistic ensemble, following Refs. [Allesina and Tang, 2012; Cicuta and Molinari, 2016] (see Sec. 1.6), and to the latter as the mixture ensemble. In Fig. 2.1 we provide a sketch of these two models.

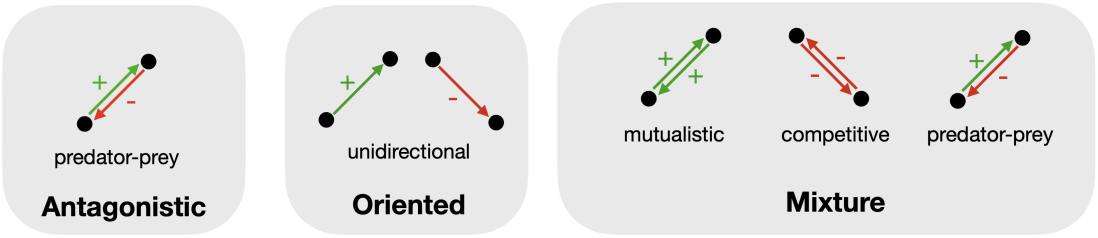

Figure 2.1: Sketch of the interactions in the two main models, the antagonistic and mixture model, that we study in this thesis, as well as in the oriented ensemble studied before in Refs. [Metz and Neri, 2020; Metz et al., 2019; Neri and Metz, 2016].

2.1 The general model: sparse random matrices with pairwise correlated interactions

We consider sparse random matrices $\mathbf{A} = \{A_{ij}\}$, which are defined as the following element-wise product

$$A_{ij} = C_{ij} J_{ij}, \qquad i, j \in (1, \dots, N), \tag{2.1}$$

where $\mathbf{C} = \{C_{ij}\}$ is an adjacency matrix of a sparse, undirected, random graph (see Sec. 1.5), i.e., $C_{ij} \in \{0, 1\}$, characterised by a prescribed degree distribution (see Sec. 1.4.2.1) $p_{\text{deg}}(k)$ with mean degree

$$c = \sum_{k=0}^{\infty} p_{\text{deg}}(k)\, k. \tag{2.2}$$

Example of prescribed degree distributions are mentioned in Sec. 1.5, for example, we remind here the binomial and poissonian degree distribution in Eq. (1.35) and Eq. (1.36). The real variables J_{ij}, forming the interaction matrix $\mathbf{J} = \{J_{ij}\}$ within the linearised dynamics approach (see Ch. 1), specify the effect that the degree of freedom j has on the degree of freedom i. Our aim is to study interactions focusing only on the correlations between the elements opposite to the diagonal, neglecting other residual correlations. This translates in assuming the real pairs (J_{ij}, J_{ji}) to be independent and identically distributed (i.i.d.), i.e., each pair $(J_{ij}, J_{ji}) : 1 \leq i < j \leq N$ is distributed according to a probability distribution $p(u, l)$, independently from i, j. Since we focus on the role of the interactions J_{ij}, J_{ji}, we also set the diagonal terms to be zeros, i.e., $J_{ii} = 0$, corresponding to simple graphs. We observe that the off-diagonal pairs (J_{ij}, J_{ji}) are as in the condition in Def. A.2.1, used in the hypothesis of the dense elliptic Theorem 3.

We can define now the general model of this thesis, which is characterised by the assumptions presented above. Sparse random matrices $\mathbf{A}$ as in Eq. (2.1), where the underlying random graph is characterised by a prescribed degree distribution $p_{\text{deg}}(k)$, with the interaction matrix $\mathbf{J}$ formed by i.i.d. off-diagonal pairs $(J_{ij}, J_{ji}) \sim p(u, l)$, and the diagonal terms are zero, define the general model of this thesis, which we refer to as sparse random matrices with pairwise correlated interactions. Since such ensemble is defined on random graphs with a prescribed degree distribution p_{deg}, then it is a locally treelike model of graphs (see Sec. 1.4.2.2).

Before specifying the probability distributions implemented in this thesis, we discuss how some ensembles already studied in the literature (see Sec. 1.5) can be obtained within our formalism from Eq. (2.1).

2.1.1 Symmetric, i.i.d. non-Hermitian and oriented sparse matrices

Sparse and symmetric random matrices, where elements opposite to the diagonal are the same [Abou-Chacra et al., 1973; Bordenave and Lelarge, 2010; Fyodorov and Mirlin, 1991; Kabashima et al., 2010; Kühn, 2008; Rogers et al., 2008; Semerjian and Cugliandolo, 2002; Susca et al., 2019] are obtained by setting

$$p(u, l) = p^{\text{S}}(u, l) = \tilde{p}(u)\delta(u - l). \tag{2.3}$$

Sparse and non-Hermitian random matrices with i.i.d. interactions strength, i.e., without any type of correlations [Metz et al., 2019; Rogers and Pérez Castillo, 2009], for which

$$p(u,l) = p^{\mathrm{N-H}}(u,l) = \tilde{p}(u)\tilde{p}(l), \tag{2.4}$$

or for oriented random matrices [Metz et al., 2019; Neri and Metz, 2016, 2020; Rogers and Pérez Castillo, 2009; Tarnowski et al., 2020], for which

$$p(u,l) = p^{\mathrm{O}}(u,l) = \frac{1}{2}\tilde{p}(u)\delta(l) + \frac{1}{2}\tilde{p}(l)\delta(u), \tag{2.5}$$

where $\tilde{p}$ is a probability density generally supported on $(-\infty,\infty)$. In the oriented case, interactions are unidirectional, as illustrated in Fig. 2.1, corresponding to random fully directed graph.

In the next subsection, we present two ensembles in a form that has not discussed before in the literature (antagonistic matrices in the literature are discussed in Sec. 1.6), namely, antagonistic random matrices in Sec. 2.1.2, for which $p(u,l)$ represents predator-prey interactions, and mixture matrices in Sec. 2.1.3, for which $p(u,l)$ represents a mixture of predator-prey, competitive, and mutualistic interactions.

2.1.2 Antagonistic ensemble

Here we define the antagonistic ensemble that we consider in this thesis, which is characterised by predator-prey interactions, where

$$J_{ij}J_{ji} < 0, \tag{2.6}$$

which generalises anti-symmetric matrices since the antagonistic ensemble studied here has generally $|J_{ij}| \neq |J_{ji}|$, whereas anti-symmetric matrices are defined by $J_{ij} = -J_{ji}$. The joint probability density of antagonistic matrices we refer to in this work is given by

$$p(u,l) = p^{\mathrm{A}}(u,l) = \frac{1}{2}\tilde{p}(|u|)\tilde{p}(|l|)\left[\theta(u)\theta(-l) + \theta(-u)\theta(l)\right], \tag{2.7}$$

where $\tilde{p}$ is a probability density with positive support $\mathbb{R}^+ = ([0,\infty))$ and normalised to one. The θ-s are the Heaviside functions defined by

$$\theta(x) = \begin{cases} 0 & x < 0, \\ 1 & x \geq 0, \end{cases} \tag{2.8}$$

that imposes the opposite sign constraint $J_{ij}J_{ji} < 0$ for each pair of indices $i \neq j$, which account for the sign constraints of predator-prey interactions. The antagonistic probability distribution in Eq. (2.7) is not the most general joint distribution that one can consider to study antagonistic systems. However, our research aims to characterise the properties of the spectra of antagonistic random matrices characterised by having oppo-

site entries with opposite sign, in order to account for the predator-prey signs constraint in Eq. (2.6). Accordingly, the choice for the model in Eq. (2.7) fully includes this feature. Finally, it is important to observe that antagonistic matrices defined by Eq. (2.7) are a generalisation of anti-symmetric matrices, since generally $|u| \neq |l|$.

Schematic summary of the assumptions on Eq. (2.7) Here we provide a schematic summary (see Appendix A.3 for a more detailed discussion) of the assumptions that we considered for defining Eq. (2.7) from, and including the assumptions therein, Eqs. (2.1) and (A.11):

1. i.i.d. pairs $p^{\mathrm{A}}_{i,j}(J_{ij}, J_{ji}) = p^{\mathrm{A}}(J_{ij}, J_{ji}) = p^{A}(u, l)$;
2. internal permutation symmetry $p^{\mathrm{A}}(u, l) = p^{\mathrm{A}}(l, u)$;
3. independence of magnitudes $p_2(u, l)\theta(-ul) = p_1(u)p_1(l)\theta(-ul)$;
4. predator-prey symmetry $p_1(x) = p_1(-x) = \tilde{p}(|x|)/2$.

In particular, 2) implies that $\langle u \rangle_{p^{\mathrm{A}}} = \langle l \rangle_{p^{\mathrm{A}}}$, and 4) implies that

$$\langle u \rangle_{p^{\mathrm{A}}} = 0, \tag{2.9}$$

such that on average the interactions of a node are balanced, which is a reasonable assumption for systems dominated by predator-prey interactions [Allesina and Tang, 2012].
We remark that the hypotheses 3) and 4) are made only for simplicity of our study, but our theory can deal with the hypotheses 1) and 2), which are intrinsic in the model in Eq. (2.1) for a more general p^{A} in Eq. (A.11).

2.1.3 Mixture ensemble

We define now the mixture ensemble that we consider in this thesis, which is characterised by a mixture of predator-prey interactions, as in Sec. 2.1.2, for which

$$J_{ij}J_{ji} < 0, \tag{2.10}$$

mutualistic interactions, for which

$$J_{ij} > 0 \text{ and } J_{ji} > 0, \tag{2.11}$$

and competitive interactions, for which

$$J_{ij} < 0 \text{ and } J_{ji} < 0. \tag{2.12}$$

By following the same logic used to define the antagonistic ensemble, within the assumptions discussed in Appendix A.3 and summarised in Sec. 2.1.2, the following probability distribution characterises the mixture ensemble, i.e.,

$$p(u,l) = p^{\mathrm{M}}(u,l) = \pi^{\mathrm{A}} p^{\mathrm{A}}(u,l) + (1-\pi^{\mathrm{A}}) p^{\mathrm{CM}}(u,l), \tag{2.13}$$

where $\pi^{\mathrm{A}} \in [0,1]$ accounts for the density of antagonistic interactions, p^{A} is the distribution defined in Eq. (2.7) that models predator-prey interactions, and p^{CM} is the distribution

$$p^{\mathrm{CM}}(u,l) = \tilde{p}(|u|)\tilde{p}(|l|)\left[\pi^{\mathrm{M}}\theta(u)\theta(l) + \left(1-\pi^{\mathrm{M}}\right)\theta(-u)\theta(-l)\right], \tag{2.14}$$

that includes both mutualistic and competitive interactions, with densities determined by $\pi^{\mathrm{M}} \in [0,1]$. Hence, for mixture matrices the couple (u,l) has a predator-prey-like interaction with probability π^{A}, while it is mutualistic with probability $(1-\pi^{\mathrm{A}})\pi^{\mathrm{M}}$ or competitive with probability $(1-\pi^{\mathrm{A}})(1-\pi^{\mathrm{M}})$.

2.1.4 Variance and covariance of the antagonistic and mixture probability distributions

In Appendix A.4 we derive the relations between the moments of the joint probability distributions $p(u,l)$ with support on $\mathbb{R}^2$ in terms of the moments of the auxiliary probability distribution $\tilde{p}$ with support on $\mathbb{R}^+$, for the antagonistic distribution p^{A} in the Eq. (2.7), and the mixture distribution p^{M} in the Eqs. (2.13) and (2.14). Here we show only the variance and the covariance (for the derivation see Appendix A.4), for general $\pi^{\mathrm{A}}, \pi^{\mathrm{M}} \in [0,1]$, which will be used in Sec. 2.2.

The variance of $p^{\mathrm{A}}(u,l)$ in Eq. (2.7) reads

$$\left\langle u^2 \right\rangle_{p^{\mathrm{A}}} - \cancelto{0}{\langle u \rangle^2_{p^{\mathrm{A}}}} = \left\langle u^2 \right\rangle_{\tilde{p}}, \tag{2.15}$$

and the covariance of $p^{\mathrm{A}}(u,l)$ reads

$$\langle ul \rangle_{p^{\mathrm{A}}} - \cancelto{0}{\langle u \rangle_{p^{\mathrm{A}}} \langle l \rangle_{p^{\mathrm{A}}}} = -\langle u \rangle_{\tilde{p}} \langle l \rangle_{\tilde{p}}. \tag{2.16}$$

From Eq. (2.13) the variance of $p^{\mathrm{M}}(u,l)$ reads

$$\left\langle u^2 \right\rangle_{p^{\mathrm{M}}} - \langle u \rangle^2_{p^{\mathrm{M}}} = \left\langle u^2 \right\rangle_{\tilde{p}} - 4\left(1-\pi^{\mathrm{A}}\right)^2 \left(\pi^{\mathrm{M}} - \frac{1}{2}\right)^2 \langle u \rangle^2_{\tilde{p}}, \tag{2.17}$$

which correctly recovers the variance of p^{A} in Eq. (A.20) when $\pi^{\mathrm{A}} = 1$, and the covariance

of $p^{\mathrm{M}}(u,l)$ reads

$$\langle ul\rangle_{p^{\mathrm{M}}} - \langle u\rangle_{p^{\mathrm{M}}}\langle l\rangle_{p^{\mathrm{M}}} = \langle u\rangle_{\tilde{p}}\langle l\rangle_{\tilde{p}}\left[1-2\pi^{\mathrm{A}}-4(1-\pi^{\mathrm{A}})^2\left(\pi^{\mathrm{M}}-\frac{1}{2}\right)^2\right], \tag{2.18}$$

which correctly recovers the covariance of p^{A} in Eq. (A.21) when $\pi^{\mathrm{A}}=1$.

2.2 Two reference examples for this thesis: Model A and Model B

Here we specify the probability distributions introduced in the general model in Eq. (2.1) that we typically consider in this thesis. First in regards to the network structure, i.e., p_{deg}, and then in regards to the interactions, i.e., the probability $\tilde{p}$ in the joint probabilities for antagonistic matrices in Eq. (2.7), and for the mixture matrices in Eqs. (2.14) and (2.13), together with the parameters $\pi^{\mathrm{A}},\pi^{\mathrm{M}}$. As we discuss below, the choices of these parameters define the reference models of this thesis, which we will often refer to in our studies at the moment of numerical implementations, that we call Model A and Model B.

As for the network structure, we often consider Erdős-Rényi graphs within the $G(N,p)$ model (see Sec. 1.5), where N is the size of the graph and p the probability of two nodes to be interacting. As we discussed at the beginning of this chapter, in this thesis we focus on the finite connectivity regime, i.e., $p=c/(N-1)$ and $\alpha=0$ in Eqs. (1.33)-(1.36), with mean degree c. The prescribed degree distributions are, in this case, binomial for finite N in Eqs. (1.33), poissonian in the $N\to\infty$ limit in Eq. (1.36). This defines the p_{deg} of both Model A and Model B. Sometimes, when specified, we also consider random regular graphs, which are defined by $p_{\mathrm{deg}}(k)=\delta_{k,c}$, or degree distributions which are linear combinations of random regular and of Erdős-Rényi graphs.

Let us now discuss the choices for the interactions distributions parameters. As for the interaction strength, we typically consider the $\tilde{p}$ in Eqs. (2.7) and (2.13) to be a uniform distribution with support on $[0,b]$, namely,

$$\tilde{p}(x)=\frac{1}{b}\left[1-\theta(x-b)\right], \quad x\geq 0, \tag{2.19}$$

where the value of b is chosen such that the variance of $p^{\mathrm{A}}(u,l)$ in Eq. (2.7), by Eq. (2.15), is one, i.e.

$$1=\left\langle u^2\right\rangle_{\tilde{p}}=\frac{1}{b}\int_0^b \mathrm{d}u\, u^2=\frac{b^2}{3}, \tag{2.20}$$

which gives $b=\sqrt{3}$. These choices of $b,\tilde{p}$ complete the definition of the Model A, which is an antagonistic ensemble.

We consider, within the mixture ensemble in Sec. 2.1.3, the probability $\tilde{p}$ to be the uniform distribution in Eq. (2.19) that we chose for Model A, with $b=\sqrt{3}$. We also

choose an equal probability for an interaction to be mutualistic or competitive, i.e., $\pi^{\mathrm{M}} = 0.5$ in Eq. (2.14), and one has that the interactions are balanced on average, i.e.,

$$\langle u \rangle_{p^{\mathrm{M}}} = 0, \tag{2.21}$$

similarly to the antagonistic model (see Eq. (2.9)). Accordingly, for this choice of π^{M}, the variance of $p^{\mathrm{M}}(u, l)$ in Eq. (2.17) simplifies to

$$\langle u^2 \rangle_{p^{\mathrm{M}}} - \cancelto{0}{\langle u \rangle^2_{p^{\mathrm{M}}}} = \langle u^2 \rangle_{\tilde{p}} = 1, \tag{2.22}$$

which equals the variance of $p^{\mathrm{A}}(u, l)$ in Eq. (2.15), independently from the value of π^{A}, and the covariance of $p^{\mathrm{M}}(u, l)$ in Eq. (2.18) simplifies to

$$\begin{aligned} \langle ul \rangle_{p^{\mathrm{M}}} - \cancelto{0}{\langle u \rangle_{p^{\mathrm{M}}} \langle l \rangle_{p^{\mathrm{M}}}} &= \langle u \rangle_{\tilde{p}} \langle l \rangle_{\tilde{p}} \left(1 - 2\pi^{\mathrm{A}}\right) \\ &= \frac{b^2}{4} \left(1 - 2\pi^{\mathrm{A}}\right). \end{aligned} \tag{2.23}$$

Within the mixture ensemble, we are interested to study how a small fraction of mutualistic or competitive interactions impacts a preponderance of predator-prey interaction, and so we set $\pi^{\mathrm{A}} = 0.9$; accordingly, the covariance of $p^{\mathrm{M}}(u, l)$ in Eq. (2.23) reads

$$\begin{aligned} \langle ul \rangle_{p^{\mathrm{M}}} &= -\frac{4}{5}\frac{b^2}{4} \\ &= -\frac{b^2}{5} = -\frac{3}{5}. \end{aligned} \tag{2.24}$$

Finally, the main difference between model A and model B is that all couples in model A interact in a predator-prey dynamics, while in model B a small fraction of interacting couples are either mutualistic or competitive, with same small probability.

Chapter 3

Cavity method for the spectral distribution of sparse non-Hermitian random matrices

In this chapter we summarise the cavity method, which is a method to determine the spectral distribution of sparse non-Hermitian random matrices [Metz et al., 2010, 2019; Rogers et al., 2008; Rogers and Pérez Castillo, 2009]. The cavity method originated from the physics of spin glasses [Mézard et al., 1987] and its core ideas have been developed in other contexts such as in computer science [Chertkov et al., 2010; Krzakala et al., 2015; Pearl, 1988].

This chapter is organised as follows. Sections 3.1-3.5 derive a set of closed equations named cavity equations for sparse non-Hermitian random matrices that are locally treelike, and present a formula for the spectral distribution expressed in terms of the solution of these equations. Finally, in Sec. 3.6 we discuss a class of solutions of the cavity equations from which the boundary of the support of the spectral distribution can be determined.

3.1 The empirical spectral density in terms of the resolvent

Here we introduce a formula for the empirical spectral density in Eq. (1.19) of a matrix $\mathbf{A}$ in terms of its resolvent, on which the rest of the chapter is based.

The resolvent $\mathbf{G}_{\mathbf{A}}(z)$ of a matrix $\mathbf{A}$ is defined as [1]

$$\mathbf{G}_{\mathbf{A}}(z) := (\mathbf{A} - z\mathbf{1}_N)^{-1}, \quad \text{with} \quad z \in \mathbb{C} \setminus \sigma(\mathbf{A}), \tag{3.1}$$

where here $()^{-1}$ denotes the matrix inverse. As we show in Appendix A.5, it is possible to express the empirical spectral density in terms of the resolvent $\mathbf{G}_{\mathbf{A}}(z)$ in Eq. (3.1) as follows

$$\rho_{\mathbf{A}}(z) = -\frac{1}{\pi N}\partial_{\bar{z}} \operatorname{Tr} \mathbf{G}_{\mathbf{A}}(z), \tag{3.2}$$

[1] An alternative but equivalent definition of the resolvent can be found in literature, f.e. [Sommers et al., 1988], with an opposite sign

where Tr is the trace operator, and where the partial derivative $\partial_{\bar{z}}$ is the following complex conjugate derivative, i.e.,

$$\partial_{\bar{z}} := \frac{\partial}{\partial \bar{z}} = \frac{1}{2}\left(\frac{\partial}{\partial x} + \mathrm{i}\frac{\partial}{\partial y}\right). \tag{3.3}$$

We observe that the resolvent $\mathbf{G}_{\mathbf{A}}(z)$ in Eq. (3.1) is well defined only outside the spectrum of $\mathbf{A}$. Since the complex conjugate derivative of a complex-valued function is zero where the function is analytic (see Appendix A.6), the left hand side of Eq. (3.2) is zero when the diagonal terms of the resolvent are analytic, which is the case outside the spectrum $\sigma(\mathbf{A})$.

Eq. (3.2) holds for both hermitian and non-Hermitian matrices $\mathbf{A}$. However, the analysis differentiates between these two cases when performing the limit for $N \to \infty$, as it is discussed in next section.

3.2 Infinite size limit: the Hermitisation method

We present now a regularisation of Eq. (3.2) that allows us to perform the limit for $N \to \infty$. The final aim is to obtain the limiting spectral distribution ρ of the empirical spectral density $\rho_{\mathbf{A}}(z)$, i.e.,

$$\rho(z) := \lim_{N\to\infty} \rho_{\mathbf{A}}(z). \tag{3.4}$$

We assume that the spectral distribution ρ is self-averaging (hence deterministic) and that it is continuous, similarly to other random matrices ensembles, as discussed in Ch. 1, and therefore the limit $N \to \infty$ in Eq. (3.4) exists.

The formula in Eq. (3.2) can not be used as it is, in the limit $N \to \infty$. It requires a bit more elaboration. Indeed, Eq. (3.2) in the limit $N \to \infty$ would give an infinite sum of delta distributions, while from the assumptions above it is expected to be a continuous distribution. In order to find a regular form of ρ, one has to find first an opportune analytic continuation $\rho_{\mathbf{A}}(z, \eta)$, i.e., a regularisation of the empirical spectral density in Eq. (3.2), so that

$$\rho_{\mathbf{A}}(z) = \lim_{\eta\to 0} \rho_{\mathbf{A}}(z, \eta). \tag{3.5}$$

Second, although a rigorous proof of the exchange of limits for general non-Hermitian matrices remains an open problem [Metz et al., 2019; Rogers, 2010b; Trefethen et al., 2005], we assume here and in the rest of the thesis that one can take first the limit $N \to \infty$, and then the limit $\eta \to 0$, so that the limiting spectral distribution is given by

$$\rho(z) = \lim_{\eta\to 0} \lim_{N\to\infty} \rho_{\mathbf{A}}(z, \eta). \tag{3.6}$$

We remark that the regularisation in Eq. (3.5) is not needed if the goal is to study the discrete spectrum of a matrix of finite size N, whereas it is an intermediate step towards the determination of the limiting spectral distribution for $N \to \infty$. Accordingly, we focus

now on finding an analytic continuation $\rho_{\mathbf{A}}(z,\eta)$ as in Eq. (3.5), aware that the final aim is to use such regularisation as in Eq. (3.6). While in the Hermitian case it is simpler to find a regularisation of the resolvent, since the support of the spectrum for hermitian matrices has zero Lebesgue measure in $\mathbb{C}$, a particular method has been developed for non-Hermitian matrices, where the spectrum has non-zero Lebesgue measure in $\mathbb{C}$: we summarise below the Hermitisation method [Feinberg and Zee, 1997; Girko, 1985; Metz et al., 2019; Rogers, 2010a; Rogers and Pérez Castillo, 2009], which maps the non-Hermitian problem to a Hermitian approach and it provides an opportune regularisation of for the empirical spectral density as in Eq. (3.2).

The first step of the Hermitisation method, is to double the size N of a given non-Hermitian matrix $\mathbf{A}$ to the following $2N \times 2N$ Hermitian matrix

$$\mathbf{H}_0(z;\mathbf{A}) := \begin{pmatrix} \mathbf{0}_N & z\mathbf{1}_N - \mathbf{A} \\ (z\mathbf{1}_N - \mathbf{A})^\dagger & \mathbf{0}_N \end{pmatrix}, \tag{3.7}$$

made of four $N \times N$ blocks. The second step is to add a diagonal regulator η to $\mathbf{H}_0$ as follows

$$\begin{aligned} \mathbf{H}_\eta(z;\mathbf{A}) :&= \mathrm{i}\mathbf{H}_0(z;\mathbf{A}) + \eta\mathbf{1_{2N}} \\ &= \begin{pmatrix} \eta\mathbf{1}_N & \mathrm{i}(z\mathbf{1}_N - \mathbf{A}) \\ \mathrm{i}(z\mathbf{1}_N - \mathbf{A})^\dagger & \eta\mathbf{1}_N \end{pmatrix}, \end{aligned} \tag{3.8}$$

which we call Hermitisation matrix, and where both $\mathbf{H}_0$ and $\mathbf{H}_\eta$ are made of four $N \times N$ blocks.

The utility of the Hermitisation matrix is that the lower left block of $\mathbf{H}_\eta^{-1}$ for small η reads (see the next page for a derivation)

$$-\mathrm{i}(z\mathbf{1}_N - \mathbf{A})^\dagger \left[\eta^2\mathbf{1}_N + (z\mathbf{1}_N - \mathbf{A})(z\mathbf{1}_N - \mathbf{A})^\dagger\right]^{-1} = \mathrm{i}\mathbf{G}_{\mathbf{A}}(z) + \mathcal{O}(\eta^2). \tag{3.9}$$

Hence it provides the resolvent, needed in the empirical spectral density as in Eq. (3.2), at the leading order in η.

Accordingly, the regularisation of the empirical spectral density in Eq. (3.2) given by the Hermitisation method reads

$$\rho_{\mathbf{A}}(z,\eta) = \frac{\mathrm{i}}{\pi N}\partial_{\bar{z}} \sum_{j=1}^{N} \left[\mathbf{H}_\eta^{-1}(z;\mathbf{A})\right]_{j+N,j}, \tag{3.10}$$

which in the end provides the limiting spectral distribution in Eq. (3.6), as discussed above. We remark that for all $z \in \mathbb{C}$, including the spectrum $\sigma_{\mathbf{A}}(z)$, and for $\eta \neq 0$, the Hermitisation matrix is invertible, and then the right hand side of Eq. (3.10) is continuous in z. In this sense $\rho_{\mathbf{A}}(z,\eta)$ provides a regularisation for the empirical spectral density in in Eq. (3.2) of general non-Hermitian matrices.

Note that there exists another formula for the empirical spectral density[2] , which is equivalent to Eq. (3.2), of non-Hermitian random matrices [Feinberg and Zee, 1997; Rogers and Pérez Castillo, 2009]. However, the regularisation in this other formula is also expressed in terms of $\mathbf{H}_\eta$ in Eq. (3.8), which highlights the importance of the Hermitian method as the reference regularisation in the study of non-Hermitian random matrices.

[2]which in turn is based on a representation of the delta in the complex plane that is different, but equivalent, to the representation of the delta on which Eq. (3.2) is based

Derivation of Eq. (3.9) We use here the following formula for the inversion of a block matrix $\mathbf{A}$ (see Appendix A.7), that we name Schur formula, i.e.,

$$\mathbf{A}^{-1} = \begin{pmatrix} \mathbf{s_d} & -\mathbf{s_d}\mathbf{b}\mathbf{d}^{-1} \\ -\mathbf{d}^{-1}\mathbf{c}\mathbf{s_d} & \mathbf{d}^{-1}\mathbf{c}\mathbf{s_d}\mathbf{b}\mathbf{d}^{-1} + \mathbf{d}^{-1} \end{pmatrix}, \tag{3.11}$$

where $\mathbf{s_d} := (\mathbf{a} - \mathbf{b}\mathbf{d}^{-1}\mathbf{c})^{-1}$ is the Schur complement of $\mathbf{d}$. Therefore, the inverse of block matrix $\mathbf{H}_\eta$, which exits for $\eta \neq 0$, can be computed straightforwardly. We are interested in the lower left block of $\mathbf{H}_\eta^{-1}$, and here we want to show that it is equal to the left hand side of Eq. (3.9). In order to apply Eq. (3.11) to $\mathbf{H}_\eta^{-1}$, we identify (see Sec. A.7)

$$\mathbf{a} := \eta \mathbf{1}_N, \tag{3.12}$$
$$\mathbf{b} := \mathrm{i}(z\mathbf{1}_N - \mathbf{A}), \tag{3.13}$$
$$\mathbf{c} := \mathrm{i}(z\mathbf{1}_N - \mathbf{A})^\dagger, \tag{3.14}$$
$$\mathbf{d} := \eta \mathbf{1}_N, \tag{3.15}$$

from which the Schur complement $\mathbf{s_d}$ reads

$$\mathbf{s_d} = \left[\eta \mathbf{1}_N + \frac{(z\mathbf{1}_N - \mathbf{A})\mathbf{1}_N(z\mathbf{1}_N - \mathbf{A})^\dagger}{\eta} \right]^{-1}. \tag{3.16}$$

The lower left block of $\mathbf{H}_\eta^{-1}$ is given by $-\mathbf{d}^{-1}\mathbf{c}\mathbf{s_d}$, i.e.,

$$\begin{aligned} -\mathbf{d}^{-1}\mathbf{c}\mathbf{s_d} &= -\frac{\mathrm{i}\mathbf{1}_N}{\eta}(z\mathbf{1}_N - \mathbf{A})^\dagger \left[\eta \mathbf{1}_N + \frac{(z\mathbf{1}_N - \mathbf{A})\mathbf{1}_N(z\mathbf{1}_N - \mathbf{A})^\dagger}{\eta} \right]^{-1} \\ &= -\mathrm{i}(z\mathbf{1}_N - \mathbf{A})^\dagger \left[\eta^2 \mathbf{1}_N + (z\mathbf{1}_N - \mathbf{A})(z\mathbf{1}_N - \mathbf{A})^\dagger \right]^{-1}, \end{aligned} \tag{3.17}$$

which coincides with the left hand side of Eq. (3.9). In order to obtain the right hand side of Eq. (3.9), we consider the inversion formula of a perturbed matrix, i.e.,

$$(\mathbf{1}_N + \alpha \mathbf{B})^{-1} = \mathbf{1}_N - \alpha \mathbf{B} + \mathcal{O}(\alpha^2), \tag{3.18}$$

which can be applied to the right hand side of Eq. (3.17), with $\eta^2 = \alpha$ and $\mathbf{B} = \left[(z\mathbf{1}_N - \mathbf{A})(z\mathbf{1}_N - \mathbf{A})^\dagger \right]^{-1}$, as follows

$$\begin{aligned} -\mathrm{i}(z\mathbf{1}_N - \mathbf{A})^\dagger \mathbf{B} \left(\eta^2 \mathbf{B} + \mathbf{1}_N \right)^{-1} &= -\mathrm{i}(z\mathbf{1}_N - \mathbf{A})^\dagger \mathbf{B}(\mathbf{1}_N + \mathcal{O}(\eta^2)) \\ &= -\mathrm{i}(z\mathbf{1}_N - \mathbf{A})^{-1} + \mathcal{O}(\eta^2) \\ &= \mathrm{i}\mathbf{G}_\mathbf{A}(z) + \mathcal{O}(\eta^2), \end{aligned} \tag{3.19}$$

which completes the derivation of Eq. (3.9).

□

3.3 Inversion of the Hermitisation matrix for general matrices

In order to evaluate the inverse of the Hermitisation matrix in Eq. (3.10), we consider a convenient permutation of the rows and columns of $\mathbf{H}_\eta$ in Eq. (3.8). The action of this permutation is defined as

$$(j+\alpha N, k+\beta N) \to (2j-1+\alpha, 2k-1+\beta), \quad \forall\, j,k=1,\dots,N, \quad \forall\, \alpha,\beta=0,1, \tag{3.20}$$

that puts next to each other the elements of the nodes (j,k), which resulted to be separated by N rows or/and columns in $\mathbf{H}_\eta$, as a consequence of the size extension of the Hermitisation in Eq. (3.8). We represent this permutation with a orthogonal matrix $\mathbf{P}$, i.e., $\mathbf{P}\mathbf{P}^{\mathrm{T}}=\mathbf{1}$, that acts on the Hermitisation matrix as follows

$$\tilde{\mathbf{H}} := \mathbf{P}\mathbf{H}_\eta\mathbf{P}^{\mathrm{T}}, \tag{3.21}$$

which results to be a matrix made of N^2 blocks $\tilde{\mathsf{H}}_{j,k}$, where each of these blocks is a two-by-two matrix defined as

$$\tilde{\mathsf{H}}_{jk} := \begin{pmatrix} \left[\tilde{\mathbf{H}}\right]_{2j-1,2k-1} & \left[\tilde{\mathbf{H}}\right]_{2j-1,2k} \\ \left[\tilde{\mathbf{H}}\right]_{2j,2k-1} & \left[\tilde{\mathbf{H}}\right]_{2j,2k} \end{pmatrix} = \begin{pmatrix} [\mathbf{H}_\eta]_{j,k} & [\mathbf{H}_\eta]_{j,k+N} \\ [\mathbf{H}_\eta]_{j+N,k} & [\mathbf{H}_\eta]_{j+N,k+N} \end{pmatrix}, \tag{3.22}$$

where $j,k=1,\dots,N$. Making explicit the elements of the Hermitisation matrix in Eq. (3.8), the two-by-two diagonal blocks in Eq. (3.22) read

$$\mathrm{i}\tilde{\mathsf{H}}_j = \mathsf{A}_{jj} - \mathsf{z}_\eta, \tag{3.23}$$

where we set for simplicity the notation $\tilde{\mathsf{H}}_j := \tilde{\mathsf{H}}_{jj}$, and the off-diagonal blocks in Eq. (3.22) read

$$\mathrm{i}\tilde{\mathsf{H}}_{jk} = \mathsf{A}_{jk}, \tag{3.24}$$

where

$$\mathsf{A}_{jk} := \begin{pmatrix} 0 & A_{j,k} \\ \bar{A}_{k,j} & 0 \end{pmatrix}, \quad \mathsf{z}_\eta = \begin{pmatrix} -\mathrm{i}\eta & z \\ \bar{z} & -\mathrm{i}\eta \end{pmatrix}. \tag{3.25}$$

From Eqs. (3.24)-(3.25) one can think at the off-diagonal $\tilde{\mathbf{H}}$ as an adjacency matrix made of two-by-two blocks $\tilde{\mathsf{H}}_{jk}$, which are non-zero if and only if there is a link between j and k (it can be (j,k), or (k,j)). In particular, if there is a graph structure in $\{A_{ij}\}=\{C_{ij}J_{ij}\}$, encoded in the adjacency matrix $\mathbf{C}$, then for one has that $\tilde{\mathsf{H}}_{j\neq k}\neq 0$ if and only if $C_{j\neq k}=1$ or $C_{k\neq j}=1$, while the diagonal $\tilde{\mathsf{H}}_j\neq 0$ for finite η.

The action of the permutation in Eq. (3.21) commutes with the matrix inverse operation, i.e.,

$$\tilde{\mathbf{H}}^{-1} = \mathbf{P}\mathbf{H}_\eta^{-1}\mathbf{P}^{\mathrm{T}}. \tag{3.26}$$

The commutation property in Eq. (3.26) translates into the fact that the action of the

permutation on the matrix inverse $\mathbf{H}_\eta^{-1}$ is the same as on the Hermitisation matrix in Eq. (3.22), i.e., it puts next to each other the elements of the nodes (j,k). Accordingly, $\tilde{\mathbf{H}}^{-1}$ results to be a matrix made of N^2 blocks G_{jk}, where each of these blocks is a two-by-two matrix defined as

$$\mathsf{G}_{jk} := \mathrm{i} \begin{pmatrix} \left[\tilde{\mathbf{H}}^{-1}\right]_{2j-1,2k-1} & \left[\tilde{\mathbf{H}}^{-1}\right]_{2j-1,2k} \\ \left[\tilde{\mathbf{H}}^{-1}\right]_{2j,2k-1} & \left[\tilde{\mathbf{H}}^{-1}\right]_{2j,2k} \end{pmatrix} = \mathrm{i} \begin{pmatrix} \left[\mathbf{H}_\eta^{-1}\right]_{j,k} & \left[\mathbf{H}_\eta^{-1}\right]_{j,k+N} \\ \left[\mathbf{H}_\eta^{-1}\right]_{j+N,k} & \left[\mathbf{H}_\eta^{-1}\right]_{j+N,k+N} \end{pmatrix}, \quad (3.27)$$

where $j,k = 1,\ldots,N$, and we note that we added by convention the prefactor i in the definition of G_{jk} (see Eq. (3.28)). The two-by-two matrices G_{jk} are the key objects of this section, as we will show below. From Eq. (3.10) one recognises that the diagonal blocks G_{jj}, which for simplicity we abbreviate into G_j are related to the regularisation of empirical spectral density as follows

$$\rho_{\mathbf{A}}(z,\eta) = \frac{1}{\pi N} \partial_{\bar{z}} \sum_{i=1}^{N} [\mathsf{G}_j]_{21}\,, \quad (3.28)$$

which highlights the role of the two-by-two matrices G_j for our study, and we discuss below how they can be determined. We note that by putting the prefactor i in the prefactor of Eq. (3.27), it does not appear in the formula Eq. (3.28). The Eq. (3.27) allows to evaluate systematically the inverse $\tilde{\mathbf{H}}^{-1}$ by decomposing the problem in determining the two-by-two matrices G_{jk}. As we show below, this can be achieved by relating the G_{jk} to the two-by-two matrices H_{jk} by using the Schur formula in Eq. (3.11). In order to reveal this strategy, we first rewrite the matrix $\mathrm{i}\tilde{\mathbf{H}}^{-1}$, which is of size $2N \times 2N$, in terms of the blocks H_{jk} and G_{jk}, which are matrices of sizes 2×2, as follows

$$\mathrm{i}\tilde{\mathbf{H}}^{-1} = \mathrm{i} \begin{pmatrix} \tilde{\mathsf{H}}_1 & \ldots & & \tilde{\mathsf{H}}_{1N} \\ \vdots & \ddots & & \vdots \\ & & \tilde{\mathsf{H}}_j & \\ & & & \ddots \\ \tilde{\mathsf{H}}_{N1} & \ldots & & \tilde{\mathsf{H}}_N \end{pmatrix}^{-1} = \begin{pmatrix} \mathsf{G}_1 & \ldots & & \mathsf{G}_{1N} \\ \vdots & \ddots & & \vdots \\ & & \mathsf{G}_j & \\ & & & \ddots \\ \mathsf{G}_{N1} & \ldots & & \mathsf{G}_N \end{pmatrix}, \quad (3.29)$$

where we remind that we chose for simplicity the notation $\tilde{\mathsf{H}}_j, \mathsf{G}_j$ for the diagonal blocks $\tilde{\mathsf{H}}_{jj}, \mathsf{G}_{jj}$, respectively. Now, by using again the fact that an operation of permutation of rows and columns commutes with the inverse operator, similarly to Eq. (3.26), we can move to the top left, i.e., at the first row and column, the blocks referring to the node j

in Eq. (3.29) as follows

$$
\begin{pmatrix}
\tilde{\mathsf{H}}_j & \tilde{\mathsf{H}}_{j1} & \dots & \tilde{\mathsf{H}}_{j(j-1)} & \tilde{\mathsf{H}}_{j(j+1)} & \dots & \tilde{\mathsf{H}}_{jN} \\
\tilde{\mathsf{H}}_{1j} & & & & & & \\
\vdots & & & & & & \\
\tilde{\mathsf{H}}_{(j-1)j} & & & \tilde{\mathbf{H}}^{(j)} & & & \\
\tilde{\mathsf{H}}_{(j+1)j} & & & & & & \\
\vdots & & & & & & \\
\tilde{\mathsf{H}}_{Nj} & & & & & &
\end{pmatrix}^{-1} =
$$

$$
-\mathrm{i}
\begin{pmatrix}
\mathsf{G}_j & \mathsf{G}_{j1} & \dots & \mathsf{G}_{j(j-1)} & \mathsf{G}_{j(j+1)} & \dots & \mathsf{G}_{jN} \\
\mathsf{G}_{1j} & \mathsf{G}_1 & \dots & & & & \mathsf{G}_{1N} \\
\vdots & \vdots & \ddots & & & & \vdots \\
\mathsf{G}_{(j-1)j} & & & \mathsf{G}_{j-1} & & & \\
\mathsf{G}_{(j+1)j} & & & & \mathsf{G}_{j+1} & & \\
\vdots & & & & & \ddots & \\
\mathsf{G}_{Nj} & \mathsf{G}_{N1} & \dots & & & & \mathsf{G}_N
\end{pmatrix}, \tag{3.30}
$$

where $\tilde{\mathbf{H}}^{(j)}$ is a $(2(N-1)\times 2(N-1))$ submatrix[3] of $\tilde{\mathbf{H}}$ obtained by deleting from $\tilde{\mathbf{H}}$ the (two) rows and (two) columns crossing the (two-by-two) matrix $\tilde{\mathsf{H}}_j$. Accordingly, by following Eqs. (3.26)-(3.22), $\tilde{\mathbf{H}}^{(j)}$ corresponds to removing the $(2j-1)$-th and the $2j$-th rows and columns of $\tilde{\mathbf{H}}$, and equivalently the j-th and the $j+N$-th rows and columns of $\mathbf{H}$.

The key point of Eq. (3.30) is to focus on the G_j on the right hand side, and to recognise that the left hand side is the inverse of a block matrix: accordingly, we can use the Schur complements approach in Sec. A.7 and apply the formula in Eq. (3.11), through the following mapping

$$\mathbf{a} := \tilde{\mathsf{H}}_j, \tag{3.31}$$

$$\mathbf{b} := \left(\tilde{\mathsf{H}}_{j1}, \dots, \tilde{\mathsf{H}}_{j(j-1)}, \tilde{\mathsf{H}}_{j(j+1)}, \dots, \tilde{\mathsf{H}}_{jN}\right), \tag{3.32}$$

$$\mathbf{c} := \left(\tilde{\mathsf{H}}_{1j}, \dots, \tilde{\mathsf{H}}_{(j-1)j}, \tilde{\mathsf{H}}_{(j+1)j}, \dots, \tilde{\mathsf{H}}_{Nj}\right)^{\mathrm{T}}, \tag{3.33}$$

$$\mathbf{d} := \tilde{\mathbf{H}}^{(j)}, \tag{3.34}$$

$$\mathbf{s_d} = (\mathbf{a} - \mathbf{b}\mathbf{d}^{-1}\mathbf{c})^{-1} = -\mathrm{i}\mathsf{G}_j, \tag{3.35}$$

where $\mathbf{s_d}$ is the Schur complement of d. It is evident, from the evaluation of $\mathbf{s_d}$, that the inversion of $\mathbf{d}$ is the same problem that we started in Eq. (3.29), but with the removal

[3] also known as cavity matrix

of j-th rows and columns, i.e.,

$$\mathrm{i}\left(\tilde{\mathbf{H}}^{(j)}\right)^{-1} = \mathrm{i}\begin{pmatrix} \tilde{\mathsf{H}}_1 & \dots & \tilde{\mathsf{H}}_{1(j-1)} & \tilde{\mathsf{H}}_{1(j+1)} & \dots & \tilde{\mathsf{H}}_{1N} \\ \vdots & \ddots & & & \vdots & \\ \tilde{\mathsf{H}}_{(j-1)1} & & \tilde{\mathsf{H}}_{j-1} & & & \\ \tilde{\mathsf{H}}_{(j+1)1} & & & \tilde{\mathsf{H}}_{j+1} & & \\ \vdots & & & & \ddots & \\ \tilde{\mathsf{H}}_{N1} & \dots & & & & \tilde{\mathsf{H}}_N \end{pmatrix}^{-1}$$
$$=: \begin{pmatrix} \mathsf{G}_1^{(j)} & \dots & \mathsf{G}_{1(j-1)}^{(j)} & \mathsf{G}_{1(j+1)}^{(j)} & \dots & \mathsf{G}_{1N}^{(j)} \\ \vdots & \ddots & & & \vdots & \\ \mathsf{G}_{(j-1)1}^{(j)} & & \mathsf{G}_{j-1}^{(j)} & & & \\ \mathsf{G}_{(j+1)1}^{(j)} & & & \mathsf{G}_{j+1}^{(j)} & & \\ \vdots & & & & \ddots & \\ \mathsf{G}_{N1}^{(j)} & \dots & & & & \mathsf{G}_N^{(j)} \end{pmatrix} = \mathrm{i}\mathbf{d}^{-1}, \tag{3.36}$$

where the prefactor i used to define the elements $\mathsf{G}_{ii'}^{(j)}$ is put for consistency with Eq. (3.27) and Eq. (3.29), the superscript (j) in the $\mathsf{G}^{(j)}$-s distinguishes them from the elements of the right hand side of Eq. (3.30), i.e., under general assumptions $\mathsf{G}_{kl}^{(j)} \neq \mathsf{G}_{kl}$, for any $k, l \neq j$.

Now, we can write Eq. (3.35) in terms of Eqs. (A.75)-(3.34) and of Eq. (3.36), which reads

$$\mathsf{G}_j = \left(-\mathrm{i}\tilde{\mathsf{H}}_j + \sum_{k=1,(k\neq j)}^{N} \sum_{l=1,(l\neq j)}^{N} \tilde{\mathsf{H}}_{jk} \mathsf{G}_{kl}^{(j)} \tilde{\mathsf{H}}_{lj}\right)^{-1}, \tag{3.37}$$

with $j = 1, \dots, N$, where the two sums made explicit the matrix multiplications in Eq. (3.35). By using the definitions (3.23) and (3.24), the relation between the G-s and the $\mathsf{G}^{(j)}$-s is given by the following equation

$$\mathsf{G}_j = \left(\mathsf{z}_\eta - \mathsf{A}_{jj} - \sum_{k=1,(k\neq j)}^{N} \sum_{l=1,(l\neq j)}^{N} \mathsf{A}_{jk} \mathsf{G}_{kl}^{(j)} \mathsf{A}_{lj}\right)^{-1}, \tag{3.38}$$

with $j = 1, \dots, N$, where $\mathsf{z}_\eta, \mathsf{A}_{jk}$ are two-by-two matrices defined in Eq. (3.25). The set of Eqs. (3.38), for each node j, are known as cavity equations or generalised resolvent equations for non-Hermitian random matrices. The expression cavity refers to the fact that the node j (and the corresponding rows and columns) has been removed in the $\tilde{\mathbf{H}}$, leaving a cavity in the first graph, which is then also called cavity graph. The set of Eqs. (3.38) expresses the two-by-two matrix G_j as a function, among the others, of the two-by-two matrices $\mathsf{G}_{kl}^{(j)}$, which are the $(N-1)^2$ blocks elements of the inverse $\mathrm{i}\left(\tilde{\mathbf{H}}^{(j)}\right)^{-1}$, as in Eq. (3.36). Accordingly, these equations are not closed yet, since the $\mathsf{G}_{kl}^{(j)}$ have to be determined. In the next section we show some characterisations of the

matrices $\mathrm{i}\left(\tilde{\mathbf{H}}^{(j)}\right)^{-1}$ and $\mathrm{i}\left(\tilde{\mathbf{H}}\right)^{-1}$ that help in closing the equations above, when there is a network structure.

3.4 Simplifications for trees

In the previous section we focused on the diagonal blocks G_j of Eq. (3.30), since we are interested in the spectral density in Eq. (3.28). However, we observe now that the off-diagonal blocks G_{kl} and $\mathsf{G}_{kl}^{(j)}$ satisfy important properties when there is a network structure, which results in simplifying Eq. (3.37) when the graph is a tree. In particular, we show here that for a tree the number of non-zero terms in the sums in the right hand side of Eq. (3.37) is significantly reduced.

We consider now the graph structure to be encoded in an adjacency matrix $\mathbf{C}$ such that

$$A_{ij} = C_{ij} J_{ij}, \tag{3.39}$$

and we denote the associated graph by $\mathcal{G}$.

We now focus on the off-diagonal blocks G_{kl}. While the off-diagonal blocks $\tilde{\mathsf{H}}_{kl}$ in Eq. (3.22) are non-zero if and only if $C_{kl} = 1$ or $C_{lk} = 1$, the off-diagonal blocks G_{kl} of the inverse $\mathrm{i}\tilde{\mathbf{H}}^{-1}$ can be non-zero even if there is not a link between k and l. In particular, the implication: if $\mathsf{G}_{k\neq l}$ is non-zero then $C_{kl} = 1$ or $C_{lk} = 1$ is generally false. Indeed, by applying recursively the Schur formula in Eq. (3.11) for the off-diagonal blocks G_{kl}, similarly to Eq. (3.36), it is possible to show that a weaker condition relates the graph structure to the G_{kl} for $k \neq l$, i.e.,

$$\begin{aligned} \mathsf{G}_{kl} \neq 0 \implies & \text{the nodes } k \text{ and } l \text{ belong to the same connected component in the} \\ & \text{graph } \mathcal{G}. \end{aligned} \tag{3.40}$$

We observe that the condition on the right is equivalent (see Sec. 1.4.1) to the existence of a path of any length in the graph passing through the nodes k and l, which happens when $\sum_{i\geq 0}(\mathbf{C}^{i+1})_{kl} > 0$.

We consider now the off-diagonal blocks $\mathsf{G}_{kl}^{(j)}$ in Eq. (3.37). They satisfy the implication in Eq. (3.40) in the place of G_{kl}, where $\mathcal{G}$ is replaced by the cavity matrix $\mathcal{G}^{(j)}$, i.e.,

$$\begin{aligned} \mathsf{G}_{kl}^{(j)} \neq 0 \implies & \text{the nodes } k \text{ and } l \text{ belong to the same connected component in the} \\ & \text{cavity graph } \mathcal{G}^{(j)}. \end{aligned} \tag{3.41}$$

We focus now on the term in the sums of Eq. (3.37), i.e.,

$$\tilde{\mathsf{H}}_{jk} \mathsf{G}_{kl}^{(j)} \tilde{\mathsf{H}}_{lj}, \quad \text{with} \quad k, l \neq j, \tag{3.42}$$

for a fixed j, and in particular we are interested to find necessary conditions to be non-zero. First, the presence of $\tilde{\mathsf{H}}_{jk}$ and $\tilde{\mathsf{H}}_{lj}$ ensures that nodes k and l have to be among the neighbours of node j, i.e,

$$\tilde{\mathsf{H}}_{jk}, \tilde{\mathsf{H}}_{lj} \neq 0 \implies k, l \in \partial_j. \tag{3.43}$$

Moreover, if $k = l$ then the diagonal terms satisfy the following implication

$$\tilde{\mathsf{H}}_{jk} \mathsf{G}_k^{(j)} \tilde{\mathsf{H}}_{kj} \neq 0 \implies k \in \partial_j. \tag{3.44}$$

Second, we consider the off-diagonal terms in Eq. (3.42) with $k \neq l$. In this case, one can verify that the intersection of the conditions in Eqs. (3.41),(3.43) can be expressed with a condition on the cycles in the full graph $\mathcal{G}$, i.e,

$$\tilde{\mathsf{H}}_{jk} \mathsf{G}_{kl}^{(j)} \tilde{\mathsf{H}}_{lj} \neq 0 \implies \exists \text{ cycle in } \mathcal{G} \text{ of the kind } j \to k \to \{i\} \to l \to j, \tag{3.45}$$

with $k \neq l$ and $k, l \neq j$, and where here we denoted by $\{i\}$ any path of any length larger than one along distinct vertices $i \neq j, k, l$.

We show now the implication in Eq. (3.45), by considering a tree graph. Indeed, by definition of trees (see Sec. 1.4.1), the condition on the right is always false, and we show now that the only non-zero terms in Eq. (3.42) are of the kind $k = l \in \partial_j$.

Given a central node j, one can verify that $\tilde{\mathbf{H}}^{(j)}$ is a block diagonal matrix (up to a permutation), with $|\partial_j|$ blocks, each of the blocks corresponds to the connected components that become disconnected from each other after the removal of node j. Since from the Schur formula the inverse of a block diagonal matrix is block diagonal, the off-diagonal blocks of $\tilde{\mathbf{H}}^{(j)}$ lead to zero $\mathsf{G}_{kl}^{(j)}$ off-diagonal, where k and l belong to two connected components that are disconnected from each other. The size of the remaining blocks on the diagonal is equal to the size of the connected components in which they correspond to. Each of these component is a (connected) tree. Using again the Schur formula for these blocks on the diagonal of $\tilde{\mathbf{H}}^{(j)}$, one obtains that the blocks $\mathsf{G}_{pq}^{(j)}$, with $p \neq q$ in a given component, are in general non zero, but either $\tilde{\mathsf{H}}_{jp}$ or $\tilde{\mathsf{H}}_{qj}$ are zero on a tree. Indeed, $\tilde{\mathsf{H}}_{jp}$ and $\tilde{\mathsf{H}}_{qj}$ $(q \neq p)$ are both non-zero if and only if there exists one cycle of the kind: $j \to k \to \{i\} \to l \to j$, which never happens on a tree by definition. So the only non-zero terms in Eq. (3.42) are of the kind $\tilde{\mathsf{H}}_{jk} \mathsf{G}_k^{(j)} \tilde{\mathsf{H}}_{kj}$, with $k \in \partial_j$.

If j is a peripheral node, i.e., with $|\partial_j| = 1$, the matrix $\tilde{\mathbf{H}}^{(j)}$ has no block structure, but the only non-zero terms in Eq. (3.42) are of the kind $\tilde{\mathsf{H}}_{jk} \mathsf{G}_k^{(j)} \tilde{\mathsf{H}}_{kj}$, with $k \in \partial_j$, since Eq. (3.43) is possible only for $k = l$ when $|\partial_j| = 1$. □

We show in the next section how the Eqs. (3.38) can be closed when the underlying graph $\mathcal{G}$ is locally treelike, in light of the properties discussed in this section.

3.5 Spectral distribution of locally treelike matrices

Here we derive the spectral distribution for locally treelike matrices. In this work, when we say that a matrix is locally treelike, or it has a locally treelike structure, when its underlying graph has this property (see Sec. 1.4.2.2). For this class of sparse matrices the derivation of the Sec. 3.3 simplifies, since the inversion algorithm of the Hermitisation matrix provides closed recursive equation in light of Sec. 3.4, as we show below.

In the previous section, we have shown that for a tree of size N the only non-zero terms in Eq. (3.42) are given by terms of the kind

$$\tilde{\mathsf{H}}_{jk}\mathsf{G}_k^{(j)}\tilde{\mathsf{H}}_{kj}, \quad \text{with} \quad k \in \partial_j, \forall j = 1, \ldots, N. \tag{3.46}$$

Therefore, there are only $|\partial_j|$ non-zero square diagonal blocks $\mathsf{G}_k^{(j)}$, with $k \neq j$, one for each of the neighbours of j, that play a role to determine G_j in the Eq. (3.37). Accordingly, for any node j, we have that the sums in Eqs. (3.37)-(3.38) restrict to the neighbourhood of node j only, i.e., (for simplicity we apply this straightforward to Eq. (3.38))

$$\sum_{k=1,(k\neq j)}^{N} \sum_{l=1,(l\neq j)}^{N} \mathsf{A}_{jk}\mathsf{G}_{kl}^{(j)}\mathsf{A}_{lj} = \sum_{k\in\partial_j} \mathsf{J}_{jk}\mathsf{G}_k^{(j)}\mathsf{J}_{kj}, \tag{3.47}$$

where

$$\mathsf{J}_{jk} := \begin{pmatrix} 0 & J_{j,k} \\ \bar{J}_{k,j} & 0 \end{pmatrix}. \tag{3.48}$$

We note that we derived Eq. (3.47) by assuming $\mathbf{C}$ to be a tree of size N; however, we are interested in locally treelike graphs, for which the equality in Eq. (3.47) is valid in the $N \to \infty$ limit almost surely. As observed in Sec. 1.4.2.2, there exists a finite number of finite (short) cycles in the $N \to \infty$ limit, for locally treelike graphs. Hence, we can see Eq. (3.47) as a good approximation for locally treelike graphs, according to which we can say that with good approximation Eq. (3.38) for locally treelike matrices simplifies to

$$\mathsf{G}_j = \left(\mathsf{z}_\eta - \mathsf{J}_{jj} - \sum_{k\in\partial_j} \mathsf{J}_{jk}\mathsf{G}_k^{(j)}\mathsf{J}_{kj} \right)^{-1}, \tag{3.49}$$

with $j = 1, \ldots, N$, where J_{jk} is defined in Eq. (3.48) and z_η defined in Eq. (3.25). The Eqs. (3.38) are known as the first set of cavity equations or generalised resolvent equations for locally treelike non-Hermitian random matrices [Metz et al., 2010, 2019; Rogers et al., 2008; Rogers and Pérez Castillo, 2009]. They say that for every node j of a locally treelike matrix the two-by-two matrix G_j defined in Eq. (3.27) is a function, among the others, of the weights J_{jk} and of the diagonal blocks $\mathsf{G}_k^{(j)}$, defined in Eq. (3.36), only for the neighbours k belonging to the neighbourhood ∂_j of j. However, the Eqs. (3.38) are not closed yet, because the $\mathsf{G}_k^{(j)}$ have to be determined.

The strategy is to realise that the $\mathsf{G}_k^{(j)}$, being the diagonal blocks of $\mathrm{i}\left(\tilde{\mathbf{H}}^{(j)}\right)^{-1}$,

can be obtained through the same algorithm for which the G_j have been obtained from Eq. (3.30), i.e., by inverting a block matrix. In this way we are going to build a system of hierarchical recursive equations, as we show below. Since for consistency with Eq. (3.49) we want to focus again on the neighbourhood of j, we consider at first the cavity matrix $\mathrm{i}\left(\tilde{\mathbf{H}}^{(\ell)}\right)^{-1}$ where the node ℓ has been removed. Second, as in Eq. (3.30), we isolate at the top left of $\mathrm{i}\left(\tilde{\mathbf{H}}^{(\ell)}\right)^{-1}$ the block $\mathsf{G}_j^{(\ell)}$, while the remaining $(N-2)^2$ other blocks $\tilde{\mathsf{H}}_{ki}$ with $k \neq \ell, j$ and $i \neq \ell, j$ on the bottom right define the cavity matrix $\tilde{\mathbf{H}}^{(\ell,j)}$. Let us now define $\mathsf{G}_{ki}^{(\ell,j)}$ as the elements of the inverse $\mathrm{i}\left(\tilde{\mathbf{H}}^{(\ell,j)}\right)^{-1}$. As argued above, when determining $\mathsf{G}_j^{(\ell)}$ with the Schur formula, the only non-zero terms $\tilde{\mathsf{H}}_{jk}\mathsf{G}_{ki}^{(\ell,j)}\tilde{\mathsf{H}}_{ij}$ with $k \neq \ell, j$ and $i \neq \ell, j$, are of the kind $\tilde{\mathsf{H}}_{jk}\mathsf{G}_{k}^{(\ell,j)}\tilde{\mathsf{H}}_{kj}$ with $k \in \partial_j \setminus \{\ell\}$, almost surely for locally treelike graphs. Accordingly, the equation that relates the $\mathsf{G}_j^{(\ell)}$-s to the $\mathsf{G}_k^{(\ell,j)}$-s, similarly to Eq. (3.49), reads

$$\mathsf{G}_j^{(\ell)} = \left(\mathsf{z}_\eta - \mathsf{J}_{jj} - \sum_{k \in \partial_j \setminus \{\ell\}} \mathsf{J}_{jk}\mathsf{G}_k^{(\ell,j)}\mathsf{J}_{kj} \right)^{-1}, \tag{3.50}$$

with $j, \ell = 1, \ldots, N$ and $j \neq \ell$, where J_{jk} is defined in Eq. (3.48) and z_η defined in Eq. (3.25). It is evident now that Eqs. (3.49) and (3.50) lead to a system of hierarchical recursive equations where the recursiveness is given by keep removing nodes to determine cavity matrices. The advantage of locally treelikeness is to close the Eqs. (3.49) and (3.50) with the approximation [Metz et al., 2019; Rogers and Pérez Castillo, 2009]

$$\mathsf{G}_k^{(\ell,j)} = \mathsf{G}_k^{(j)}, \quad \text{with} \quad k \in \partial_j \setminus \{\ell\}, \tag{3.51}$$

$$\mathsf{G}_j^{(\ell)} = \left(\mathsf{z}_\eta - \mathsf{J}_{jj} - \sum_{k \in \partial_j \setminus \{\ell\}} \mathsf{J}_{jk}\mathsf{G}_k^{(j)}\mathsf{J}_{kj} \right)^{-1}, \tag{3.52}$$

with $j, \ell = 1, \ldots, N$ and $j \neq \ell$, where J_{jk} is defined in Eq. (3.48) and z_η is defined in Eq. (3.25), and where the $\mathsf{G}_k^{(j)}$ are evaluated on the cavity graph obtained by the removal of node j.

The idea behind Eq. (3.51) is that (see Fig. 3.1), for trees, for a fixed node j, its neighbours k-s except of ℓ become disconnected in the cavity graph obtained by removing node j; equivalently, the corresponding blocks $\mathsf{G}_k^{(j)}$ in the corresponding cavity matrix become statistically uncorrelated. Consequently, the additional removal of node ℓ does not have any effect on the neighbours k-s. The Eq. (3.51) and Eq. (3.47) are exact on trees, while for locally treelike graphs hold almost surely locally. However, in the limit $N \to \infty$, the presence of long cycles of divergent length does not break the validity of Eq. (3.51), since the correlations between two nodes in an infinite cycle vanish, and hence the variables $\mathsf{G}_k^{(j)}$ in the cavity matrix become statistically uncorrelated, similarly to what happens in finite trees as discussed above. Accordingly, excluding the effect of the presence of a finite number of short cycles — i.e., of finite length in the limit $N \to \infty$ — the approximation in Eq. (3.51), together with the equations derived so far, becomes

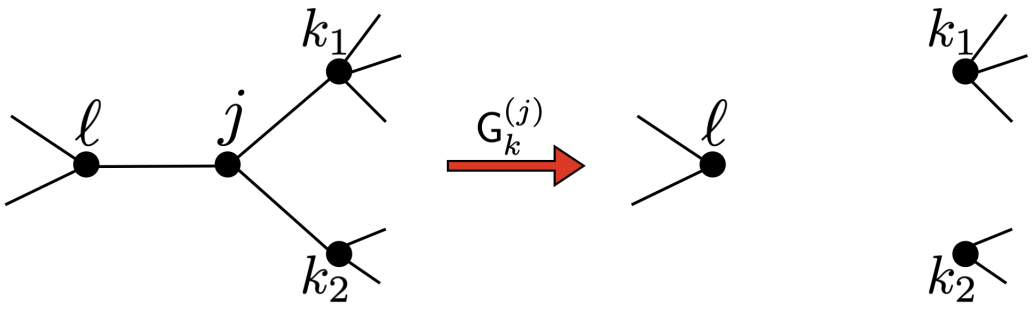

Figure 3.1: Illustration to support the reasoning behind the approximation in Eq. (3.51) for locally treelike graphs: given the tree on the left and focusing on the neighbourhood of a node j the nodes k_1, k_2, which form the neighbourhood ∂_j except of ℓ, are linked indirectly through node j only. Accordingly, when on the right we consider the cavity graph obtained by removing the node j, the three nodes k_1, k_2, ℓ belong to three different connected components that are disconnected from each other. The key point is then that the additional removal of node ℓ from the cavity graph on the right does not have any further effect on the nodes k_1, k_2.

exact in the limit $N \to \infty$.

The Eqs. (3.49) and (3.52) are known as the the cavity equations or generalised resolvent equations for non-Hermitian random matrices that are locally treelike. They need to be solved, in the limit $N \to \infty$ — for the locally treelike approximation to be valid — and for a finite, but small, η. Indeed, first one needs to determine the $\mathsf{G}_k^{(j)}$ from Eq. (3.52), and second the G_j from the Eqs. (3.49), both for a finite, but small, η. These solutions are needed then to evaluate the limiting distribution ρ, defined in Eq. (3.4), in the limits $\eta \to 0$ and $N \to \infty$ (as discussed in Sec. 3.2), of the regularisation of the empirical spectral density in Eq. (3.28), i.e.,

$$\rho(z) = \lim_{\eta \to 0} \lim_{N \to \infty} \frac{1}{\pi N} \sum_{j=1}^{N} \partial_{\bar{z}} \left[\mathsf{G}_j\right]_{21} , \tag{3.53}$$

which we refer to as the spectral distribution of the locally treelike ensemble under study.

3.6 Boundary of the support of the spectral distribution

We present in this section the method to determine the boundary of the support of the spectral distribution ρ in Eq. (3.53), by using stability properties of the solutions of the cavity equations (3.49) and (3.52). The support of ρ is defined as

$$\mathcal{S} := \overline{\{z \in \mathbb{C} : \rho(z) \neq 0\}}, \tag{3.54}$$

where $\overline{\Phi}$ denotes the closure of a set Φ.

We briefly show here that the support $\mathcal{S}$ defined in Eq. (3.54), with the spectrum $\sigma(\mathbf{A})$ for general sparse non-Hermitian random matrices, and in particular that the support coincides with the continuous part of the spectrum in the infinite size limit. In the limit $N \to \infty$ the closure of the discrete spectrum $\sigma(\mathbf{A})$ converges to

$$\lim_{N\to\infty} \overline{\sigma(\mathbf{A})} = \sigma_{\mathrm{c}} \cup \sigma_{\mathrm{p}}, \tag{3.55}$$

where σ_{c} is the continuous part of the spectrum, while σ_{p} is the point part of the spectrum [Reed et al., 1980]. The point spectrum is characterised by outliers, that can be deterministic or stochastic[a]. Typically [Neri and Metz, 2016, 2020], the point spectrum has zero Lebesgue measure, since in the limit $N \to \infty$ in Eq. (3.53) the outliers of the point spectrum give typically a sub-leading contribution to the sum, which divided by N gives a zero contribution to the spectral distribution. Accordingly, both stochastic and deterministic outliers are not seen by ρ, hence they are not included in $\mathcal{S}$. Finally, in relation with $\mathcal{S}$, one has that

$$\mathcal{S} = \sigma_{\mathrm{c}}, \tag{3.56}$$

i..e, the support set $\mathcal{S}$ coincides with the continuous part of the spectrum.

[a] the presence of a finite number of cycles of fixed length — as discussed earlier in this section, they can exist in the $N \to \infty$ limit, even for locally treelike graphs — may produce stochastic outliers [Bonneau et al., 2017; Neri and Metz, 2020]

The strategy to obtain the boundary of the support $\mathcal{S}$ is as follows: first we introduce and discuss the trivial solution that is defined outside the support in Sec. 3.6.1, second we determine the boundary with the stability analysis of the trivial solution in Sec. 3.6.2.

3.6.1 The trivial solution of the cavity equations

We consider a class of solutions of the cavity equations (3.49) and (3.52) that, as we are going to show, is valid outside the support $\mathcal{S}$. This class, which we name trivial solution [Metz et al., 2019], can be obtained by setting to zero the diagonal terms of the G_j-s and of the $\mathsf{G}_j^{(l)}$-s, i.e.,

$$\mathsf{G}_j^0 := \begin{pmatrix} 0 & -\bar{g}_j \\ -g_j & 0 \end{pmatrix}, \qquad \mathsf{G}_j^{0,(\ell)} := \begin{pmatrix} 0 & -\bar{g}_j^{(\ell)} \\ -g_j^{(\ell)} & 0 \end{pmatrix}, \tag{3.57}$$

with $j, \ell = 1, \ldots, N$ and $j \neq \ell$, and the apex ^{0} is added to refer to the trivial solution. The off-diagonal terms $-g_j, -g_j^{(\ell)}$ satisfy, respectively,

$$-g_j = \frac{1}{z - J_{jj} + \sum_{k \in \partial_j} J_{jk} g_k^{(j)} J_{kj}}, \tag{3.58}$$

$$-g_j^{(\ell)} = \frac{1}{z - J_{jj} + \sum_{k \in \partial_j \setminus \{\ell\}} J_{jk} g_k^{(j)} J_{kj}}, \tag{3.59}$$

with $j, \ell = 1, \ldots, N$ and $j \neq \ell$. It is straightforward to verify that Eqs. (3.57)-(3.59) satisfy the cavity equations (3.49) and (3.52) for $\eta = 0$. The relevance of the trivial solution in Eqs. (3.57)-(3.59) is its relation with the spectrum $\sigma(\mathbf{A})$. Indeed, it is possible to show [Metz et al., 2019], through the inversion algorithm via the Schur complements (see Sec. A.7), that the diagonal elements of the resolvent $\mathbf{G}_{\mathbf{A}^{(\ell)}}(z)$ of non-Hermitian matrices, defined in Eq. (3.1), satisfy Eqs. (3.59) in the place of $g_j^{(\ell)}$. Accordingly, $g_j^{(\ell)}$ in Eq. (3.59) can be identified with the diagonal elements of the resolvent $\mathbf{G}_{\mathbf{A}}(z)$. Since the resolvent $\mathbf{G}_{\mathbf{A}}(z)$ is well defined (analytic) for $z \notin \sigma(\mathbf{A})$, through this identifications it means that the trivial solution is well defined for $z \notin \sigma(\mathbf{A})$. In particular, in the infinite size limit the spectral distribution in Eq. (3.53) for the trivial solution G_j^0 satisfies

$$\rho(z) = -\lim_{N \to \infty} \frac{1}{\pi N} \sum_{j=1}^{N} \partial_{\bar{z}} g_j = 0 \quad \text{if } z \notin \mathcal{S}, \tag{3.60}$$

since the complex conjugate derivative of a function is zero where it is analytic (see Appendix A.6.1).

Finally, what we have shown is the fact that the Eqs. (3.57)-(3.59) provide a solution (which we name the trivial solution) of the cavity equations (3.49) and (3.52), for $\eta = 0$, in a region of the complex plane that turns out to be the complementary set of $\mathcal{S}$. This reasoning is the core of the logical method to determine the support $\mathcal{S}$ of the spectral distribution ρ, in the $\lim N \to \infty$, for non-Hermitian random matrices that are locally treelike. In the following section we discuss how the method of determining the boundary of the support $\mathcal{S}$ can build upon this reasoning.

3.6.2 Linear stability analysis of the trivial solution

We want to understand here what happens to the trivial solution when we consider a small but non-zero η. Indeed, in Eq. (3.53) the non-zero spectral distribution is obtained from the nontrivial solution of the cavity equations for finite η, in the limit $\eta \to 0$, and defined inside the support $\mathcal{S}$. We consider a diagonal perturbation of the trivial solution, which is expected, following the reasoning above, to be stable only outside the support $\mathcal{S}$. The perturbation consists in adding the following diagonal two-by-two matrix $\Delta_j^{(\ell)}$

to the trivial solution $\mathsf{G}_j^{0,(\ell)}$ in Eq. (3.57), i.e.,

$$\Delta_j^{(\ell)} := \begin{pmatrix} \epsilon_j^{(\ell)} & 0 \\ 0 & \delta_j^{(\ell)} \end{pmatrix}, \qquad \text{with} \quad |\epsilon_j^{(\ell)}|, |\delta_j^{(\ell)}| \ll 1, \tag{3.61}$$

with $j, \ell = 1, \ldots, N$ and $j \neq \ell$. The idea is now to perform a linear stability analysis of the perturbed trivial solution in Eq. (3.61), in order to determine the domain of the trivial solution. Inserting the perturbed $\mathsf{G}_j^{(\ell)}$ in Eq. (3.52) we have that

$$\begin{aligned}
\mathsf{G}_j^{0,(\ell)} + \Delta_j^{(\ell)} &= \begin{pmatrix} \epsilon_j^{(\ell)} & -\bar{g}_j^{(\ell)} \\ -g_j^{(\ell)} & \delta_j^{(\ell)} \end{pmatrix} = \\
&= \left(\begin{pmatrix} 0 & z - J_{jj} \\ \bar{z} - \bar{J}_{jj} & 0 \end{pmatrix} - \sum_{k \in \partial_j \setminus \{\ell\}} \begin{pmatrix} 0 & J_{jk} \\ \bar{J}_{kj} & 0 \end{pmatrix} \begin{pmatrix} \epsilon_k^{(j)} & -\bar{g}_k^{(j)} \\ -g_k^{(j)} & \delta_k^{(j)} \end{pmatrix} \begin{pmatrix} 0 & J_{kj} \\ \bar{J}_{jk} & 0 \end{pmatrix} \right)^{-1} \qquad (3.62) \\
&= \begin{pmatrix} -\sum_{k \in \partial_j \setminus \{\ell\}} \delta_k^{(j)} |J_{jk}|^2 & z - J_{jj} + \sum_{k \in \partial_j \setminus \{\ell\}} g_k^{(j)} J_{jk} J_{kj} \\ \bar{z} - \bar{J}_{jj} + \sum_{k \in \partial_j \setminus \{\ell\}} \bar{g}_k^{(j)} \bar{J}_{jk} \bar{J}_{kj} & -\sum_{k \in \partial_j \setminus \{\ell\}} \epsilon_k^{(j)} |J_{kj}|^2 \end{pmatrix}^{-1} \\
&= \frac{\begin{pmatrix} -\sum_{k \in \partial_j \setminus \{\ell\}} \epsilon_k^{(j)} |J_{kj}|^2 & -z + J_{jj} - \sum_{k \in \partial_j \setminus \{\ell\}} g_k^{(j)} J_{jk} J_{kj} \\ -\bar{z} + \bar{J}_{jj} - \sum_{k \in \partial_j \setminus \{\ell\}} \bar{g}_k^{(j)} \bar{J}_{jk} \bar{J}_{kj} & -\sum_{k \in \partial_j \setminus \{\ell\}} \delta_k^{(j)} |J_{jk}|^2 \end{pmatrix}}{D_1 - D_2}, \qquad (3.63)
\end{aligned}$$

where we defined

$$D_1 := \left(\sum_{k \in \partial_j \setminus \{\ell\}} \delta_k^{(j)} |J_{jk}|^2 \right) \left(\sum_{k \in \partial_j \setminus \{\ell\}} \epsilon_k^{(j)} |J_{kj}|^2 \right) = \mathcal{O}(\epsilon\delta) \tag{3.64}$$

$$D_2 := \left| z - J_{jj} + \sum_{k \in \partial_j \setminus \{\ell\}} g_k^{(j)} J_{jk} J_{kj} \right|^2 = \left| g_j^{(l)} \right|^{-2}, \tag{3.65}$$

and where we used that the $g_j^{(l)}$-s satisfy Eq. (3.59), with $j, \ell = 1, \ldots, N$ and $j \neq \ell$. We see that the denominator in Eq. (3.63) can be expanded to the leading order in $\epsilon\delta$ as follows

$$\frac{1}{D_1 - D_2} = -\left| g_j^{(l)} \right|^2 + \mathcal{O}(\epsilon\delta), \tag{3.66}$$

so by setting the diagonal elements of both sides of Eq. (3.63) to be equal we get

$$\epsilon_j^{(\ell)} = \left|g_j^{(l)}\right|^2 \sum_{k\in\partial_j\setminus\{\ell\}} \epsilon_k^{(j)}|J_{kj}|^2 + \mathcal{O}(\epsilon^2\delta), \tag{3.67}$$

$$\delta_j^{(\ell)} = \left|g_j^{(l)}\right|^2 \sum_{k\in\partial_j\setminus\{\ell\}} \delta_k^{(j)}|J_{jk}|^2 + \mathcal{O}(\epsilon\delta^2), \tag{3.68}$$

which decouple at the leading orders in ϵ, δ. Finally, the linear stability analysis of the perturbed trivial solutions leads to the two following decoupled systems of self-consistent equations for the sets of variables $\{\epsilon_j^{(\ell)}\}, \{\delta_j^{(\ell)}\}$

$$\epsilon_j^{(\ell)} = \left|g_j^{(l)}\right|^2 \sum_{k\in\partial_j\setminus\{\ell\}} \epsilon_k^{(j)}|J_{kj}|^2, \tag{3.69}$$

$$\delta_j^{(\ell)} = \left|g_j^{(l)}\right|^2 \sum_{k\in\partial_j\setminus\{\ell\}} \delta_k^{(j)}|J_{jk}|^2, \tag{3.70}$$

with $j, \ell = 1, \ldots, N$ and $j \neq \ell$, where the $g_j^{(\ell)}$-s satisfy the self-consistent equations

$$-g_j^{(\ell)} = \frac{1}{z - J_{jj} + \sum_{k\in\partial_j\setminus\{\ell\}} J_{jk} g_k^{(j)} J_{kj}}, \tag{3.71}$$

with $j, \ell = 1, \ldots, N$ and $j \neq \ell$.

The region of the complex plane where the solutions of Eqs. (3.69)-(3.70) remain small and the perturbation is reabsorbed to zero defines the complementary set of the support $\mathcal{S}$ of the spectral distribution ρ. We observe that, although the Eqs. (3.69)-(3.70) are decoupled in the two sets of variables the sets of variables $\{\epsilon_j^{(\ell)}\}$ and $\{\delta_j^{(\ell)}\}$, these last two sets of variables are not generally statistically independent, through the $g_j^{(\ell)}$-s, and when the weights J_{jk}, J_{kj} are dependent random variables and drawn from a joint $p(J_{jk}, J_{kj})$, as it considered in this thesis.

In Ch. 4 we implement this theory to determine the boundary of the ensembles studied in this thesis, i.e., the Model A and Model B defined in Ch. 2.

3.7 Summary of this chapter

We determined the spectral distribution in Eq. (3.53) for sparse and non-Hermitian random matrices on locally treelike graphs. The method we used is based on the regularisation for the empirical spectral density given by Eq. (3.10), which requires to invert the Hermitisation block matrix $\mathbf{H}_\eta^{-1}$ defined in Eq. (3.8). For general matrices, the inversion algorithm consists in applying recursively the Schur formula in Eq. (3.11). For locally treelike graphs, the inversion algorithm can be closed and it leads to a set of closed equations, i.e., the cavity equations in the Eqs. (3.49) and (3.52). In order to close the recursive the equations, we used the Eqs. (3.47) and Eq. (3.51), which are exact on finite trees. On locally treelike graphs, these assumptions are approximations that become exact in the limit $N \to \infty$ to determine ultimately self-averaging quantities, such as the spectral distribution and its support $\mathcal{S}$.

Finally, we presented how the boundary of the support $\mathcal{S}$ for locally tree like matrices can be determined from the cavity equations Eqs. (3.49) and (3.52). This method is based on a linear stability analysis of the trivial solution, which is a class of solution, defined in Eqs. (3.57)-(3.59) of the cavity equations. The properties of the trivial solution is that it is defined outside $\mathcal{S}$ and that it is stable from a diagonal perturbation only outside $\mathcal{S}$. The linear stability analysis of the trivial solution leads to a set of linear self-consistent equations for the perturbation parameters: the region of the complex plane where such a perturbation converges to zero defines the complementary set of the support of the spectral distribution.

Chapter 4

Theory for the spectra of sparse random matrices with pairwise correlated interactions

In this chapter we apply the theoretical framework developed in Ch. 3, based on the cavity method for locally treelike and non-Hermitian random matrices, to the general model defined in Ch. 2, i.e., sparse random matrices with pairwise correlated interactions. We remind that since the general model is defined on random graphs with a prescribed degree distributions (see Sec. 1.4), it is a locally treelike ensemble. We assume from this chapter on that the weights J_{ij} to be real, and the diagonal terms to be zero, i.e., $J_{jj} = 0$. We observe that we considered interactions to be balanced on average — see Eqs. (2.9) and (2.21) — hence the associated spectra do not contain (deterministic) outliers [Neri and Metz, 2016].

In Secs. 4.1-4.3 we apply the equations for the spectral distribution and the boundary of its support to the general, which leads to distributional recursive equations. In order to check the validity of the equations that we derived, in Sec. 4.4 we apply them to limiting cases already known in literature, i.e., the oriented and dense ensembles. Sections 4.5-4.6 present the numerical algorithms that we use to solve the equations of the theory in Secs. 4.1-4.3 for the spectral distribution and for its support, respectively. Finally, in Sec. 4.7, we derive an adaption of the elliptic law for sparse systems, which we use as comparison when presenting the numerical results of the spectra in Ch. 5.

4.1 Spectral distribution

Here we use the cavity method for locally treelike and non-Hermitian random matrices, to derive a set of equations for the spectral distribution of the general model. We start by considering the cavity Eqs. (3.49) and (3.52).

Since we are interested in exploring the properties of the spectra of sparse matrices in the limit $N \to \infty$, we map here the cavity equations (3.49) and (3.52) into recursive distributional cavity equations [Kabashima et al., 2010; Metz et al., 2019]. The advantage of this approach is that it allows to sample directly the $N \to \infty$ limit of the sparse non-

Hermitian ensemble under study, as we explain now. The strategy is to map of the cavity equations (3.49) and (3.52) into distributional equations in terms of distributions of the random variables G_j and $\mathsf{G}_j^{(\ell)}$ in the infinite size limit. The idea behind this mapping is that the neighbourhoods of any couple of distinct nodes in the infinite graph are statistically equivalent, which is the case for random graphs with prescribed degree distributions. Accordingly, the concepts of nodes j, l and of their neighbourhoods are lost, together with the concept of cavity graph. Since the random variables in the right hand side of (3.49) are independent, as well as the random variables in the right hand side of (3.52), one has that the G_j and $\mathsf{G}_j^{(\ell)}$ are generally described by different distributions. Accordingly, we can define the following two distributions

$$\tilde{q}(\mathsf{g}) := \lim_{N\to\infty} \frac{1}{N} \sum_{j=1}^{N} \delta(\mathsf{g} - \mathsf{G}_j), \tag{4.1}$$

and

$$q(\mathsf{g}) := \lim_{N\to\infty} \frac{1}{cN} \sum_{j=1}^{N} \sum_{\ell\in\partial_j} \delta(\mathsf{g} - \mathsf{G}_j^{(\ell)}). \tag{4.2}$$

In terms of these two distributions the cavity equations (3.49) and (3.52) can be written as the following implicit distributional equations[1][2]

$$\tilde{\mathsf{g}} \overset{\mathrm{d}}{=} \left(\mathsf{z}_\eta - \sum_{\ell=1}^{K} \mathsf{J}_\ell \mathsf{g}_\ell \mathsf{J}_\ell^{\mathrm{T}} \right)^{-1}, \tag{4.3}$$

$$\mathsf{g} \overset{\mathrm{d}}{=} \left(\mathsf{z}_\eta - \sum_{\ell=1}^{K'-1} \mathsf{J}_\ell \mathsf{g}_\ell \mathsf{J}_\ell^{\mathrm{T}} \right)^{-1}, \tag{4.4}$$

where $\overset{\mathrm{d}}{=}$ denotes equality in the distributions, i.e. they represent self-consistent equations for the distributions $\tilde{q}$ and q of the random variables $\tilde{\mathsf{g}}$ and g in Eq. (4.1)-(4.2), respectively, and where the J-s are defined as follows

$$\forall j,k = 1,\dots,N \text{ with } j \neq k: \quad \mathsf{J}_{jk} \to \mathsf{J}_\ell := \begin{pmatrix} 0 & u_\ell \\ l_\ell & 0 \end{pmatrix}, \quad \text{with} \quad (u_\ell, l_\ell) \sim p(u_\ell, l_\ell), \tag{4.5}$$

where p is a joint distribution for the i.i.d. pairs of weights, such as the ones introduced in Ch. 2. Within this distributional approach, the integer numbers K, K' are drawn from two different, but related degree distributions, as we explain now. Indeed, while K is drawn from the degree distribution obtained by randomly picking up a vertex in the graph, which is the prescribed degree distribution p_{deg}, K' is drawn from the branching degree distribution q_{deg}, i.e. the degree distribution obtained by randomly picking up an

[1] we used here a short notation for $\tilde{\mathsf{g}}$ to remind that $\tilde{\mathsf{g}} \sim \tilde{q}(\mathsf{g})$ while $\mathsf{g} \sim q(\mathsf{g})$. However, when the distribution $\tilde{q}$ is specified, as in the rest of the chapter, the tilde on $\tilde{\mathsf{g}}$ is not necessary

[2] we use the transpose symbol $\mathsf{J}_\ell^{\mathrm{T}}$ since we consider only real values to model interactions. In the general theory for non-Hermitian matrices one would have $\mathsf{J}_\ell^\dagger$ instead

edge in the graph, and then asking what is the degree of one of its end vertices. As it is shown below q_{deg} and p_{deg} are related trough the simple equation

$$\forall k \in \mathbb{N}: \quad q_{\mathrm{deg}}(k) = \frac{k p_{\mathrm{deg}}(k)}{\langle k \rangle_{p_{\mathrm{deg}}}}. \tag{4.6}$$

The Eqs. (4.3) and (4.4) are implicit distributional equations, where the probability distributions from which the random variables are drawn do not appear yet. With the considerations made above, the distributional cavity equations Eqs. (4.3) and (4.4), in terms of the distributions $\tilde{q}$ and q in Eqs. (4.1) and (4.2), become explicit into

$$\tilde{q}(\mathsf{g}) = \sum_{k=0}^{\infty} p_{\mathrm{deg}}(k) \int \prod_{\ell=1}^{k} \mathrm{d}\mathsf{g}_\ell q(\mathsf{g}_\ell) \int \prod_{\ell=1}^{k} p(u_\ell, l_\ell) \mathrm{d}u_\ell \mathrm{d}l_\ell \; \delta\left(\mathsf{g} - \left(\mathsf{z}_\eta - \sum_{\ell=1}^{k} \mathsf{J}_\ell \mathsf{g}_\ell \mathsf{J}_\ell^{\mathrm{T}}\right)^{-1}\right), \tag{4.7}$$

and

$$q(\mathsf{g}) = \sum_{k=1}^{\infty} \frac{k p_{\mathrm{deg}}(k)}{c} \int \prod_{\ell=1}^{k-1} \mathrm{d}\mathsf{g}_\ell q(\mathsf{g}_\ell) \int \prod_{\ell=1}^{k-1} p(u_\ell, l_\ell) \mathrm{d}u_\ell \mathrm{d}l_\ell \; \delta\left(\mathsf{g} - \left(\mathsf{z}_\eta - \sum_{\ell=1}^{k-1} \mathsf{J}_\ell \mathsf{g}_\ell \mathsf{J}_\ell^{\mathrm{T}}\right)^{-1}\right), \tag{4.8}$$

where $\langle k \rangle_{p_{\mathrm{deg}}} = c$ is the mean degree, z_η is defined in Eq. (3.25), and J_ℓ is defined in Eq. (4.5). In Eq. (4.8) and Eq. (4.8), and in the rest of the chapter, we use the simple notation $\mathrm{d}\mathsf{g}_\ell$ for the Lebesgue measure in the space $\mathbb{C}^{2\times 2}$ of two-by-two complex matrices. The distributional cavity equations Eqs. (4.7) and (4.8) are recursive distributional equations that can be solved numerically via the population dynamics algorithm, as discussed in Sec. 4.5. The solutions then can be used to evaluate the spectral distribution in Eq. (3.53), which reads

$$\rho(z) = \lim_{\eta \to 0} \frac{1}{\pi} \partial_{\bar{z}} \int \mathrm{d}\mathsf{g} \; \tilde{q}(\mathsf{g}) \, [\mathsf{g}]_{21}. \tag{4.9}$$

The branching degree distribution

In this paragraph we derive Eq. (4.6).
We consider an undirected simple graph $\mathcal{G}$ of size N, described by the adjacency matrix $\mathbf{C}$ with prescribed degree distribution $p_{\text{deg}}(k|N)$. We define the joint distribution of degrees of connected node pairs in $\mathcal{G}$ as

$$\forall k, k' \in \mathbb{N}: \quad W(k, k'|N) = \frac{\sum_{i=1}^{N} \sum_{j=1,(j\neq i)}^{N} \delta_{k,k_i(\mathbf{C})} \delta_{k',k_j(\mathbf{C})} C_{ij}}{\sum_{i=1}^{N} \sum_{j=1,(j\neq i)}^{N} C_{ij}}. \tag{4.10}$$

The joint distribution in Eq. (4.10) represents the fraction of links in $\mathcal{G}$ that connect a node of degree k to another distinct node of degree k'. Accordingly, its marginal with respect to k' gives the fraction of links between two nodes where one of the two nodes has degree k, which coincides with the definition of q_{deg} in the main text. In other words, q_{deg} can be obtained as

$$\begin{aligned} q_{\text{deg}}(k|N) &= \sum_{k'=0}^{\infty} W(k, k'|N) \\ &= \sum_{k'=0}^{\infty} \frac{\sum_{i=1}^{N} \sum_{j=1,(j\neq i)}^{N} \delta_{k,k_i} \delta_{k',k_j} C_{ij}}{\sum_{i=1}^{N} \sum_{j=1,(j\neq i)}^{N} C_{ij}} \\ &= \frac{\sum_{i=1}^{N} \delta_{k,k_i} k_i}{N \langle k \rangle_{p_{\text{deg}}}} \\ &= \frac{k \sum_{i=1}^{N} \delta_{k,k_i}}{N \langle k \rangle_{p_{\text{deg}}}} \\ &= \frac{k p_{\text{deg}}(k|N)}{\langle k \rangle_{p_{\text{deg}}}}, \end{aligned} \tag{4.11}$$

which leads to Eq. (4.6) in the limit $N \to \infty$.

4.2 Alternative formula for the spectral distribution

Here we derive an alternative theoretical formula for the spectral distribution ρ, which turns out to be more applicable, at the numerical implementation level, than Eq. (4.9). Indeed, in principle ρ can be determined from Eq. (4.9) by taking the numerical derivative $\partial_{\bar{z}}$. However, it is possible to circumvent this step by considering a joint distribution for G and its derivative $\partial_{\bar{z}}\mathsf{G}$ of the cavity equations (3.49) and (3.52) [Metz et al., 2019; Rogers and Pérez Castillo, 2009]. We apply now this approach to find an alternative expression for the spectral distribution in Eq. (4.9), and then, in Sec. 5.1.2 and Sec. 5.2.2, we present numerical results for the spectral distribution of sparse random matrices with pairwise correlated interactions. We want to calculate the derivative $\partial_{\bar{z}}$ of the cavity equations

(3.49) and (3.52); the right hand sides of these two equations are inverse of matrices, which, due to commutation rules, reads

$$\partial_{\bar{z}}(\mathbf{K}^{-1}) = -\mathbf{K}^{-1}(\partial_{\bar{z}}\mathbf{K})\mathbf{K}^{-1}, \tag{4.12}$$

By using it, we can now compute the derivative $\partial_{\bar{z}}$ of the cavity equations (3.49) and (3.52), which read

$$\partial_{\bar{z}}\mathsf{G}_j = -\mathsf{G}_j \left[\sigma_- - \sum_{k\in\partial_j} \mathsf{J}_{jk}\left(\partial_{\bar{z}}\mathsf{G}_k^{(j)}\right)\mathsf{J}_{kj}\right]\mathsf{G}_j, \tag{4.13}$$

and

$$\partial_{\bar{z}}\mathsf{G}_j^{(\ell)} = -\mathsf{G}_j^{(\ell)} \left[\sigma_- - \sum_{k\in\partial_j\setminus\{l\}} \mathsf{J}_{jk}\left(\partial_{\bar{z}}\mathsf{G}_k^{(j)}\right)\mathsf{J}_{kj}\right]\mathsf{G}_j^{(\ell)}, \tag{4.14}$$

where

$$\sigma_- = \partial_{\bar{z}}\mathsf{z}_\eta = \begin{pmatrix} 0 & 0 \\ 1 & 0 \end{pmatrix}. \tag{4.15}$$

By following the same approach that we used in Sec. 4.1 to derive the distributional version of the cavity equations (3.49) and (3.52), we can write now the distributional equations for the following distributions

$$\tilde{q}(\mathsf{g},\mathsf{g}') := \lim_{N\to\infty}\frac{1}{N}\sum_{j=1}^{N}\delta(\mathsf{g}-\mathsf{G}_j)\delta(\mathsf{g}'-\partial_{\bar{z}}\mathsf{G}_j), \tag{4.16}$$

and

$$q(\mathsf{g},\mathsf{g}') := \lim_{N\to\infty}\frac{1}{cN}\sum_{j=1}^{N}\sum_{\ell\in\partial_j}\delta(\mathsf{g}-\mathsf{G}_j^{(\ell)})\delta(\mathsf{g}'-\partial_{\bar{z}}\mathsf{G}_j^{(\ell)}), \tag{4.17}$$

which read

$$\begin{aligned}\tilde{q}(\mathsf{g},\mathsf{g}') = \sum_{k=0}^{\infty} p_{\deg}(k)\int\prod_{\ell=1}^{k}\mathrm{d}\mathsf{g}_\ell\mathrm{d}\mathsf{g}'_\ell q(\mathsf{g}_\ell,\mathsf{g}'_\ell)\int\prod_{\ell=1}^{k}\mathrm{d}u_\ell\mathrm{d}l_\ell\, p(u_\ell,l_\ell)\\ \times\delta\left[\mathsf{g}-\left(\mathsf{z}_\eta-\sum_{\ell=1}^{k}\mathsf{J}_\ell\mathsf{g}_\ell\mathsf{J}_\ell^{\mathrm{T}}\right)^{-1}\right]\delta\left[\mathsf{g}'+\mathsf{g}\left(\sigma_- - \sum_{\ell=1}^{k}\mathsf{J}_\ell\mathsf{g}'_\ell\mathsf{J}_\ell^{\mathrm{T}}\right)\mathsf{g}\right],\end{aligned} \tag{4.18}$$

and

$$\begin{aligned}q(\mathsf{g},\mathsf{g}') = \sum_{k=1}^{\infty}\frac{kp_{\deg}(k)}{c}\int\prod_{\ell=1}^{k-1}\mathrm{d}\mathsf{g}_\ell\mathrm{d}\mathsf{g}'_\ell\, q(\mathsf{g}_\ell,\mathsf{g}'_\ell)\int\prod_{\ell=1}^{k-1}\mathrm{d}u_\ell\mathrm{d}l_\ell\, p(u_\ell,l_\ell)\\ \times\delta\left[\mathsf{g}-\left(\mathsf{z}_\eta-\sum_{\ell=1}^{k-1}\mathsf{J}_\ell\mathsf{g}_\ell\mathsf{J}_\ell^{\mathrm{T}}\right)^{-1}\right]\delta\left[\mathsf{g}'+\mathsf{g}\left(\sigma_- - \sum_{\ell=1}^{k-1}\mathsf{J}_\ell\mathsf{g}'_\ell\mathsf{J}_\ell^{\mathrm{T}}\right)\mathsf{g}\right].\end{aligned} \tag{4.19}$$

We refer to the Eqs. (4.18) and (4.19) as the "distributional cavity equations that include the derivatives". By using the Eqs. (4.18) and (4.19) the spectral density can be evaluated as follows

$$\rho(z) = \lim_{\eta\to 0} \frac{1}{\pi} \int \mathrm{d}\mathbf{g}\mathrm{d}\mathbf{g}'\, \tilde{q}(\mathbf{g},\mathbf{g}')[\mathbf{g}']_{21}, \tag{4.20}$$

where, differently from Eq. (4.9), the derivative is includes implicitly in $\mathbf{g}'$. Finally, by inserting Eq. (4.18) into Eq. (4.20) the spectral distribution can be expressed in terms of the distribution q as follows

$$\begin{aligned}
\rho(z) &= \lim_{\eta\to 0^+} \frac{1}{\pi} \int \mathrm{d}\mathbf{g}\mathrm{d}\mathbf{g}'\, \tilde{q}(\mathbf{g},\mathbf{g}')[\mathbf{g}']_{21} \\
&= \lim_{\eta\to 0^+} \frac{1}{\pi} \sum_{k=0}^{\infty} \int p_{\mathrm{deg}}(k) \prod_{\ell=1}^{k} \mathrm{d}\mathbf{g}_\ell \mathrm{d}\mathbf{g}'_\ell\, q(\mathbf{g}_\ell,\mathbf{g}'_\ell) \int \prod_{l=1}^{k} \mathrm{d}u_\ell \mathrm{d}l_\ell p(u_\ell,l_\ell) \\
&\times \int \mathrm{d}\mathbf{g}\mathrm{d}\mathbf{g}' \delta\left[\mathbf{g} - \left(\mathbf{z}_\eta - \sum_{\ell=1}^{k} \mathsf{J}_\ell \mathbf{g}_\ell \mathsf{J}_\ell^{\mathrm{T}}\right)^{-1}\right] \delta\left[\mathbf{g}' + \mathbf{g}\left(\sigma_- - \sum_{\ell=1}^{k} \mathsf{J}_\ell \mathbf{g}'_\ell \mathsf{J}_\ell^{\mathrm{T}}\right)\mathbf{g}\right] [\mathbf{g}']_{21} \\
&= \lim_{\eta\to 0^+} \frac{1}{\pi} \sum_{k=0}^{\infty} \int p_{\mathrm{deg}}(k) \prod_{\ell=1}^{k} \mathrm{d}\mathbf{g}_\ell \mathrm{d}\mathbf{g}'_\ell\, q(\mathbf{g}_\ell,\mathbf{g}'_\ell) \int \prod_{l=1}^{k} \mathrm{d}u_\ell \mathrm{d}l_\ell p(u_\ell,l_\ell) \\
&\times \left[-\left(\mathbf{z}_\eta - \sum_{\ell=1}^{k} \mathsf{J}_\ell \mathbf{g}_\ell \mathsf{J}_\ell^{\mathrm{T}}\right)^{-1} \left(\sigma_- - \sum_{\ell=1}^{k} \mathsf{J}_\ell \mathbf{g}'_\ell \mathsf{J}_\ell^{\mathrm{T}}\right) \left(\mathbf{z}_\eta - \sum_{\ell=1}^{k} \mathsf{J}_\ell \mathbf{g}_\ell \mathsf{J}_\ell^{\mathrm{T}}\right)^{-1} \right]_{21},
\end{aligned} \tag{4.21}$$

where we integrated over the variables $\mathbf{g}, \mathbf{g}'$. The spectral distribution ρ can be evaluated via a Monte-Carlo numerical integration procedure, once the distribution q has reached a stable solution via the population dynamics algorithm (see Sec. 4.5). The Eq. (4.21) is a key result of this thesis, which provides the spectral distribution of sparse random matrices with pairwise correlated interactions and on locally treelike graphs, and which is not available in this form in the existing literature.

4.3 Boundary of the support of the spectral distribution

In Sec. 3.6 we showed how to evaluate the boundary of the support, in the complex plane, of the spectral distribution of locally treelike and non-Hermitian random matrices. The key equations that we derived for this purpose are Eqs. (3.69),(3.70) and Eq. (3.71). Here we apply them to the general model and we derive their distributional counterpart, similarly to Sec. 4.1.

In light of the linear stability analysis performed in Sec. 3.6, and similarly to Sec. 4.1, we introduce the following distribution

$$Q(g,h,h') := \lim_{N\to\infty} \frac{1}{cN} \sum_{j=1}^{N} \sum_{\ell\in\partial_j} \delta(g - g_j^{(\ell)}) \delta(h - \epsilon_j^{(\ell)}) \delta(h' - \delta_j^{(\ell)}), \tag{4.22}$$

in terms of which the Eqs. (3.69),(3.70) and Eq. (3.71) can be mapped to the following distributional self-consistent equation, to the leading order in the perturbation, i.e.,

$$Q(g,h,h') = \sum_{k=1}^{\infty} \frac{k\, p_{\deg}(k)}{c} \int \prod_{\ell=1}^{k-1} \mathrm{d}g_\ell \mathrm{d}h_\ell \mathrm{d}h'_\ell \, Q(g_\ell, h_\ell, h'_\ell) \int \prod_{\ell=1}^{k-1} \mathrm{d}u_\ell \mathrm{d}l_\ell \, p(u_\ell, l_\ell)$$
$$\times \delta\left(g + \left(z + \sum_{\ell=1}^{k-1} u_\ell g_\ell l_\ell\right)^{-1}\right) \delta\left(h - |g|^2 \sum_{\ell=1}^{k-1} h_\ell u_\ell^2\right) \delta\left(h' - |g|^2 \sum_{\ell=1}^{k-1} h'_\ell l_\ell^2\right), \quad (4.23)$$

where we used the compact notation $\mathrm{d}g$, and equivalently $\mathrm{d}h\mathrm{d}h'$ to denote the (bi-dimensional) Lebesgue measure in $\mathbb{C}$. We observe that in Eq. (4.23), the recursions for h and h' are decoupled. Hence, since $p(u_\ell, l_\ell) = p(l_\ell, u_\ell)$ is assumed to be symmetric, we can marginalise Q with respect to anyone of h or h', so that the information on the stability is preserved but with one variable less[3]. Accordingly, we have that the marginal self-consistent distributional equation reads

$$\begin{aligned} Q(g,h) &= \int \mathrm{d}h' \, Q(g,h,h') \\ &= \sum_{k=1}^{\infty} \frac{k p_{\deg}(k)}{c} \int \prod_{\ell=1}^{k-1} \mathrm{d}g_\ell \mathrm{d}h_\ell Q(g_\ell, h_\ell) \int \prod_{\ell=1}^{k-1} p(u_\ell, l_\ell) \mathrm{d}u_\ell \mathrm{d}l_\ell \\ &\times \delta\left(h - |g|^2 \sum_{\ell=1}^{k-1} h_\ell l_\ell^2\right) \delta\left(g + \left(z + \sum_{\ell=1}^{k-1} u_\ell g_\ell l_\ell\right)^{-1}\right). \end{aligned} \quad (4.24)$$

The self-consistent equation (4.24) for the distribution $Q(g,h)$ is the key equation that governs the boundary of the support $\mathcal{S}$ of the spectral distribution. Together with the Eq. (4.21), Eq. (4.24) is a key result of this thesis, which provides the boundary of the support the spectral distribution of sparse random matrices with pairwise correlated interactions and on locally treelike graphs, and which is not available in this form in the existing literature. Indeed, as discussed in Sec. 3.6, the property that a perturbation of the trivial solution is stable only outside $\mathcal{S}$, is mapped into the criterion that for $z \notin \mathcal{S}$ the solution of Eq. (4.24) converges to a stable solution that is the trivial solution in the distributional approach, which factorises as follows

$$Q(g,h) = q^{(0)}(g)\delta(h), \quad (4.25)$$

$$\begin{aligned} q^{(0)}(g) &= \sum_{k=1}^{\infty} \frac{k p_{\deg}(k)}{c} \int \prod_{\ell=1}^{k-1} \mathrm{d}g_\ell q^{(0)}(g_\ell) \int \prod_{\ell=1}^{k-1} p(u_\ell, l_\ell) \mathrm{d}u_\ell \mathrm{d}l_\ell \\ &\times \delta\left(g + \left(z + \sum_{\ell=1}^{k-1} u_\ell g_\ell l_\ell\right)^{-1}\right), \end{aligned} \quad (4.26)$$

[3]Otherwise, if p were not symmetric, one should marginalise with respect to each of the variables h, h', which would give rise to two independent distributional equations that need to be studied separately

while the solution Eqs. (4.25),(4.26) is unstable for $z \in \mathcal{S}$. The distributional trivial solution $q^{(0)}$ corresponds to the trivial solution that we introduced in Sec. 3.6.1, and for which the spectral distribution is zero outside the support. Accordingly, the edge of stability of the perturbation in Eq. (4.24) at the trivial solution in Eq. (4.25) defines the boundary of $\mathcal{S}$. We note that the same equation Eq. (4.24) with the criterion Eqs. (4.25),(4.26) can be obtained [Mambuca et al., 2020] equivalently by a linear stability analysis applied directly to the distributional equation of the trivial solution of the cavity equations. In Sec. 4.4, we apply Eq. (4.24) to obtain the boundary in limiting cases which have been already studied in literature, i.e., oriented matrices and dense matrices. In both cases the theory above has successfully provided the analytical equations for the boundary of these benchmark ensembles.

4.4 Limiting cases

In the previous section we derived an exact formula for the boundary of the support $\mathcal{S}$ of the spectral distribution ρ of random matrices in the general model. In particular, we have shown that the boundary of $\mathcal{S}$ is given by the edge of stability of Eq. (4.24) at the distributional trivial solution given by Eq. (4.25). Here we show that the boundary of $\mathcal{S}$ obtained from the stability analysis of Eq. (4.24) corresponds with results obtained previously in the literature for the limiting cases of oriented sparse random matrices (see Ref. [Neri and Metz, 2020] and Ch. 2), for which $J_{ij}J_{ji} = 0$, and of dense matrices (see Refs. [Götze et al., 2015; Sommers et al., 1988] and Ch. 1), for which $c \to \infty$.

4.4.1 Oriented ensemble

In the oriented ensemble, $p(u, d)$ is of the form given by Eq. (2.5), such that, $J_{ij}J_{ji} = 0$ for each pair of indices i and j. We show in this section that for oriented matrices the boundary of the continuous part of the spectrum is given by values of $z \in \mathbb{C}$ for which

$$|z|^2 = \frac{\langle k(k-1) \rangle_{p_{\text{deg}}}}{2c} \left\langle l^2 \right\rangle_{\tilde{p}}, \tag{4.27}$$

where $\tilde{p}$ is the distribution that appears on the right-hand side of Eq. (2.5). First, we show that Eq. (4.27) determines the edge of stability of Eqs. (4.24) at the solution (4.25), and second we show the correspondence with the results for the boundary of $\mathcal{S}$ in Ref. [Neri and Metz, 2020].

4.4.1.1 Derivation of the boundary of the support from the distributional approach

In the oriented ensemble, the denominators in the delta distributions of Eq. (4.24) simplify since $u_\ell l_\ell = 0$. As a consequence, Eq. (4.24) reads

$$Q(g,h) = \delta\left(g + \frac{1}{z}\right) R(h), \tag{4.28}$$

where R solves

$$R(h) = \sum_{k=1}^{\infty} \frac{k p_{\deg}(k)}{c} \int \prod_{\ell=1}^{k-1} \mathrm{d}h_\ell R(h_\ell) \int \prod_{\ell=1}^{k-1} \mathrm{d}u_\ell \mathrm{d}l_\ell \, p^{\mathrm{O}}(u_\ell, l_\ell) \, \delta\left(h - \frac{\sum_{\ell=1}^{k-1} h_\ell l_\ell^2}{|z|^2}\right), \tag{4.29}$$

where p^{O} is the distribution defined in Eq. (2.5). Eq. (4.28) implies that for oriented matrices the variables g and h decouple. Hence, it suffices to study the stability of Eq. (4.29) at the trivial solution $R_0(h) = \delta(h)$.

Evaluating the average value of h, we readily obtain

$$\begin{aligned} \langle h \rangle_Q &= \int \mathrm{d}g\mathrm{d}h \; h \, Q(g,h) = \int \mathrm{d}g\mathrm{d}h \; h \, \delta\left(g + \frac{1}{z}\right) R(h) \\ &= \int \mathrm{d}h R(h) h = \langle h \rangle_R = \frac{\langle k(k-1) \rangle_{p_{\deg}}}{2c} \left\langle l^2 \right\rangle_{\tilde{p}} \frac{\langle h \rangle_R}{|z|^2}, \end{aligned} \tag{4.30}$$

where $\tilde{p}$ is the distribution appearing on the right-hand-side of Eq. (2.5). Hence, the edge of stability is given by the values of z for which Eq. (4.27) holds, which is what we were meant to show.

4.4.1.2 Derivation of the boundary of the support from the theory in Ref. [Neri and Metz, 2020]

We derive the result Eq. (4.27) from the results obtained in Ref. [Neri and Metz, 2020]. There, the random matrices $\mathbf{A}$ are of the form

$$\mathbf{A} = \tilde{\mathbf{J}} \circ \tilde{\mathbf{C}}, \tag{4.31}$$

where $\tilde{\mathbf{C}}$ is the adjacency matrix of a random, directed graph with a prescribed joint degree distribution $p^{\mathrm{d}}_{\deg}(k_{\mathrm{in}}, k_{\mathrm{out}})$ of indegrees k_{in} and outdegrees k_{out}, and where $\tilde{\mathbf{J}}$ is a random matrix with real-valued i.i.d. entries drawn from a distribution $\tilde{p}(x)$.

According to Ref. [Neri and Metz, 2020], in the limit $N \to \infty$ the boundary of the continuous part of the spectrum of $\mathbf{A}$ is given by the values $z \in \mathbb{C}$ for which

$$|z|^2 = \tilde{c}(\rho + 1)\langle x^2 \rangle_{\tilde{p}}, \tag{4.32}$$

where $\tilde{c}$ is the mean indegree (or outdegree)

$$\tilde{c} = \langle k_{\text{in}} \rangle_{p^{\text{d}}_{\text{deg}}} = \langle k_{\text{out}} \rangle_{p^{\text{d}}_{\text{deg}}}, \tag{4.33}$$

where we denoted the expectation over the degree distribution $p^{\text{d}}_{\text{deg}}(k_{\text{in}}, k_{\text{out}})$ as $\langle \rangle_{p^{\text{d}}_{\text{deg}}}$, with $k_{\text{in}}, k_{\text{out}} \in \mathbb{N}$, and where ρ is the degree correlation coefficient

$$\rho = \frac{\langle k_{\text{in}} k_{\text{out}} \rangle_{p^{\text{d}}_{\text{deg}}} - \tilde{c}^2}{\tilde{c}^2}. \tag{4.34}$$

Note that Eq. (4.31) considers a random, directed graph $\tilde{\mathbf{C}}$ with symmetric couplings $\tilde{\mathbf{J}}$, while Eq. (1.42) with $p = p^{\text{O}}$ considers a random, undirected graph $\mathbf{C}$ with asymmetric couplings $\mathbf{J}$. Both models are related through the correspondence

$$p^{\text{d}}_{\text{deg}}(k_{\text{in}}, k_{\text{out}}) = \sum_{k=0}^{\infty} p_{\text{deg}}(k) \frac{1}{2^k} \sum_{n=0}^{k} \binom{k}{n} \delta_{k_{\text{in}},n} \delta_{k_{\text{out}},k-n} \tag{4.35}$$

between the degree distributions $p^{\text{d}}_{\text{deg}}, p_{\text{deg}}$ of the directed and undirected graphs, respectively.

We now show that Eq. (4.27) is consistent with Eq. (4.32). From Eq. (4.35) we can express the correlation $\langle k_{\text{in}} k_{\text{out}} \rangle_{p^{\text{d}}_{\text{deg}}}$ as follows

$$\begin{aligned}
\langle k_{\text{in}} k_{\text{out}} \rangle_{p^{\text{d}}_{\text{deg}}} = \tilde{c}^2 (\rho + 1) &= \sum_{k_{\text{in}}=0}^{\infty} \sum_{k_{\text{out}}=0}^{\infty} k_{\text{in}} k_{\text{out}} \sum_{k=0}^{\infty} p_{\text{deg}}(k) \frac{1}{2^k} \sum_{n=0}^{k} \binom{k}{n} \delta_{k_{\text{in}},n} \delta_{k_{\text{out}},k-n} \\
&= \sum_{k=0}^{\infty} p_{\text{deg}}(k) \frac{1}{2^k} \sum_{n=0}^{k} \binom{k}{n} n(k-n) \\
&= \left\langle \frac{1}{2^k} \sum_{n=0}^{k} \binom{k}{n} n(k-n) \right\rangle_{p_{\text{deg}}}.
\end{aligned} \tag{4.36}$$

In order to evaluate Eq. (4.36) we introduce the moment generating function

$$g(x) := \sum_{n=0}^{k} \binom{k}{n} e^{nx} = (1 + e^x)^k, \tag{4.37}$$

with derivatives

$$g'(x) := \frac{\mathrm{d}}{\mathrm{d}x} g(x) = \sum_{n=0}^{k} \binom{k}{n} e^{nx}\, n = k(1 + e^x)^{k-1} e^x, \tag{4.38}$$

$$g''(x) := \frac{\mathrm{d}^2}{\mathrm{d}x^2} g(x) = \sum_{n=0}^{k} \binom{k}{n} e^{nx}\, n^2 = k(1 + e^x)^{k-2} e^x (k e^x + 1), \tag{4.39}$$

so that in terms of $g(x)$ and its derivatives we have

$$\begin{aligned}\tilde{c}^2\,(\rho+1) &= \left\langle p_{\rm deg}(k)\frac{k}{2^k}g'(x=0)\right\rangle_{p_{\rm deg}} - \left\langle \frac{1}{2^k}g''(x=0)\right\rangle_{p_{\rm deg}} \\ &= \left\langle \frac{k^2}{2}\right\rangle_{p_{\rm deg}} - \left\langle \frac{k(k+1)}{2^2}\right\rangle_{p_{\rm deg}} \\ &= \left\langle \frac{k^2-k}{2^2}\right\rangle_{p_{\rm deg}} \\ &= \frac{1}{4}\left\langle k(k-1)\right\rangle_{p_{\rm deg}}. \end{aligned} \tag{4.40}$$

Similarly to Eq. (4.40), one has also that

$$\tilde{c} = \left\langle \frac{g'(x=0)}{2^k}\right\rangle_{p_{\rm deg}} = \frac{c}{2}. \tag{4.41}$$

By using Eqs. (4.40)-(4.41), we have that Eq. (4.32) recovers Eq. (6.6) for the boundary of an oriented ensemble, i.e.

$$\frac{|z|^2}{\langle x^2\rangle_{\tilde{p}}} = \tilde{c}\,(\rho+1) = \frac{\langle k(k-1)\rangle_{p_{\rm deg}}}{4\tilde{c}} = \frac{\langle k(k-1)\rangle_{p_{\rm deg}}}{2c}, \tag{4.42}$$

which confirms the consistency with Ref. [Neri and Metz, 2020].

4.4.2 Large connectivity limit

We take the limit $c \to \infty$, with $c/N \sim_\infty 0$, where $\sim_\infty$ means the asymptotic equivalence in the limit $c \to \infty$ and $N \to \infty$, where the latter is implicit in the distributional approach, and we find the elliptic law given by

$$\rho(z) = \begin{cases} \dfrac{\sigma^2}{\pi(\sigma^4-\tau^2)} & \text{if} \quad z \in \mathcal{S}, \\ 0 & \text{if} \quad z \notin \mathcal{S}, \end{cases} \tag{4.43}$$

with

$$\tau := c\,\langle ul\rangle_p\,, \quad \text{and} \quad \sigma^2 := c\,\langle u^2\rangle_p\,, \tag{4.44}$$

where p is the distribution of u and l in the general model, and where we rescaled here u, l by $1/\sqrt{c}$ so that σ and τ in Eq. (4.44) remain finite in the limit $c \to \infty$. The support is given by

$$\mathcal{S} := \left\{ z \in \mathbb{C} : \frac{\Re(z)^2}{(\sigma^2+\tau)^2} + \frac{\Im(z)^2}{(\sigma^2-\tau)^2} \le \frac{1}{\sigma^2} \right\}, \tag{4.45}$$

which is consistent with the elliptic law Eq. (4.43), in the sense that the integral (with the Lebesgue measure in $\mathbb{C}$) of ρ over the support $\mathcal{S}$ is one.

The elliptic law in Eq. (4.43)-(4.45) — with σ and τ as in Eq. (4.44) —, is equivalent to the elliptic law for i.i.d. matrices in Eq. (1.22) and Eq. (1.23) with rescaled variance

and correlation.

4.4.2.1 Support

We first derive now an expression for the support $\mathcal{S}$. We show that the edge of stability of the Eq. (4.24) at the trivial solution Eq. (4.25) provides us with the boundary of the elliptic law in Eqs. (4.43). Using the law of large numbers, we can identify the sums inside the delta distributions on the right-hand-side of Eq. (4.24) with their mean values, i.e., for $c \to \infty$

$$\sum_{\ell=1}^{k-1} u_\ell g_\ell d_\ell \sim_\infty \tau \hat{g}, \tag{4.46}$$

$$\sum_{\ell=1}^{k-1} h_\ell l_\ell^2 \sim_\infty \sigma^2 \hat{\epsilon}. \tag{4.47}$$

As a consequence, to the leading order $1/c$, the distribution Q takes the form

$$Q(g,h) = \delta\left(g + \frac{1}{z+\tau\hat{g}}\right)\delta\left(h - \sigma^2|\hat{g}|^2\hat{h}\right). \tag{4.48}$$

By evaluating ensemble averages $\langle g\rangle_Q$, $\langle h\rangle_Q$, with Q as in Eq. (4.48) which equal the mean values $\hat{g}$ and $\hat{h}$, respectively, one finds the self-consistent equations

$$\hat{g} = -\frac{1}{z+\tau\hat{g}}, \tag{4.49}$$

and

$$\hat{h} = \sigma^2\hat{h}|\hat{g}|^2. \tag{4.50}$$

The edge of stability of the previous equation is given by $\hat{g} = \hat{g}(z)$ such that

$$|\hat{g}|^2 = \frac{1}{\sigma^2}. \tag{4.51}$$

From Eq. (4.49) we have the following identity

$$|\hat{g}|^2 = \hat{g}\bar{\hat{g}} = \frac{1}{(z+\tau\hat{g})(\bar{z}+\tau\bar{\hat{g}})}, \tag{4.52}$$

and from Eq. (4.51) it follows that

$$(z+\tau\hat{g})(\bar{z}+\tau\bar{\hat{g}}) = \sigma^2; \tag{4.53}$$

we have also that

$$\hat{g} + \bar{\hat{g}} = -\frac{1}{z+\tau\hat{g}} - \frac{1}{\bar{z}+\tau\bar{\hat{g}}} = -\frac{\bar{z}+\tau\bar{\hat{g}}+z+\tau\hat{g}}{\sigma^2} = -(\hat{g}+\bar{\hat{g}})\frac{\tau}{\sigma^2} - \frac{z+\bar{z}}{\sigma^2}, \tag{4.54}$$

and multiplying by σ^2 and factorising on the left hand side $\hat{g} + \bar{\hat{g}}$ we have

$$\hat{g} + \bar{\hat{g}} = -\frac{z + \bar{z}}{\sigma^2 + \tau}, \tag{4.55}$$

which can be expressed in terms of the real parts as

$$\Re(\hat{g}) = -\frac{\Re(z)}{\sigma^2 + \tau}. \tag{4.56}$$

Similarly one can get an equation for the difference

$$\hat{g} - \bar{\hat{g}} = -\frac{1}{z + \tau\hat{g}} + \frac{1}{\bar{z} + \tau\bar{\hat{g}}} = \frac{-\bar{z} - \tau\bar{\hat{g}} + z + \tau\hat{g}}{\sigma^2} = (\hat{g} - \bar{\hat{g}})\frac{\tau}{\sigma^2} + \frac{z - \bar{z}}{\sigma^2}, \tag{4.57}$$

and multiplying by σ^2 and factorising on the left hand side $\hat{g} - \bar{\hat{g}}$ we have

$$\hat{g} - \bar{\hat{g}} = \frac{z - \bar{z}}{\sigma^2 - \tau}, \tag{4.58}$$

which can be expressed in terms of the imaginary parts as

$$\Im(\hat{g}) = \frac{\Im(z)}{\sigma^2 - \tau}. \tag{4.59}$$

Finally, since from Eqs. (4.52),(4.53) we have that

$$(\Re(\hat{g}))^2 + (\Im(\hat{g}))^2 = \frac{1}{\sigma^2}, \tag{4.60}$$

plugging (4.56) and (4.59) we have the equation for the boundary of the support in the large connectivity limit as

$$\left(\frac{\Re(z)}{\sigma^2 + \tau}\right)^2 + \left(\frac{\Im(z)}{\sigma^2 - \tau}\right)^2 = \frac{1}{\sigma^2}, \tag{4.61}$$

which is equivalent to Eq. (4.45).

4.4.2.2 Spectral distribution

We compute the spectral distribution in the large connectivity limit. In this case, we rely on the Eqs. (4.7-4.9). Similarly to the previous derivation of the boundary in Sec. 4.4.2.1, in the limit $c \to \infty$, we can apply the law of large numbers inside the Dirac distributions of Eqs. (4.7-4.8), leading to

$$\tilde{q}(\mathsf{g}) = q(\mathsf{g}) = \delta\left(\mathsf{g} - \begin{pmatrix} -\sigma^2\hat{g}_{22} & z - \tau\hat{g}_{21} \\ \bar{z} - \tau\hat{g}_{12} & -\sigma^2\hat{g}_{11} \end{pmatrix}^{-1}\right), \tag{4.62}$$

where we set $\eta = 0$, and we explicitly express the elements of the matrix products, replacing them with their mean values, similarly to Eqs. (4.46)-(4.47). As in Sec. 4.4.2.1, by evaluating ensemble averages $\langle \mathsf{g} \rangle_q$, with q as in Eq. (4.62) which equals the mean value $\hat{\mathsf{g}}$, one finds the self-consistent equation where $\hat{\mathsf{g}}$ solves the self-consistent equation

$$\begin{aligned} \hat{\mathsf{g}} = \begin{pmatrix} \hat{g}_{11} & \hat{g}_{12} \\ \hat{g}_{21} & \hat{g}_{22} \end{pmatrix} &= \begin{pmatrix} -\sigma^2 \hat{g}_{22} & z - \tau \hat{g}_{21} \\ \bar{z} - \tau \hat{g}_{12} & -\sigma^2 \hat{g}_{11} \end{pmatrix}^{-1} \\ &= \frac{1}{\hat{g}_{11}\hat{g}_{22}\sigma^4 - (\bar{z} - \tau \hat{g}_{12})(z - \tau \hat{g}_{21})} \begin{pmatrix} -\sigma^2 \hat{g}_{11} & -z + \tau \hat{g}_{21} \\ -\bar{z} + \tau \hat{g}_{12} & -\sigma^2 \hat{g}_{22} \end{pmatrix}, \end{aligned} \tag{4.63}$$

and the spectral distribution is given by

$$\rho(z) = \frac{1}{\pi} \partial_{\bar{z}}\, \hat{g}_{21}. \tag{4.64}$$

Equation (4.63) implies that

$$\hat{g}_{11}\hat{g}_{22} = \frac{\hat{g}_{11}\hat{g}_{22}\sigma^4}{\left[\hat{g}_{11}\hat{g}_{22}\sigma^4 - (\bar{z} - \tau \hat{g}_{12})(z - \tau \hat{g}_{21})\right]^2}, \tag{4.65}$$

such that either

$$\hat{g}_{11} = \hat{g}_{22} = 0, \tag{4.66}$$

or

$$\left[\hat{g}_{11}\hat{g}_{22}\sigma^4 - (\bar{z} - \tau \hat{g}_{12})(z - \tau \hat{g}_{21})\right]^2 = \sigma^4. \tag{4.67}$$

Equation (4.66) is the trivial solution and Eq. (4.67) is the nontrivial solution.

In Sec. 4.4.2.1, we have shown that the trivial solution Eq. (4.72) is stable for all z for which

$$\left(\frac{\Re(z)}{\sigma^2 + \tau}\right)^2 + \left(\frac{\Im(z)}{\sigma^2 - \tau}\right)^2 > \frac{1}{\sigma^2}, \tag{4.68}$$

while the nontrivial solution holds for

$$\left(\frac{\Re(z)}{\sigma^2 + \tau}\right)^2 + \left(\frac{\Im(z)}{\sigma^2 - \tau}\right)^2 \leq \frac{1}{\sigma^2}. \tag{4.69}$$

In what follows, we first compute the spectral distribution for the trivial solution and then we compute it for the nontrivial solution.

Trivial solution. For the trivial solution, Eq. (4.63) reduces to the two equations

$$\hat{g}_{21} = \frac{1}{z - \tau \hat{g}_{21}}, \tag{4.70}$$

$$\hat{g}_{12} = \frac{1}{\bar{z} - \tau \hat{g}_{12}}, \tag{4.71}$$

which admit two complex solutions

$$\hat{g}_{21} = \frac{z \pm \sqrt{z^2 - 4\tau}}{2\tau}. \tag{4.72}$$

For $|z| > 2\sqrt{|\tau|}$, this is an analytical function in z, and therefore

$$\partial_{\bar{z}}\, \hat{g}_{21} = 0. \tag{4.73}$$

Since for all z for which Eq. (4.68) holds, it also holds that $|z| > 2\sqrt{|\tau|}$, we obtain that

$$\rho(z) = 0 \quad \text{if} \quad \left(\frac{\Re(z)}{\sigma^2 + \tau}\right)^2 + \left(\frac{\Im(z)}{\sigma^2 - \tau}\right)^2 > \frac{1}{\sigma^2}. \tag{4.74}$$

Nontrivial solution. For the nontrivial solution Eq. (4.67) we obtain

$$\hat{\mathbf{g}} = \begin{pmatrix} \hat{g}_{11} & \hat{g}_{12} \\ \hat{g}_{21} & \hat{g}_{22} \end{pmatrix} = \pm\frac{1}{\sigma^2} \begin{pmatrix} -\sigma^2 \hat{g}_{11} & -z + \tau \hat{g}_{21} \\ -\bar{z} + \tau \hat{g}_{12} & -\sigma^2 \hat{g}_{22} \end{pmatrix}, \tag{4.75}$$

and therefore

$$\pm\sigma^2 \hat{g}_{21} = -\bar{z} + \tau \hat{g}_{12}, \tag{4.76}$$

$$\pm\sigma^2 \hat{g}_{12} = -z + \tau \hat{g}_{21}. \tag{4.77}$$

From these equations we obtain a closed equation for $\hat{g}_{21}$, i.e.,

$$\hat{g}_{21} = \mp\frac{\sigma^2}{\sigma^4 - \tau^2}\bar{z} - \frac{\tau}{\sigma^4 - \tau^2} z, \tag{4.78}$$

and accordingly

$$\rho(z) = \frac{1}{\pi}\partial_{\bar{z}}\, \hat{g}_{21} = \frac{1}{\pi}\frac{\sigma^2}{\sigma^4 - \tau^2}, \tag{4.79}$$

if we select the positive solution.

4.5 Computing the spectral distribution: the population dynamics algorithm

Here we detail the numerical algorithm that can be used to obtain the spectral distribution ρ from the theoretical derivation in Sec. 4.2. We implement this method to determine ρ for the antagonistic matrices, and present the results in Ch. 5. We first present the population dynamics algorithm, which is a numerical method to solve self consistently equations of the form Eq. (4.19), and from its stable solution ρ can be estimated via a Mont-Carlo integration, as discussed at the end of this section.

Recursive distributional equations of the form Eq. (4.19) have been previously found, in the literature, in different contexts. For example, to study spin glasses on a Bethe lattice [Mézard and Parisi, 2001], where $q(\mathsf{g}, \mathsf{g}')$ (there named $Q(h)$) represents the probability density of local fields h_i on each spin sites i, and in the theory of localisation of electrons [Abou-Chacra et al., 1973]. In the context of symmetric sparse random matrices, recursive distributional equations have been derived through an approach based on replicas [Kühn, 2008], and on the cavity method [Metz et al., 2010]. Similar recursive equations have been found within the study of message-passing problems (or belief propagation) [Chertkov et al., 2010; Krzakala et al., 2015]. In all these separated problems, these equations are essentially described by ensemble averages: an average over the disorder of the interactions (in Eq. (4.19) it is given by $p(u, l)$), an average over the degree distribution ($p_{\text{deg}}(k)$) and the average over the distribution (q).

The numerical algorithm introduced to solve these self consistent equations, which analytically would be hardly solvable, is called population dynamics: the probability distribution to be determined is parametrised by a large number N_{p} of variables which arrange in a population; its dynamics is given by the update rule according to the argument of the delta in the self-consistent equation that, accordingly, depends on the specific case under study. This dynamics defines a Markov chain on the space of the N_{p} variables of the population [Mézard and Parisi, 2001]. In particular, this chain has a stationary distribution which is reached after some transient time. In the limit N_{p}, the stationary distribution satisfies the self-consistent equation. As agued in Ref. [Mézard and Parisi, 2001], it would be possible to show that the corrections to this limit are proportional to N_{p}^{-1}. The procedure for practical applications consists in fixing the value of N_{p} ($\approx 10^4 - 10^5$ for example), iterating the update rules for the dynamics many times in such a way as to obtain the spectral distribution at fixed N_{p}, and finally extrapolating the results to the limit $N_{\text{p}} \to \infty$. We explain more in detail the algorithm below.

We represent the distributions $q(\mathsf{g}, \mathsf{g}')$ with a population of pairs $(\mathsf{g}^{(j)}, \mathsf{g}'^{(j)})$ of two-by-two matrices $\mathsf{g}^{(j)}$ and $\mathsf{g}'^{(j)}$ with complex entries.

The population is initialised and updated as follows:

1. Initialise the population by drawing N_{p} independent realisations of random variables $(\mathsf{g}^{(i)}, \mathsf{g}'^{(i)})$ from a certain distribution $p_{\text{init}}(\mathsf{g}, \mathsf{g}')$;

2. Generate a degree k from the distribution $\frac{k}{c} p_{\text{deg}}(k)$;

3. Uniformly and randomly select $k-1$ elements $(\mathsf{g}_\ell, \mathsf{g}'_\ell)$ from the population and draw $k-1$ random variables (u_ℓ, l_ℓ) from the distribution $p(u_\ell, l_\ell)$, with $\ell = 1, 2, \ldots, k-1$;

4. Compute

$$\mathsf{g} = \left(\mathsf{z}_\eta - \sum_{\ell=1}^{k-1} \mathsf{J}_\ell \mathsf{g}_\ell \mathsf{J}_\ell^{\mathrm{T}} \right)^{-1}, \text{ and } \quad \mathsf{g}' = -\mathsf{g} \left(\sigma_- - \sum_{\ell=1}^{k-1} \mathsf{J}_\ell \mathsf{g}'_\ell \mathsf{J}_\ell^{\mathrm{T}} \right) \mathsf{g}; \tag{4.80}$$

5. Uniformly and randomly select an index $i \in \{1, \ldots, N_p\}$ and replace $(\mathbf{g}^{(i)}, \mathbf{g}'^{(i)})$ by $(\mathbf{g}, \mathbf{g}')$.

In this case, the precise form of the distribution p_{init} does not matter. The steps (2-5) are repeated a number N_{eq} of times until the estimated distribution

$$\hat{q}(\mathbf{g}, \mathbf{g}') = \frac{1}{N_{\text{p}}} \sum_{j=1}^{N_{\text{p}}} \delta(\mathbf{g} - \mathbf{g}^{(j)}) \delta(\mathbf{g}' - \mathbf{g}'^{(j)}) \tag{4.81}$$

has converged to its stationary value.

After the distribution $\hat{q}(\mathbf{g}, \mathbf{g}')$ has converged, we compute a first estimate $\hat{\rho}_1$ of ρ from Eqs. (4.21) and (4.19) with a Monte-Carlo integration algorithm. We then repeat the steps (2-5) a number N_{p} of times and then compute a second estimate of $\hat{\rho}_2$ of ρ. We repeat this procedure a number n_ρ of times to obtain the final estimate

$$\hat{\rho} = \frac{1}{n_\rho} \sum_{i=1}^{n_\rho} \hat{\rho}_i. \tag{4.82}$$

The error on $\hat{\rho}$ is computed based on the standard deviation of the set of sampled $\hat{\rho}_i$.

4.6 Computing the boundary of the support with the population dynamics algorithm

Here we detail the numerical method that we used to obtain the boundary of the support $\mathcal{S}$, for which we present the results in Ch. 5 applied to the models in Ch. 2. The method is based on a population dynamics algorithm similar to the one described in Sec. 4.5 to solve the Eq. (4.19).

The population dynamics algorithm for the boundary represents the distribution $Q(g, h)$ in Eq. (4.24) with a population of N_{p} realisations of the random variables (g, h). The population is initialised and updated as follows:

1. Initialise the population by drawing N_{p} independent realisations of random variables $(g^{(i)}, h^{(i)})$ from a certain distribution $p_{\text{init}}(g, h)$;

2. Generate a degree k from the distribution $\frac{k}{c} p_{\text{deg}}(k)$;

3. Uniformly and randomly select $k-1$ elements (g_ℓ, h_ℓ) from the population and draw $k-1$ random variables (u_ℓ, l_ℓ) from the distribution $p(u_\ell, l_\ell)$, with $\ell = 1, 2, \ldots, k-1$;

4. Compute

$$g = -\left[z + \sum_{\ell=1}^{k-1} u_\ell g_\ell l_\ell \right]^{-1}, \text{ and } \quad h = |g|^2 \sum_{\ell=1}^{k-1} h_\ell \, |l_\ell|^2 ; \tag{4.83}$$

5. Uniformly and randomly select an index $i \in \{1, \ldots, N_p\}$ and replace $(g^{(i)}, h^{(i)})$ by (g, h).

Steps (2-5) are repeated for a certain number $N_{\rm s} = n_{\rm s} N_{\rm p}$ of iterations, where $n_{\rm s}$ is the number of sweeps for which the whole population is updated. After $n_{\rm s}$ sweeps, the steps (2-5) are repeated for another number $N_{\rm r} = n_{\rm r} N_{\rm p}$ of iterations after which the distribution $Q(g, h)$ is estimated as

$$\hat{Q}(g, h) = \frac{1}{n_{\rm r} N_{\rm p}} \sum_{j=1}^{n_{\rm r} N_{\rm p}} \delta(g - g^{(j)}) \delta(h - h^{(j)}). \tag{4.84}$$

If $N_{\rm p} \to \infty$, then the pairs $(g^{(j)}, h^{(j)})$ in the population are independent realisations drawn from the distribution $Q(g, h)$ and the algorithm is exact.

Since the Eq. (4.24) follows from a stability analysis, it holds that if the initial population is of the form given by Eq. (4.25), then

$$\lim_{n_{\rm s} \to \infty} \lim_{N_{\rm p} \to \infty} \langle |h| \rangle_{\hat{Q}} = \begin{cases} 0, & z \notin \mathcal{S}, \\ \infty, & z \in \mathcal{S}. \end{cases} \tag{4.85}$$

Hence, we obtain the boundary of $\mathcal{S}$ by determining the value of z that separates the region where $\langle |h| \rangle_{\hat{Q}}$ diverges from the region where $\langle |h| \rangle_{\hat{Q}}$ converges to zero.

4.7 Adaptation of the elliptic law for sparse matrices

Here we derive an adaptation of the elliptic law in Eq. (1.22) and Eq. (1.23) to sparse matrices, equivalently, for example, to what has been done in [Allesina and Tang, 2012], as discussed in Ch. 1.

As discussed in Sec. 1.3 and Sec. 1.6, the elliptic law has been applied to random matrices of finite but large size N, where a couple of opposite entries (A_{ij}, A_{ji}) is non-zero with probability C. At the level of the elliptic domain, this case amounts to a rescaling of the semiaxes $a_{x,y}$ of the elliptic support, as in Eq. (1.45). Such elliptic law, which is derived to describe the boundary of the spectra of dense matrices is, by definition, independent of the network topology. Here we want to make evidence of the progress that our study gives to the current literature, and to highlight the importance of the influence of network topology on the spectral properties of sparse random matrices with pairwise correlated interactions. Accordingly, we further adapt the elliptic law to sparse random matrices of the general model that we study in this thesis, as they were dense matrices, and thus ignoring the network structure. This adaptation is simply given by mapping the mean degree c of the sparse ensemble that we study to the connectance C through $C = c/N$. Equivalently, this mapping defines an effective i.i.d. matrix ensemble with entries (A_{ij}, A_{ji}) with correlation τ and variance σ^2 as in Eq. (4.44), for finite c, that satisfies the elliptic law in Eq. (4.43),(4.45). The relation between the covariance

and the variance of the two ensemble is a simple rescaling by c: for example, in the case of the interactions of Model A, they are $\sigma^2 = c$ and $\tau = -3c/4$.

We make explicit now the semiaxes $a_{\Re,\Im}$, on the real and imaginary axes, respectively, of the elliptic boundary in $\mathcal{S}$ for this adaptation of the elliptic law, i.e.,

$$a_{\Re,\Im} = \sigma(1 \pm \tau/\sigma^2), \tag{4.86}$$

which, as discussed above, correspond to the semiaxes in Eq. (1.45) where $c = CN$ is included in the definitions of τ, σ^2 as in Eq. (4.44).

The first consequence of this adaptation is that the elliptic law has finite support for $N \to \infty$, differently from what happens for dense matrices with finite elements. In other words, the elliptic law adapted to the sparse ensembles predicts that systems whose interactions are described by sparse matrices can be stable in all cases as the leading eigenvalue does not diverge with N.

When we present the numerical results in Chs. 5-6, we also show in the figures the analytical curves corresponding to the adaptation of the elliptic law as derived in Eqs. (4.43)-(4.45).

4.8 Summary of this chapter

We adopted a distributional approach to determine the central equations for the spectral distribution and its support for the general model in Sec. 2.1.

First, we obtained the distributional cavity equation that include the derivatives in Eq. (4.19), from which the spectral distribution is given by Eq. (4.21).

Second, we obtained the self-consistent equation (4.24), that outside the support $\mathcal{S}$ converges to the distributional trivial solution in Eq. (4.26), and hence it establishes a criterion to determine the boundary of $\mathcal{S}$.

Chapter 5

Results for the spectra of sparse random matrices with pairwise correlated interactions

This chapter presents results for the spectra of antagonistic and mixture random matrices. In particular, we focus here on the spectral distribution ρ and its support $\mathcal{S}$. In order to corroborate the theory developed in Ch. 4, we compare the results obtained from direct diagonalization of matrices of finite sizes N with the theoretical predictions for infinitely large matrices. The numerical methods, that have been implemented to obtain the boundary of the support and the spectral distribution, are based on the population dynamics algorithm, as discussed in Sec. 4.5 and in Sec. 4.6. In order to evidence the role of the network structure, we also discuss the differences between the spectra of sparse matrices and those of effective dense matrices defined through the adaption of the elliptic law in Eqs. (4.43)-(4.45), as discussed in Sec. 4.7.

First, Sec. 5.1 considers sparse antagonistic matrices on random regular graphs , for which the degree distribution has bounded support. Then, Sec. 5.2 presents the spectra of matrices in Model A defined in Sec. 2.2, in order to consider the effects of an unbounded degree distribution and of degree fluctuations on the spectra of antagonistic matrices. Finally, Sec. 5.3 shows the spectra of matrices in Model B defined in Sec. 2.2, since we want to understand the differences between the antagonistic and mixture ensembles at the level of their spectra.

5.1 Antagonistic matrices on random regular graphs

We consider here the spectra of antagonistic matrices on random regular graphs with the degree distribution

$$p_{\rm deg}(k) = \delta_{k,c}, \tag{5.1}$$

and with the interactions of only predator-prey kind, as in Model A. In Sec. 5.1.1 we present results for the support of the spectral distribution and then in Sec. 5.1.2 results on the spectral distribution.

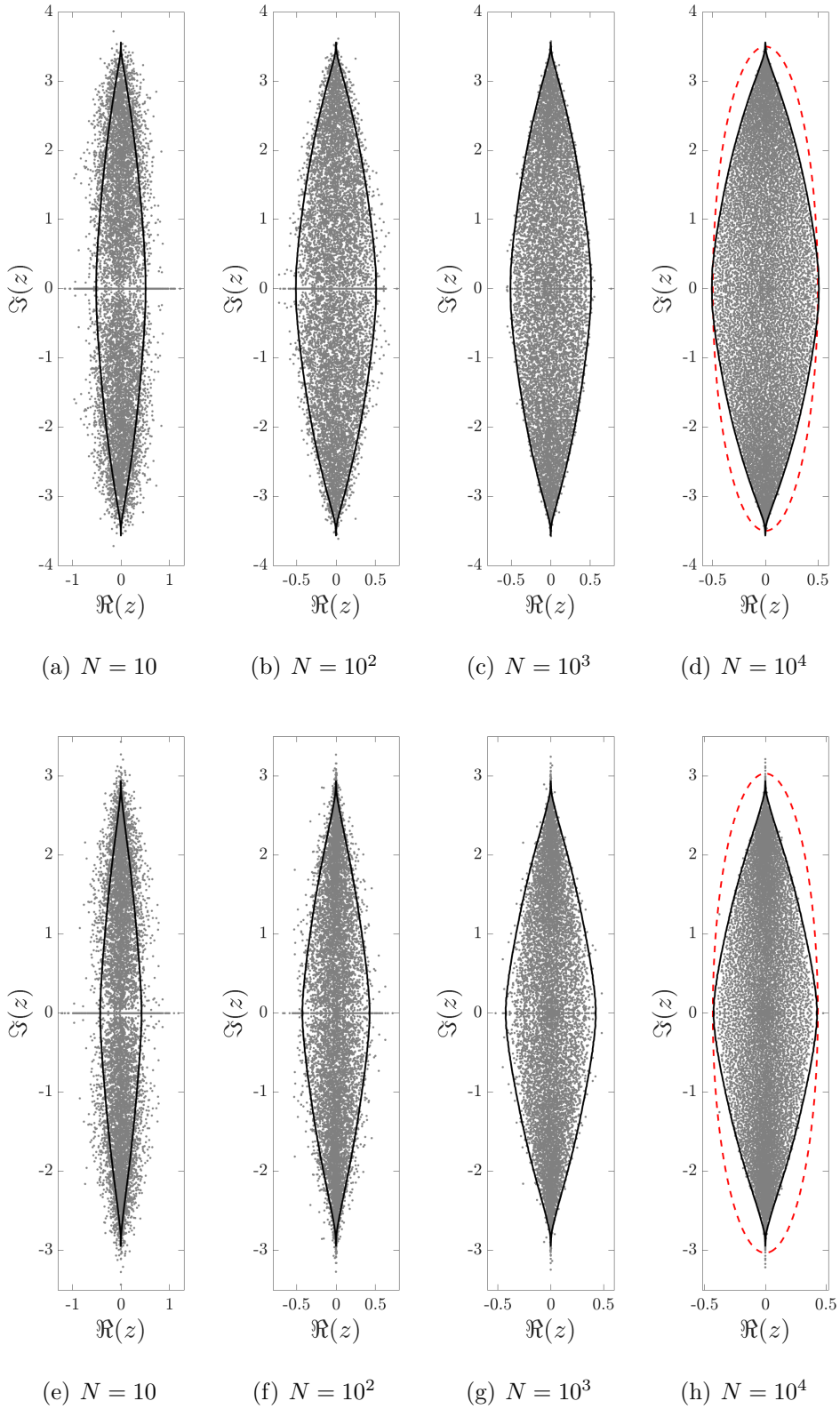

(a) $N = 10$ (b) $N = 10^2$ (c) $N = 10^3$ (d) $N = 10^4$

(e) $N = 10$ (f) $N = 10^2$ (g) $N = 10^3$ (h) $N = 10^4$

Figure 5.1: Spectra of antagonistic random matrices on random regular graphs with degree $c = 4$ (panels from (a) to (d)) and $c = 3$ (panels from (e) to (h)), the interactions are as in Model A in Sec. 2.2. Gray markers are the eigenvalues of m_s matrices of size N, with $m_s = 10^4/N$, that are randomly drawn from this ensemble and are obtained through direct diagonalization routines. Continuous black lines are theoretical results for $N \to \infty$ obtained with the theory of Sec. 4.3. Red dashed lines shown in panels (d) and (h) represent the boundary of the elliptic law given by Eqs. (4.43-4.45) with $\sigma^2 = c$ and $\tau = -3c/4$. Note that the horizontal and vertical scales are not fixed, for visualisation purposes.

5.1.1 Support of the spectral distribution

Figure 5.1 shows the spectra of antagonistic matrices on graphs with degrees $c = 3$ and $c = 4$. Each panel contains 10^4 eigenvalues obtained from direct diagonalization of $m_s = 10^4/N$ matrices, where we keep the product $m_s N$ fixed. The plots show also the boundary of the spectra as mentioned above. There is a very good correspondence between the boundary of theory and the spectra of eigenvalues from direct diagonalization already at $N \approx 10^3$, while for smaller N deviations appear, which are due to fluctuations in the spectral properties for matrices of finite size. For example, from Fig. 5.1 it appears that the leading eigenvalue at small values of $N = 10$ is larger than the leading eigenvalue at $N = 10^4$, for fixed value of c. Indeed, there are tails of eigenvalues that extend beyond the boundary of the support on the real axis that appear for small values of N. These tails in the antagonistic case are probably due to cycles in the graph which are more abundant for non-sparse realisations, as it is the case for small values of $N \approx 10$, while the tails disappear for larger N, where there is a smaller fraction of cycles. This is an example of finite size effects, and we study in more detail the dependence on N of the leading eigenvalue in Ch. 6.

We observe that the adaptation of the elliptic law in Eqs. (4.43)-(4.45), as discussed in Sec. 4.7, provides a very good approximation for the leading eigenvalue of an antagonistic matrix with $c = 3, 4$ on random regular graphs. However, stronger and stronger discrepancies appear in the boundary towards the intersection with the imaginary axis.

In Sec. 5.1.2 we look at the spectral distribution ρ, to validate our theory and to further characterise deviations from the adaptation of the elliptic law.

5.1.2 Spectral distribution

We present results about the spectral distribution of antagonistic random matrices on random regular graphs. We focus here on mean connectivity $c = 4$, the spectra of this ensemble are shown in Fig. 5.1 (panels (a)-(d)). We select cuts parallel to the real or imaginary axes in the complex plane, as shown in Fig. 5.2, which indicates the number of the figure in which we show the spectral distribution. The empirical spectral density of the eigenvalues evaluated by diagonalising 10^4 matrices of size 5000 is compared with the theoretical evaluation of the spectral distribution. As discussed in Sec. 4.5, the latter amounts to first solve Eq. (4.19) with a population dynamics algorithm, and second to a Monte-Carlo integration of Eq. (4.21) to finally estimate the spectral distribution ρ.

The results in Fig. 5.3 show an excellent agreement between theory and numerical experiments. The distribution displays some qualitative similarities between the three cuts: the peak is for $\Re(z) = 0$, and there is an evident change of the slope in proximity of the boundary, where it becomes steeper. However, some care should be taken to interpret the results in Fig. 5.3(c). Indeed, there exists an accumulation of eigenvalues on the real line, which is a known phenomenon in RMT where the number of real

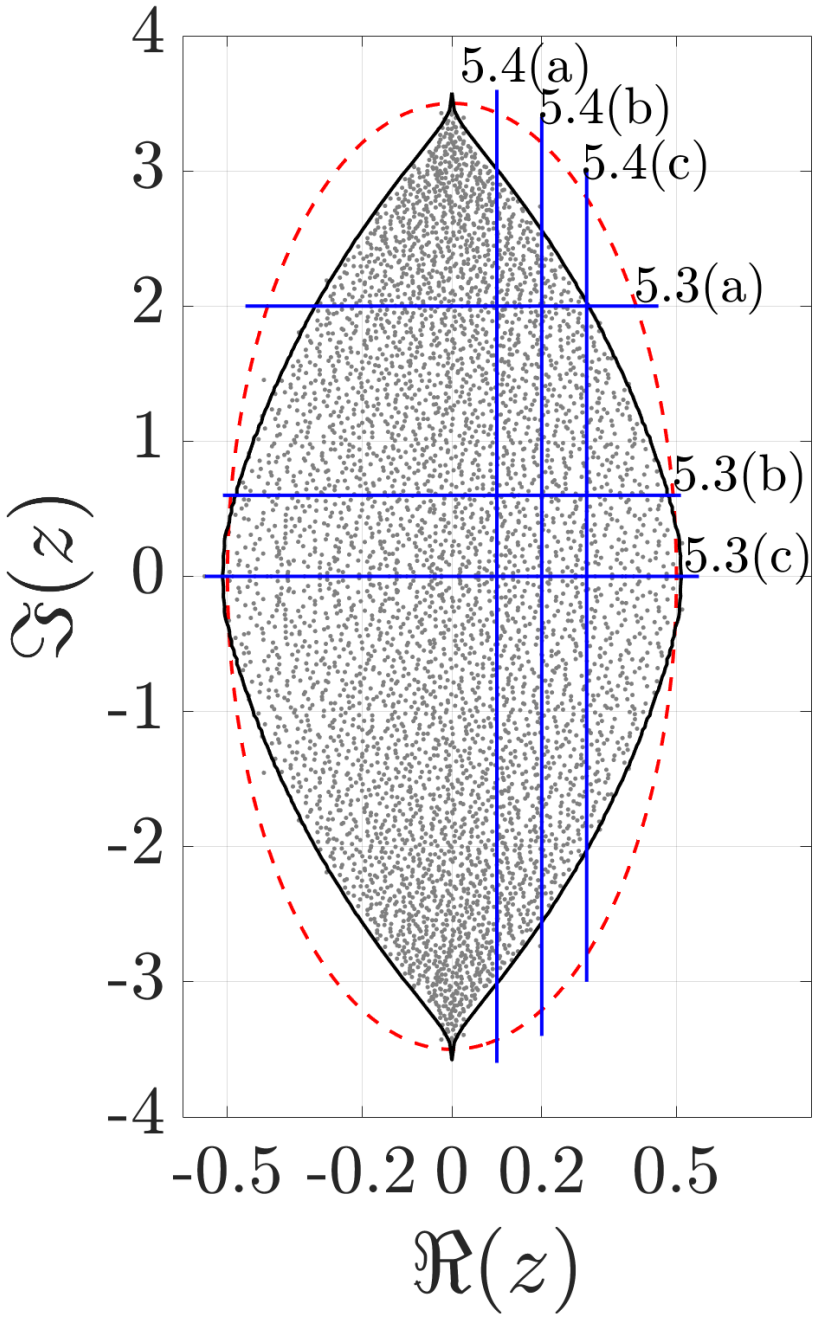

Figure 5.2: Eigenvalues of one matrix sampled from antagonistic random matrices on random regular graphs with $c = 4$, as in Fig. 5.1, now one sample with $N = 5000$. The blue lines denote the cuts along which we compute the spectral distribution ρ in Figs. 5.3 and 5.4. The red dashed line is the elliptic law given by Eqs. (4.43-4.45) with $\sigma^2 = c$ and $\tau = -3c/4$.

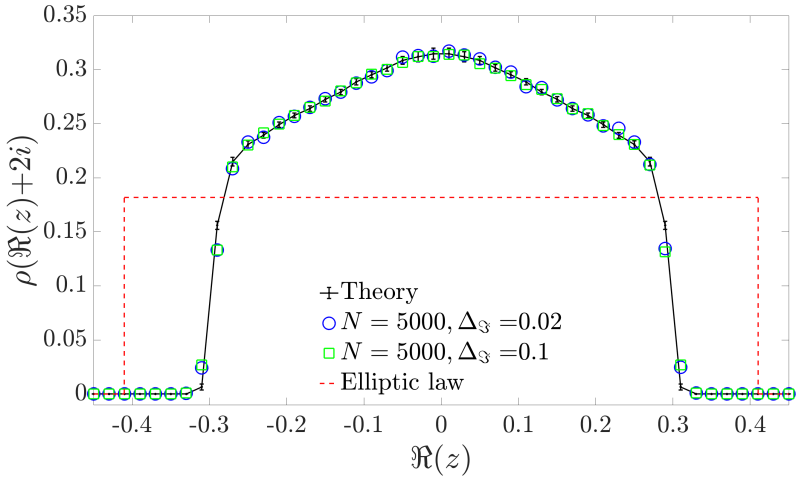

(a) $\Im(z) = 2$

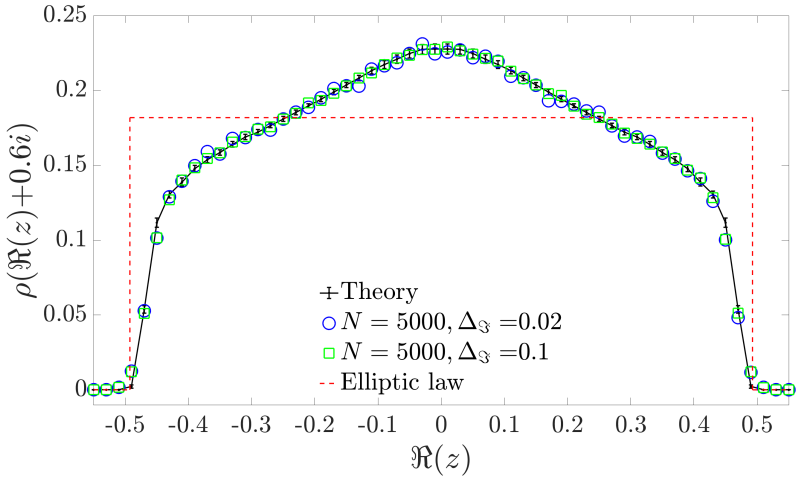

(b) $\Im(z) = 0.6$

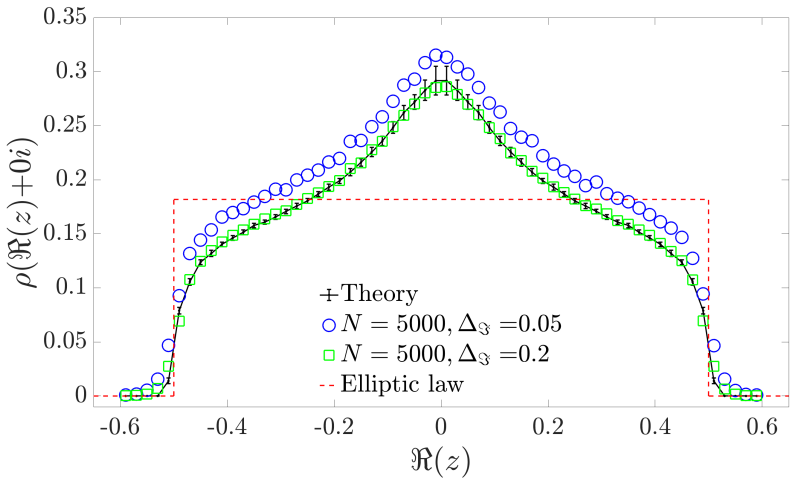

(c) $\Im(z) = 0$

Figure 5.3: The spectral distribution ρ along cuts parallel to the real axis for antagonistic random matrices on random regular graphs with $c = 4$. The values of $\Im(z)$ are indicated in the captions and the cuts are shown in Fig. 5.2. Theoretical results from the cavity (solid black line) are compared with histograms obtained by numerically diagonalising 10^4 matrices of size $N = 5000$ and collecting all eigenvalues in a strip of width $\Delta_\Im$ (markers). The spectral distribution is also compared with the elliptic law given by Eqs. (4.43-4.44) with $\sigma^2 = c$ and $\tau = -3c/4$ (red dashed line). Error bars denote the numerical error on the ρ value computed with population dynamics, as explained in Sec. 4.5.

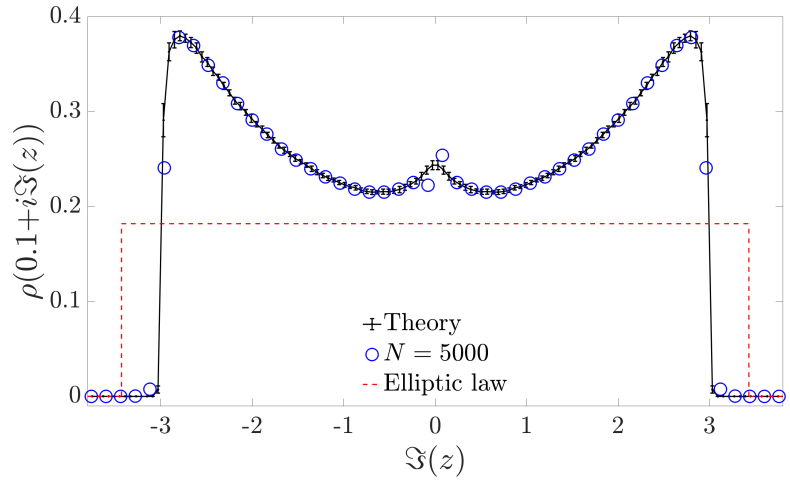

(a) $\Re(z) = 0.1$

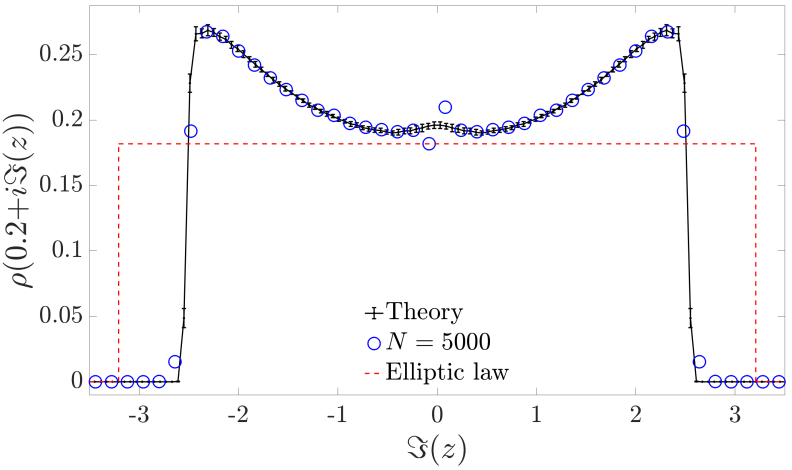

(b) $\Re(z) = 0.2$

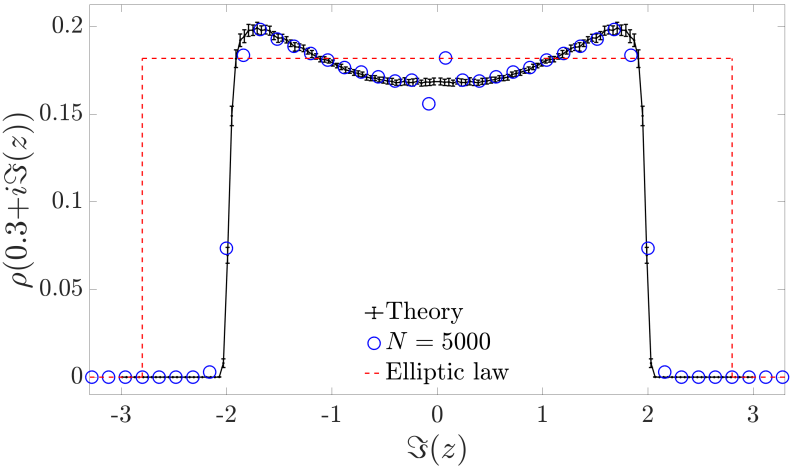

(c) $\Re(z) = 0.3$

Figure 5.4: The spectral distribution ρ along cuts parallel to the imaginary axis for antagonistic random matrices on random regular graphs with $c = 4$. The present figure is similar to Fig. 5.3, with the difference that the spectral distribution ρ shown is for cuts parallel to the imaginary axis. The values of $\Re(z)$ are given and the width $\Delta_{\Re} = 0.02$.

eigenvalues is of order $\mathcal{O}(\sqrt{N})$ [Edelman et al., 1994; Metz et al., 2019]. In presence of such a singular behaviour, the binning resolution of width $\Delta_{\Im}$ affects the estimate of the spectral distribution, hence different binning choices can give different estimates. On the other side, in the population dynamics we can compute ρ exactly. Accordingly, the discrepancy in Fig. 5.3(c) is not due to a disagreement with the theory, instead it is a systematic deviation of the empirical estimate of ρ due to the singular accumulation of real eigenvalues. Although the adaptation of the elliptic law provides a good estimate of the leading eigenvalue, as it can be seen also in Fig. 5.3(c), it provide significative discrepancies on the spectral distribution, which is not uniform.

The three cuts parallel to the imaginary axis in Fig. 5.4 show also an excellent agreement with the theory. In this case there is not a singular accumulation of eigenvalues, hence only one and equal binning choice is reported for all the three panels. Remarkably, here the highest values of the distribution are not at the centre, i.e., here at $\Im(z) = 0$, but in proximity of the boundary. However, also in this case the slope becomes steep in proximity of the boundary. The adaptation of the elliptic law in this case display discrepancies both in the boundary and in particular in the distribution, which is not uniform.

Figs. 5.3 and 5.4 also compare ρ with the adaptation of the elliptic law given by Eqs. (4.43-4.44), which here amounts to $\sigma^2 = c$ and $\tau = -3c/4$. While the boundary of the spectrum is well predicted by the elliptic law, a feature already observed in Fig. 5.1, this is not the case for the spectral distribution ρ.

5.2 Antagonistic matrices on Erdős-Rényi graphs

In order to study the effects of the degree fluctuations in the local network structure, together with the irregularity given by the unbounded degree distribution p_{deg}, here we consider the spectra of antagonistic matrices given by Model A. In this case the distribution $p(u, l)$ of the interactions is the same as in Sec. 5.1; however, differently from the random regular graphs considered in Sec. 5.1, in the Model A the network structure is given by Erdős-Rényi graphs.

5.2.1 Reentrance effect

Figure 5.5 presents the spectra of antagonistic matrices on Erdős-Rényi graphs with mean degrees $c = 4$ and $c = 2$. As in Fig. 5.1, each panel shows 10^4 eigenvalues obtained from direct diagonalization of $m_{\text{s}} = 10^4/N$ matrices, together with the boundary of the spectrum for N infinitely large, which is obtained from the theory of Ch. 4.

The most striking feature observed in Fig. 5.5 is the qualitative difference between $c = 4$ and $c = 2$ in the boundaries of the spectra of antagonistic matrices, for $N \to \infty$. For $c = 4$, the boundary of the spectrum has a shape similar to the elliptic law given by Eqs. (4.43-4.45), and as it was for the random regular, the adapted elliptic law

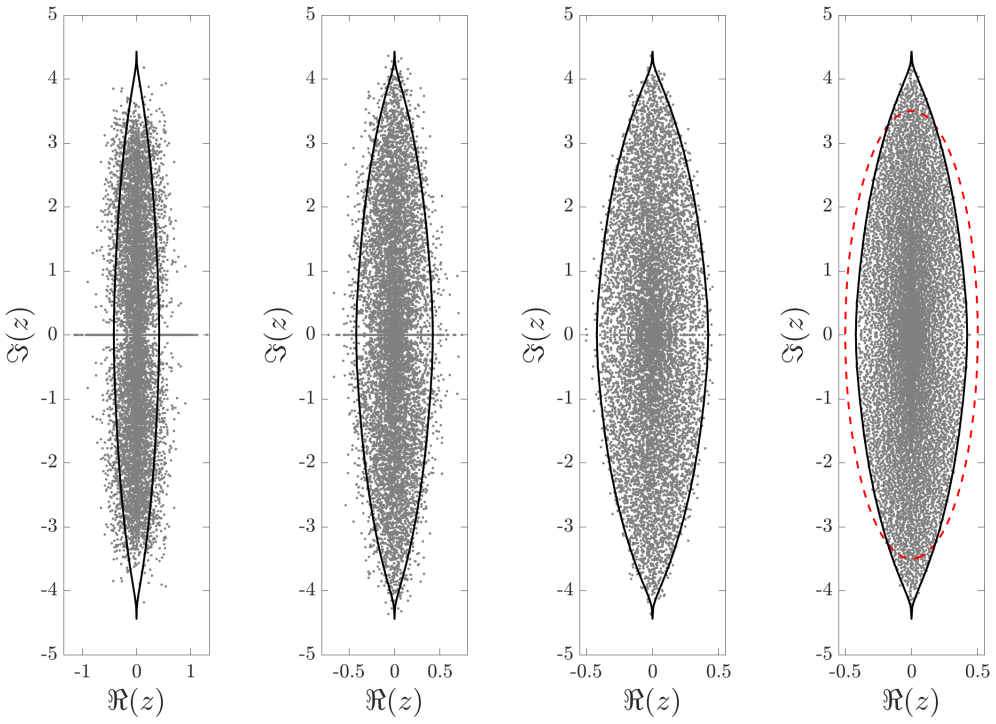

(a) $N = 10$ (b) $N = 10^2$ (c) $N = 10^3$ (d) $N = 10^4$

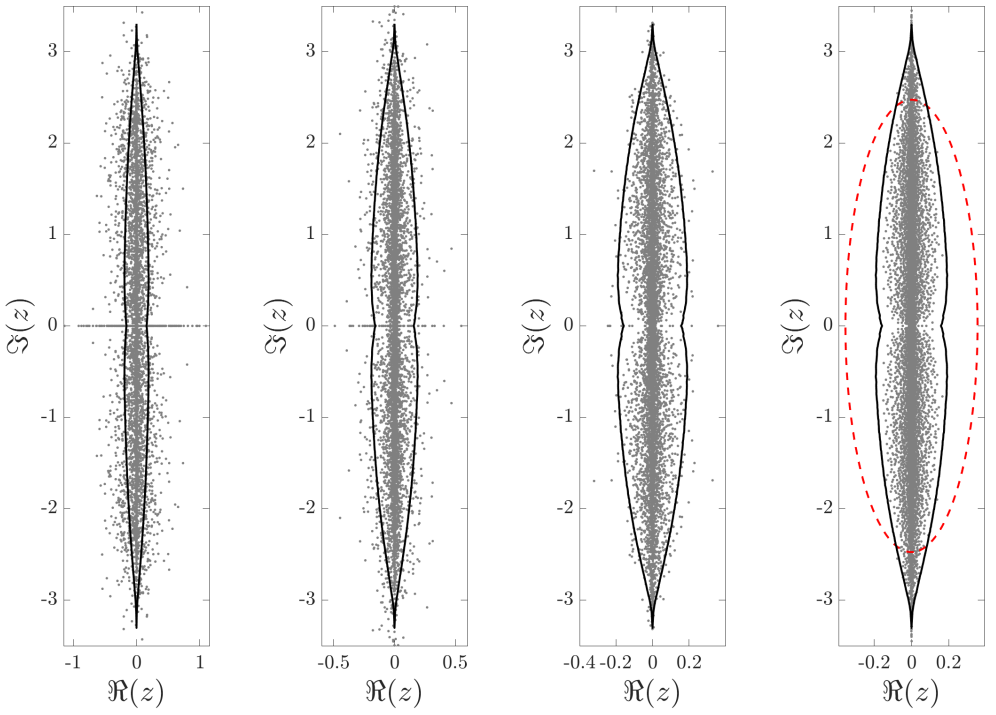

(e) $N = 10$ (f) $N = 10^2$ (g) $N = 10^3$ (h) $N = 10^4$

Figure 5.5: Spectra of antagonistic random matrices on Erdős-Rényi graphs (Model A in Sec. 2.2) with mean degree $c = 4$ (panels from (a) to (d)) and $c = 2$ (panels from (e) to (h)). Gray markers are the eigenvalues of m_s matrices of size N, with $m_s = 10^4/N$, that are randomly drawn from this ensemble and are obtained through direct diagonalization routines. Continuous black lines are theoretical results for $N \to \infty$ obtained with the theory of Sec. 4.3. Red dashed lines shown in panels (d) and (h) represent the boundary of the elliptic law given by Eqs. (4.43-4.45) with $\sigma^2 = c$ and $\tau = -3c/4$. Note that the horizontal and vertical scales are not fixed, for visualisation purposes.

provides a good estimate for the boundary of the spectrum and the leading eigenvalue of antagonistic matrices with $c = 4$. However, in this case the actual spectrum is more shrunk on the real axis than in the correspondent ensemble on random regular graphs, hence the adapted elliptic law here slightly overestimates the leading eigenvalue. For $c = 2$ completely new features appear in the shape of the boundary of the support. The spectrum and the leading eigenvalue for this sparse ensemble with $c = 2$ deviate significantly from the elliptic ensembles. The difference is in this case mainly due to a "reentrance" phenomenon in the support when approaching the real axis, and its effect is that the leading eigenvalue is complex. The reentrance effect comes as a surprising result, since it is is absent in the dense models, where the leading eigenvalue is real.

Similarly to the random regular spectra in Fig. 5.1, we observe a very good correspondence between theory and the eigenvalues from direct diagonalization, in particular the leading eigenvalue, already at sizes $N \approx 10^3 - 10^4$, while only for smaller N deviation appears, due to fluctuations in the spectral properties for matrices of finite size. Even though the theory is exact in the limit $N \to \infty$ to reveal the locally treelike structure, it is quite remarkable to have such a good agreement in antagonistic matrices at values of $N \approx 10^3 - 10^4$, since for these values there are still many cycles in the graphs.

5.2.2 Spectral distribution

We complete here the study on the spectra of Model A by presenting results about the spectral density, in analogy with Sec. 5.1.2. We focus here on mean connectivity $c = 4$. Similarly to Fig. 5.3 and Fig. 5.4 for random regular graphs, also the results of antagonistic matrices on Erdős-Rényi graphs provide an excellent agreement between the empirical density of eigenvalues, obtained by direct diagonalization, and the numerical solutions from the theory based on cavity method. This correspondence further validates the theory that we developed to analyse the spectra of antagonistic matrices.

In analogy with Fig. 5.3(c), we find also in Fig. 5.7(c) that the estimates of the density on the $\Im(z) = 0$ cut behaves singularly for the Erdős-Rényi graphs. This behaviour has been discussed in Sec. 5.1.2, and is expected to be a common feature for general non-Hermitian sparse ensemble. However, Fig. 5.7(c) reveals a new feature which was not present in its regular counterpart. From Fig. 5.7(c) , we observe that the spectral distribution of antagonistic matrices on Erdős-Rényi graphs diverges for $z \to 0$. Interestingly, this divergence is also observed in the adjacency matrices of undirected Erdős-Rényi graphs, see Ref. [Kühn, 2008], and in the adjacency matrices of directed Erdős-Rényi graphs, see Ref. [Metz et al., 2019]. On the other hand, the divergence does not occur in regular graphs. Hence, the divergence of the spectral distribution for $z \to 0$ is a generic feature due to network topology and is independent of the nature of the interactions J_{ij}. It would be interesting to have a precise understanding of the origin of the peak.

A comparison with the adapted elliptic law prediction reveals that also in this case the distribution is significantly not uniform; other than the peak in the origin discussed

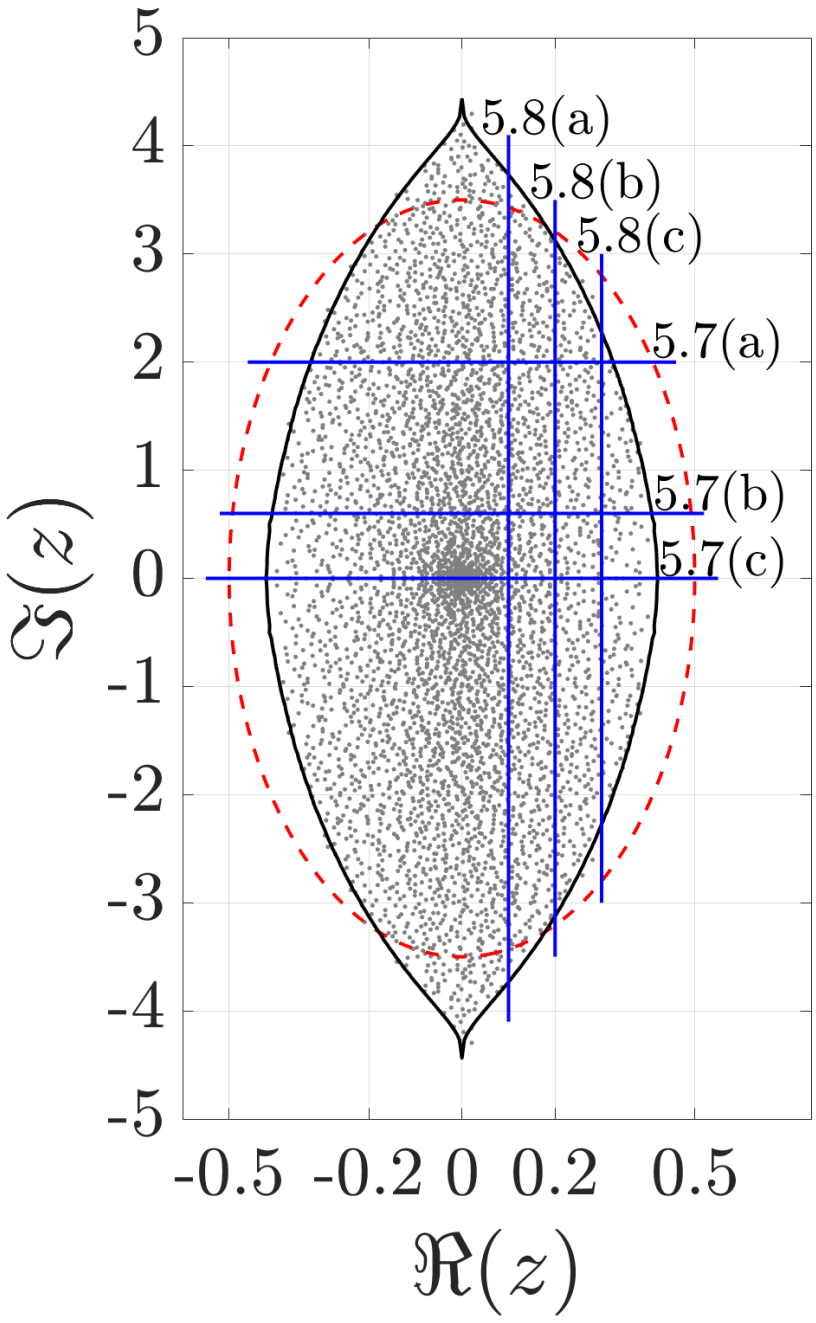

Figure 5.6: Eigenvalues of one matrix sampled from Model A with $c = 4$, as in Fig. 5.5, but now with $N = 5000$. The blue lines denote the cuts along which we compute the spectral distribution ρ in Figs. 5.7 and 5.8. The red dashed line is the elliptic law given by Eqs. (4.43-4.45) with $\sigma^2 = c$ and $\tau = -3c/4$.

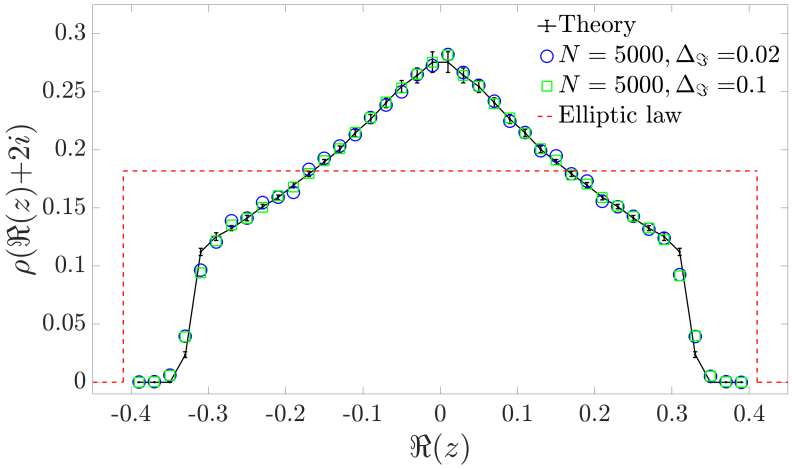

(a) $\Im(z) = 2$

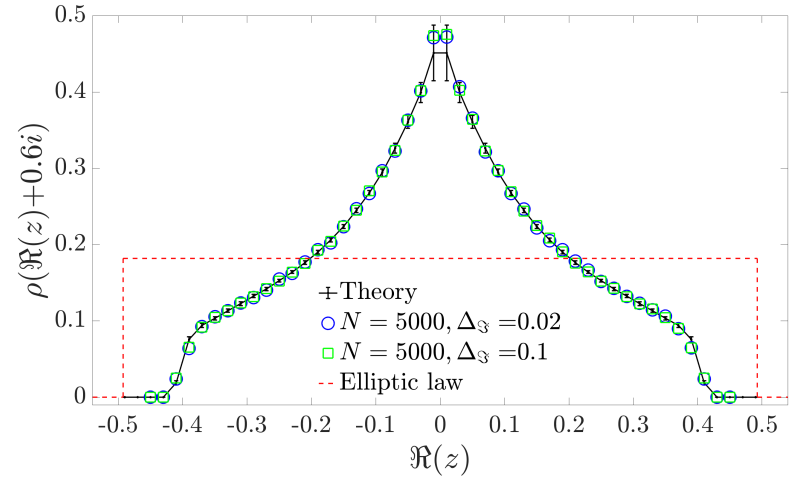

(b) $\Im(z) = 0.6$

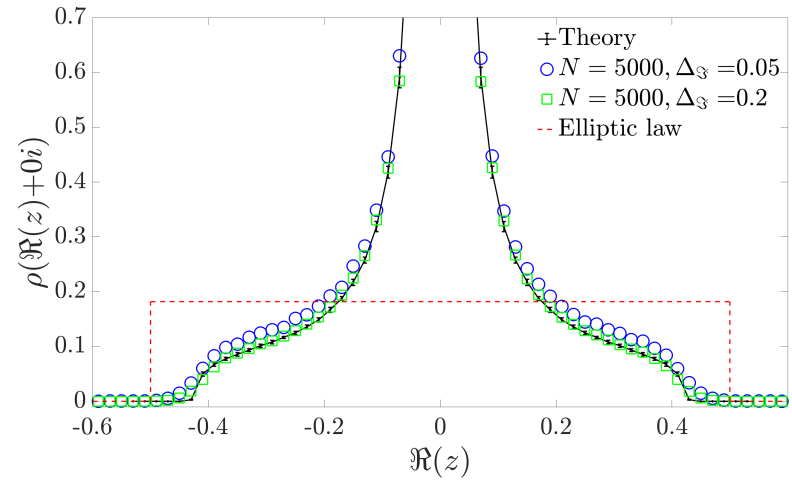

(c) $\Im(z) = 0$

Figure 5.7: The spectral distribution ρ along cuts parallel to the real axis for random matrices of Model A with $c = 4$. The values of $\Im(z)$ are indicated in the captions and the cuts are shown in Fig. 5.6. Theoretical results from the cavity method (solid black line) are compared with histograms obtained by numerically diagonalising 10^4 matrices of size $N = 5000$ and collecting all eigenvalues in a strip of width $\Delta_\Im$ (markers). The spectral distribution is also compared with the elliptic law given by Eqs. (4.43-4.44) with $\sigma^2 = c$ and $\tau = -3c/4$ (red dashed line). Error bars denote the numerical error on the ρ value computed with population dynamics, as explained in Sec. 4.5.

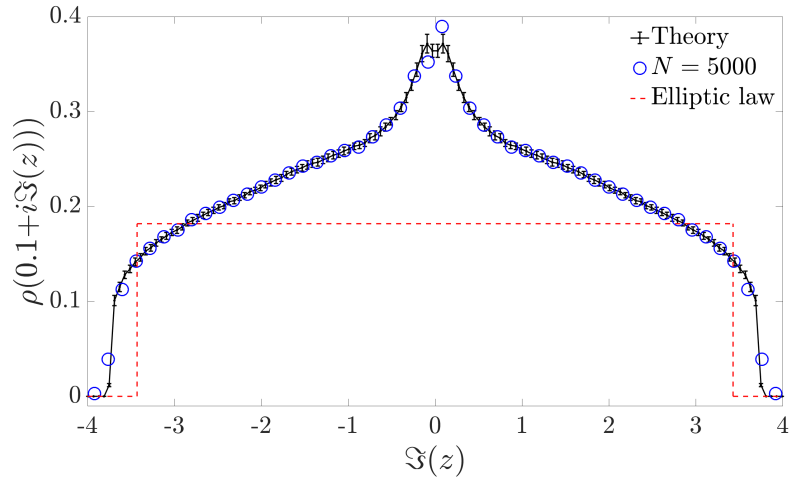

(a) $\Re(z) = 0.1$

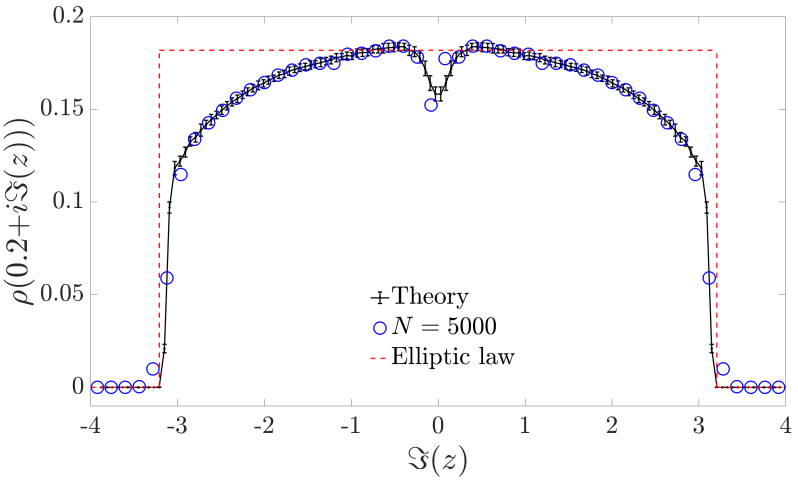

(b) $\Re(z) = 0.2$

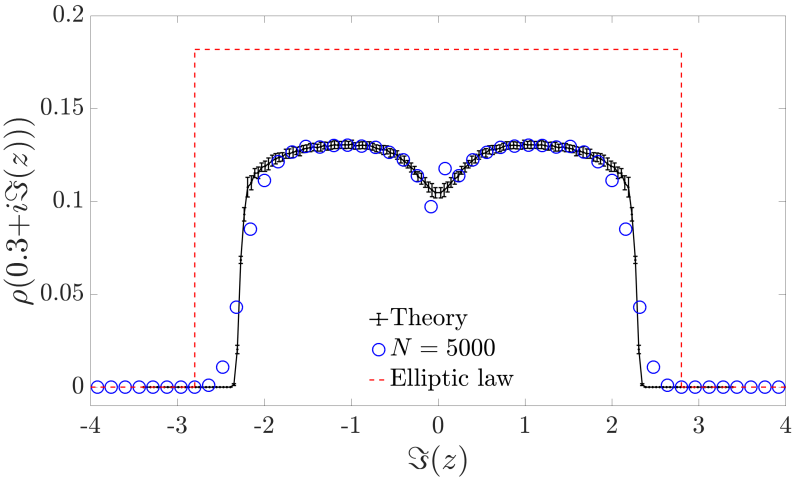

(c) $\Re(z) = 0.3$

Figure 5.8: The spectral distribution ρ along cuts parallel to the imaginary axis for random matrices of Model A with $c = 4$. The present figure is similar to Fig. 5.3, with the difference that the spectral distribution ρ shown is for cuts parallel to the imaginary axis. The values of $\Re(z)$ are given and the width $\Delta_{\Re} = 0.02$.

above, there are strong non-uniformity in the slopes of the profiles, in particular in correspondence of the intersections with the imaginary and real axes.

5.3 Emergence of long tails in the spectra of mixture matrices on Erdős-Rényi graphs

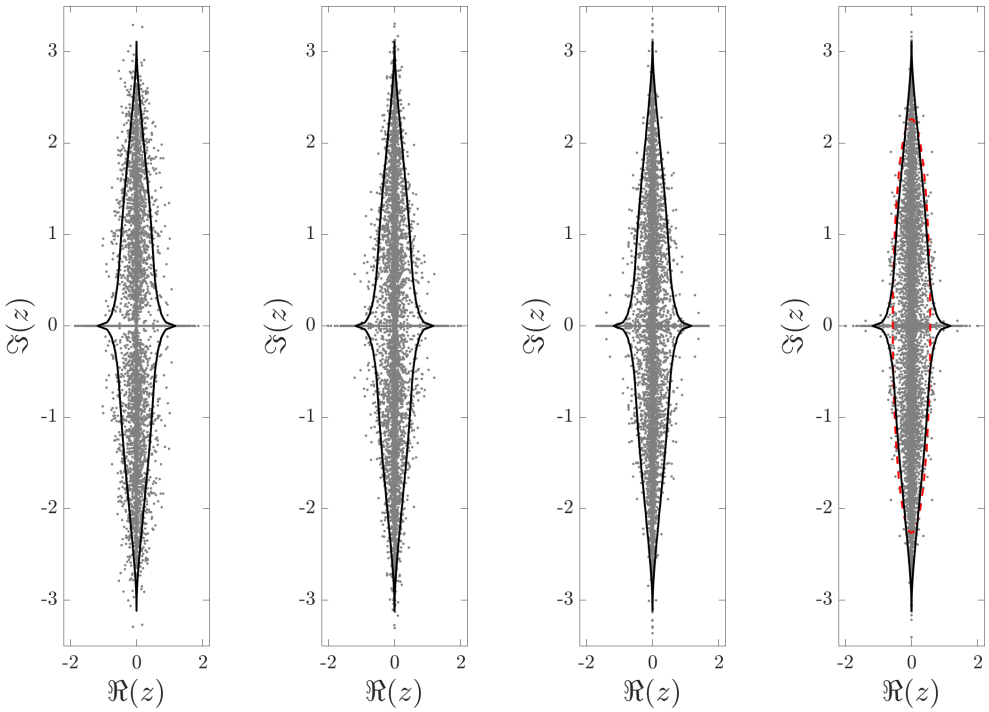

(a) $N = 10$ (b) $N = 10^2$ (c) $N = 10^3$ (d) $N = 10^4$

Figure 5.9: Spectra of mixture random matrices on Erdős-Rényi graphs with mean degree $c = 2$ (Model B in Sec. 2.2). Gray markers are the eigenvalues of m_s matrices of size N, with $m_s = 10^4/N$, randomly drawn from this ensemble and obtained through direct diagonalization routines. Continuous black lines are theoretical results for $N \to \infty$ obtained with the cavity theory of Sec. 4.3. Red dashed lines shown in panel (d) represents the boundary of the elliptic law given by Eqs. (4.43-4.45) with $\sigma^2 = c$ and $\tau = -3c/5$.

In the study of antagonistic matrices we saw that for small mean degrees and on Erdős-Rényi graphs we saw the emergence of the reentrance phenomenon in the spectra, which was absent in the random regular case. Here we address the study to answer the question whether a reentrance can be found also in mixture matrices on Erdős-Rényi graphs with mean degree $c = 2$. Accordingly, we focus here on the boundary of $\mathcal{S}$ for matrices of Model B, namely, mixture matrices in for which 90% of the interactions are of the predator-prey type, 5% of competitive interactions, and 5% are mutualistic interactions.

Figure 5.9, shows a very good agreement between eigenvalues from direct diagonalization and the boundary of the spectrum as predicted by the theory for $N \to \infty$, a part from the sample fluctuations for small sizes, similarly to the antagonistic counterparts Fig. 5.5, panels (e)-(h). Remarkably, the big difference with the antagonistic case is evident when approaching the real axis, where here the boundary of the support shows opposite convexity and the eigenvalues extend on the real axis. The reentrant behaviour observed at $c = 2$ for antagonistic matrices (see Fig. 5.5) has disappeared for mixture matrices. In addition, we observe that mixture matrices are characterised by long tails of eigenvalues on the real axis that persist for large sizes N, whereas they are absent in the spectra of antagonistic matrices when increasing the system size N. These observed tails are reminiscent of the Lifshitz tails in symmetric and sparse random matrices [Bapst and Semerjian, 2011; Khorunzhiy et al., 2006; Kühn, 2008; Rodgers and Bray, 1988; Slanina, 2012], where the support $\mathcal{S}$ covers the whole real axis. The tails of eigenvalues on the real axis are typical in the spectra of sparse random matrices on undirected random graphs defined on unbounded degree distributions, as discussed in Ch. 1, and their absence in the antagonistic matrices renders this ensemble a very interesting exception. Such tails suggest a potential divergence of the leading eigenvalue of sparse large matrices. We investigate more about the potential divergence of the leading eigenvalue and the tails of the spectrum in antagonistic and mixture matrices in Ch. 6.

We discuss finally about the estimate of the boundary provided by the adaptation of the elliptic law in Eqs. (4.43-4.45). Discrepancies emerge also for mixture matrices, as shown in Fig. 5.9, and this time are due to the emergence of tails on the real line as discussed above, which cannot be described with the elliptic law. Therefore, especially for mixture matrices, the predictions on the leading eigenvalue that can be obtained by neglecting the local graph topology and using a adaptation of the elliptic law to the sparse case are completely unreliable, and more studies on the leading eigenvalue are needed (see Ch. 6).

5.4 Summary of this chapter: the main results

We found a reentrance in the boundary of the support of the spectral distribution for matrices of model A with mean degree $c = 2$, namely for antagonistic matrices on Erdős-Rényi graphs (see Fig. 5.5). We named this phenomenon as the reentrance effect. Remarkably, this behaviour characterises antagonistic matrices of Model A, where the degree distribution has fluctuations and the interactions are of only predator-prey kind. Indeed, the reentrance effect disappear when changing one of the two features: when the degree distribution is regular (see Fig. 5.1), and when interactions contains also a small fraction of mutualistic or competitive kind (see Fig. 5.9).

Another important result that we found is the appearance of long tails on the real axis in the spectra of mixture matrices, which persist at large system sizes. These tails are surprisingly absent in the antagonistic case. The existence of these tails suggests a potential divergence of the leading eigenvalue as a function of the system size.

Finally, we have corroborated our theory on the spectral distribution and its support for infinitely large sparse matrices with pairwise correlated interactions by comparing the theoretical predictions with data obtained from direct diagonalization of finite matrices. Remarkably, already at system sizes of $\mathcal{O}(10^3)$ the theory and the direct diagonalization data result to be in very good agreement.

Chapter 6

The leading eigenvalue: stability and dynamical implications

In this chapter we aim to characterise more in detail the existence of tails of eigenvalues and the reentrance effect found in Ch. 5, by focusing on the leading eigenvalue λ_1. As discussed in Ch. 1, λ_1 is also the key variable for the stability and dynamical properties in the proximity of the fixed points of the dynamics. Chapter 5 has shown also that the theory that we have developed in Ch. 4 is robust in predicting the support $\mathcal{S}$ and the spectral distribution ρ for large sparse random matrices with pairwise correlated interactions. Equipped with this powerful theory, this chapter presents a quantitative study on the leading eigenvalue. In Sec. 6.1 we briefly discuss properties of the leading eigenvalue and how it can be determined from the theory of Ch. 4. Section 6.2 studies the dependence of the leading eigenvalue on the system size for matrices of Model A (antagonistic) and Model B (mixture), defined in Sec. 2.2. Section 6.3 presents a numerical study for the theoretical prediction of the leading eigenvalue of Model A and Model B. In Sec. 6.4 we discuss the studies of Secs. 6.2-6.3 in light of the stability of the associated fixed points. Section 6.5 explores the role of the network topology on the leading eigenvalue and its impact on the stability. In Sec. 6.6 we characterise the reentrance effect of Model A by studying the imaginary part of the leading eigenvalue as a function of the mean degree. Finally, we explore the consequences of the reentrance effect and of the study in Sec. 6.7 at the level of the dynamics of antagonistic systems in the vicinity of fixed points.

6.1 The leading eigenvalue of sparse random matrices

In general the leading eigenvalue of sparse random matrices is not self-averaging. This can be understood from the fact that small cycles persist in the limit $N \to \infty$ for sparse random matrices when the underlying graph has a giant component (in Appendix A.8 we discuss the criteria for the existence of a giant component in various random graph models). Indeed, the small cycles may create stochastic outlier eigenvalues in the point

spectrum that may also be leading eigenvalues, as discussed in Ref. [Bonneau et al., 2017; Neri and Metz, 2020]. Accordingly, when considering the leading eigenvalue λ_1, there is a finite, albeit small, probability that λ_1 is contributed by a cycle of finite length, and therefore the leading eigenvalue is not a self-averaging quantity. On the other side we remind that, as discussed in Sec. 3.6, the support $\mathcal{S}$ is equal (see Eq. (3.56)) to the continuous part of the spectrum that is self-averaging. Although we cannot compute the exact contribution of cycles to λ_1, we can use the theory presented in Ch. 4, to compute, when the underlying graph has a giant component, the typical value λ_1^* of the leading eigenvalue from the support, as follows

$$\lambda_1^* = \text{argmax}\left\{\Re(z) : z \in \mathcal{S}\right\}, \tag{6.1}$$

where in Eq. (6.1), as in Eq. (A.1), we use the convention to choose the value with the largest imaginary part in case there are several eigenvalues with a maximum $\Re(z)$. We remind that, as discussed in Ch. 3, the cavity method for locally treelike matrices become exact in the limit of $N \to \infty$ to determine self-averaging quantities, such as the spectral distribution, its support $\mathcal{S}$ and the typical value λ_1^*. In fact, these self-averaging quantities are not influenced by the finite number of finite length cycles that can exist in the limit of $N \to \infty$, which at most produces stochastic outliers.

We note that, as argued in Ref. [Neri and Metz, 2020], when there exists a giant component it is expected that the contribution of the small cycles to the leading eigenvalue is small, even in the limit of $N \to \infty$, and λ_1 is dominated by its typical value λ_1^*. In this Chapter we focus on the regime when there exists a giant component.

Below we discuss how the typical value λ_1^* of the leading eigenvalue can be obtained by using Eq. (6.1).

6.1.1 Determination of the leading eigenvalue

We show here how we have implemented Eq. (6.1) to obtain λ_1^*, i.e., the typical value of the leading eigenvalue for antagonistic matrices of Model A, from the population dynamics results for the boundary of the support $\mathcal{S}$ (that can be determined as explained in Sec. 4.6).

Since for antagonistic matrices the slope of the boundary of $\mathcal{S}$ is vertical, as shown in Fig. 5.5, one needs to control the fluctuations in the population dynamics algorithm to obtain an accurate value of λ_1^*. To this aim, we use a cubic fit on the values for the boundary of $\mathcal{S}$ obtained with the population dynamics algorithm. This procedure is shown in Fig. 6.1, which shows data points for the boundary of $\mathcal{S}$ in the vicinity of λ_1^* for three values of the mean degree c and also shows a cubic fit through these data points. We finally obtain an accurate estimate of λ_1^* by computing the maximum value of the fitted cubic polynomial.

In this chapter we apply the same method discussed here to determine the typical

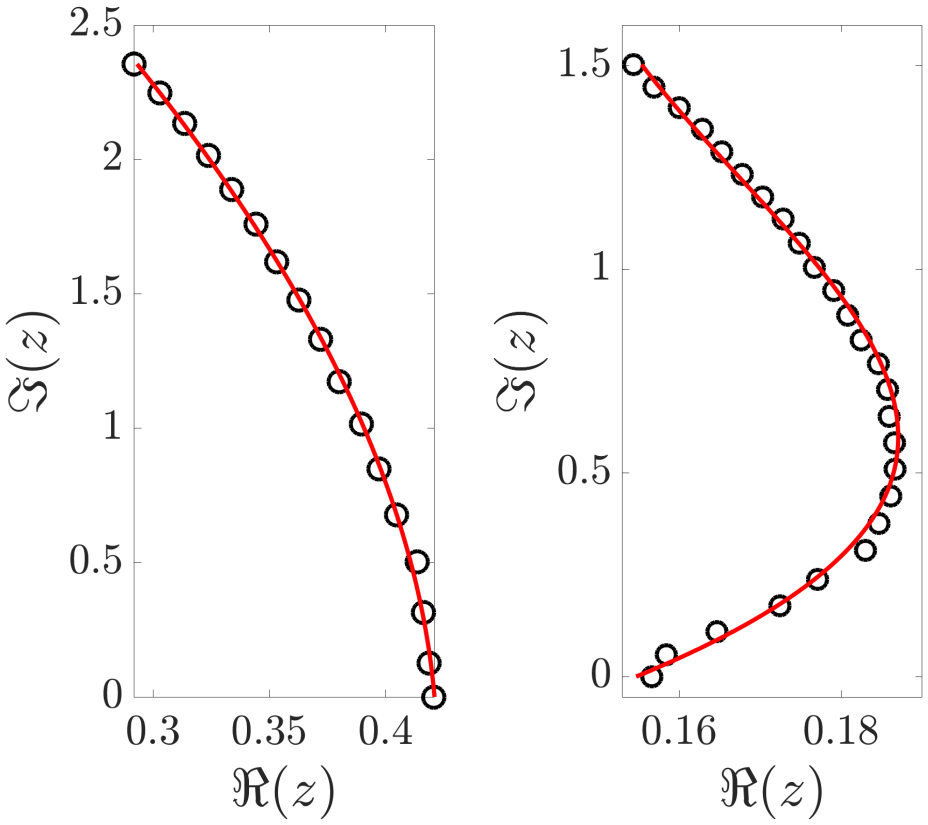

(a) $c = 4$ (b) $c = 2$

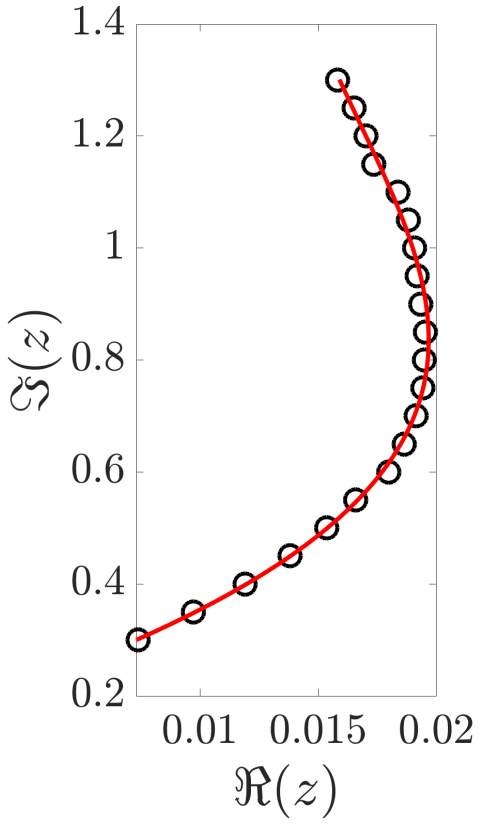

(c) $c = 1.3$

Figure 6.1: Cubic fits to the data points, obtained with the population dynamics algorithm described in Sec. 4.6, for the boundary of the support set in the vicinity of λ_1^*. Results shown are for Model A with mean degrees $c = 4$, $c = 2$ and $c = 1.3$. Panels (a) and (b) are a zoom of the spectra shown in Fig. 5.5.

value of the leading eigenvalue from the theory.

6.2 Dependence of the leading eigenvalue on the system size for antagonistic and mixture matrices

Inspired by the results on the boundary of the support that we presented in Ch. 5, in particular the differences between the spectra of Model A (antagonistic) in Fig. 5.5 and of Model B (mixture) in Fig. 5.9, we present here a study on the leading eigenvalue as a function of the system size N for matrices of Model A and of Model B at a fixed value of the mean degree c. We diagonalise 10^3 matrices sampled from Model A and Model B with $c = 4$ as a function of N, and compute the sample means of the leading eigenvalue λ_1. The sample means are estimates of the mean value

$$\langle \Re(\lambda_1) \rangle := \langle \Re(\lambda_1(\mathbf{A})) \rangle_{\mathcal{A}} \tag{6.2}$$

of the leading eigenvalue λ_1, where by $\langle \rangle_{\mathcal{A}}$ we denoted the ensemble average over the space $\mathcal{A}$ of random matrices $\mathbf{A}$, which here is either Model A or Model B.

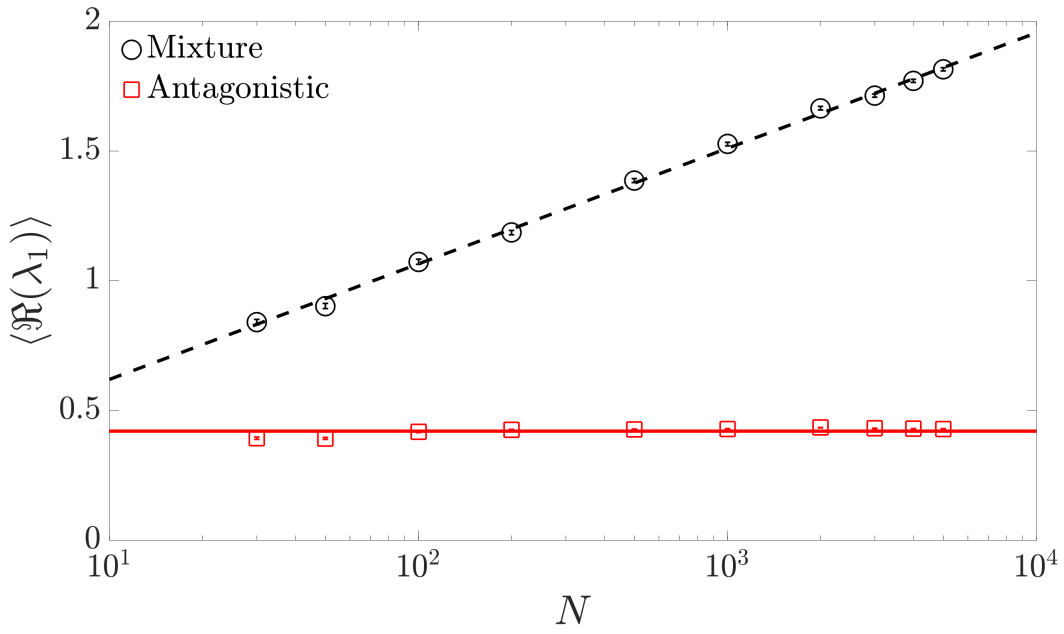

Figure 6.2: Real part $\langle \Re[\lambda_1] \rangle$ of the mean value of the leading eigenvalue λ_1 as a function of N for antagonistic matrices (Model A) and mixture matrices (Model B) on Erdős-Rényi graphs with mean degree $c = 4$. Markers are sample means of λ_1 obtained from directly diagonalising 10^3 matrices. The continuous red line is the typical value of $\Re(\lambda_1^*)$ obtained with the theory based on the cavity method, as discussed in Sec. 6.1, and the black dashed line is obtained from fitting the function $a \log(N) + b$ to the data.

Figure 6.2 shows the results. On one side, for antagonistic random matrices $\langle \Re[\lambda_1] \rangle$ is almost independent of N, and it exhibits very small fluctuations, on the other side for mixture matrices $\langle \Re[\lambda_1] \rangle$ diverges logarithmically as a function of N. We remind

here that, by definition of the models A and B (see Ch. 2), 100% of the interactions are predator-prey like in Model A, whereas 90% of the interactions are predator-prey like in Model B, and the remaining interactions are present in the same probability, i.e., 5% are mutualistic and 5% competitive. The result found here means that only a small non-zero fraction of mutualistic or competitive interactions is enough to imply major changes in the behaviour of the leading eigenvalue.

In Figure 6.2 we show also for Model A only the typical value λ_1^* of the leading eigenvalue evaluated from the theory, as discussed in Sec. 6.1, which is in very good agreement with the sample means data from direct diagonalization already at small values of $N \approx 10^2$. As we show in the next section, the theory in the large N limit provides a finite value λ_1^* for antagonistic matrices, while for mixture matrices we obtain that λ_1^* is infinitely large.

6.3 Theoretical predictions for the leading eigenvalue of antagonistic and mixture matrices: a numerical study

Here we discuss the theoretical predictions on the typical value λ_1^* of the leading eigenvalue for infinitely large matrices of Model A and Model B with $c = 4$, consistently with Fig. 6.2, in order to highlight the differences between these two models at the level of λ_1^*. In order to do so, we present now a numerical study on the boundary of the support. Indeed, as discussed in Sec. 6.1, λ_1^* can be determined from the support $\mathcal{S}$. Accordingly, a detailed numerical study on the boundary of $\mathcal{S}$ can lead to important conclusions on λ_1^*, in particular to determine whether it is finite or not.

As explained more in detail in Sec. 4.6, the boundary of $\mathcal{S}$ is obtained by determining the value of z that separates the region where $\langle |h| \rangle_{\hat{Q}}$ diverges from the region where $\langle |h| \rangle_{\hat{Q}}$ converges to zero, where $\hat{Q}$ is the population of size N_p, obtained with the population dynamics algorithm, that estimates the solution of the distributional equation in Eq. (4.24). We focus on the real axis, that is where λ_1^* lies for matrices of Model A and Model B with $c = 4$.

Practically, we evaluate $\langle |h| \rangle_{\hat{Q}}$ as follows. We initialise the $(g^{(i)}, h^{(i)})$ with the uniform distribution

$$p_{\text{init}}(g, h) = \frac{1}{\Delta^2}, \quad g \in [-\Delta, \Delta], h \in [-\Delta, \Delta], \tag{6.3}$$

for which we have set $\Delta = 10$, but the precise value of Δ does not influence the results. Subsequently, we compute

$$\langle |h| \rangle_{\hat{Q}} = \frac{1}{n_{\text{r}} N_{\text{p}}} \sum_{j=1}^{n_{\text{r}} N_{\text{p}}} |h^{(j)}|, \tag{6.4}$$

with $n_{\text{r}} = 500$. In addition, in order to obtain an estimate of the fluctuations in $\langle |h| \rangle_{\hat{Q}}$ between different realisations of the population dynamics algorithm, we repeat this procedure a $\mathcal{N} = 10$ times, i.e., we compute $\langle |h| \rangle_{\hat{Q}}$ for $\mathcal{N}$ runs of the population dynamics

algorithm with different initial realisations of $(g^{(i)}, h^{(i)})$.

Figure 6.3 shows the mean of $\log \langle |h| \rangle_{\hat{Q}}$ taken over the $\mathcal{N}$ realisations of the population dynamics algorithm as a function of $\Re(z)$ for Model A and Model B with mean degree $c = 4$ and $\Im(z) = 0$. Plots show $\log \langle |h| \rangle_{\hat{Q}}$ for various values of the population size $N_{\rm p}$ and we evaluate it at different number $n_{\rm s}$ of sweeps ($n_{\rm s}$ is proportional to the number of iterations of the population dynamics algorithm, see Sec. 4.6). The error on the mean value of $\log \langle |h| \rangle_{\hat{Q}}$ is obtained from the standard deviation of $\log \langle |h| \rangle_{\hat{Q}}$ on the sample of $\mathcal{N} = 10$ realisations.

In the case of antagonistic matrices, all lines intersect in a common point, which provides the estimate of the boundary of the support set $\mathcal{S}$. On the other hand, in the case of mixture matrices, the intersection point for different $n_{\rm s}$ increases as a function of the population size $N_{\rm p}$. This fact implies that the intersection point diverges as a function of $N_{\rm p}$ and the real axis belongs to the support set $\mathcal{S}$.

In terms of the typical value λ_1^* of the leading eigenvalue, the results obtained here imply that λ_1^* is not finite for model B, while it is finite for Model A. As we anticipated before, these results λ_1^* corroborates the result of Fig. 6.2 that shows that the leading eigenvalue of mixture matrices diverges as a function of N, while the leading eigenvalue of antagonistic matrices converges to a finite value as a function of N. Although we can not compute exactly the contribution of small cycles on the leading eigenvalue, as discussed in Sec. 6.1, Fig. 6.2 suggests some qualitative considerations on this contribution. More in detail, the very good agreement between the direct diagonalization results on the sample means already at small values of N, where there are many cycles, and the typical value from the theory indicates that the contribution of small cycles to the leading eigenvalue is small, and λ_1 results to be dominated by its typical value λ_1^*.

The results found for mixture matrices of Model B, both in terms of the logarithmic dependence on the system size of the mean $\langle \Re[\lambda_1] \rangle$ in Fig. 6.2, and of the theoretical prediction of the divergence of its typical value λ_1^* in the infinite size limit as discussed above, provide a more quantitative characterisation of the tails observed in the spectra of matrices of Model B presented in Fig. 5.9. We observe that these results found in mixture matrices are similar to the divergent behaviour of the leading eigenvalue of undirected graphs, and to the Lifshitz tails in the spectrum of sparse and symmetric matrices, where the support of the spectral distribution contain the whole real axis (see Ch. 1).

6.4 Large antagonistic systems can be stable, while mixture can not

The different results on the leading eigenvalue of matrices of Model A and Model B presented in Sec. 6.2 and in Sec. 6.3 lead to important implications at the level of the stability of the associated fixed points. Indeed, within the linearised dynamics approach presented in Ch. 1, the stability criteria in Eq. (1.13) assures that, when a system is

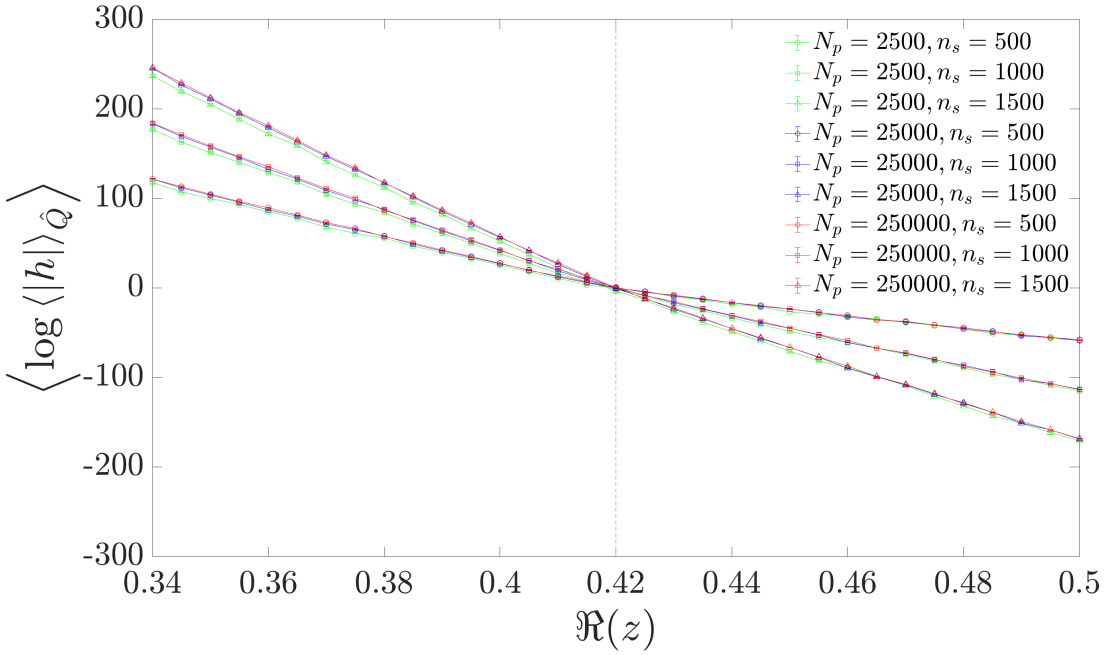

(a) Antagonistic

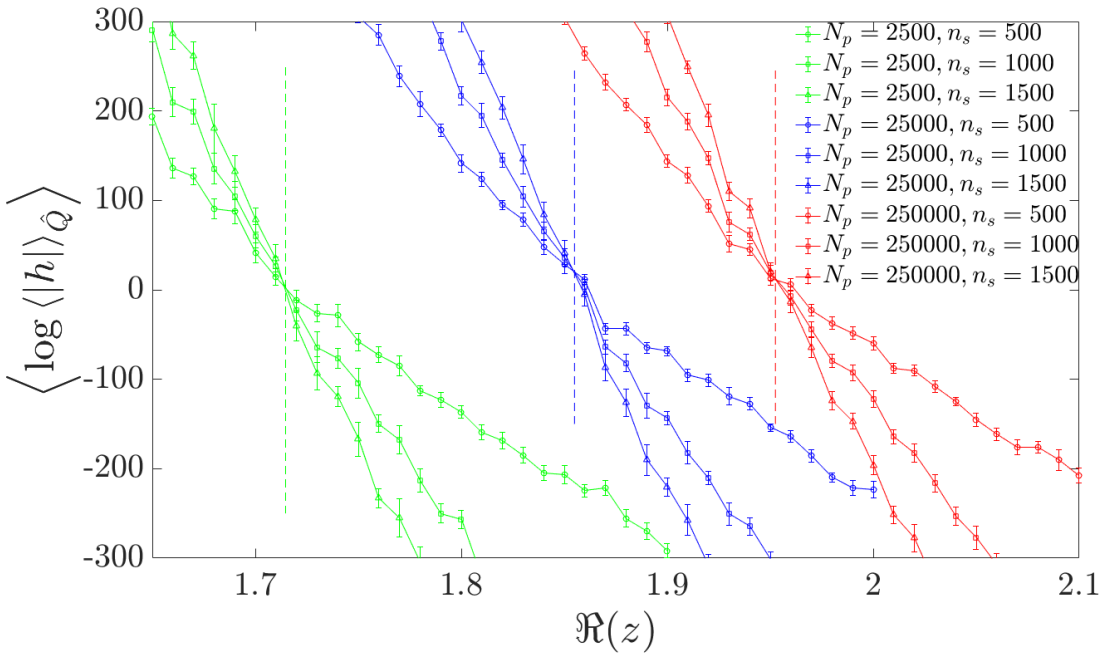

(b) Mixture

Figure 6.3: Plots of $\log \langle |h| \rangle_{\hat{Q}}$ as a function of $\Re(z)$ for antagonistic matrices (Model A in Sec. 2.2, panel (a)) and mixture matrices (Model B in Sec. 2.2, panel (b)). The mean degree $c = 4$ and $\Im(z) = 0$. The markers are obtained with the population dynamics algorithm described in Sec. 4.6 with the population size N_p and the number of sweeps n_s as given in the legend, and the error bars denote the estimated error obtained with repeated realisations of the population dynamics algorithm.

characterised by a finite self-regulation parameter d that is large enough, if the real part of the leading eigenvalue does not increase as a function of N, then the fixed points are stable. We found that this is the case for antagonistic matrices of Model A, i.e., infinitely large systems with predator-prey interactions can be stable. On the other side, for mixture matrices of Model B a finite but large d can not guarantee the stability of the fixed point, since the leading eigenvalue grows with N and the system becomes almost surely unstable for large N. In other words, infinitely large systems that contain mutualistic and competitive interactions are always unstable.

Remarkably, the results for mixture matrices have been obtained using $\pi^{\mathrm{A}} = 0.9$ for Model B, indicating that a small fractions of competitive (i.e., 5%) and mutualistic i.e., (5%) interactions are sufficient to render a system unstable in the infinite size limit. As a consequence, sparse and large dynamical systems are in general unstable, unless they only contain predator-prey interactions. This behaviour represents a surprising result in the stability of complex systems, because the dense ensembles with predator prey interactions become unstable when large enough, as well as sparse systems with symmetric interactions (see Ch. 1). We remind that the sparse oriented ensemble (see Ch. 2 and Sec. 4.4.1), characterised by unidirectional interactions on sparse directed random graphs, is also another example of stable system in the infinite size limit.

Given these results, in the next section we investigate how the system stability, represented by the leading eigenvalue, is influenced by the mean degree and the degree fluctuations.

6.5 Influence of network topology on the leading eigenvalue

Here we study how the leading eigenvalue depends on the network topology, in particular the mean degree c and the degree fluctuations. Given that antagonistic systems can be stable, as shown in Sec. 6.4, we focus on this ensemble to infer more stability properties.

By first looking at the differences between the spectra of large antagonistic matrices on random regular graphs and Erdős-Rényi graphs presented in Ch. 5, for a fixed value of the mean degree $c = 4$, we can set the study on how the network topology influences the stability properties of antagonistic systems. In particular, we look at one realisation of a large matrix of size $N = 10^4$, which are panels (d) of Fig. 5.1 and Fig. 5.5, and we put them next to each other in panels (a) and (b) of Fig. 6.4, where we set the same horizontal and vertical scales. More in detail, we set the horizontal range to be equal to the biggest projection of the two spectra on the real axis (which is given by the random regular, in panel (a)), and we set the vertical range to be equal to the biggest projection of the two spectra on the imaginary axis (which is given by the Erdős-Rényi, in panel (b)). Fig. 6.4 clearly shows the qualitative difference between the two spectra: from panel (a) to panel (b), the eigenvalues shrink on the real axis, and elongate on the imaginary axis. This shrinking behaviour translates, in particular, into the fact that the

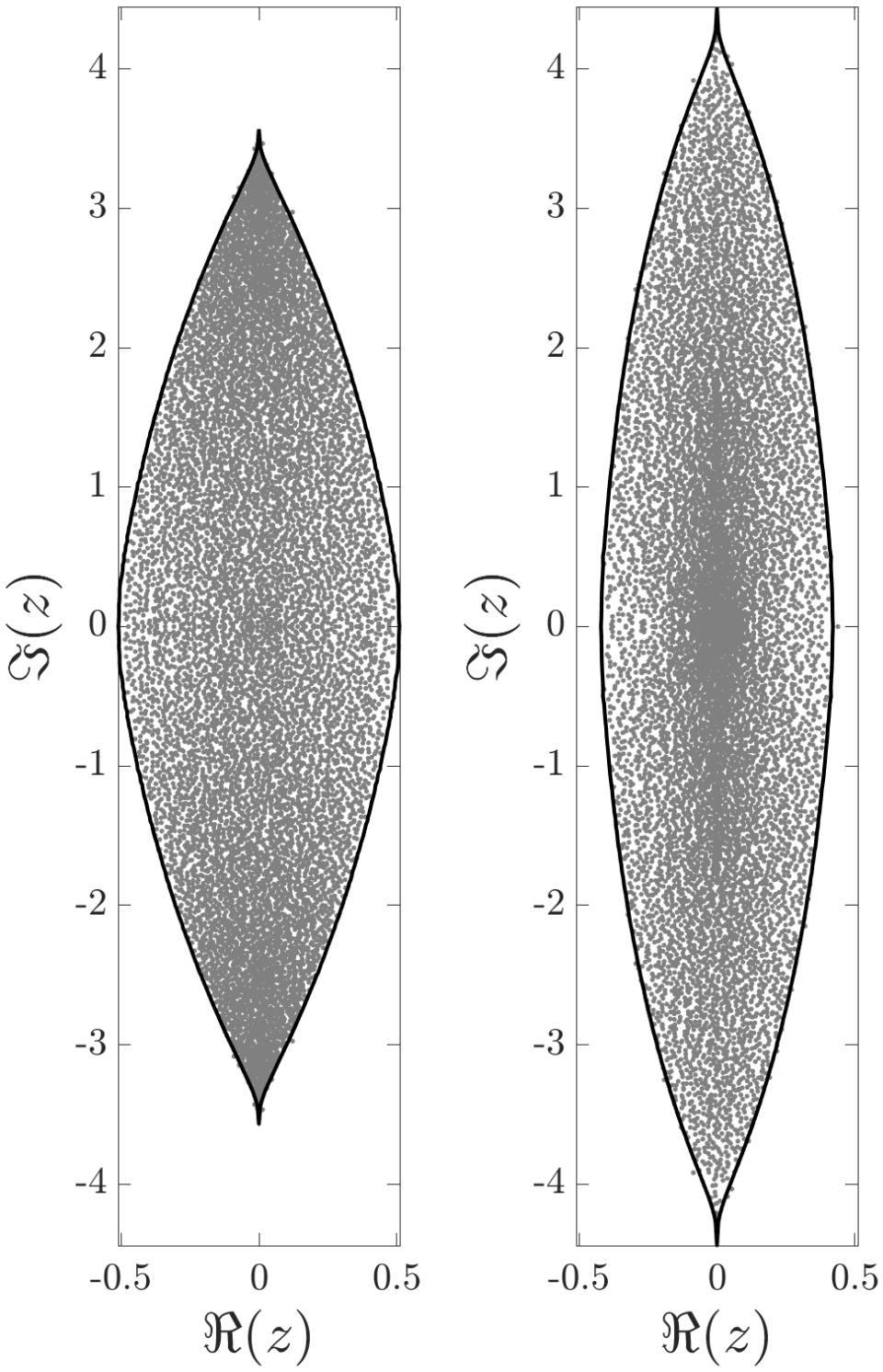

(a) Random regular

(b) Erdős-Rényi

Figure 6.4: Spectra of antagonistic random matrices on a random regular graph (panel (a)) and on a Erdős-Rényi graph (panel (b)) (Model A in Sec. 2.2) with mean degree $c = 4$, as in panels (d) of Fig. 5.1 and Fig. 5.5. To facilitate the visual comparison, we set here the same horizontal and vertical scales in the two panels: the horizontal and vertical ranges are set exactly to cover the biggest projections, among the two spectra in the two panels, of the support on the real and imaginary axes.

typical value λ_1^* of the leading eigenvalue of antagonistic matrices on Erdős-Rényi graphs is smaller than the one on random regular graphs, for $c = 4$.

In terms of stability, this means that a smaller d is needed to have stability for antagonistic matrices on Erdős-Rényi graphs than on random regular graphs. Equivalently, for all the values of d that are greater than the leading eigenvalue of antagonistic matrices on Erdős-Rényi graphs, but smaller than antagonistic matrices on random regular graphs, one has that the first systems are stable, while the second are not. In synthesis, for $c = 4$, antagonistic systems on Erdős-Rényi graphs seem to be more stable than antagonistic matrices on random regular graphs. This surprising effect, derived for a fixed value of the mean degree c, is a nontrivial stabilising effect that is due only to the degree fluctuations in the network topology of Erdős-Rényi graphs. In the next subsection, we analyse what happens when we vary the mean degree c, in order to systematically confirm or not this behaviour.

Since we want to understand also if the effects of network topology are generic or depend on the interactions, we consider the oriented random matrices (see Ch. 2), where the interactions are unidirectional, because also in this ensemble the leading eigenvalue of an infinitely large matrix is finite (see Ch. 1 and [Neri and Metz, 2020]). For the antagonistic ensemble, we consider the distribution $\tilde{p}$ given by Eq. (2.19), and for the oriented ensemble $\tilde{p}$ is an arbitrary distribution with unit variance and zero mean. Indeed, for oriented matrices the precise form of $\tilde{p}$ does not matter as $\Re(\lambda_1)$ only depends on its variance and mean value.

We present now two analyses. First, in Sec. 6.5.1, we study how the leading eigenvalue of antagonistic and oriented matrices depends on the mean degree of the underlying graph, for random regular and Erdős-Rényi graphs. Second, in Sec. 6.5.2, we consider the antagonistic and oriented matrices on a random graph ensemble described by a prescribed degree distribution p_{deg} that allows to control variance

$$\mathrm{Var}(k) = \langle k^2 \rangle_{p_{\mathrm{deg}}} - c^2, \tag{6.5}$$

in order to study how the degree fluctuations impact the stability.

6.5.1 Dependence of the leading eigenvalue on the mean degree

Here we study the dependence of the typical value of the leading eigenvalue on the mean degree c, for infinitely large antagonistic and oriented matrices on Erdős-Rényi graphs and random regular graphs, from the theory as discussed in Sec. 6.1. The aim is to understand systematically whether the stabilising effect of Erdős-Rényi graphs for antagonistic matrices, discussed above, depends on the mean degree and the role of the nature of interactions.

We perform our analyses in the regimes above the percolation threshold, i.e., where a large connected, component exist for undirected graphs (for the antagonistic ensembles),

and where a large strongly connected component exists for directed graphs (for the oriented ensembles). Otherwise, below the percolation threshold, small cycles give a dominant contribution on the leading eigenvalue [Neri and Metz, 2020] and Sec. 6.1). We discuss the criteria for the existence of a giant component in Appendix A.8. These regimes are given by $c > 1$ for Erdős-Rényi graphs, $c > 2$ for random regular graphs for the undirected ensembles, and by $c > 2$ Erdős-Rényi graphs, $c > 3$ for the random regular graphs for the directed ensembles.

Figure 6.5(a) shows $\Re(\lambda_1^*)$ for the antagonistic ensemble on Erdős-Rényi graphs (Model A), and on random regular graphs, as a function of c. First, we find that the value $\Re(\lambda_1^*)$ monotonically increases as a function of c for every ensemble. Second, in light of the discussions on stability made above, Fig. 6.5(a) shows that if interactions are of the predator-prey type, then Erdős-Rényi graphs are more stable than random regular graphs for all values of c, since the $\Re(\lambda_1^*)$ of Erdős-Rényi graphs is always smaller than the one correspondent to random regular ones.

Figure 6.5(b) presents the real part of the leading eigenvalue as a function of c for oriented matrices, for a comparison with the study for antagonistic matrices in Fig. 6.5(a). The interactions (J_{ij}, J_{ji}) for oriented matrices are random variables drawn from the distribution given by Eq. (2.5) with $\tilde{p}$ an arbitrary distribution with zero mean and unit variance, i.e., $\langle l^2 \rangle_{\tilde{p}} = \langle u^2 \rangle_{\tilde{p}} = 1$. In this case, the boundary of the support set $\mathcal{S}$ is given by [Neri and Metz, 2020]

$$|z|^2 = \frac{\langle k(k-1) \rangle_{p_{\text{deg}}}}{2c}, \tag{6.6}$$

as derived also in Appendix 4.4 from the theory based on the cavity method presented in Ch. 4, and therefore

$$\Re(\lambda_1^*) = \sqrt{\frac{\text{Var}(k) + c^2 - c}{2c}}. \tag{6.7}$$

Comparing the values of the typical value $\Re(\lambda_1^*)$ of the leading eigenvalue in Figs. 6.5(a) and 6.5(b), we observe that dynamical systems with predator-prey interactions are more stable than those with unidirectional interactions. Moreover, we find that for antagonistic systems, characterised by having only predator-prey interactions, on Erdős-Rényi graphs are more stable than when on random regular graphs, while for oriented systems, characterised by unidirectional interactions, it is the other way around. We study more in detail the dependence of the leading eigenvalue on the degree fluctuations in the next section

Figs. 6.5(a) and 6.5(b) show also the leading eigenvalue that is obtained from the adaptation of the elliptic law in Sec. 4.7. Comparing the results for sparse matrices obtained with the cavity method with the predictions from the adaptation of the elliptic law, which ignores the presence of an underlying network, we find that the elliptic law provides a reasonable quantitative prediction of the leading eigenvalue of antagonistic matrices only for values $c \gtrsim 4$, and that the best agreement is given by random regular graphs. On the other side, for oriented matrices we found that the adapted elliptic law

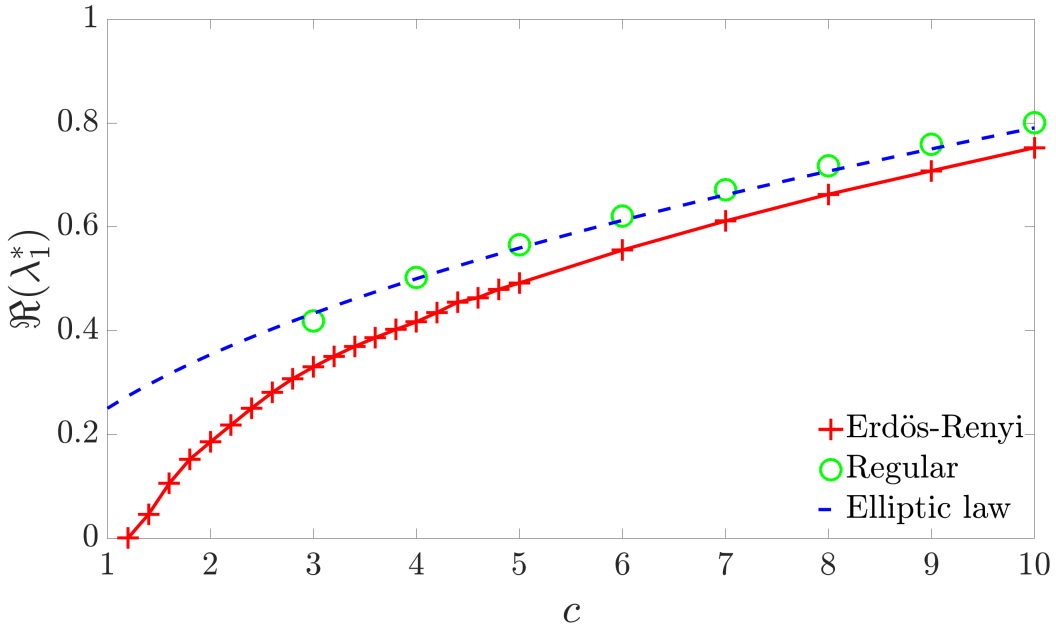

(a) Antagonistic

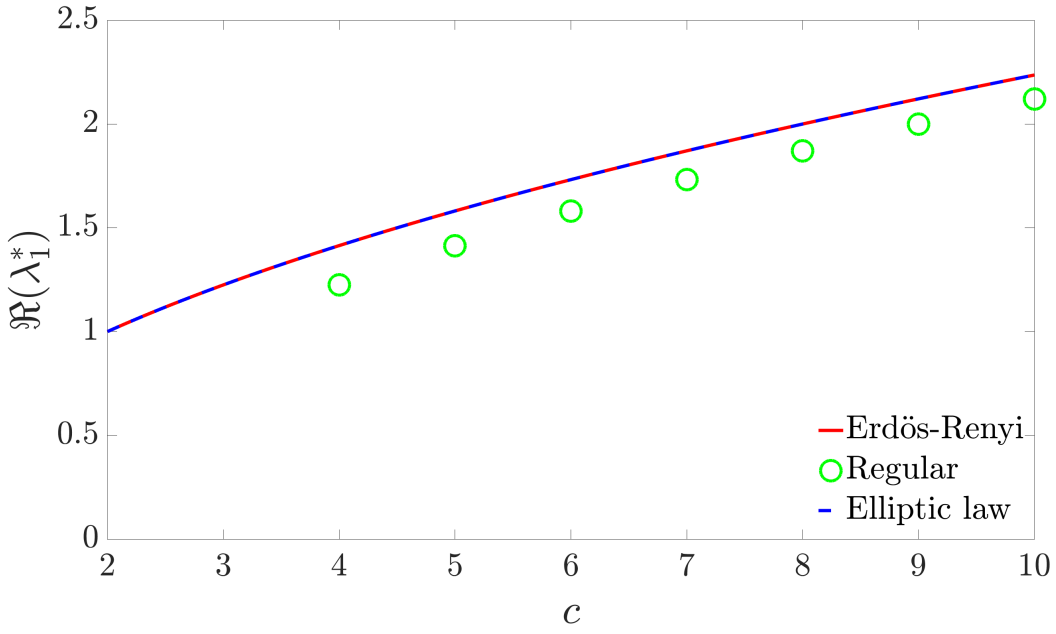

(b) Oriented

Figure 6.5: Real part $\Re(\lambda_1^*)$ of the typical leading eigenvalue value as a function of the mean degree c for antagonistic matrices [Panel (a)] and oriented matrices [Panel (b)], both defined on either Erdős-Rényi or regular graphs. For antagonistic matrices $\tilde{p}$ is given by Eq. (2.19) and for oriented matrices $\tilde{p}$ is an arbitrary distribution with unit variance and zero mean. Panel (a): predictions from the theory, as discussed in Sec. 6.1, (markers) are compared with the elliptic law given by Eqs. (4.43-4.45) (dashed blue line). The red line connecting the red crosses is a guide to the eye. Panel (b): analytical predictions from Eq. (6.7) are compared with the elliptic law given by Eqs. (4.43-4.45).

predictions match very well the theory for Erdős-Rényi graphs, while it systematically deviates from the random regular data.

From the study in this section, we can conclude that independently from the interactions and the underlying graph structure, the fixed points of the corresponding systems are more likely to be unstable when increasing the mean degree, as it was first shown in dense graphs in terms of connectance [May, 1972].

We investigate more on the role of the network topology on stability in the next section where we directly study how the degree fluctuations affect system stability, by interpolating between the two extreme cases of Erdős-Rényi (maximum degree fluctuations) and random regular graphs (no degree fluctuations).

6.5.2 Dependence on the degree fluctuations

Here we explore the role of degree fluctuations in oriented and antagonistic ensembles, in order to characterise the impact on stability for the corresponding systems.

We are interested to study the stability properties of infinitely large matrices, as in the previous Sec. 6.5.1, with the theoretical approach to determine the real part of λ_1^*, as discussed in Sec. 6.1. From Figs. 6.5(a) and 6.5(b) we gathered first evidences that degree fluctuations can have both a stabilising and a destabilising effect on system stability, depending on the kind of the interactions. Here, we aim at systematically studying the effect of degree fluctuations on system stability by analysing the dependency of the leading eigenvalue on the variance of the degree distribution at a fixed value of the mean degree c, interpolating between the random regular and Erdős-Rényi graphs discussed in the previous section. In other words, we study here the leading eigenvalue at fixed values of c in Figs. 6.5(a) and 6.5(b), where the independent variable is now the variance $\mathrm{Var}(k)$.

We therefore consider random graphs characterised by the prescribed degree distribution

$$p_{\mathrm{deg}}(k) = a\delta_{k,c} + (1-a)e^{-c}\frac{c^k}{k!}, \tag{6.8}$$

where $a \in [0,1]$. By varying the parameter a, we also modulate the variance of this degree distribution, which, as it can be easily verified, is given by

$$\mathrm{Var}(k) = c(1-a), \tag{6.9}$$

while keeping the mean degree c fixed.

In Fig. 6.6(a), we plot the real part of the leading eigenvalue $\Re(\lambda_1^*)$ for antagonistic matrices with $\tilde{p}$ given by Eq. (2.19) as a function of the variance of the degree distribution p_{deg} in Eq. (6.8) for different small discrete values of c. To facilitate the interpretation of the figure, we look at the extremal cases. On one side, at the left of the plot, when $\mathrm{Var}(k) = 0$, it corresponds $a = 1$, i.e., the underlying graph is a random regular graph.

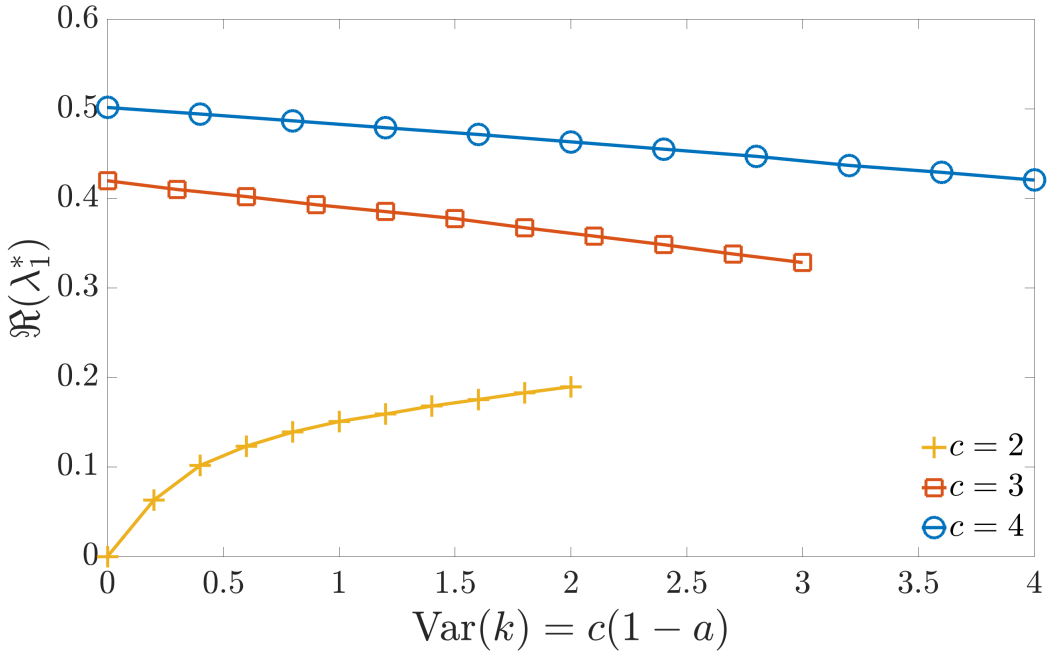

(a) Antagonistic

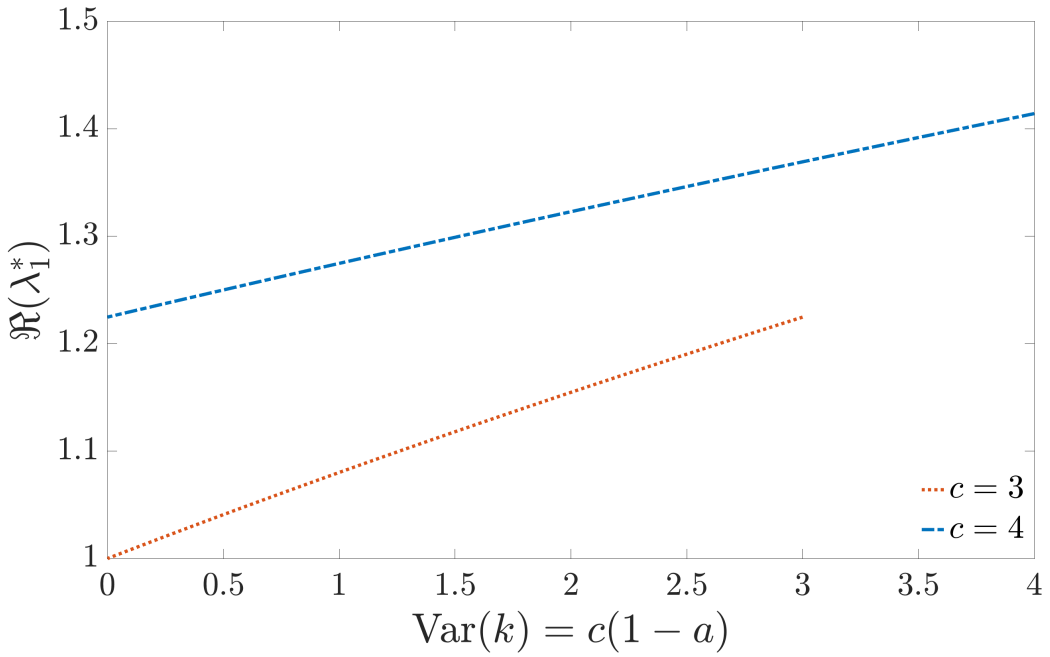

(b) Oriented

Figure 6.6: Real part of the leading eigenvalue $\Re(\lambda_1^*)$ as a function of the variance $\mathrm{Var}(k)$ for antagonistic and oriented random matrices, both defined on random graphs with the prescribed degree distribution Eq. (6.8). For antagonistic matrices $\tilde{p}$ is given by Eq. (2.19) and for oriented matrices $\tilde{p}$ is an arbitrary distribution with unit variance and zero mean. The markers in Panel (a) are obtained with the theory as discussed in Sec. 6.1, and lines are guides to the eye. The lines in Panel (b) are the theoretical results given by Eq. (6.7).

On the other side, at the right of the plot, when $\mathrm{Var}(k) = c$, — and hence the max value on the horizontal axis is determined by the value of c — it corresponds $a = 0$, i.e., the underlying graph is a Erdős-Rényi graph, in the infinite size limit. We observe that degree fluctuations tend to stabilise antagonistic dynamical systems as the real part of the leading eigenvalue decreases as a function of $\mathrm{Var}(k)$ for $c = 3, 4$. We find this fact as another very interesting behaviour of the antagonistic ensemble, since the leading eigenvalue typically grows with the maximal degree in sparse ensembles (see Ref. [Chung et al., 2004; Krivelevich and Sudakov, 2003] and Ch. 1), which is larger when the degree fluctuations increase, at fixed c. We do not represent here larger values of c, since we found that their content is equivalent to what has been found for $c = 3, 4$. A notable exception is instead when the mean degree $c = 2$, in which case $\Re(\lambda_1^*)$ increases as a function of the degree fluctuations.

In Fig. 6.6(b), we plot the leading eigenvalue for oriented matrices with $\tilde{p}$ an arbitrary distribution with zero mean and unit variance. Remarkably, in this case we obtain the opposite result, namely, that degree fluctuations always destabilise systems with unidirectional interactions, which is equivalent to the fact that in Fig. 6.5 the Erdős-Rényi curve is always above the points corresponding to random regular graphs. In fact, this result follows readily from Eq. (6.7). The interesting variability in the behaviour of the leading eigenvalues for antagonistic and oriented matrices, that we found in Sec. 6.5.1 and in Sec. 6.5.2, with also different behaviours for $c = 2$ than $c = 3, 4$ in Fig. 6.6(a), allows further considerations on the relation between system stability and the topology of the associated graph. Naively, one could make the hypothesis that the stability of systems defined on a graph is related to the size of its giant, i.e., largest connected, component. In particular a big giant component may have high chances that one of its nodes is unstable to local perturbations that diffuse to the whole giant component, giving rise to a global instability if the connected component spans the entire system. If this were the case, graphs with giant components should be associated to less stable systems and the different behaviour of the leading eigenvalue as a function of the degree fluctuations should be originated by opposite trends of the size of the giant component in antagonistic and oriented matrices. We explore this possibility in Appendix A.8 by evaluating the size of the giant component in the two cases. This comparison does not confirm the hypothesis, interestingly showing that the size of the giant component of the underlying interaction network does not directly influence the stability property of the system. Finally, the result we found suggest that the stabilising effects due to the networks topology depend intrinsically on the nature of the interactions.

6.6 Phase transition on the imaginary part of the leading eigenvalue for antagonistic systems

In Sec. 5.2 we found a reentrance phenomenon in the boundary of the support $\mathcal{S}$ of Model A (see Sec. 2.2) when $c = 2$ (see Fig. 5.5). Here we aim to systematically characterise this behaviour in terms of the imaginary part of the leading eigenvalue. Indeed, the reentrance effect translates into the fact that the typical eigenvalue λ_1^* (see Sec. 6.1) has a non-zero imaginary part. Remarkably, we observed that the reentrance phenomenon is absent in Model B, which has only a small fractions of competitive (i.e., 5%) and mutualistic i.e., (5%) interactions, and the majority (i.e., 90%) of predator-prey interactions. Indeed, the spectra of matrices with $c = 2$, shown in Fig. 5.9, are qualitatively completely different from the corresponding Model A with $c = 2$, and they are also characterised by tails of real eigenvalues. Accordingly, the reentrance phenomenon is a special feature that is found in antagonistic matrices with only predator-prey interactions, and it is lost when a small fraction of not predator-prey interactions are added. Here we aim to study the imaginary part of the leading eigenvalue as a function of the mean degree c, which determines also for which values of c there exists a reentrance effect in the corresponding support.

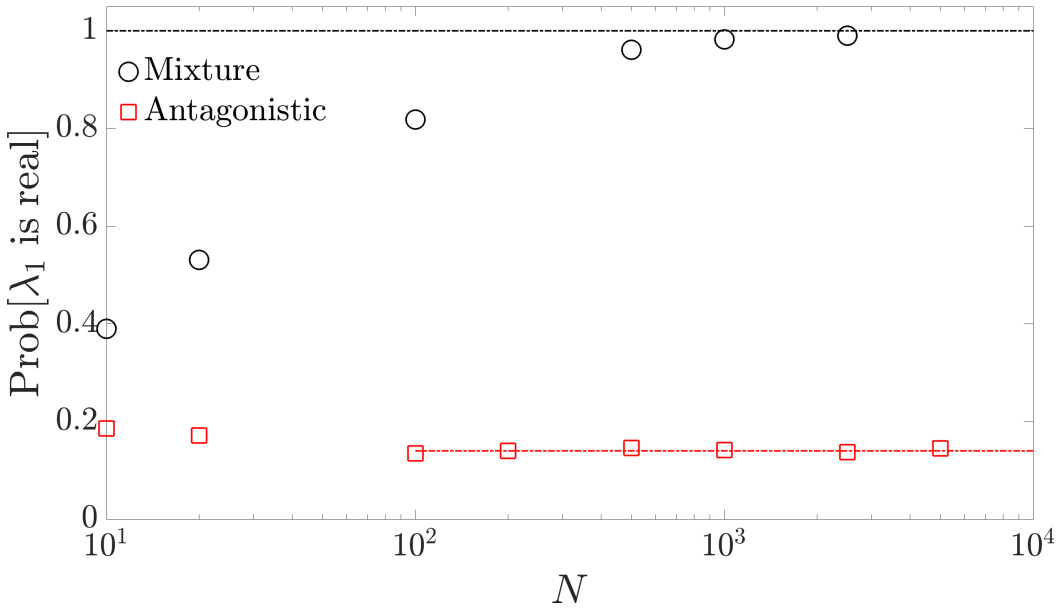

Figure 6.7: Probability Prob[$\lambda_1 \in \mathbb{R}$] that λ_1 is located on the real line as a function of N. Markers are numerical results obtained from directly diagonalising 10^4 matrices from the antagonistic ensemble (Model A, red squares) and 10^3 matrices from the mixture ensemble (Model B, black circles), both for Erdős-Rényi graphs with a mean degree $c = 2$.

First, we considered direct diagonalization results of matrices with mean degree $c = 2$,

and we compute the probability $\pi_{\Re}$ that their leading eigenvalue is real, i.e.,

$$\pi_{\Re} = \text{Prob}[\lambda_1 \in \mathbb{R}]. \tag{6.10}$$

In particular, we study this probability $\pi_{\Re}$, estimated over a sample of 10^3 matrices, as a function of the system size N, for antagonistic matrices of Model A and also for mixture matrices of Model B, in order to highlight the differences between these two ensembles also at finite sizes. We have obtained these results by using the criterion $\Im(\lambda_1) < 10^{-13}$ to identify an eigenvalue as real, where 10^{-13} is much smaller than the typical distance between two eigenvalues. The Figure 6.7 shows that the distinction between these two ensembles is evident already at small values $\approx 10^2$ of the system size, where the probability that λ_1 is real for mixture matrices is more than four times larger than it is for antagonistic matrices. Also, for mixture matrices $\pi_{\Re}$ approaches fast the value of one, i.e., already when $N = 10^3$ the leading eigenvalue is real with probability one. On the other side, for antagonistic matrices λ_1 always has a non-zero imaginary part with finite probability. Remarkably, just as in Fig. 6.2, and in the spectra in Figs. 5.5,5.9, it is sufficient to have a small fraction of mutualistic and competitive interactions to obtain completely different results, which here is a real-valued λ_1. Hence, all interactions must be of the predator-prey type in order to have a non-real leading eigenvalue. From Fig. 6.7, it is evident that λ_1 is not self-averaging, consistently with Sec. 6.1: Indeed, if the leading eigenvalue were self-averaging, then $\pi_{\Re}$ in Eq. (6.10) should tend either to one or zero in the limit $N \to \infty$. Figure 6.7 implies also that there are strong fluctuations in the imaginary part of the leading eigenvalue of antagonistic matrices. Indeed, Fig. 6.7 shows that λ_1 is typically imaginary, but it is real with a finite, albeit small, probability, and this probability decreases very slowly when increasing N. Although we can not compute the exact contribution of small cycles on the leading eigenvalue and on its distribution, the spectra of antagonistic matrices in Fig. 5.5 suggest that many real eigenvalues are contributed by cycles, which are more abundant at small values of N.

We focus now on Model A. Since λ_1 is a random variable such that its imaginary part displays strong fluctuations and with a non-zero probability to be real at fixed N, we assume here that the distribution of the imaginary part of the leading eigenvalue takes the form

$$p\left(\Im(\lambda_1)\right) = \pi_{\Re}\, \delta(\Im(\lambda_1)) + (1 - \pi_{\Re}) p_{\text{c}}(\Im(\lambda_1)), \tag{6.11}$$

where $\pi_{\Re}$ is defined in Eq. (6.10), and it is estimated as in Fig. 6.7 for a fixed value of N, and where $p_{\text{c}}(\Im(\lambda_1))$ a continuous distribution for non-real values of $\Im(\lambda_1)$. From general considerations on sparse graphs, it is expected that in the limit $N \to \infty$ the continuous component tends to [Neri and Metz, 2020]

$$p_{\text{c}}(x) = a\delta(x - \Im(\lambda_1^*)) + (1 - a) p_{\text{cycle}}(x), \tag{6.12}$$

where $\Im(\lambda_1^*)$ is the typical value of $\Im(\lambda_1)$ and $p_{\text{cycle}}(x)$ is the remaining distribution describing the nontypical values of $\Im(\lambda_1)$, which are originated due to the presence of small cycles in the graph [Bonneau et al., 2017]. Above the percolation threshold, it is expected that the leading eigenvalue is dominated by its typical value $\Im(\lambda_1^*)$, and hence its weight in the distribution dominates over the contribution of cycles, i.e., $a \approx 1$ [Neri and Metz, 2020]. Conveniently, as discussed in Sec. 6.1, the imaginary part of the typical value $\Im(\lambda_1^*)$ can be predicted, in the limit $N \to \infty$ by the theory based on the cavity method that we presented in detail Ch. 3,4.

From direct diagonalization of antagonistic matrices, we can evaluate the following distribution at finite sizes of the imaginary part of λ_1, i.e.,

$$p_{\Im(\lambda_1)}(x) := \langle \delta(x - \Im(\lambda_1(\mathbf{A}))) \rangle_{\mathcal{A}} \ , \tag{6.13}$$

where by $\langle \rangle_{\mathcal{A}}$, as in Eq. (6.2), we denote the ensemble average over the space $\mathcal{A}$ of random matrices $\mathbf{A}$, which here is Model A. In Fig. 6.8, $p_{\Im(\lambda_1)}(x)$ is plotted for antagonistic matrices of finite size $N = 5000$.

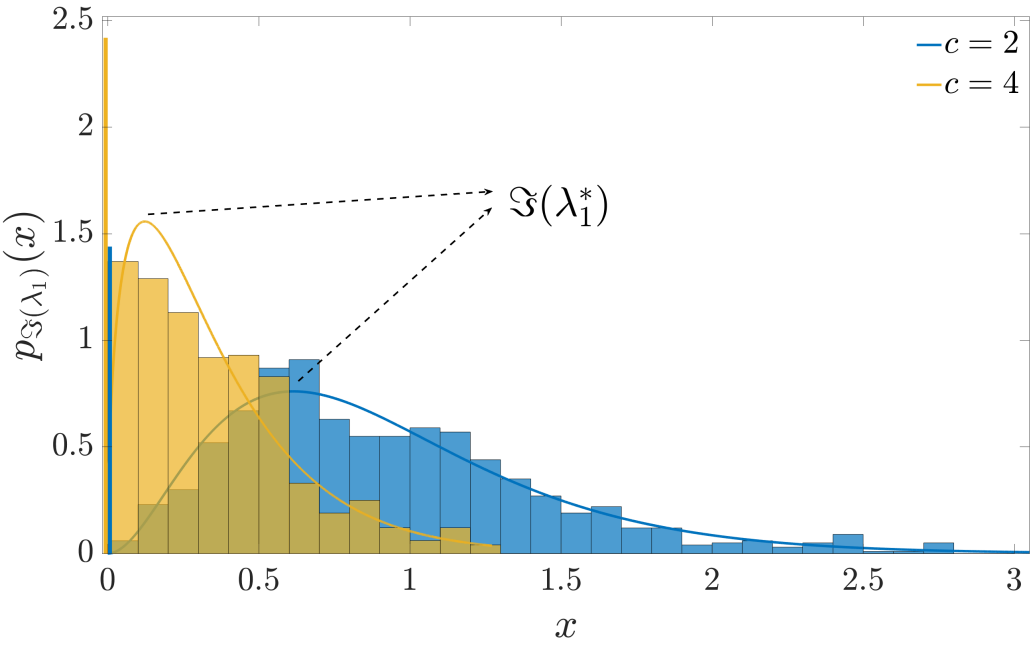

Figure 6.8: Histograms of the imaginary part $\Im(\lambda_1)$ of the leading eigenvalue λ_1 in antagonistic matrices defined on Erdős-Rényi graphs (Model A) with mean degrees $c = 2$ (blue) and $c = 4$ (yellow). Results shown are obtained from diagonalising 10^3 matrices of size $N = 5000$. The thick vertical line at $\Im(\lambda_1) = 0$ has height $\text{Prob}[\lambda_1 \in \mathbb{R}]/\delta$, with $\delta = 0.1$ the width of the intervals in the histogram. Continuous lines are gamma distributions, see Eq. (6.14), fitted to the histograms [fitted parameters are $\alpha = 3.04$ and $\beta = 3.31$ (blue) and $\alpha = 1.53$ and $\beta = 4.35$ (yellow)].

From finite N results, as shown in Fig. 6.8, we get an independent estimate of the typical $\Im(\lambda_1^*)$ (see Appendix A.9 for a more detailed finite size study) by identifying it

with the mode of a gamma distribution

$$\gamma(x;\alpha,\beta) = (1-\pi_{\Re})\frac{\beta^{\alpha}x^{\alpha-1}e^{-\beta x}}{\Gamma(\alpha)}, \tag{6.14}$$

fitted on the histogram of non real values $\Im(\lambda_1)$, with $\Gamma(\alpha)$ the gamma function and $\beta, \alpha \in \mathbb{R}_+$ two fitting parameters.

We study now the typical value $\Im(\lambda_1^*)$ as a function of the mean degree c, that we obtained from both the theory for $N \to \infty$, and from the estimate at finite N, as explained above. Figure 6.9 shows that these two independent methods give compatible results on the typical value of antagonistic random matrices, although strong finite size effects affect the estimates of $\Im(\lambda_1^*)$ from direct diagonalization data, since as discussed above the imaginary part of the leading eigenvalue has strong fluctuations. We study more in detail the distributions $p(\Im(\lambda_1))$ at different sizes in Appendix A.9. Remarkably,

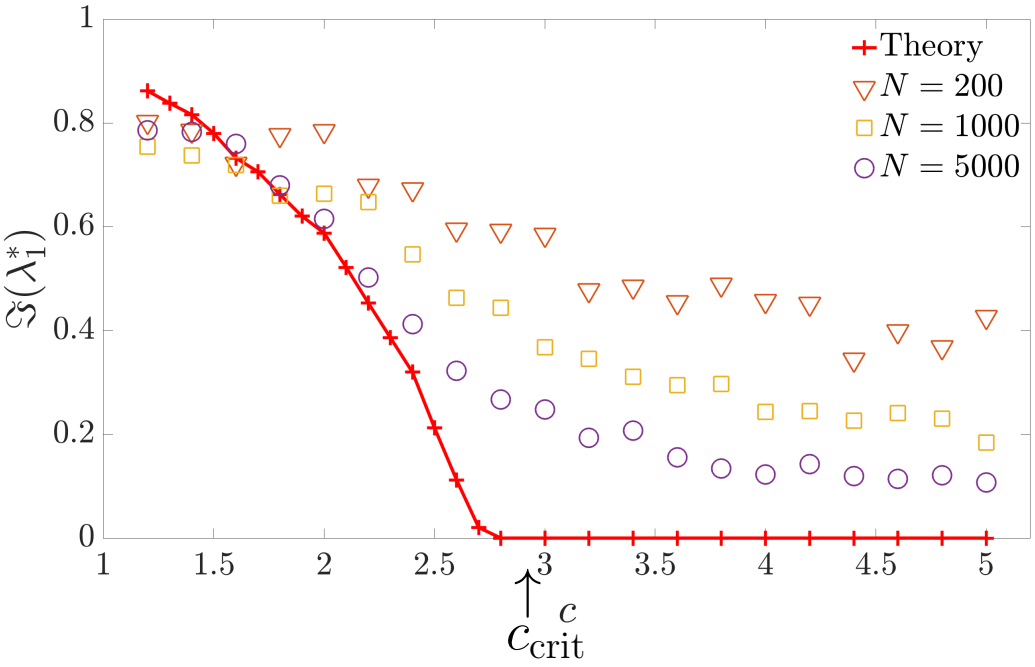

Figure 6.9: Imaginary part of the typical value $\Im(\lambda_1^*)$ of the leading eigenvalue λ_1 as a function of the mean degree c for antagonistic matrices defined on Erdős-Rényi graphs (Model A). Red crosses denote $\Im(\lambda_1^*)$ in the limit of $N \to \infty$ computed with the cavity method (see Sec.6.1), while the solid line is a guide to the eye. Unfilled markers denote $\Im(\lambda_1^*)$ obtained from directly diagonalising 10^3 matrices of a given size N as shown in Fig. 6.8. Results shown are for $c > 1$ since Erdős-Rényi graphs do not have a giant component when $c < 1$.

we find that $\Im(\lambda_1^*)$ exhibits a continuous phase transition, in the limit $N \to \infty$, as a function of the mean degree c. In particular, Fig. 6.9 shows that there exists a critical c_{crit} such that $\Im(\lambda_1^*)$ converges as $N \to \infty$ towards zero for $c > c_{\text{crit}}$ and to a non-zero value for $c < c_{\text{crit}}$. Such continuous transition corresponds to a continuous deformation of the support whose effect is the appearance of a reentrant behaviour below a critical value c_{crit} of the mean degree. We have quantified the reentrance effect seen in Fig. 5.5,

which systematically activates below the critical value $c_{\rm crit}$, and becomes stronger and stronger when approaching the percolation transition at $c = 1$.

In the next section, we explore more in detail another very important consequence of such continuous transition, at the level of the dynamics of large complex systems in the vicinity of fixed points. Indeed, as discussed in Ch. 1, the imaginary part of the leading eigenvalue determines how a complex system dynamically recovers from a perturbation at fixed points.

6.7 Dynamical oscillations for large antagonistic systems

Here we present the implications that the continuous phase transition shown in Fig. 6.9 has on the dynamics, in the vicinity of stable fixed points (see Ch. 1), of complex systems of large size N. In light of the conditions on the imaginary part of the leading eigenvalue in Eq. (1.15) and Eq. (1.16), by assuming that we are in the vicinity of a stable fixed point, the critical $c_{\rm crit} \approx 2,7$ separates a phase characterised by small mean degrees, where large and stable antagonistic systems typically oscillate towards the fixed point after a small perturbation, from a phase characterised by larger connectivities, where large antagonistic systems relax monotonically to the fixed point.

To illustrate this behaviour, we study the time dependence of the vector $\vec{y}(t)$, representing the deviation from a stable fixed point, within the following linearised dynamics

$$\partial_t \vec{y} = -\mathbf{d}\,\vec{y} + \mathbf{A}\vec{y}, \tag{6.15}$$

where $\mathbf{d}$ is a diagonal matrix where we assume for simplicity that all diagonal elements are equal to d, and $\mathbf{A}$ is an antagonistic matrix of Model A. We assume that

$$d > \Re(\lambda_1(\mathbf{A})), \tag{6.16}$$

which guarantees the fixed point $\vec{y} = \vec{0}$ is stable. Figure 6.10 illustrates the distinction between the dynamics at $c = 2 < c_{\rm crit}$ and $c = 4 > c_{\rm crit}$ by plotting trajectories of $\vec{y}$ as a function of t for three different matrix realisations $\mathbf{A}$ drawn from the Model A. Since $\vec{y}(t)$ is a vector in a high dimensional space, we plot its projection $\vec{y}(t) \cdot \vec{y}(0)/|\vec{y}(0)|^2$ on the initial state, for which we have set all entries equal to one, i.e., $\vec{y}(0) = (1, 1, \ldots, 1)^T$. We observe a clear qualitative difference between the $c = 2$ and $c = 4$ trajectories of $\vec{y}(t)$: for $c = 2$ the trajectory is reminiscent of a harmonic oscillator in the underdamped regime while for $c = 4$ the trajectory is reminiscent of a harmonic oscillator in the over damped regime.

We make now a careful analysis of the different timescales involved in the linearised dynamics in Eq. (6.15) of the relaxation towards the stable fixed point. Indeed, as shown in Appendix A.1, the long term dynamics is governed by three timescales. First,

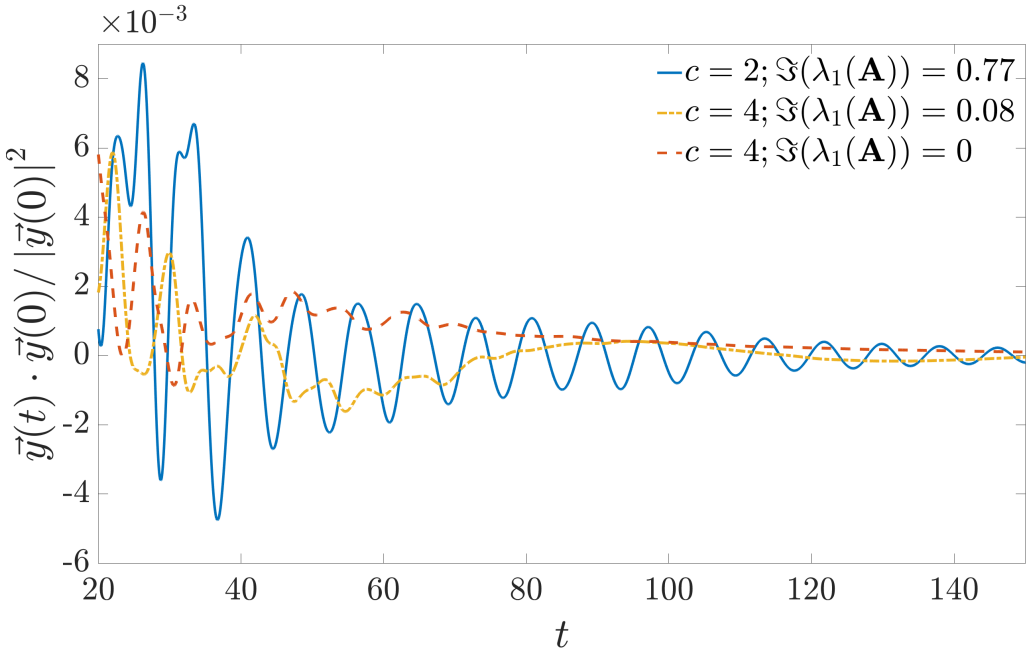

Figure 6.10: Plot of $\vec{y}(t)\cdot\vec{y}(0)/|\vec{y}(0)|^2$ as a function of t for three different realisations of antagonistic matrices $\mathbf{A}$ drawn from Model A with $N = 10^4$, and with $c = 2$ or $c = 4$ as denoted in the legend. We have chosen matrix realisations such that the $\Im(\lambda_1(\mathbf{A}))$ (numerical values reported in the figure) correspond to the typical values of $\Im(\lambda_1)$ in Fig. 6.8.

the timescale $\tau_{\rm rel}$ that a stable system needs to relax to its fixed point is given by

$$\tau_{\rm rel} := \frac{1}{d - \Re(\lambda_1)}, \tag{6.17}$$

where $\lambda_1 = \lambda_1(\mathbf{A})$ is the leading eigenvalue of the matrix $\mathbf{A}$. The spectral gap $\Re(\lambda_1) - \Re(\lambda_2)$,[1] where $\Re(\lambda_2)$ denotes the second largest value of the real parts of the eigenvalues of $\mathbf{A}$, sets a second important timescale, i.e., the transient timescale $\tau_{\rm gap}$

$$\tau_{\rm gap} := \frac{1}{\Re(\lambda_1) - \Re(\lambda_2)}. \tag{6.18}$$

As shown in Appendix A.1, the long time dynamics is dominated by the leading eigenvalue if and only if

$$\tau_{\rm rel} \gtrsim \tau_{\rm gap}. \tag{6.19}$$

In other words, if $\tau_{\rm rel}$ is smaller than $\tau_{\rm gap}$, then the system relaxes to the fixed point too fast for the mode associated to the leading eigenvalue to be visible, since the contribution of more than one mode, associated to eigenvalues λ_i such that $\Re(\lambda_i) > 2\Re(\lambda_1) - d$, will be visible at the same time eigenvalues will dominate the dynamics. The third and last timescale, relevant for the long time dynamics, is given by the oscillations timescale $\tau_{\rm oscil}$,

[1] for simplicity we assume here that there can exist only the complex conjugate $\bar{\lambda}_1$ that has the same real part of λ_1; otherwise, instead of λ_2 one would have λ_{M+1} when there are $M > 1$ degenerate leading eigenvalues, up to complex conjugation

defined by

$$\tau_{\text{oscil}} := \frac{1}{\Im(\lambda_1)}. \tag{6.20}$$

Now, provided that the condition in Eq. (6.19) is satisfied, the leading eigenvalue, and in particular its imaginary part $\Im(\lambda_1)$, distinguishes two scenarios, as follows

$$\vec{y}(t) : \begin{cases} \text{NO oscillations,} & \text{if} \quad \tau_{\text{oscil}} \gg \tau_{\text{rel}}; \\ \text{Oscillations,} & \text{if} \quad \tau_{\text{oscil}} \ll \tau_{\text{rel}}. \end{cases} \tag{6.21}$$

In words, the dynamical vector $\vec{y}(t)$ shows simple exponential recovery to the fixed point if τ_{oscil} is much larger than τ_{rel}; otherwise, $\vec{y}(t)$ shows an oscillatory dynamics during relaxation towards equilibrium if τ_{oscil} is much smaller than τ_{rel}.

For large systems, where the spectral gap is expected to be small and vanishing in the limit $N \to \infty$, the condition in Eq. (6.19) can be obtained only at the verge of instability, i.e. for $d - \Re(\lambda_1)$ even smaller than the spectral gap (hence large τ_{rel}). In this setting, systems with λ_1 typically real, or that due to finite size fluctuations of $\Im(\lambda_1)$ can have a large but finite τ_{oscil}, will mostly present a non-oscillatory relaxation dynamics. This occurs for antagonistic systems characterised by mean degree $c > c_{\text{crit}}$. For example, in Fig. 6.10 we show two realisations with $c = 4$: the dashed red line represents an instance with a real leading eigenvalue λ_1, and with a spectral gap of 0.03 ($\tau_{\text{gap}} \approx 30$); the yellow dot-dashed line has a complex leading eigenvalue with a non-zero, but small, imaginary part ($\tau_{\text{oscill}} \approx 10$), due to finite size fluctuations as discussed above, and with a spectral gap of 0.02 ($\tau_{\text{gap}} = 50$). In this example already a $\tau_{\text{rel}} = 40$ is enough to have the dominating mode to emerge at around $t = 60$, after a short transient. Note that some oscillation is still visible in the antagonistic realisation characterised by a complex leading eigenvalue, but with a timescale $\tau_{\text{rel}} \lesssim \tau_{\text{gap}}$. The oscillations are expected to disappear completely for $N \to \infty$, as they are originated by finite size fluctuations of the λ_1.

On the contrary, antagonistic systems with $c = 2 < c_{\text{crit}}$ are characterised by a finite typical $\Im(\lambda_1^*)$ in the large size limit, and most of the times they be characterised by $\tau_{\text{oscil}} \ll \tau_{\text{rel}}$. Provided that the condition in Eq. (6.19)is satisfied, these systems will typically present evident oscillatory dynamics in the relaxation towards the fixed points as in the example of Fig. 6.10 where the gap is 0.02, $\tau_{\text{gap}} = 50$ and again we have set $\tau_{\text{rel}} = 40$.

Remarkably, evidences of similar oscillatory recovery of the fixed point after a perturbation has been observed in ecosystems [Arnoldi et al., 2018; Hermann and Touboul, 2012], and in the context of neural networks [Massimini et al., 2005; Rogasch and Fitzgerald, 2013], suggesting a potential relation with the dynamical results presented here for antagonistic matrices.

Chapter 7

Conclusions and perspectives

In this thesis we shed new light on the interplay between complexity and stability.

By taking inspiration from the ecosystems on food webs, we modelled the Jacobian of the dynamics of complex systems with sparse random matrices on random graphs with predator-prey, competitive or mutualistic interactions. We referred to the antagonistic ensemble when only predator-prey interactions are present, and to the mixture ensemble when one allows for all the three kinds of interactions, in given proportions. More in detail, we assumed that the off-diagonal part $\mathbf{A}$ of the Jacobian of the dynamics evaluated at the fixed points is approximated by sparse random matrices with pairwise correlated interactions, while the diagonal elements of the Jacobian are assumed to be positive real numbers to guarantee the stability of the fixed points in the absence of interactions. For simplicity, we assumed also the diagonal elements to be all equal to d. A first approach to the study of the dynamical behaviour is to infer the stability properties of the fixed points of the dynamics. In the random matrix approach, the leading eigenvalue of $\mathbf{A}$ governs the stability properties of the fixed points. In particular, if its real part is finite in the infinite size limit, then there can exist a large enough but finite value of d that guarantees the stability of the fixed points in the presence of interactions. Vice versa, if the real part of the leading eigenvalue of $\mathbf{A}$ is not finite in the infinite size limit, then there does not exist a finite value of d that is large enough to guarantee the stability of the fixed points. We found unexpected results on the stability properties of fixed points of complex systems, under the assumptions on their Jacobian that we mentioned above. These results significantly distinguish from both dense random matrices, characterised by the absence of a network structure, and sparse random matrices that are symmetric or oriented. As we showed in this thesis, such differences emerge in at least three aspects, that we summarise below.

7.1 The three main results

Here we summarise the three main results obtained in this thesis.

7.1.1 Large antagonistic systems can be stable, while mixture can not

The first question we answered is whether infinite sparse systems with pairwise correlated interactions can be stable or not. We found that the fixed points of large dynamical antagonistic systems can be stable, while the ones modelled with mixture matrices become unstable almost surely for large enough systems. More specifically, we showed that the real part of the leading eigenvalue λ_1 is finite for infinitely large antagonistic matrices, while it diverges with the system size in mixture matrices (see Fig. 6.2 and Fig. 6.3). Remarkably, it is sufficient a non-zero fraction of non predator-prey interactions This result for antagonistic systems comes as surprise as large complex systems are typically unstable, as discussed in Ch. 1. Indeed, there are two mechanisms for which the instability can emerge. First, the leading eigenvalue of dense matrices diverges with probability one with the system size when the variance of the interactions is independent of the system size, for any kind of interactions [Allesina and Tang, 2012; May, 1972]. Second, it is known that the leading eigenvalue of undirected random graphs defined with prescribed degree distribution with unbounded support diverges almost surely for large graphs [Chung et al., 2004]. Such divergence is reflected in symmetric and sparse random matrices, where the spectral distribution displays Lifshitz tails that extend on the real axis [Kühn, 2008; Rodgers and Bray, 1988].

We can provide a simple explanation of the stability of infinitely large antagonistic matrices. This explanation is based on the fact that all the eigenvalues of antagonistic tree matrices lie on the imaginary axis, as one can verify with examples of finite trees. Therefore, antagonistic systems on finite trees are stable when they are stable in the absence of interactions, independently from the supports of the degree distribution and the interactions strength being bounded or not. Accordingly, the antagonistic ensemble defines locally a dynamical system that is stable because they are locally treelike. In contrast, in a mixture model with a small percentage of interactions with same sign, i.e., mutualistic or competitive interactions, and a much larger percentage of predator-prey interactions, the leading eigenvalue of finite trees has unbounded real part when either the degree distribution or the coupling have unbounded support. This translates into the fact that for any fixed value $d > 0$ infinitely large mixture matrices contains almost surely a local neighbourhood whose leading eigenvalue is larger than d, i.e., they are unstable with probability one. The theoretical results that we obtained for the stability of infinite antagonistic and mixture matrices are consistent with their local neighbourhood properties.

It is important to note that in the sparse models of this thesis the interaction intensities do not depend on the system size N. This is a reasonable assumption for real networked systems, since the interactions within a local neighbourhood are insensitive in first approximation to a change of the whole system size, while keeping the mean degree fixed. On the other side, one can rescale the interactions in any model by a function of the system size, so that the leading eigenvalue can stay finite in the infinite size limit.

The specific function depends on the model. This approach is done, for example, in dense systems, to have a compact support of the spectral distribution in the infinite size limit (see Ch. 1), where in this case the rescaling is given by $\sqrt{N}$. One can use this rescaling approach to keep the leading eigenvalue finite also in sparse systems. As discussed in Ch. 1, the leading eigenvalue of undirected graphs scales as $\mathcal{O}(\sqrt{k_{\max}})$. The specific dependence of $k_{\max}$ on the system size N depends on the specific sparse network model, and in particular on the degree distribution. For example, in the Erdős-Rényi model for symmetric adjacency matrices this dependence is known analytically (see Eq. (1.39)) in the finite connectivity regime, consequently it provides the rescaling of the interactions that would make the leading eigenvalue finite. In regards to the sparse models studied in this thesis, we have empirically found that the scaling with N of the leading eigenvalue of mixture matrices of Model B is given by $\log N$ (see Fig. 6.2). It would be interesting to have an analytic formula for the leading eigenvalue of mixture matrices that can confirm this behaviour.

7.1.2 Influence of network topology on the leading eigenvalue

The second question we wanted to understand is how the local network topology affects the stability of large antagonistic systems. First, we showed that the mean degree of a graph has always destabilising effect on the system stability, as it was first shown in dense graphs [May, 1972]. Second, we quantitatively characterised the effect of the degree fluctuations in the network structure, by considering antagonistic matrices on a random graph ensemble with a prescribed degree distribution that interpolates between a random regular graph and a Erdős-Rényi one. We found that the leading eigenvalue of sparse antagonistic matrices decreases upon increasing the degree fluctuations for large mean degrees, while it increases if the mean degree is small (see Fig. 6.6(a)). Accordingly, fluctuations in the network topology stabilise antagonistic systems except if the degree is small. We performed the same analysis on oriented sparse matrices, characterised by unidirectional links, which is another sparse ensemble known to be stable in the infinite size limit [Neri and Metz, 2020]. The degree fluctuations have always destabilising effects on the stability of infinite oriented systems, i.e., we found that the leading eigenvalue in this case always increases upon increasing these fluctuations (see Fig. 6.6(b)). The opposite trends between antagonistic and oriented ensembles that have been observed in the dependence of the leading eigenvalue on the degree fluctuations suggest that the stabilising effects due to the degree fluctuations in the network topology depend on the nature of the interactions.

7.1.3 Phase transition on the imaginary part of the leading eigenvalue for antagonistic systems

Finally, we analysed how antagonistic and mixture sparse systems respond dynamically to a perturbation in proximity of a stable fixed point. Remarkably, we found that large antagonistic systems with small values of the mean degree typically display an oscillatory relaxation towards the fixed points after a perturbation (see Fig. 6.10). This phenomenon is a direct consequence of a reentrance effect in the spectrum of large antagonistic matrices for small enough mean degrees, where the leading eigenvalue is typically complex (see Fig. 5.5). Instead, for large mean degrees the leading eigenvalue of large antagonistic matrices is typically real. The reentrance effect is a surprising feature of the antagonistic sparse ensemble, since for non-symmetric random matrices the leading eigenvalue is typically real (for symmetric ensembles is trivially real always). For example, as discussed in Ch. 1, it is real in the dense and dilute regimes, where it holds the elliptic law [Allesina and Tang, 2012]; for directed and sparse random graphs with i.i.d. interactions [Neri and Metz, 2020], and for general sparse non-symmetric random matrices with i.i.d. entries [Allesina and Tang, 2012; Amir et al., 2016; Metz et al., 2019; Rogers and Pérez Castillo, 2009]. In addition, the results on the imaginary part of the leading eigenvalue for antagonistic matrices persist in the infinite size limit, where the leading eigenvalue remains finite, as we discussed above. Indeed, such peculiar dynamical behaviour of the antagonistic model characterises a continuous phase transition for the imaginary part of the typical value of the leading eigenvalue as a function of the mean degree c, with a critical value c_{crit} that separates a phase where the leading eigenvalue is complex to one where it is real (see Fig. 6.9). At variance, large mixture matrices have typically a monotonic recovery to a fixed point after a perturbation. Indeed, in this case the leading eigenvalue is with probability one real for finite but large mixture matrices, even for small mean degree (see Fig. 6.7). This behaviour for mixture matrices is due to the appearance of extended tails in the spectrum on the real axis (see Fig. 5.9), which are responsible also for the divergence of the leading eigenvalue that we discussed above. These tails are reminiscent of Lifshitz tails in the spectra of symmetric and sparse random matrices [Bapst and Semerjian, 2011; Khorunzhiy et al., 2006; Slanina, 2012]. Remarkably, our results suggest that a sufficient and necessary condition for the appearance of these tails is the existence of a non-zero fraction of competitive and mutualistic interactions. Indeed, the novel oscillatory behaviour for antagonistic matrices can happen because in this case the spectra do not develop extended tails on the real axis.

We use simple arguments to derive the functional dependence of the imaginary part of the leading eigenvalue close to the critical point c_{crit}. Inspired by the theory on continuous transitions [Landau, 1937], we identify the imaginary part of the leading eigenvalue as an order parameter, whereas the mean degree plays the role of the temperature. Following this approach and respecting the symmetries of the spectra of antagonistic matrices

explored in Ch. 5, we can express the real part of the leading eigenvalue as a function of c_{crit} near the critical point as follows, i.e.,

$$\Re(\lambda_1^*) = a + \Delta(c_{\text{crit}} - c)(\Im(\lambda_1^*))^2 - b(\Im(\lambda_1^*))^4, \tag{7.1}$$

where a, Δ, b are positive real parameters that up to the leading order are independent of c. In order to find the maximal value of $\Re(\lambda_1^*)$ as a function of $\Im(\lambda_1^*)$, with the other parameters kept fixed, we evaluate the derivative of Eq. (7.1) with respect to $\Im(\lambda_1^*)$ and then set it to zero; this gives the solution $\Im(\lambda_1^*) = 0$ for $c > c_{\text{crit}}$ and the following nontrivial solution for $c < c_{\text{crit}}$, i.e.,

$$\Im(\lambda_1^*) = \sqrt{\frac{\Delta(c_{\text{crit}} - c)}{2b}}, \tag{7.2}$$

which describes the leading behaviour of the phase transition close to the critical point c_{crit}.

7.2 Future perspectives

We conclude by discussing possible future research perspectives.

7.2.1 Hypotheses relaxation

We discuss now some future research perspectives that can generalise the results of this thesis, by relaxing some of the assumptions that we used here to obtain them.

First, a possible direction that we think is worth to explore is to relax the assumption $d_j = d$ for any node j for the diagonal part of the Jacobian at the fixed points, as well as to relax the symmetry of interactions with zero mean, i.e., balanced interactions on average, (see Eq. (2.9) and Eq. (2.21)). The first would mean to introduce diagonal disorder for the self-regulation mechanisms in the absence of interactions that in principle can be different for different species, whereas the second would account, for example in the case of predator-prey interactions, for different average strength between predators and preys. In the first case we expect that one would obtain qualitatively equivalent results for the leading eigenvalue, since the network structure would be unchanged. However, in the second case we expect from other studies [Allesina and Tang, 2012; Neri and Metz, 2016, 2020] that such an asymmetry would lead to eigenvalue outliers in the spectrum, which are absent in the balanced case. It is important to understand if the results on the leading eigenvalue and hence on the stability properties of the fixed points are affected. In particular, an interesting question is whether the oscillatory to monotonic transition persists in the non-balanced case.

A second interesting challenge is to go beyond the classical assumption of substituting the true Jacobian of the dynamics at the fixed points with a random matrix, in order

to account for more realistic features of the community structure at the fixed points. Although in the model considered in this thesis we went beyond the classical approach of random matrix theory by including a sparse network structure and interactions that are pairwise correlated, such as predator-prey ones, this hypothesis potentially neglects further structural properties of the fixed point that may be relevant. A possible strategy is to simulate the non-linearised dynamics on many realisations, and infer properties of the Jacobian at convergence, where the community is selected dynamically. For example, for dense models it has been found [Biroli et al., 2018] that in phases characterised by large variability the specific structure of the original community is preserved, although with reduced diversity, so that the model in this case remains statistically equivalent with rescaled parameters. It would be interesting to understand if this statistical equivalence is also found for the sparse systems that we study.

A third important research question is whether the relaxation of the locally treelike assumption in the network structure would preserve or not the stability properties that we showed for antagonistic systems. In particular it would be interesting to include and quantify the effects of cycles on the leading eigenvalue and hence on stability, as they can appear in food webs [Dunne et al., 2002a; Williams and Martinez, 2000]. More in detail, as argued by [Neri and Metz, 2020], for sparse random matrices the distribution of the leading eigenvalue in the limit of large system size is expected to be a weighted sum of a delta function at its typical value and a continuous part due to small cycles. The continuous part is supported on the half real line with the lower bound at the typical value of the leading eigenvalue. The delta is expected to have the weight ν that is close to one when there is a giant component, whereas below the percolation threshold the small cycles give a dominating contribution to the leading eigenvalue, i.e., the weight of the continuous part of the distribution has weight $(1 - \nu)$ is close to one. The results from direct diagonalization of antagonistic matrices above the percolation threshold (see Fig. 5.5 and Fig. 6.2) suggest that $\nu \approx 1$ for this model. It would be interesting to perform a quantitative study to determine ν first in the antagonistic matrices considered in this thesis, and second in antagonistic models defined on other sparse graphs that are sparse but not necessarily locally treelike, and finally to compare them. In this way one could have a more quantitative characterisation of the effect of small cycles on the leading eigenvalue and hence on the system stability.

7.2.2 Building upon the current results

We conclude now with future research directions that can build upon the results presented here or be related to them, that add on the perspectives discussed above.

First, it would be interesting to understand whether the results on the leading eigenvalue and on system stability for the antagonistic and mixture matrices are sensitive to the choice of the degree distribution and of the interaction strength distribution $\tilde{p}$ in Eq. (2.7) (antagonistic) and in Eq. (2.13) (mixture). We remark that the theory that

we developed in Ch. 4 can be applied to the general model defined on random graph ensemble with a prescribed degree distribution, and characterised by pairwise correlated interactions. We expect that the change of the distribution of the interaction strength, in particular by considering ones with unbounded support, as well as considering other degree distributions, for example the exponential or power law distributions, might introduce strong finite size effects both at the level of direct diagonalization of finite matrices and of the population dynamics algorithm to solve the theoretical equations for the infinite size limit. An important choice that plays a role for the behaviour of the leading eigenvalue is whether the degree distribution has bounded support or not, since typically the leading eigenvalue of random graphs scales as $\mathcal{O}(k_{\max})$. For example, mixture models where both the distributions of the interaction strength and of the degree have bounded supports could have a finite leading eigenvalue in the infinite size limit. For antagonistic matrices, the fact that the typical leading eigenvalue converges to a finite value is suggested to be in the nature of the interactions, and so it could be generalised to other distributions. Confirming this fact would be a signal of universality for antagonistic ensembles. At the level of the phase transition of the imaginary part of the leading eigenvalue as a function of the mean degree for antagonistic matrices, it is difficult to make hypothesis if it can be found also with other distributions, especially at the level of the degree distribution, since the change of the network topology typically affects the spectra in the sparse regime: for example, we found that antagonistic random matrices on random regular graphs have always real leading eigenvalue when there is a giant component, although in this case it is worth to say that the degrees are restricted to integer values and that the degree distribution has bounded support with no degree fluctuations. In the case that such transition is found also on models of antagonistic matrices defined on other distributions, it can be another signal of universal behaviour of antagonistic systems.

A second interesting question is whether the phase transition from a non-oscillatory to an oscillatory behaviour for antagonistic matrices as a function of the mean degree can be related to a localisation-delocalisation phase transition of their right and left eigenvectors. Indeed, it is known that the right eigenvectors of directed random graphs localise at small values of the mean degree [Metz and Neri, 2020], as well as the eigenvectors in symmetric and sparse random matrices [Kühn, 2008]. Accordingly, the fact that for small mean degree the leading eigenvalue is typically imaginary for large antagonistic matrices and in particular the reentrance effect in the spectrum could be related to the existence of localised eigenstates. If this were the case, such localisation transition can give insights also on the universality features of the phase transition discovered for antagonistic matrices in this thesis. In addition, it is known that Lifshitz tails of sparse and symmetric random matrices correspond to localised states in the spectrum [Kühn, 2008]. Consequently, it would be interesting to understand if the extended tails found in mixture matrices are associated to such localisation transition.

A third question is related to the surprising result, summarised above, that degree fluctuations stabilise antagonistic systems when the mean degree is large enough (see Fig. 6.6(a)). It would be interesting to study an antagonistic model on a random graph ensemble defined with a prescribed degree distribution that can have larger values of the variance, for example a power law distribution, in order to understand whether the real part of the typical leading eigenvalue could eventually reach the zero value, or it saturates to a finite value.

A fourth interesting question is to understand for which scaling of $f(N) = 1 - \pi^{\mathrm{A}}(N)$ with the system size N the leading eigenvalue of a mixture ensemble remains finite in the limit of large N. We first look at this problem in the case of symmetric matrices. As discussed in Ch. 1, for symmetric and sparse random matrices the leading eigenvalue is governed by the maximal degree $k_{\max}$, so the problem can be tackled in this case by studying the maximal degree. As discussed above, this quantity depends on the specific ensemble, and in particular on the degree distribution. In particular, if one knows its scaling with N, as in the case of symmetric adjacency matrices of the Erdős-Rényi model, then one can rescale accordingly the interactions in order to compensate for the divergence behaviour. In the case of non symmetric matrices there exist no results that relate the leading eigenvalue to the maximal degree, and therefore the problem is harder to study.

Finally, one can study the spectral properties on specific network realisations of ecosystems, neural networks, or other complex systems, that can be compared with our theoretical predictions. Interestingly, oscillations in the dynamical recovery towards fixed points are found in several contexts in real-world systems, suggesting a possible relation with the theoretical results that we predicted. For example, oscillatory responses are found as a response to perturbations in the context of the brain activity during sleep phases [Massimini et al., 2005; Rogasch and Fitzgerald, 2013], as well as in oscillatory phases in large ecosystems [Arnoldi et al., 2018; Hermann and Touboul, 2012].

Appendix A

Appendices

We end this thesis with a set of appendices, where we present the technical, i.e., mathematical and numerical, tools that we implemented to derive the results obtained in the main chapters of the thesis. Appendix A.1 reviews the derivation of the stability criteria given by Eqs. (1.13)-(1.16). In Appendix A.2 we expose in more detail the theorems for the universal laws in random matrix theory (RMT), presented in Sec. 1.3 and in Sec. 1.5. Appendix A.3 explains deeper and step by step the assumptions within the definition of the antagonistic ensemble in Ch. 2, and in Appendix A.4 we present explicitly the formulas for the generic moments of the probability distributions of the antagonistic and mixture ensemble. In Appendix A.5 we derive the formula for the empirical spectral density in terms of the resolvent of a matrix, that we used in Ch. 3. Appendix A.6 shows the derivation of Cauchy-Pompeiu formula, which is a generalisation of the Cauchy integral formula in complex analysis, that we used to derive the formula for the empirical spectral density in Appendix A.5. In Appendix A.7 we derive the inverse of a block matrix in terms of Schur complements, i.e., the Schur formula, that we used in Ch. 3. Appendix A.8 revise the percolation theory for the existence of giant components in undirected and directed graphs, and present a study on how the size of the largest connected component depends on graph topology, both for undirected and directed graphs. Finally, Appendix A.9 presents a finite size study of the leading eigenvalue of random antagonistic matrices and mixture matrices.

A.1 Leading eigenvalue: stability criterion and frequency of oscillations

Here we show that the leading eigenvalue λ_1 of $\mathbf{A}$ governs the long time dynamics of $\vec{y}(t)$, i.e., in the limit $t \gg 1$. In particular, we derive the conditions given by Eqs. (1.13) and (1.14) for the stability of linearised dynamics of complex systems and the conditions given by Eqs. (1.15) and (1.16) for the oscillations in the dynamical response to a perturbation in the vicinity of fixed points.

We order the eigenvalues of the $N \times N$ matrix $\mathbf{A}$ such that

$$\Re(\lambda_1) \geq \Re(\lambda_2) \geq \ldots \geq \Re(\lambda_N), \tag{A.1}$$

where if two consequent eigenvalues, say λ_j and λ_{j+1}, have the same real part, then we use the convention that $\Im(\lambda_j) \geq \Im(\lambda_{j+1})$.

We assume here that the matrix $\mathbf{A}$ is diagonalisable so that it can be decomposed as

$$\mathbf{A} = \sum_{j=1}^{N} \lambda_j \vec{R}_j \vec{L}_j^{\dagger}, \tag{A.2}$$

where $\vec{R}_j$ is a right eigenvector associated with λ_j, $\vec{L}_j$ is a left eigenvector associated with λ_j, and $\vec{L}_j^{\dagger}$ denotes the complex conjugate of $\vec{L}_j$. We normalise left and right eigenvectors, such that,

$$\vec{R}_j \cdot \vec{L}_k = \delta_{j,k}, \tag{A.3}$$

for all $j, k \in \{1, 2, \ldots, N\}$.

Substitution of Eq. (A.2) in Eq. (1.10) yields for $d_j = d$,

$$\vec{y}(t) = e^{-dt} \sum_{j=1}^{N} e^{\lambda_j t} [\vec{L}_j \cdot \vec{y}(0)] \vec{R}_j. \tag{A.4}$$

Hence, in the limit $t \to \infty$, we obtain

$$\vec{y}(t) = e^{(\Re(\lambda_1)-d)t} \left[\sum_{j=1}^{M} e^{\mathrm{i}\Im(\lambda_j)t} [\vec{L}_j \cdot \vec{y}(0)] \vec{R}_j + \mathcal{O}\left(e^{(\Re(\lambda_{M+1})-\Re(\lambda_1))t}\right) \right], \tag{A.5}$$

where M denotes the number of eigenvalues for which $\Re(\lambda_1) = \Re(\lambda_2) = \ldots = \Re(\lambda_M)$. From Eq. (A.5) both the stability conditions, given by Eqs. (1.13) and (1.14), and the conditions for oscillations in $\vec{y}(t)$, given by Eqs. (1.15) and (1.16), readily follow. In particular, Eq. (A.5) set the timescales discussed in Sec. 6.7.

The conditions Eqs. (1.13)-(1.16) also apply when $\mathbf{A}$ is nondiagonalisable. However, in this case we cannot employ the eigendecomposition Eq. (A.2) and we should instead rely on a Jordan decomposition, see Ref. [Neri and Metz, 2020].

A.2 Random Matrix theory: theorems for the universal laws

We discuss in this appendix the main theorems in RMT that establish the universal laws (see Sec. 1.3).

Given the spectrum in Eq. (1.11), an important mathematical object is the empirical spectral measure[1] $\mu_{\mathbf{A}}$ (see for example [Götze et al., 2015; Naumov, 2013; Nguyen and O'Rourke, 2015]), which is the following discrete probability measure on $\mathbb{C}$, defined on a subset E

$$\mu_{\mathbf{A}}(E) := \frac{1}{N}|\{1 \leq i \leq N : \lambda_i(\mathbf{A}) \in E\}|, \quad \text{with} \quad E \in \mathcal{B}(\mathbb{C}), \tag{A.6}$$

where $\mathcal{B}(\mathbb{C})$ is a Borel σ-algebra of $\mathbb{C}$, i.e., for example, E is an open subset of $\mathbb{C}$, and where $|\{\}|$ denotes the cardinality of the set $\{\}$. When the matrices $\mathbf{A}$ are random, i.e drawn from a probability distribution on $\mathbb{C}^{N\times N}$, $\mu_{\mathbf{A}}$ is a random discrete probability measure on $\mathbb{C}$, i.e. it is a random variable taking values in the space of discrete probability measures on $\mathbb{C}$. We observe that the empirical spectral density in Eq. (1.19) is the density associated to the measure in Eq. (A.6), i.e., [Billingsley, 1986]

$$\mu_{\mathbf{A}}(E) = \int_E \rho_{\mathbf{A}}(z)\, \mathrm{d}x\, \mathrm{d}y, \quad \text{with} \quad E \in \mathcal{B}(\mathbb{C}), \tag{A.7}$$

where $\mathrm{d}x\ \mathrm{d}y$ is the (two-dimensional) Lebesgue measure in the complex plane, with $z = x + \mathrm{i}y$.

A fundamental problem in RMT is to determine the limiting spectral measure μ, if it exists, and under which hypotheses, of the sequence of measures $\mu_{\mathbf{A}/\sqrt{N}}$, as the size N of the random matrix tends to infinity. We observe than when μ exists, typically it is deterministic, whereas $\mu_{\mathbf{A}}$ are random objects, and this fact is an example of self-averaging objects in disordered systems. As discussed in Sec. 1.3, the fundamental object in RMT, on which the universal laws are expressed, is the limiting distribution ρ, which is the (deterministic) density associated to the (deterministic) measure μ, similarly to Eq. (A.7).

The theorems that we present in this appendix are on the convergence of the empirical spectral measure defined in Eq. (A.6). More in detail, a sequence of measures $\mu_{\mathbf{A}}/\sqrt{N}$ is said to converge to a measure μ if, for every test function $\phi : \mathbb{C} \to \mathbb{C}$ that is continuous and compactly supported in $\mathbb{C}$, the difference of the Lebesgue integral of ϕ with respect to the measures $\mu_{\mathbf{A}}/\sqrt{N}$ and μ, i.e.,

$$\Delta\phi_\mu := \int_{\mathbb{C}} \phi(z)\, \mathrm{d}\mu_{\mathbf{A}/\sqrt{N}} \ - \ \int_{\mathbb{C}} \phi(z)\, \mathrm{d}\mu \tag{A.8}$$

converges to zero when $N \to \infty$. We mention here two ways that the difference in

[1] this object can be found [Tao and Vu, 2010; Wood, 2012] also under the name of empirical spectral distribution.

Eq. (A.8) can converge. First, the convergence in probability, which happens when

$$\lim_{N\to\infty} \text{Prob}\left[|\Delta\phi_\mu| \geq \epsilon\right] = 0, \tag{A.9}$$

for every $\epsilon > 0$. Second, the almost sure (also named as almost everywhere or with probability one) convergence, which is given if, with probability one, the difference $\Delta\phi_\mu$ converges to zero for all ϕ, i.e.,

$$\text{Prob}\left[\lim_{N\to\infty} |\Delta\phi_\mu| = 0\right] = 1, \tag{A.10}$$

which is a stronger condition than Eq. (A.9), i.e., it typically implies convergence in probability.

We consider in the next section the case of dense random matrices.

A.2.1 Dense Matrices

We consider first the Hermitian random matrices, for which the universal law is given by Eq. (1.20). We state here the most recent version of the theorem for the dense semi-circular law, i.e., under weakest hypotheses.

Theorem 1 (Dense semi-circular law [Bai, 1999])**.** *Let ζ be a real random variable, and let ξ be a complex random variable with variance one. For each $N \geq 1$, assume $\boldsymbol{A}$ to be a $N \times N$ Hermitian matrix whose entries on or above the diagonal are independent. Further assume that the diagonal entries are i.i.d. copies of ζ and those above the diagonal are i.i.d. copies of ξ. Then the empirical spectral density of the rescaled matrix $\boldsymbol{A}/\sqrt{N}$ converges almost surely (and in probability) to the semi-circular law in Eq.* (1.20) *as $N \to \infty$.*

As for non-Hermitian matrices $\mathbf{A}$ with independent and identical distributed (i.i.d.) entries A_{ij}, the empirical spectral measure of $\mathbf{A}/\sqrt{N}$ approaches the distribution for the uniform probability measure on the unit disk in the complex plane in Eq. (1.21) as N goes to infinity, a phenomenon known in the literature as the *circular* law. The dense (i.e., non-sparse) circular law has been proven in many special cases by many authors, starting from [Mehta, 1967] (Gaussian case), [Girko, 1985, 2004], [Edelman, 1988], [Ginibre, 1965] (real Gaussian case), [Bai and Silverstein, 2010; Bai, 1997] [continuous case with bounded $(2+\delta)$-th moment, for $\delta > 0$], [Götze and Tikhomirov, 2007] (sub-Gaussian case) and [Götze and Tikhomirov, 2007] (bounded $(2 + \delta)$-th moment, for $\delta > 0$), [Pan and Zhou, 2010] (bounded 4-th moment), [Tao and Vu, 2008] (bounded $(2 + \delta)$-th moment, for $\delta > 0$). The following theorem 2 is the current best result, due to [Tao and Vu, 2010], requiring only zero mean and unit variance (see also [Tao and Vu, 2009]).

Theorem 2 (Dense circular law [Tao and Vu, 2010])**.** *Let ξ be a complex random variable with mean zero and variance one. For each $N \geq 1$, assume that the entries of $\boldsymbol{A}$ are*

i.i.d. copies of ξ. Then the empirical spectral measure of the rescaled matrix $\boldsymbol{A}/\sqrt{N}$ converges almost surely (and in probability) to a measure with density that satisfies the circular law in Eq. (1.21) *as $N \to \infty$.*

There have been recently interests in generalising Theorem 2 to random matrix ensembles where the finite variance hypothesis is relaxed [Bordenave et al., 2011].

For a general class of matrices $\{\mathbf{A}\}_{N\geq 1}$ satisfying the following condition A.2.1, we state below the theorem for the elliptic law, as formulated by [Naumov, 2013], requiring finite fourth moment. and satisfying the following condition:

Definition A.2.1. (Condition for the elliptic law.) Let (u, l) be a random vector in $\mathbb{R}^2$ where both u and l have mean zero and variance one. Let $\{(A_{ij}, A_{ji})\}$ be an infinite double array of random variables on $\mathbb{R}$. For each $N \geq 1$ we define the random $N \times N$ matrix $\mathbf{A} = (A_{ij})_{1\leq i,j\leq N}$. The sequence of random matrices $\{\mathbf{A}\}_{N\geq 1}$ is said to satisfy the condition for the elliptic law with atom variables (u, l) if the following conditions hold:

(i) (Independence): $\{A_{ii} : i \geq 1\} \cup \{(A_{ij}, A_{ji}) : 1 \leq i < j\}$ is a collection of independent random elements;

(ii) (Common distribution): each pair $(A_{ij}, A_{ji}) : 1 \leq i < j$ is an i.i.d. copy of (u, l) — pairs independent and identically distributed — ;

(iii) (Flexibility of the main diagonal): the diagonal elements $\{A_{ii} : i \geq 1\}$ are i.i.d. with mean zero and finite variance.

Theorem 3 (Dense elliptic law [Naumov, 2013])**.** *Let $\{\mathbf{A}\}_{N\geq 1}$ be a sequence of real random matrices that satisfy condition in Def. A.2.1 with atom variables (u, l) where $\langle ul\rangle = \tau$ where $-1 < \tau < 1$. Also, assume that $\langle u^4\rangle, \langle l^4\rangle < \infty$. Then the empirical spectral measure of the rescaled matrix $\mathbf{A}/\sqrt{N}$ converges in probability to a measure with density that satisfies the elliptic law with parameter τ in Eq.* (1.22) *as $N \to \infty$.*

The hypothesis of finite fourth moment has been weaken and the theorem generalised for complex matrices in Refs. [Götze et al., 2015; Nguyen and O'Rourke, 2015]. Moreover, in the light of universality principle [Tao and Vu, 2010], [Wood, 2012], it has been conjectured [Nguyen and O'Rourke, 2015] that the elliptic theorem continues to hold when $\langle |u|^2\rangle = \langle |l|^2\rangle = 1$ and $\langle ul\rangle = \tilde{\tau}$, where $\tilde{\tau}$ is a complex number such that $|\tilde{\tau}| < 1$.

A.2.2 Dilute matrices

The mathematical literature in dilute random matrices is much less rich than in dense matrices. However, here we state the theorem on the circular law for dilute random matrices; the case of sparse matrices with $\alpha = 0$ is an exception.

Theorem 4 (Dilute circular law [Wood, 2012]). *Let* $0 < \alpha \leq 1$ *be a constant, and let* J_{ij} *be a real*[2] *random variable with mean zero and variance one,* $\forall i, j = 1, \ldots, N$. *Let* $\mathbf{A}$ *be the random matrix in Eq.* (1.42) *with the random adjacency matrix* $\mathbf{C}$ *as in Eq.* (1.31) *with* p *as in Eq.* (1.33). *Then the empirical spectral measure of* $\mathbf{A}/\sqrt{pN}$ *with* p *as in Eq.* (1.33) *converges in probability to the uniform distribution on the unit disk; in other words, the density of the empirical spectral measure converges to the circular law in Eq.* (1.21).

[2] it can be complex, and the theorem is still valid

A.3 Assumptions in the definition of the antagonistic ensemble

Here we make explicit the assumptions needed to define the antagonistic ensemble in Sec. 2.1.2, determined by Eq. (2.7), starting from Eq. (2.1), which is the model for sparse random matrices with pairwise correlated weights. We show first the most general antagonistic ensemble that one can study with the model in the Eq. (2.1). Then, we build progressively the definition of the antagonistic ensemble as in Eq. (2.7), which is the one used in this thesis to model antagonistic matrices.

The generic joint probability density of the antagonistic ensemble is given by

$$p(u,l) = p^{\mathrm{A}}(u,l) := \alpha\, p_2(u,l)\theta(-ul), \tag{A.11}$$

with

$$\int_{\mathbb{R}^2} \mathrm{d}u\, \mathrm{d}l\, p^{\mathrm{A}}(u,l) = \int_{\mathbb{R}^2} \mathrm{d}u\, \mathrm{d}l\, p_2(u,l) = 1, \tag{A.12}$$

where $p_2(u,l)$ is a general joint probability density with support on $\mathbb{R}^2$. The theta functions, defined in Eq. (2.8), account for the sign constraints of predator-prey interactions. The factor α accounts for normalisation of p^{A}, and it can depend on the symmetry properties of p_2 (for example, if $p_2(u,l) = p_2(-u,l)$ or $p_2(u,l) = p_2(u,-l)$ for $u,l \in \mathbb{R}$ then $\alpha = 2$). We observe that the model in the Eq. (2.1) admits an internal symmetry for node labelling order: the choice of ordering (i,j) in (J_{ij}, J_{ji}) is not physical (internal permutation symmetry of the model). This translates into the fact that the configuration (u,l), with $ul < 0$, must be equivalent to the configuration (l,u). In other words, if for example in the couple (i,j) i is a predator of j, and j is a prey of i, in a random network model as in the Eq. (2.1), it is possible relabel the pair so that j is a predator of i, and i is a prey of j. Before relabelling, the interaction of the pair (i,j) is represented by (u,l) with $u > 0, l < 0$; after relabelling, the interaction of the same pair (i,j) is represented by (u',l') with $u' = l < 0, l' = u > 0$. Therefore, the probability p_2 admits a symmetry for $(u,l) \to (l,u)$, i.e., $p_2(u,l) = p_2(l,u)$, which we call internal permutation symmetry. Because of the definition in Eq. (A.11), this condition is reflected on p^{A}, i.e., $p^{\mathrm{A}}(u,l) = p^{\mathrm{A}}(l,u)$ and, for general joint p from the model in Eq. (2.1).

We observe that this assumption of symmetry does not imply that the probability of being a predator coincides with the probability of being a prey. Indeed, the first quantity is $\langle \theta(u) + \theta(l) \rangle_{p^{\mathrm{A}}}$, with p^{A} as in Eq. (A.11), which is equal to $2\langle \theta(u) \rangle_{p^{\mathrm{A}}}$ for the symmetry of p_2 just discussed. The second quantity is $\langle \theta(-u) + \theta(-l) \rangle_{p^{\mathrm{A}}} = 2\langle \theta(-u) \rangle_{p^{\mathrm{A}}}$, which is generally different from $2\langle \theta(u) \rangle_{p^{\mathrm{A}}}$ (similarly, the average strength of predator $2\langle u\theta(u) \rangle_{p^{\mathrm{A}}}$ and prey $-2\langle u\theta(-u) \rangle_{p^{\mathrm{A}}}$ are generally different). However, these quantities become equal with the assumption $p_2(u,l) = p_2(-l,-u)$, which we call predator-prey symmetry. Since we are interested in the role of the sign constraint in the model, we assume for simplicity that the correlation between the random variables u, l holds only at the level of their

signs, and not of their magnitudes. Therefore, Eq. (A.11) can be simplified into

$$p^{\mathrm{A}}(u,l) = \alpha\, p_1(u)p_1(l)\theta(-ul), \tag{A.13}$$

where p_1 is a probability density with support on $\mathbb{R}$, normalised to one. Finally, we assume p_1 to be symmetric in $\mathbb{R}$, reflecting the fact we do not distinguish between the magnitudes of different kinds of interaction, i.e., between the strength of predators and preys: $p_1(x) = p_1(-x)$, with x a real number. With these symmetry properties, it is easy to verify that

$$\alpha = 2. \tag{A.14}$$

Now we can define from p_1 a probability density $\tilde{p}$ with positive support ($[0,\infty)$) and normalised to one such that

$$2p_1(x) = \tilde{p}(|x|), \tag{A.15}$$

from which we can obtain finally the joint probability density of antagonistic matrices in Eq. (2.7)

A.4 Formulas for the moments of the antagonistic and mixture ensembles

Here we want to express the moments of the joint probabilities $p(u,l)$ with support on $\mathbb{R}^2$ in terms of the moments of the auxiliary probability distribution $\tilde{p}$ with support on $\mathbb{R}^+$, in the Eqs. (2.7), (2.14) and (2.13).

As for the antagonistic ensemble, the generic moment for the joint $p(u,l) = p^{\mathrm{A}}(u,l)$ in Eq. (2.7) reads

$$\langle u^m l^n \rangle_{p^{\mathrm{A}}} = \frac{1}{2} \langle u^m \rangle_{\tilde{p}} \langle l^n \rangle_{\tilde{p}} \left[(-1)^m + (-1)^n \right], \tag{A.16}$$

with m, n integer numbers. In particular from Eq. (A.16) we have

$$\left\langle u^{2m+1} \right\rangle_{p^{\mathrm{A}}} = 0, \tag{A.17}$$

$$\left\langle u^{2m} \right\rangle_{p^{\mathrm{A}}} = \left\langle u^{2m} \right\rangle_{\tilde{p}}, \tag{A.18}$$

$$\left\langle u^{2m+1} l^{2n+1} \right\rangle_{p^{\mathrm{A}}} = - \left\langle u^{2m+1} \right\rangle_{\tilde{p}} \left\langle l^{2n+1} \right\rangle_{\tilde{p}}, \tag{A.19}$$

which hold similarly also for $\langle l^n \rangle_{p^{\mathrm{A}}}$. From Eqs. (A.17)-(A.19) we have that the variance of $p^{\mathrm{A}}(u,l)$ reads

$$\left\langle u^2 \right\rangle_{p^{\mathrm{A}}} - \cancelto{0}{\langle u \rangle^2_{p^{\mathrm{A}}}} = \left\langle u^2 \right\rangle_{\tilde{p}}, \tag{A.20}$$

while the covariance of $p^{\mathrm{A}}(u,l)$ reads

$$\langle ul \rangle_{p^{\mathrm{A}}} - \cancelto{0}{\langle u \rangle_{p^{\mathrm{A}}} \langle l \rangle_{p^{\mathrm{A}}}} = - \langle u \rangle_{\tilde{p}} \langle l \rangle_{\tilde{p}}. \tag{A.21}$$

Similarly, the generic moment for the joint $p(u,l) = p^{\mathrm{CM}}(u,l)$ in Eq. (2.14) reads

$$\langle u^m l^n \rangle_{p^{\mathrm{CM}}} = \langle u^m \rangle_{\tilde{p}} \langle l^n \rangle_{\tilde{p}} \left[\pi^{\mathrm{M}} + (1 - \pi^{\mathrm{M}})(-1)^{m+n} \right], \tag{A.22}$$

with m, n integer numbers.

As for the mixture ensemble, the generic moment for the joint $p(u,l) = p^{\mathrm{M}}(u,l)$ in Eq. (2.13) reads

$$\langle u^m l^n \rangle_{p^{\mathrm{M}}} = \langle u^m \rangle_{\tilde{p}} \langle l^n \rangle_{\tilde{p}} \left[\frac{\pi^{\mathrm{A}}}{2} \left((-1)^m + (-1)^n \right) + \left(1 - \pi^{\mathrm{A}} \right) \left(\pi^{\mathrm{M}} + (1 - \pi^{\mathrm{M}})(-1)^{m+n} \right) \right], \tag{A.23}$$

with m, n integer numbers. From Eqs. (A.22) and (A.23) we have that the first moment ($m = 1$ and $n = 0$) is

$$\langle u \rangle_{p^{\mathrm{M}}} = 2(1 - \pi^{\mathrm{A}}) \left(\pi^{\mathrm{M}} - \frac{1}{2} \right) \langle u \rangle_{\tilde{p}}, \tag{A.24}$$

while the second moment

$$\left\langle u^2 \right\rangle_{p^{\mathrm{M}}} = \left[\pi^{\mathrm{A}} + (1 - \pi^{\mathrm{A}}) \left(\pi^{\mathrm{M}} + (1 - \pi^{\mathrm{M}}) \right) \right] \left\langle u^2 \right\rangle_{\tilde{p}} = \left\langle u^2 \right\rangle_{\tilde{p}}. \tag{A.25}$$

From Eqs. (A.24) and (A.25) the variance of $p^{\mathrm{M}}(u, l)$ reads

$$\left\langle u^2 \right\rangle_{p^{\mathrm{M}}} - \langle u \rangle_{p^{\mathrm{M}}}^2 = \left\langle u^2 \right\rangle_{\tilde{p}} - 4\left(1 - \pi^{\mathrm{A}}\right)^2 \left(\pi^{\mathrm{M}} - \frac{1}{2}\right)^2 \langle u \rangle_{\tilde{p}}^2 , \tag{A.26}$$

which correctly recovers the variance of p^{A} in Eq. (A.20) when $\pi^{\mathrm{A}} = 1$, while the covariance of $p^{\mathrm{M}}(u, l)$ reads

$$\langle ul \rangle_{p^{\mathrm{M}}} - \langle u \rangle_{p^{\mathrm{M}}} \langle l \rangle_{p^{\mathrm{M}}} = \langle u \rangle_{\tilde{p}} \langle l \rangle_{\tilde{p}} \left[1 - 2\pi^{\mathrm{A}} - 4(1 - \pi^{\mathrm{A}})^2 \left(\pi^{\mathrm{M}} - \frac{1}{2}\right)^2 \right] , \tag{A.27}$$

which correctly recovers the covariance of p^{A} in Eq. (A.21) when $\pi^{\mathrm{A}} = 1$.

A.5 Derivation of the formula for the empirical spectral density in terms of the resolvent

In this appendix we derive the formula Eq. (3.2) for the empirical spectral density of a matrix $\mathbf{A}$ in Eq. (1.19) in terms of the resolvent of a matrix.

First, we observe that the Eq. (1.19) is a distributional equation, i.e., it needs to be interpreted as action on a space of test functions (see, for example, [Vladimirov, 1979]). We consider here the space of smooth (see Appendix A.6.1 for the definition) functions and with compact support $D \subset \mathbb{C}$, for which the action of distributions is represented by complex integrals in D. Accordingly, given a smooth function ϕ with compact support D, such that it contains the spectrum (defined in Eq. (1.11)), i.e., $\sigma(\mathbf{A}) \subset D$, Eq. (1.19) translates into the complex integral [Reed et al., 1980], with $z = x + \mathrm{i}y$,

$$\int_D \mathrm{d}x\, \mathrm{d}y\, \rho_{\mathbf{A}}(z)\phi(z) = \frac{1}{N}\sum_{j=1}^{N}\int_D \mathrm{d}x\, \mathrm{d}y\, \delta(z-\lambda_j(\mathbf{A}))\phi(z) = \frac{1}{N}\sum_{j=1}^{N}\phi(\lambda_j(\mathbf{A})), \tag{A.28}$$

$$= \frac{1}{N}\sum_{j=1}^{N}\left(\delta_{\lambda_j(\mathbf{A})}, \phi\right), \tag{A.29}$$

where $\mathrm{d}x\,\mathrm{d}y$ is the (two-dimensional) Lebesgue measure in the complex plane, and where we introduced the following compact notation to express the action, though Lebesgue integration, of the distribution ψ on the test function ϕ in the compact support D, i.e.,

$$(\psi, \phi) := \int_D \mathrm{d}x\, \mathrm{d}y\, \psi(z)\phi(z), \tag{A.30}$$

and we denoted in Eq. (A.29) the delta distribution in the complex plane that is centred in $\lambda_j(\mathbf{A})$ by $\delta_{\lambda_j(\mathbf{A})}$. The Eq. (A.28) expresses also the usefulness of the empirical spectral density, in the sense that by integrating ϕ with respect to the empirical spectral density $\rho_{\mathbf{A}}$, one obtains the arithmetic average of ϕ evaluated at the eigenvalues of $\mathbf{A}$.

We now proceed with the derivation of Eq. (3.2). We observe that $\mathbf{A} = \mathbf{U}\mathbf{T}_N\mathbf{U}^{-1}$, by Schur's decomposition of a general matrix $\mathbf{A}$, where $\mathbf{U}$ is a unitary matrix and $\mathbf{T}_N$ is upper triangular with diagonal elements equal to the eigenvalues $\lambda_j(\mathbf{A})$. Accordingly, given the cyclicality of the trace operator and some elementary matrix operations (see for example [Petersen and Pedersen, 2012]), we have

$$\begin{aligned}\mathrm{Tr}\left[\mathbf{G}_{\mathbf{A}}(z)\right] &= \mathrm{Tr}\left[(\mathbf{A} - z\mathbf{1}_N)^{-1}\right] \\ &= \mathrm{Tr}\left[(\mathbf{T}_N - z\mathbf{1}_N)^{-1}\right] \\ &= \sum_{j=1}^{N}\frac{1}{\lambda_j(\mathbf{A}) - z}.\end{aligned} \tag{A.31}$$

In order to prove Eq. (3.2), we observe that, similarly to Eq. (1.19), also Eq. (3.2) is a

distributional equation, i.e., it needs to be interpreted as an action on a space of test functions. As above, we consider a test function ϕ that is smooth and with compact support $D \subset \mathbb{C}$, such that $\sigma(\mathbf{A}) \subset D$. By using Eq. (A.31), and similarly to Eqs. (A.28)-(A.30), the distributional Eq. (3.2) can be expressed through its action on the test function ϕ as follows

$$-\frac{1}{\pi N}\sum_{j=1}^{N}\left(\partial_{\bar{z}}\frac{1}{\lambda_j(\mathbf{A})-z},\phi\right)=\frac{1}{N}\sum_{j=1}^{N}\left(\delta_{\lambda_j(\mathbf{A})},\phi\right). \tag{A.32}$$

In order to complete the derivation of Eq. (3.2), we prove now Eq. (A.32). This can be done in two steps. First, the j-th term in the sum in the left hand side can be viewed within the distributional derivative as

$$-\left(\partial_{\bar{z}}\frac{1}{\lambda_j(\mathbf{A})-z},\phi\right)=\left(\frac{1}{\lambda_j(\mathbf{A})-z},\partial_{\bar{z}}\phi\right), \tag{A.33}$$

since the boundary terms, coming from integration by parts, vanish for test functions on compact support. Second, the proof is completed by using the Cauchy-Pompeiu formula (see Appendix A.6) to the test function ϕ, that with the notation in Eq. (A.30), reads

$$\phi(\lambda_j(\mathbf{A}))=\frac{1}{\pi}\left(\frac{1}{\lambda_j(\mathbf{A})-z},\partial_{\bar{z}}\phi\right), \tag{A.34}$$

$$=-\frac{1}{\pi}\left(\partial_{\bar{z}}\frac{1}{\lambda_j(\mathbf{A})-z},\phi\right), \tag{A.35}$$

where we used Eq. (A.33) in Eq. (A.35). Finally, by using Eq. (A.29) on the left hand side of Eq. (A.35), we have proven Eq. (A.32), from which, as discussed above, the derivation of Eq. (3.2) is completed.

□

We observe also that the formula Eq. (A.32), that we have just proven, is equivalent to the following distributional equation

$$\partial_{\bar{z}}(\pi z)^{-1}=\delta(z), \tag{A.36}$$

which, mathematically speaking, is nothing but a representation of the δ in the complex plane.

A.6 The Cauchy-Pompeiu formula

In this appendix we derive the Cauchy-Pompeiu formula for complex functions (see for example Ref. [Fong, 2006a; Henrici, 1986; Hörmander, 1966]), that is the generalisation to smooth functions of the Cauchy integral formula, which holds for holomorphic functions. We make here the observation (explained in Sec. A.6.1), essential in this section, that smooth functions are not necessarily holomorphic (complex differentiable), which translates into the fact that their partial derivative $\partial_{\bar{z}}$, defined in Eq. (3.3), is generally non-zero (see Sec. A.6.1.1).

A straightforward way to obtain the Cauchy-Pompeiu formula is by using the Stokes-Cartan theorem (see below), which is a generalisation of the Stokes theorem, for differential forms [Fong, 2006b; Nahmad-Achar, 2018].

Theorem 5. *(Stokes-Cartan)[Cartan, 1945]. If ω is a $(n-1)$-form with compact support on smooth n-dimensional manifold Ω, $\partial\Omega$ denotes the boundary of Ω given the induced orientation, then*

$$\int_{\Omega} \mathrm{d}\omega = \int_{\partial\Omega} \omega|_{\partial\Omega}, \tag{A.37}$$

where the n-form $\mathrm{d}\omega$ is the exterior derivative of ω.

To proceed in the derivation of the Cauchy-Pompeiu formula, we define the 1-form

$$\chi := \frac{1}{z-\zeta}\,\mathrm{d}z, \quad \text{with} \quad z \in \mathbb{C} \setminus \{\zeta\}, \tag{A.38}$$

which satisfies

$$\mathrm{d}\chi = 0, \quad \text{with} \quad z \in \mathbb{C} \setminus \{\zeta\}, \tag{A.39}$$

as we show below.

Proposition 1. *χ is closed in $\mathbb{C} \setminus \{\zeta\}$, i.e. $\mathrm{d}\chi = 0$.*

$$\begin{aligned}
\mathrm{d}\chi &= \mathrm{d}\left(\frac{1}{z-\zeta}\right) \wedge \mathrm{d}z + \frac{1}{z-\zeta}\cancelto{0}{\mathrm{d}z \wedge \mathrm{d}z} \\
&= \left((\partial_z \frac{1}{z-\zeta})\mathrm{d}z + (\partial_{\bar{z}} \cancelto{0}{\frac{1}{z-\zeta}})\mathrm{d}\bar{z} \right) \wedge \mathrm{d}z \\
&= -\frac{1}{(z-\zeta)^2}\cancelto{0}{\mathrm{d}z \wedge \mathrm{d}z} = 0.
\end{aligned}$$

With the following we completely characterise the 1-form χ:

Proposition 2. *χ is not exact, i.e. $\int_{C_r}\chi\neq 0$ on a circumference C_r of radius $r>0$ centred in ζ.*

Consider the standard parametrisation of C_r given by $z(\theta)=\zeta+re^{\mathrm{i}\theta}$ with $\theta\in[0,2\pi)$. Then we have

$$\int_{C_r}\chi=\int_{C_r}\frac{\mathrm{d}z}{z-\zeta}=\int_0^{2\pi}\frac{\mathrm{d}(\zeta+re^{\mathrm{i}\theta})}{\zeta+re^{\mathrm{i}\theta}-\zeta}=\int_0^{2\pi}\frac{re^{\mathrm{i}\theta}\,\mathrm{i}\mathrm{d}\theta}{re^{\mathrm{i}\theta}}=\int_0^{2\pi}\mathrm{i}\mathrm{d}\theta=2\pi\mathrm{i}. \quad \text{(A.40)}$$

This means that here is no function f defined on the complex plane $\mathbb{C}\setminus\{\zeta\}$ such that $df=\chi$. If χ were exact, say $\chi=\mathrm{d}f$, we would have (applying Stokes Theorem) $\int_{C_r}\chi=\int_{C_r}\mathrm{d}f=f(z(2\pi))-f(z(0))=f(\zeta+r)-f(\zeta+r)=0$, since $e^{2\pi\mathrm{i}}=e^0=1$.

In order to derive the Cauchy-Pompeiu formula, we consider a smooth complex-valued function ϕ. We consider a compact disk $D_R\subset\mathbb{C}$, with radius R, that contains ζ, so that the hypothesis of the Stokes theorem are satisfied. We define the 1-form

$$\omega:=\phi\chi,\quad \text{with}\quad z\in\mathbb{C}\setminus\{\zeta\}, \quad \text{(A.41)}$$

from which we have that

$$\begin{aligned}\mathrm{d}\omega=\mathrm{d}(\phi\chi)&=\mathrm{d}\phi\wedge\chi+\phi\cancelto{0}{\mathrm{d}\chi}\\&=(\partial_z\phi\,\mathrm{d}z+\partial_{\bar z}\phi\,\mathrm{d}\bar z)\wedge\frac{\mathrm{d}z}{z-\zeta}\\&=\frac{\partial_{\bar z}\phi}{z-\zeta}\,\mathrm{d}\bar z\wedge\mathrm{d}z,\end{aligned} \quad \text{(A.42)}$$

where we used that χ is closed in $z\in\mathbb{C}\setminus\{\zeta\}$.

Now, consider the disk $D_{r,R}$ obtained by subtracting to D_R a small disk D_r of radius r centred on ζ. We can apply the Stokes-Cartan Theorem 5 to ω in $D_{r,R}\subset(\mathbb{C}\setminus\{\zeta\})$, i.e.

$$\begin{aligned}\int_{D_{r,R}}\mathrm{d}\omega&=\int_{\partial D_{r,R}}\omega\\&=\int_{\partial D_R}\omega-\int_{\partial D_r}\omega.\end{aligned} \quad \text{(A.43)}$$

The contour integral on the small disk reads

$$\int_{\partial D_r}\omega=\int_0^{2\pi}\frac{\phi(\zeta+re^{\mathrm{i}\theta})}{\zeta+re^{\mathrm{i}\theta}-\zeta}r\;de^{\mathrm{i}\theta}=\mathrm{i}\int_0^{2\pi}\phi(\zeta+re^{\mathrm{i}\theta})\mathrm{d}\theta. \quad \text{(A.44)}$$

By using Eq. (A.42) and Eq. (A.44), Eq. (A.43) becomes

$$\int_{D_{r,R}} \frac{\partial_{\bar{z}}\phi}{z-\zeta}\,\mathrm{d}\bar{z}\wedge\mathrm{d}z = \int_{\partial D_R} \frac{\phi}{z-\zeta}\,\mathrm{d}z - \mathrm{i}\int_0^{2\pi} \phi(\zeta + re^{\mathrm{i}\theta})\mathrm{d}\theta. \tag{A.45}$$

In the limit of the radius r going to 0, the last contribute on the right of Eq. (A.45) leads to

$$\mathrm{i}\int_0^{2\pi} \phi(\zeta + re^{\mathrm{i}\theta})\mathrm{d}\theta \to \mathrm{i}\int_0^{2\pi} \phi(\zeta)\mathrm{d}\theta = 2\pi\mathrm{i}\phi(\zeta), \tag{A.46}$$

since $\phi(\zeta + re^{\mathrm{i}\theta})$ converges to $\phi(\zeta)$ when $r \to 0$. On the other side, the disk $D_{r,R}$ fills all the disk D_R when $r \to 0$. So by taking the limit $r \to 0$ we can rewrite Eq. (A.45) as

$$\int_{D_R} \frac{\partial_{\bar{z}}\phi}{z-\zeta}\,\mathrm{d}\bar{z}\wedge\mathrm{d}z = \int_{\partial D_R} \frac{\phi}{z-\zeta}\,\mathrm{d}z - 2\pi\mathrm{i}\phi(\zeta). \tag{A.47}$$

By inverting now the Eq. (A.47), we obtain the Cauchy-Pompeiu formula, i.e.

$$\phi(\zeta) = \frac{1}{2\pi\mathrm{i}}\int_{\partial D_R} \frac{\phi}{z-\zeta}\,\mathrm{d}z - \frac{1}{2\pi\mathrm{i}}\int_{D_R} \frac{\partial_{\bar{z}}\phi}{z-\zeta}\,\mathrm{d}\bar{z}\wedge\mathrm{d}z. \tag{A.48}$$

□

If ϕ is a test function on the space of smooth (but not necessarily holomorphic, such that in general $\partial_{\bar{z}}\phi \neq 0$) complex functions with compact support $D \subset \mathbb{C}$, such that the arbitrary disc D_R contains D, we have that the contour integral in Eq. (A.48) vanishes, so that we have

$$\phi(\zeta) = -\frac{1}{2\pi\mathrm{i}}\int_D \frac{\partial_{\bar{z}}\phi}{z-\zeta}\,\mathrm{d}\bar{z}\wedge\mathrm{d}z, \tag{A.49}$$

which reduces to the Lebesgue integral, in the support $D \subset \mathbb{C}$, with the (bi-dimensional) measure $\mathrm{d}x\mathrm{d}y$, i.e.,

$$\phi(\zeta) = -\frac{1}{\pi}\int_D \frac{\partial_{\bar{z}}\phi}{z-\zeta}\,\mathrm{d}x\,\mathrm{d}y, \tag{A.50}$$

as applied in Sec. A.5.

A.6.1 Smooth complex functions and holomorphic functions

Here we discuss the observation, made in the main text, that complex functions that are smooth are not necessarily holomorphic, while the converse holds.
First, we consider a complex-valued function ϕ, i.e., $\phi : \Omega \to \mathbb{C}$, with $\Omega \subseteq \mathbb{C}$. ϕ can be represented at a given point $z = x + \mathrm{i}y \in \mathbb{C}$, in terms of its real and imaginary parts, that we define as follows

$$\phi(z = x + \mathrm{i}y) = u(x, y) + \mathrm{i}v(x, y), \tag{A.51}$$

where u, v are real valued functions. Now we discuss the smoothness and the holomorphic properties.

Smooth complex functions. The complex function ϕ in Eq. (A.51) is said to be smooth when u, v are of class C^∞, i.e., the partial derivatives of any order of u, v exist and are continuous.

Holomorphic functions. Holomorphic and complex-differentiable are synonymous[a]. Holomorphic functions are actually infinitely differentiable, and all holomorphic functions are complex analytic function that equal their own Taylor series, which is a remarkable result of complex analysis, that is based on the Cauchy integral formula (see, for example, [Rudin, 1987]). This result also implies that holomorphic functions are smooth.
We remind that a function (real or complex) is differentiable in an open set, by definition, if and only if the limiting difference quotient is well defined on any given point in the open set (see, for example, [Hörmander, 1966; Rudin, 1987]). We suppose now that u and v in Eq. (A.51) are real-differentiable in Ω'. This implies that the partial derivatives of u and v exist. This is not enough to guarantee $\phi(z)$ to be complex-differentiable for any $z \in \Omega$. In terms of the partial derivatives of u and v, the complex-differentiability is a stronger condition with respect to the real-differentiability. More in detail, other two conditions on the partial derivatives of u and v are needed for the complex-differentiability. Indeed, $\phi(z)$ is complex-differentiable at $z = x + \mathrm{i}y$ if and only if the partial derivatives of u and v satisfy the following Cauchy-Riemann equations at z, i.e.,

$$\partial_x u = \partial_y v \tag{A.52}$$

$$\partial_y u = -\partial_x v. \tag{A.53}$$

Since z is arbitrary in Ω, we have that ϕ is complex-differentiable in Ω if and only if the partial derivatives of u and v satisfy the Cauchy-Riemann equations in Eq. (A.52), Eq. (A.53) in Ω.

[a] If ϕ is complex differentiable at every point in an open set Ω, then ϕ is holomorphic on Ω. ϕ is holomorphic on some non-open set Ω if it is holomorphic in an open set containing Ω.

A.6.1.1 Holomorphicity and explicit dependence on $\bar{z}$

In this paragraph, in light of the discussion above, we show the equivalence

$$\phi \text{ is holomorphic on } \Omega \iff \partial_{\bar{z}}\phi = 0 \text{ in } \Omega, \text{ with } \Omega \subseteq \mathbb{C}, \tag{A.54}$$

which we assumed in the main text several times.
We can use the Cauchy-Riemann equations in Eq. (A.52), Eq. (A.53) to show the equivalence in Eq. (A.54), with the following Proposition.

Proposition 3. *Given a complex-valued function ϕ as in Eq.* (A.51)*, u and v are real-differentiable, we have that: ϕ satisfies the Cauchy-Riemann equations in Eq.* (A.52)*, Eq.* (A.53) *(and so ϕ is holomorphic) $\iff \partial_{\bar{z}}\phi = 0$.*

This can be shown straightforwardly, as follows

$$\begin{aligned} 2\partial_{\bar{z}}\phi &= (\partial_x + \mathrm{i}\partial_y)\,(u + iv) \\ &= \partial_x u - \partial_y v + \mathrm{i}(\partial_x v + \partial_y u). \end{aligned}$$

Then one observes that the right hand side is zero if and only if the Cauchy-Riemann equations are satisfied.

A.7 Inverse of a block matrix in terms of Schur complements

Here we show how the inverse of a block matrix can be obtained via the Schur complements [Bordenave and Lelarge, 2010; Gallier et al., 2010; Lu and Shiou, 2002; Petersen and Pedersen, 2012]. Given a general invertible square block matrix of rank $2N$ parametrised as follows

$$\mathbf{A} := \begin{pmatrix} \mathbf{a} & \mathbf{b} \\ \mathbf{c} & \mathbf{d} \end{pmatrix}, \tag{A.55}$$

where in general the blocks $\mathbf{a}, \mathbf{b}, \mathbf{c}, \mathbf{d}$ have different sizes, with $\mathbf{a}, \mathbf{d}$ square matrices and invertible. The Schur complements $\mathbf{s_a}$ of $\mathbf{a}$ and $\mathbf{s_d}$ of $\mathbf{d}$ are defined as

$$\mathbf{s_a} := (\mathbf{d} - \mathbf{c}\mathbf{a}^{-1}\mathbf{b})^{-1}, \tag{A.56}$$

$$\mathbf{s_d} := (\mathbf{a} - \mathbf{b}\mathbf{d}^{-1}\mathbf{c})^{-1}. \tag{A.57}$$

Accordingly, one way to express the inverse of $\mathbf{A}$ in terms of Schur complement $\mathbf{s_d}$ is

$$\begin{aligned} \mathbf{A}^{-1} &= \begin{pmatrix} \mathbf{a} & \mathbf{b} \\ \mathbf{c} & \mathbf{d} \end{pmatrix}^{-1} \\ &= \begin{pmatrix} \mathbf{1} & \mathbf{0} \\ -\mathbf{d}^{-1}\mathbf{c} & \mathbf{1} \end{pmatrix} \begin{pmatrix} \mathbf{s_d} & \mathbf{0} \\ \mathbf{0} & \mathbf{d}^{-1} \end{pmatrix} \begin{pmatrix} \mathbf{1} & -\mathbf{b}\mathbf{d}^{-1} \\ \mathbf{0} & \mathbf{1} \end{pmatrix} \\ &= \begin{pmatrix} \mathbf{s_d} & -\mathbf{s_d}\mathbf{b}\mathbf{d}^{-1} \\ -\mathbf{d}^{-1}\mathbf{c}\mathbf{s_d} & \mathbf{d}^{-1}\mathbf{c}\mathbf{s_d}\mathbf{b}\mathbf{d}^{-1} + \mathbf{d}^{-1} \end{pmatrix}, \end{aligned} \tag{A.58}$$

where the block structure is preserved, and the sizes of the identity and the zero matrices are related (and constrained) to the size of the matrices $\mathbf{a}, \mathbf{b}, \mathbf{c}, \mathbf{d}$. Other equivalent forms of the inverse $\mathbf{A}^{-1}$ in terms of the Schur complements $\mathbf{s_a}$ and $\mathbf{s_d}$ read

$$\mathbf{A}^{-1} = \begin{pmatrix} \mathbf{s_d} & -\mathbf{a}^{-1}\mathbf{b}\mathbf{s_a} \\ -\mathbf{s_a}\mathbf{c}\mathbf{a}^{-1} & \mathbf{s_a} \end{pmatrix} \tag{A.59}$$

$$= \begin{pmatrix} \mathbf{a}^{-1}\mathbf{b}\mathbf{s_a}\mathbf{c}\mathbf{a}^{-1} + \mathbf{a}^{-1} & -\mathbf{a}^{-1}\mathbf{b}\mathbf{s_a} \\ -\mathbf{s_a}\mathbf{c}\mathbf{a}^{-1} & \mathbf{s_a} \end{pmatrix} \tag{A.60}$$

$$= \begin{pmatrix} \mathbf{a}^{-1}\mathbf{b}\mathbf{s_a}\mathbf{c}\mathbf{a}^{-1} + \mathbf{a}^{-1} & -\mathbf{s_d}\mathbf{b}\mathbf{d}^{-1} \\ -\mathbf{d}^{-1}\mathbf{c}\mathbf{s_d} & \mathbf{d}^{-1}\mathbf{c}\mathbf{s_d}\mathbf{b}\mathbf{d}^{-1} + \mathbf{d}^{-1} \end{pmatrix}. \tag{A.61}$$

A.8 Largest connected components in graphs and comparison with the leading eigenvalue

We first revisit percolation theory for undirected random graphs [Molloy and Reed, 1998] and directed random graphs [Dorogovtsev et al., 2001], and subsequently we discuss potential connections between percolation theory and the leading eigenvalue of random graphs.

A.8.1 Revision of percolation theory

A.8.1.1 Largest connected component in undirected graphs

Let $G = (V, E)$ be a graph with V a set of vertices and E a set of undirected edges. We say that a subgraph $G' = (V', E')$ of G is connected if for each pair of vertices $i \in V'$ and $j \in V'$ there exists a path of edges that belong to E' that connect i to j. The largest connected component is the largest subgraph G' of G that is connected, i.e., both the order $|V'|$ and the size $|E'|$ of the subgraph or maximal.

The relative order of the largest connected component is defined by

$$f(G) = \frac{|V'|}{N}. \tag{A.62}$$

We consider now undirected, random graphs with a prescribed degree distribution $p_{\text{deg}}(k)$. We denote the generating function of $p_{\text{deg}}(k)$ by

$$\tilde{M}(x) := \sum_{k=0}^{\infty} x^k p_{\text{deg}}(k) = \left\langle x^k \right\rangle_{p_{\text{deg}}} \tag{A.63}$$

where we denote the expectation over the degree distribution p_{deg} as $\langle\rangle_{p_{\text{deg}}}$, with $k \in \mathbb{N}$, and we will also use the generating function

$$M(x) := \frac{1}{c} \left\langle k\, x^k \right\rangle_{p_{\text{deg}}} = \frac{\partial_x \tilde{M}(x)}{c}, \tag{A.64}$$

where c is the mean degree of $p_{\text{deg}}(k)$.

In the limit $N \to \infty$, the relative order $f(G)$ converges with probability one to a deterministic value f, which is given by [Molloy and Reed, 1998],

$$1 - f = \tilde{M}(y), \tag{A.65}$$

where y is the smallest nonnegative solution of

$$y^2 = M(y). \tag{A.66}$$

Solving Eqs. (A.65-A.66) one finds that

$$f > 0 \quad \text{if} \quad \langle k\,(k-2)\rangle_{p_{\text{deg}}} > 0 \tag{A.67}$$

and that

$$f = 0 \quad \text{if} \quad \langle k\,(k-2)\rangle_{p_{\text{deg}}} < 0 \tag{A.68}$$

Hence, the condition

$$\langle k\,(k-2)\rangle_{p_{\text{deg}}} = 0 \tag{A.69}$$

determines the percolation transition in undirected, random graphs.

A.8.1.2 Largest strongly connected component in directed graphs

Let $G = (V, E)$ be a directed graph with V a set of vertices and E a set of undirected edges. We say that a subgraph $G' = (V', E')$ of G is strongly connected if for each pair of vertices $i \in V'$ and $j \in V'$ there exists a path starting in node j and ending in node i that follows the edges in E', and there exists also a reverse path that starts in node i and ends in node j. The largest strongly connected component is the largest subgraph G' that is strongly connected.

We define the relative order of the largest strongly connected component as

$$s_{\text{sc}}(G) = \frac{|V'|}{N}. \tag{A.70}$$

Let us consider directed, random graphs with a prescribed degree distribution $p^{\text{d}}_{\text{deg}}(k_{\text{in}}, k_{\text{out}})$ of indegrees and outdegrees . Then, in the limit $N \to \infty$ it holds that [Dorogovtsev et al., 2001; Neri and Metz, 2020]

$$s_{\text{sc}} = s_{\text{in}} + s_{\text{out}} + s_{\text{t}} - s_{\text{wc}}, \tag{A.71}$$

where s_{in}, s_{out}, s_{t} and s_{wc} are the fraction of nodes that belong to the incomponent, outcomponent, tendrils and the weakly connected component, respectively. By denoting the expectation over the degree distribution $p^{\text{d}}_{\text{deg}}(k_{\text{in}}, k_{\text{out}})$ as $\langle\rangle_{p^{\text{d}}_{\text{deg}}}$, with $k_{\text{in}}, k_{\text{out}} \in \mathbb{N}$, as in Sec. 4.4.1.2, it holds that

$$s_{\text{in}} = 1 - \left\langle \alpha^{k_{\text{in}}} \right\rangle_{p^{\text{d}}_{\text{deg}}}, \tag{A.72}$$

$$s_{\text{out}} = 1 - \left\langle \beta^{k_{\text{out}}} \right\rangle_{p^{\text{d}}_{\text{deg}}}, \tag{A.73}$$

and

$$s_{\text{t}} - s_{\text{wc}} = \left\langle \alpha^{k_{\text{in}}}\, \beta^{k_{\text{out}}} \right\rangle_{p^{\text{d}}_{\text{deg}}} - 1, \tag{A.74}$$

where a and b are probability that solve (the smallest nonnegative solutions) the equations

$$\tilde{c}\,\alpha = \left\langle k_{\text{out}}\, \alpha^{k_{\text{in}}} \right\rangle_{p^{\text{d}}_{\text{deg}}}, \tag{A.75}$$

and

$$\tilde{c}\,\beta = \left\langle k_{\rm in}\,\beta^{k_{\rm out}}\right\rangle_{p^{\rm d}_{\rm deg}}, \tag{A.76}$$

where $\tilde{c}$ is the mean indegree, equal to the mean outdegree $\langle k_{\rm in}\rangle_{p^{\rm d}_{\rm deg}} = \langle k_{\rm out}\rangle_{p^{\rm d}_{\rm deg}} = \tilde{c}$.

Solving Eqs. (A.92-A.76), we obtain that [Dorogovtsev et al., 2001; Neri and Metz, 2020]

$$s_{\rm sc} > 0 \quad \text{if} \quad \langle k_{\rm in}\,k_{\rm out}\rangle_{p^{\rm d}_{\rm deg}} > \tilde{c}, \tag{A.77}$$

and

$$s_{\rm sc} = 0 \quad \text{if} \quad \langle k_{\rm in}\,k_{\rm out}\rangle_{p^{\rm d}_{\rm deg}} < \tilde{c}, \tag{A.78}$$

Hence, the condition

$$\langle k_{\rm in}\,k_{\rm out}\rangle_{p^{\rm d}_{\rm deg}} = \tilde{c}, \tag{A.79}$$

determines the percolation transition of the strongly connected component in directed, random graphs.

A.8.2 Comparison with the leading eigenvalue

A.8.2.1 Undirected random graphs

Following the theory in Sec. A.8.1.1 in the case of the the degree distribution in Eq. (6.8) we easily get

$$\tilde{M}(x) = ax^c + (1-a)e^{-c(1-x)}, \tag{A.80}$$

and

$$M(x) = ax^c + (1-a)xe^{-c(1-x)}. \tag{A.81}$$

From Eq. (A.66) we find that y is the smallest non-negative solution of

$$y^2 = ay^k + (1-a)ye^{-c(1-y)}, \tag{A.82}$$

which needs to be solved numerically for y and then the solution to be used in Eq. (A.65) to determine f.

The left hand side of critical condition for the percolation transition in Eq. (A.69) is

$$\begin{aligned}\langle k\,(k-2)\rangle_{p_{\rm deg}} &= ac(c-2) + (1-a)(c^2-c)\\ &= c-1-a,\end{aligned} \tag{A.83}$$

for $c \neq 0$ and so the critical condition reads

$$a = c - 1. \tag{A.84}$$

In the special case of $a = 0$, corresponding to the Erdős-Rényi ensemble with the Poisson degree distribution, the percolation transition takes place at $c = 1$. In Panel (a) of Fig. A.1, we plot for the relative order f of the largest connected component as a function

of the variance $\mathrm{var}(k)$ of the degree distribution for random graphs with a prescribed degree distribution given by Eq. (6.8). We obtain that for infinitely large graphs f decreases monotonically as a function of $\mathrm{var}(k)$, even for $c = 2$. Hence, there is no clear link between the functional dependencies of f and λ_1 as a function of $\mathrm{var}(k)$ (compare Panel (a) of Fig. 6.6 in the main text with Panel (a) of Fig. A.1).

A.8.2.2 Directed random graphs

We consider a random, directed graph with a prescribed degree distribution $p^{\mathrm{d}}_{\mathrm{deg}}$ given by Eq. (4.35). Such a random graph can be constructed by adding unidirectional links on an undirected graph with degree distribution $p_{\mathrm{deg}}(k)$, as we discussed in Sec. 2.1.1 and shown in Appendix 4.4.1.2. Using Eqs. (4.33)-(4.34) and (4.40)-(4.41), we find that critical condition (A.79) reads

$$\begin{aligned}\frac{c}{2} &= \langle k_{\mathrm{in}}\, k_{\mathrm{out}} \rangle_{p^{\mathrm{d}}_{\mathrm{deg}}} \\ &= \tilde{c}^2\,(\rho + 1) \\ &= \frac{1}{4}\,\langle k(k-1) \rangle_{p_{\mathrm{deg}}}\,. \end{aligned} \tag{A.85}$$

It follows that if $p_{\mathrm{deg}}(k)$ is given by Eq. (6.8), then the strongly connected component of the graph percolates when

$$\begin{aligned} 2c &= ac(c-1) + (1-a)c^2 \\ &= c^2 - ac, \\ &\implies a = c - 2, \end{aligned} \tag{A.86}$$

and in particular the relative size s_{sc} of the largest strongly connected component is larger than zero when $a < c - 2$. In the special case of an Erdős-Rényi ensemble ($a = 0$) with Poisson degree distribution (as in Eq. (1.36)) the strongly connected component percolates at $c = 2$. For a random regular graph ($a = 1$), as in Eq. (5.1), the strongly connected component percolates at $c = 3$.

Let us now determine the fraction s_{sc} of nodes in the largest strongly connected component, as in Eq. (A.92). First, we observe that, since $\binom{k}{n} = \binom{k}{k-n}$, with $n \leq k$, it follows that $p^{\mathrm{d}}_{\mathrm{deg}}$ in Eq. (4.35) is symmetric, i.e.,

$$p^{\mathrm{d}}_{\mathrm{deg}}(k_{\mathrm{in}}, k_{\mathrm{out}}) = p^{\mathrm{d}}_{\mathrm{deg}}(k_{\mathrm{out}}, k_{\mathrm{in}}). \tag{A.87}$$

Accordingly, one has that the Eqs. (A.75),(A.76) are the same equation, i.e.,

$$\begin{aligned}\alpha &= \beta \\ &= \frac{2}{c}\sum_{k=0}^{\infty}\frac{p_{\rm deg}(k)}{2^k}\sum_{n=0}^{k}\binom{k}{n}\alpha^n(k-n) \\ &= \frac{2}{c}\left\langle \frac{1}{2^k}\sum_{n=0}^{k}\binom{k}{n}\alpha^n(k-n)\right\rangle_{p_{\rm deg}},\end{aligned} \tag{A.88}$$

where we used Eq. (4.35). In order to solve Eq. (A.88), we observe that we can use the moment generating function $g(x = y\ln\alpha)$ in Eq. (4.37) as follows

$$g(x = y\ln\alpha) = \sum_{n=0}^{k}\binom{k}{n}\alpha^{ny} = (1+\alpha^y)^k. \tag{A.89}$$

Accordingly, we can express Eq. (A.88) as

$$\begin{aligned}\alpha &= \frac{2}{c}\left\langle \frac{kg(x=\ln\alpha) - g'(x=\ln\alpha)}{2^k}\right\rangle_{p_{\rm deg}} \\ &= \frac{2}{c}\left\langle k\,\left[\left(\frac{\alpha+1}{2}\right)^k - \frac{\alpha}{2}\left(\frac{\alpha+1}{2}\right)^{k-1}\right]\right\rangle_{p_{\rm deg}} \\ &= \frac{2}{c}\left\langle k\,\left(\frac{\alpha+1}{2}\right)^{k-1}\left(\frac{\alpha+1}{2} - \frac{\alpha}{2}\right)\right\rangle_{p_{\rm deg}} \\ &= \frac{1}{c}\left\langle k\,\left(\frac{\alpha+1}{2}\right)^{k-1}\right\rangle_{p_{\rm deg}}.\end{aligned} \tag{A.90}$$

We use now the degree distribution $p_{\rm deg}$ in Eq. (6.8), so that the average in Eq. (A.90) reads

$$\begin{aligned}\alpha &= \frac{1}{c}\sum_{k=0}^{\infty}k\,\left(\frac{\alpha+1}{2}\right)^{k-1}\left[a\delta_{k,c} + (1-a)e^{-c}\frac{c^k}{k!}\right] \\ &= \frac{1}{c}\left[ac\left(\frac{\alpha+1}{2}\right)^{c-1} + (1-a)\sum_{k=1}^{\infty}e^{-c}\frac{c^k}{(k-1)!}\left(\frac{\alpha+1}{2}\right)^{k-1}\right] \\ &= a\left(\frac{\alpha+1}{2}\right)^{c-1} + (1-a)e^{-c}e^{c\frac{\alpha+1}{2}} \\ &= a\left(\frac{\alpha+1}{2}\right)^{c-1} + (1-a)e^{c\frac{\alpha-1}{2}},\end{aligned} \tag{A.91}$$

which is an equation for α, that needs to be determined for the smallest non-negative $\alpha \in [0,1]$. The solution of Eq. (A.91) can be used to determine the relative size of the largest strongly connected component, where we now express it in terms of the degree distribution $p_{\rm deg}$ in Eq. (6.8). First, by the symmetry in Eq. (A.87), one has that the

Eqs. (A.72),(A.73) are actually the same equation, i.e., $s_{\rm in} = s_{\rm out}$ so that Eq. (A.92) simplifies to

$$\begin{aligned} s_{\rm sc} &= 2s_{\rm in} + s_{\rm t} - s_{\rm wc}, \\ &= 2 - 2\left\langle \left(\frac{1+\alpha}{2}\right)^k \right\rangle_{p_{\rm deg}} + \left\langle \alpha^k \right\rangle_{p_{\rm deg}} - 1 \\ &= 1 + \left\langle \alpha^k - 2\left(\frac{1+\alpha}{2}\right)^k \right\rangle_{p_{\rm deg}} \end{aligned} \tag{A.92}$$

where we used again Eq. (4.35), and where α is the solution of Eq. (A.88). Second, we have

$$\begin{aligned} s_{\rm sc} &= 1 + \sum_{k=0}^{\infty} \left[a\delta_{k,c} + (1-a)e^{-c}\frac{c^k}{k!} \right] \left[\alpha^k - 2\left(\frac{1+\alpha}{2}\right)^k \right] \\ &= 1 + a\left[\alpha^c - 2\left(\frac{\alpha+1}{2}\right)^c \right] + (1-a)e^{-c}\left\{ \sum_{k=0}^{\infty} \frac{(c\alpha)^k}{k!} - 2\sum_{k=0}^{\infty} \frac{1}{k!}\left[\frac{c(\alpha+1)}{2}\right]^k \right\} \\ &= 1 + a\left[\alpha^c - 2\left(\frac{\alpha+1}{2}\right)^c \right] + (1-a)\left[e^{c(\alpha-1)} - 2e^{c\frac{\alpha-1}{2}} \right]. \end{aligned} \tag{A.93}$$

In Panel (b) of Fig. A.1, we plot the relative order $s_{\rm sc}$ as a function of ${\rm var}(k)$ for directed graphs $p_{\rm deg}(k_{\rm in}, k_{\rm out})$ given by Eq. (4.35), and the degree distribution $p_{\rm deg}$ in Eq. (6.8). We find that $s_{\rm sc}$ increases as a function of ${\rm var}(k)$ for $c = 3$ and decreases as a function of ${\rm var}(k)$ for $c = 4$. Hence, there is again no direct link between the functional dependencies of $s_{\rm sc}$ and λ_1 on ${\rm var}(k)$ (compare Panel (b) of Fig. 6.6 in the main text with Panel (b) of Fig. A.1).

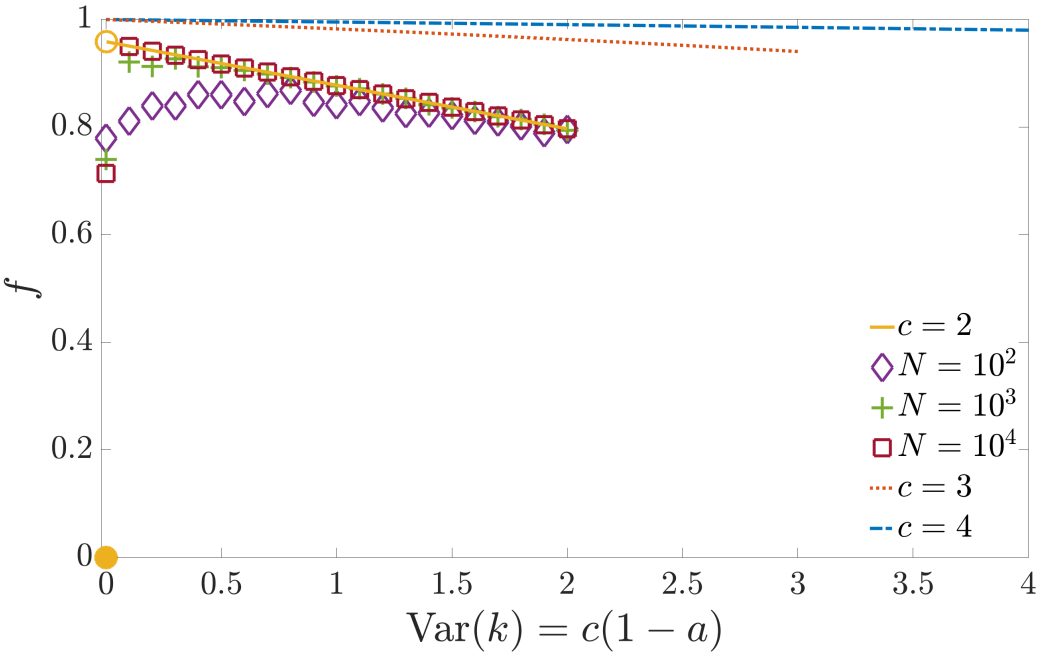

(a) undirected

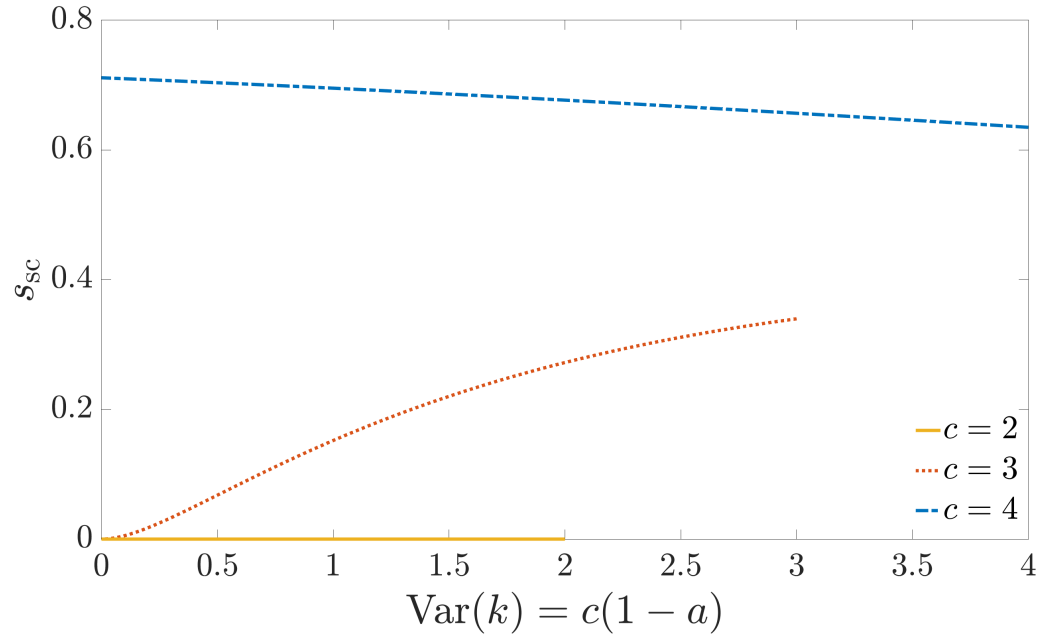

(b) directed

Figure A.1: Panel (a): Relative order f of the largest connected component of random graphs with the prescribed degree distribution given by Eq. (6.8), just as in Fig. 6.6(a). Lines correspond to theoretical results for infinitely large N obtained from solving Eqs. (A.65-A.66), while the markers are simulation results for finite N and $c = 2$; we have included simulations in order to verify the peculiar discontinuity of f at $a = 1$. Panel (b): Relative order s_{sc} of the largest strongly connected component of random, directed graphs with a joint degree distribution $p_{\mathrm{deg}}(k_{\mathrm{in}}, k_{\mathrm{out}})$ given by Eq. (4.35), just as in Fig. 6.6(b). Lines are theoretical values for infinitely large N obtained from solving Eqs. (A.92-A.76).

A.9 Finite size study of the leading eigenvalue

In this appendix we study finite size effects on the determination of the leading eigenvalue $\Im(\lambda_1^*)$, and of its distribution. Figure 6.9 shows that finite size effects are significant in sparse random matrices. Therefore, we analyze here how the distribution $p(\Im(\lambda_1))$, plotted in Fig. 6.8, depends on N.

Figure A.2 presents empirical data for the distribution of $\Im(\lambda_1)$ in antagonistic matrices with parameters that are the same as in Fig. 6.9, except for the system size N, which now takes three values $N = 200$, $N = 1000$ and $N = 5000$. Just as in Fig. 6.9, we observe that the distribution of $\Im(\lambda_1)$ consists of two parts and is of the form given by Eq. (6.11). We make a couple of interesting observations from Fig. A.2. First, we observe that $\pi_{\Re}$ in Eq. (6.10), i.e., the probability that the leading eigenvalue is real, is independent of N, consistent with the results obtained in Fig. 6.7. A possible explanation for the observed N-independence of $\pi_{\Re}$ is that the leading eigenvalue can be real when the matrix $\mathbf{A}$ contains a cycle that induces a feedback loop, that is so strong that it contributes to the spectrum with a leading eigenvalue. Since for sparse random graphs the number of cycles of a given fixed length is independent of N — and they persist in the limit $N \to \infty$ — (as discussed in the main text), and since cycles of finite length are not accounted for by the cavity method, this explanation is consistent with both the numerical diagonalization results and the theoretical results obtained in this thesis. Second, we observe that the mode $\Im(\lambda_1^*)$ of the continuous part of the distribution decreases as a function of N. For $c = 4 > c_{\text{crit}}$ the distribution moves swiftly towards zero while for $c = 2 < c_{\text{crit}}$ the mode appears to converge to a finite non-zero value, which is consistent with the phase transition at $N \to \infty$ shown in Fig. 6.9 and the conjecture that the cavity method provides an estimate for the mode of the continuous part of the distribution of $|\Im(\lambda_1)|$.

Figure A.3 plots $p(\Im(\lambda_1))$ for mixture matrices, which is the equivalent of Fig. A.2 for antagonistic matrices. Comparing the distribution in Figs. A.2 and A.3, we see that the main difference is the behaviour of $\pi_{\Re}$, which rapidly converges to 1 for mixture matrices, as also shown in Fig. 6.7. As a consequence, for mixture matrices the continuous part of the distribution $p(\Im(\lambda_1))$ disappears for large enough N, which, as shown in Fig. A.3, is enough already at $N \approx 10^2$.

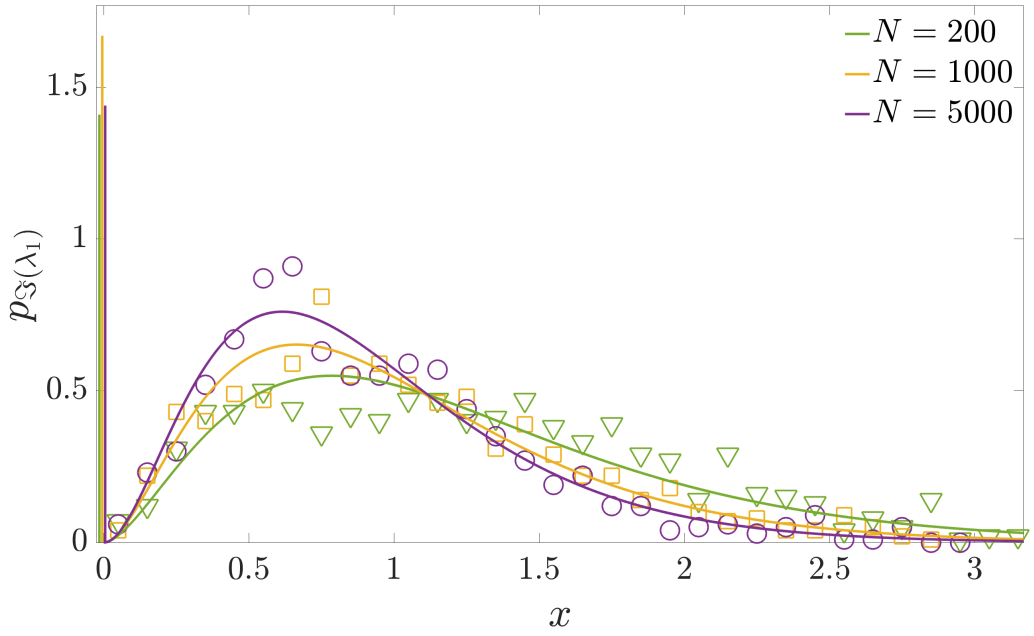

(a) $c = 2$

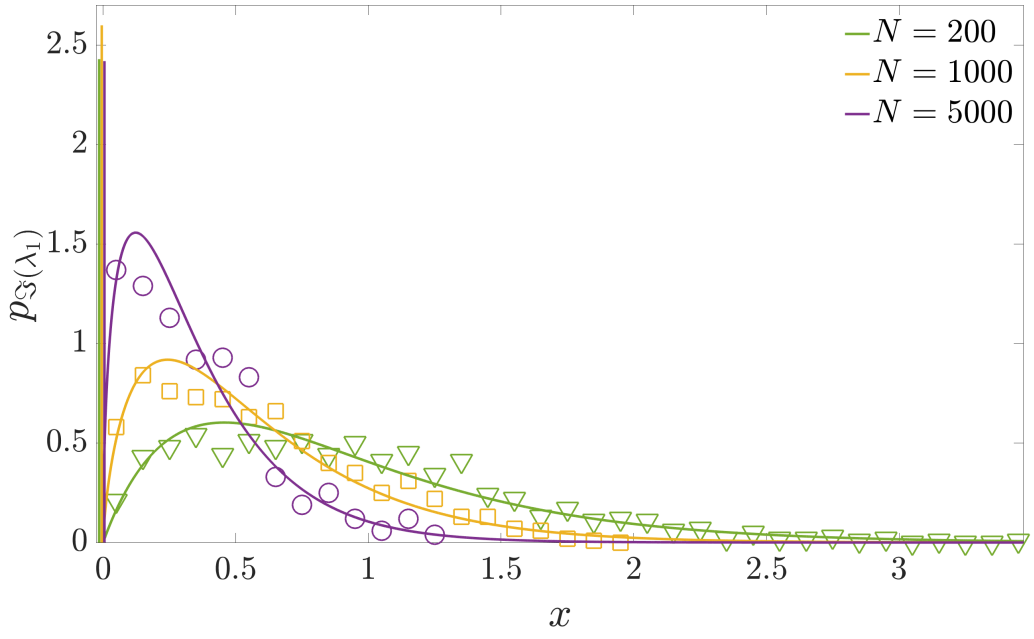

(b) $c = 4$

Figure A.2: Distributions of the imaginary part of the leading eigenvalue for antagonistic matrices (Model A) with $c = 2$ [Panel (a)] and $c = 4$ [Panel (b)]. The thick vertical line at $\Im(\lambda_1) = 0$ has height $\text{Prob}[\lambda_1 \in \mathbb{R}]/\delta$, with $\delta = 0.1$ the width of the intervals in the histogram. Markers are histograms of imaginary part of the leading eigenvalues obtained through direct diagonalization of $m_s = 1000$ antagonistic matrices for different values of N. Continuous lines are obtained by fitting the Gamma distribution on these data.

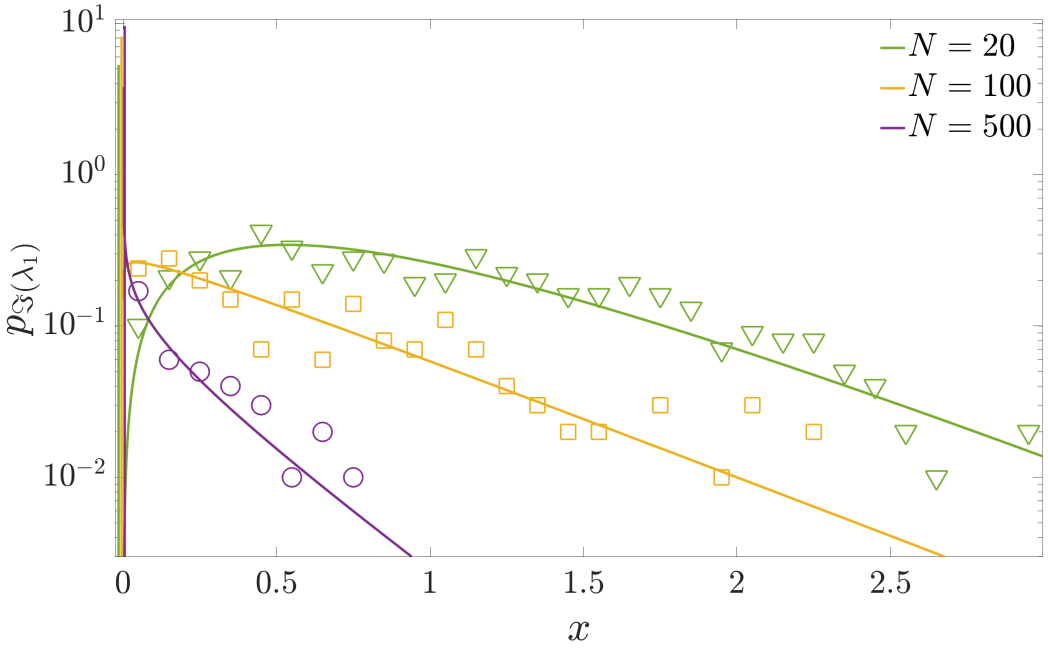

(a) $c = 2$

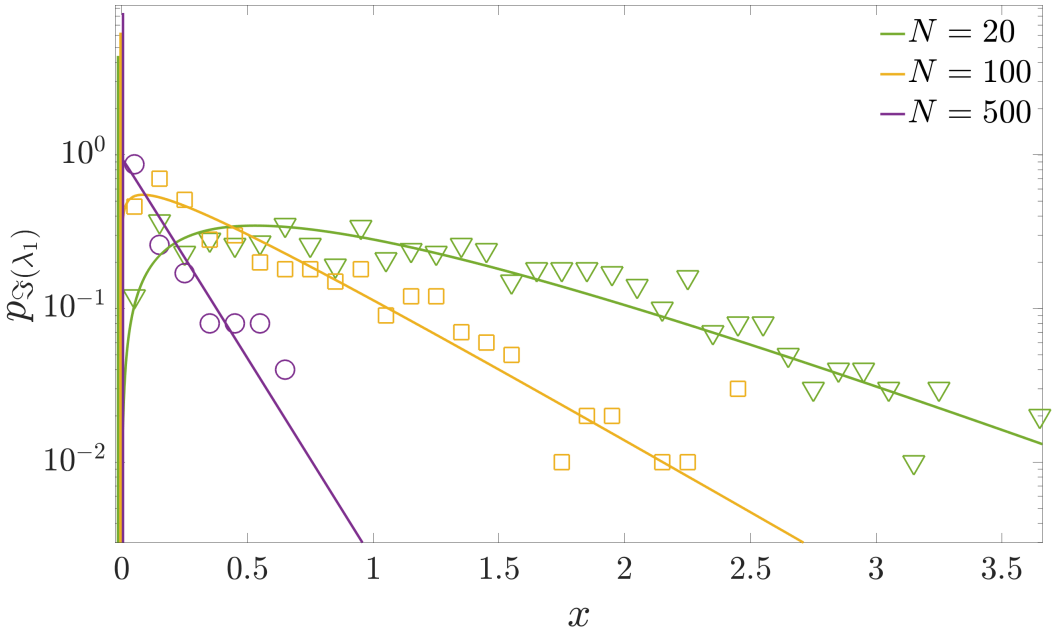

(b) $c = 4$

Figure A.3: Distributions of the imaginary part of the leading eigenvalue mixture matrices (Model B) with $c = 2$ and $c = 4$. The thick vertical line at $\Im(\lambda_1) = 0$ has height $\text{Prob}[\lambda_1 \in \mathbb{R}]/\delta$, with $\delta = 0.1$ the width of the intervals in the histogram. Markers are histograms of imaginary part of the leading eigenvalues obtained through direct diagonalization of $m_s = 1000$ mixture matrices and for different values of N. Continuous lines are obtained by fitting the Gamma distribution on these data. Vertical axes are in log-scale to make visible the continuous part of the distributions.

Bibliography

Abou-Chacra, R., Thouless, D. J., and Anderson, P. W. (1973). A selfconsistent theory of localization. *Journal of Physics C: Solid State Physics*, 6(10):1734–1752.

Ahmadian, Y., Fumarola, F., and Miller, K. D. (2015). Properties of networks with partially structured and partially random connectivity. *Phys. Rev. E*, 91:012820.

Akemann, G., Baik, J., and Di Francesco, P. (2011). *The Oxford Handbook of Random Matrix Theory*. Oxford University Press.

Albert, R. and Barabási, A.-L. (2002). Statistical mechanics of complex networks. *Rev. Mod. Phys.*, 74:47–97.

Allesina, S., Grilli, J., Barabás, G., Tang, S., Aljadeff, J., and Maritan, A. (2015). Predicting the stability of large structured food webs. *Nature communications*, 6(1):1–6.

Allesina, S. and Pascual, M. (2008). Network structure, predator–prey modules, and stability in large food webs. *Theoretical Ecology*, 1(1):55–64.

Allesina, S. and Tang, S. (2012). Stability criteria for complex ecosystems. *Nature*, 483:205–8.

Allesina, S. and Tang, S. (2015). The stability–complexity relationship at age 40: a random matrix perspective. *Population Ecology*, 57(1):63–75.

Amir, A., Hatano, N., and Nelson, D. R. (2016). Non-hermitian localization in biological networks. *Physical Review E*, 93(4):042310.

Arnoldi, J.-F., Bideault, A., Loreau, M., and Haegeman, B. (2018). How ecosystems recover from pulse perturbations: A theory of short-to long-term responses. *Journal of theoretical biology*, 436:79–92.

Backstrom, L., Boldi, P., Rosa, M., Ugander, J., and Vigna, S. (2011). Four degrees of separation. *Proceedings of the 4th Annual ACM Web Science Conference, New York, NY, USA*.

Bai, Z. and Silverstein, J. (2010). *Spectral Analysis of Large Dimensional Random Matrices*. Springer New York.

Bai, Z. D. (1997). Circular law. *The Annals of Probability*, 25(1):494–529.

Bai, Z. D. (1999). Methodologies in spectral analysis of large dimensional random matrices, a review. *Statistica Sinica*, 9(3):611–662.

Bapst, V. and Semerjian, G. (2011). Lifshitz tails on the bethe lattice: a combinatorial approach. *Journal of Statistical Physics*, 145(1):51.

Barbier, M., Arnoldi, J.-F., Bunin, G., and Loreau, M. (2018). Generic assembly patterns in complex ecological communities. *Proceedings of the National Academy of Sciences*, 115(9):2156–2161.

Bardoscia, M., Battiston, S., Caccioli, F., and Caldarelli, G. (2017). Pathways towards instability in financial networks. *Nature Communications*, 8(1):14416.

Baron, J. W. and Galla, T. (2020). Dispersal-induced instability in complex ecosystems. *arXiv preprint arXiv:2003.04206*.

Basak, A. and Rudelson, M. (2017). The circular law for sparse non-hermitian matrices. *arXiv:1707.03675 [math]*.

Battiston, S., Caldarelli, G., May, R. M., Roukny, T., and Stiglitz, J. E. (2016). The price of complexity in financial networks. *Proceedings of the National Academy of Sciences*, 113(36):10031–10036.

Battiston, S., Puliga, M., Kaushik, R., Tasca, P., and Caldarelli, G. (2012). Debtrank: Too central to fail? financial networks, the fed and systemic risk. *Nature Sci. Rep.*, 2:1–6.

Bauer, M. and Golinelli, O. (2001a). Random incidence matrices: Moments of the spectral density. *Journal of Statistical Physics*, 103(1):301–337.

Bauer, M. and Golinelli, O. (2001b). Random incidence matrices: moments of the spectral density. *Journal of Statistical Physics*, 103(1-2):301–337.

Bianconi, G. and Marsili, M. (2005). Loops of any size and hamilton cycles in random scale-free networks. *Journal of Statistical Mechanics: Theory and Experiment*, 2005(06):06005.

Billingsley, P. (1986). *Probability and Measure*. John Wiley and Sons, second edition.

Bimbard, C., Ledoux, E., and Ostojic, S. (2016). Instability to a heterogeneous oscillatory state in randomly connected recurrent networks with delayed interactions. *Phys. Rev. E*, 94:062207.

Biroli, G., Bunin, G., and Cammarota, C. (2018). Marginally stable equilibria in critical ecosystems. *New Journal of Physics*, 20(8):083051.

Bollobás, B. (2001). *Random Graphs*. Cambridge Studies in Advanced Mathematics. Cambridge University Press, 2 edition.

Bonneau, H., Hassid, A., Biham, O., Kühn, R., and Katzav, E. (2017). Distribution of shortest cycle lengths in random networks. *Phys. Rev. E*, 96:062307.

Bordenave, C., Caputo, P., and Chafaï, D. (2011). Spectrum of Non-Hermitian Heavy Tailed Random Matrices. *Communications in Mathematical Physics*, 307:513–560.

Bordenave, C. and Lelarge, M. (2010). Resolvent of large random graphs. *Random Structures & Algorithms*, 37(3):332–352.

Brunel, N. (2000). Dynamics of sparsely connected networks of excitatory and inhibitory spiking neurons. *Journal of computational neuroscience*, 8(3):183–208.

Bullmore, E. and Sporns, O. (2009). Complex brain networks: graph theoretical analysis of structural and functional systems. *Nature reviews neuroscience*, 10(3):186–198.

Caccioli, F., Barucca, P., and Kobayashi, T. (2018). Network models of financial systemic risk: a review. *Journal of Computational Social Science*, 1(1):81–114.

Cartan, E. (1945). *Les systèmes differentiels extérieurs et leur applications géométriques*. Actualités scientifiques et industrielles. Hermann & cie.

Chertkov, M., Kroc, L., Krzakala, F., Vergassola, M., and Zdeborová, L. (2010). Inference in particle tracking experiments by passing messages between images. *Proceedings of the National Academy of Sciences*, 107(17):7663–7668.

Chung, F., Lu, L., and Vu, V. (2004). The spectra of random graphs with given expected degrees. *Internet Mathematics*, 1(3):257–275.

Cicuta, G. M. and Molinari, L. G. (2016). Random antagonistic matrices. *Journal of Physics A: Mathematical and Theoretical*, 49(37):375601.

Coyte, K. Z., Schluter, J., and Foster, K. R. (2015). The ecology of the microbiome: networks, competition, and stability. *Science*, 350(6261):663–666.

de Jong, H. (2002). Modeling and simulation of genetic regulatory systems: A literature review. *Journal of computational biology : a journal of computational molecular cell biology*, 9:67–103.

Dembo, A., Montanari, A., et al. (2010). Gibbs measures and phase transitions on sparse random graphs. *Brazilian Journal of Probability and Statistics*, 24(2):137–211.

Dorogovtsev, S. N. and Mendes, J. F. (2013). *Evolution of networks: From biological nets to the Internet and WWW*. OUP Oxford.

Dorogovtsev, S. N., Mendes, J. F. F., and Samukhin, A. N. (2001). Giant strongly connected component of directed networks. *Phys. Rev. E*, 64:025101.

Dumitriu, I. and Pal, S. (2012). Sparse regular random graphs: Spectral density and eigenvectors. *The Annals of Probability*, 40(5):2197–2235.

Dunne, J. A., Williams, R. J., and Martinez, N. D. (2002a). Food-web structure and network theory: the role of connectance and size. *Proceedings of the National Academy of Sciences*, 99(20):12917–12922.

Dunne, J. A., Williams, R. J., and Martinez, N. D. (2002b). Network structure and biodiversity loss in food webs: robustness increases with connectance. *Ecology letters*, 5(4):558–567.

Duras, M. M., Sokalski, K., and Suł kowski, P. (1997). Statistical properties of sparse Gaussian random symmetrical ensemble. *Jagellonian University. Institute of Physics. Acta Physica Polonica B*, 28(5):1023–1038.

Easley, D. and Kleinberg, J. (2010). *Networks, Crowds, and Markets: Reasoning about a Highly Connected World*. Cambridge University Press.

Edelman, A. (1988). Eigenvalues and condition numbers of random matrices. *SIAM J. Matrix Anal. Appl.*, 9(4):543–560.

Edelman, A., Kostlan, E., and Shub, M. (1994). How many eigenvalues of a random matrix are real? *Journal of the American Mathematical Society*, 7(1):247–267.

Emmerson, M. and Yearsley, J. M. (2004). Weak interactions, omnivory and emergent food-web properties. *Proceedings of the Royal Society B: Biological Sciences*, 271(1537):397?405.

Erdös, P. and Rényi, A. (1959). On random graphs, I. *Publicationes Mathematicae (Debrecen)*, 6:290–297.

Erdös, P. and Rényi, A. (1960). On the evolution of random graphs. *Publications of the Mathematical Institute of the Hungarian Academy of Sciences*, 5:17–61.

Farmer, J. D. and Skouras, S. (2013). An ecological perspective on the future of computer trading. *Quantitative Finance*, 13(3):325–346.

Feinberg, J. and Zee, A. (1997). Non-hermitian random matrix theory: Method of hermitian reduction. *Nuclear Physics B*, 504(3):579 – 608.

Fong, C. (2006a). Complex 2-forms: Cauchy-pompeius formula. `http://people.math.carleton.ca/~ckfong/S32.pdf`.

Fong, C. (2006b). Formation of differential forms: Wedge products. `http://people.math.carleton.ca/~ckfong/S21.pdf`.

Fortuna, M. A., Stouffer, D. B., Olesen, J. M., Jordano, P., Mouillot, D., Krasnov, B. R., Poulin, R., and Bascompte, J. (2010). Nestedness versus modularity in ecological networks: two sides of the same coin? *Journal of Animal Ecology*, 79(4):811–817.

Fried, Y., Kessler, D., and M. Shnerb, N. (2016). Communities as cliques. 6.

Fyodorov, Y. V. and Khoruzhenko, B. A. (2016). Nonlinear analogue of the May Wigner instability transition. *Proceedings of the National Academy of Sciences*, 113(25):6827–6832.

Fyodorov, Y. V. and Mirlin, A. D. (1991). On the density of states of sparse random matrices. *Journal of Physics A: Mathematical and General*, 24(9):2219.

Galla, T. (2018). Dynamically evolved community size and stability of random lotka-volterra ecosystems. *EPL*, 123(4):48004.

Galla, T. and Farmer, J. D. (2013). Complex dynamics in learning complicated games. *Proceedings of the National Academy of Sciences*, 110(4):1232–1236.

Gallier, J. et al. (2010). The schur complement and symmetric positive semidefinite (and definite) matrices. *Penn Engineering*, pages 1–12.

Gardner, M. R. and Ashby, W. R. (1970). Connectance of large dynamic (cybernetic) systems: critical values for stability. *Nature*, 228(5273):784–784.

Gibbs, T., Grilli, J., Rogers, T., and Allesina, S. (2018). Effect of population abundances on the stability of large random ecosystems. *Physical Review E*, 98(2):022410.

Gilbert, E. N. (1959). Random graphs. *Ann. Math. Statist.*, 30(4):1141–1144.

Ginibre, J. (1965). Statistical ensembles of complex, quaternion, and real matrices. *Journal of Mathematical Physics*, 6(3):440–449.

Girko, V. L. (1985). Circular law. *Theory of Probability and Its Applications*, 29(4):694–706.

Girko, V. L. (2004). The strong circular law. Twenty years later. II. *Random Operators and Stochastic Equations*, 12(3):255–312.

Girko, V. L. (2006). The strong elliptic law. Twenty years later. I. *Random Operators and Stochastic Equations*, 14:59–102.

Götze, F., Naumov, A., and Tikhomirov, A. (2015). On a Generalization of the Elliptic Law for Random Matrices. *Acta Physica Polonica B*, 46:1737.

Götze, F. and Tikhomirov, A. (2007). On the Circular Law. *ArXiv Mathematics e-prints*.

Grela, J. (2017). What drives transient behavior in complex systems? *Phys. Rev. E*, 96:022316.

Grilli, J., Rogers, T., and Allesina, S. (2016). Modularity and stability in ecological communities. *Nature communications*, 7(1):1–10.

Grobman, D. M. (1959). Homeomorphism of systems of differential equations. *Doklady Akademii Nauk SSSR*, 128(5):880–881.

Haas, P. A., Oliveira, N. M., and Goldstein, R. E. (2020). Subpopulations and stability in microbial communities. *Physical Review Research*, 2(2):022036.

Haldane, A. and May, R. (2011). Systemic risk in banking ecosystems. *Nature*, 469:351–5.

Hartman, P. (1960). A lemma in the theory of structural stability of differential equations. *Proceedings of the American Mathematical Society*, 11(4):610–620.

Haydon, D. T. (2000). Maximally stable model ecosystems can be highly connected. *Ecology*, 81(9):2631–2636.

Henrici, P. (1986). *Applied and Computational Complex Analysis. Vol. 3*. John Wiley & Sons, Inc.

Hermann, G. and Touboul, J. (2012). Heterogeneous connections induce oscillations in large-scale networks. *Physical review letters*, 109(1):018702.

Hofbauer, J. and Sigmund, K. (1998). *Evolutionary Games and Population Dynamics*. Cambridge University Press.

Hooper, D. U., Chapin, F. S., Ewel, J. J., Hector, A., Inchausti, P., Lavorel, S., Lawton, J. H., Lodge, D. M., Loreau, M., Naeem, S., Schmid, B., Setl, H., Symstad, A. J., Vandermeer, J., and Wardle, D. A. (2005). Effects of biodiversity on ecosystem functioning: A consensus of current knowledge. *Ecological Monographs*, 75(1):3–35.

Hörmander, L. (1966). *An Introduction to Complex Analysis in Several Variables*. North-Holland mathematical library. Van Nostrand.

Kabashima, Y., Takahashi, H., and Watanabe, O. (2010). Cavity approach to the first eigenvalue problem in a family of symmetric random sparse matrices. *Journal of Physics: Conference Series*, 233:012001.

Kadmon, J. and Sompolinsky, H. (2015). Transition to chaos in random neuronal networks. *Physical Review X*, 5(4):041030.

Khorunzhiy, O., Kirsch, W., and Müller, P. (2006). Lifshitz tails for spectra of erdős–rényi random graphs. *The Annals of Applied Probability*, 16(1):295–309.

Kirk, P., Rolando, D. M. Y., MacLean, A. L., and Stumpf, M. P. H. (2015). Conditional random matrix ensembles and the stability of dynamical systems. *New Journal of Physics*, 17(8):083025.

Kondoh, M. (2003). Foraging adaptation and the relationship between food-web complexity and stability. *Science*, 299(5611):1388–1391.

Krivelevich, M. and Sudakov, B. (2003). The largest eigenvalue of sparse random graphs. *Combinatorics, Probability and Computing*, 12(1):61–72.

Krzakala, F., Ricci-Tersenghi, F., Zdeborova, L., Zecchina, R., Tramel, E. W., and Cugliandolo, L. F. (2015). *Statistical Physics, Optimization, Inference, and Message-Passing Algorithms : Lecture Notes of the Les Houches School of Physics : Special Issue, October 2013* . Oxford University Press, Oxford.

Kühn, R. (2008). Spectra of sparse random matrices. *Journal of Physics A: Mathematical and Theoretical*, 41(29):295002.

Landau, L. D. (1937). On the theory of phase transitions. I. *Phys. Z. Sowjet.*, 11:26.

Lu, T.-T. and Shiou, S.-H. (2002). Inverses of 2 x 2 block matrices. *Computers and Mathematics with Applications*, 43(1-2):119–129.

Mambuca, A. M., Balata, A., Lamperti, M., and Filia, F. (2018). How to measure the proximity to a market crash: Introducing system resilience indicators.

Mambuca, A. M., Cammarota, C., and Neri, I. (2020). Dynamical systems on large networks with predator-prey interactions are stable and exhibit oscillations. *preprint arXiv:2009.11211*.

Martí, D., Brunel, N., and Ostojic, S. (2018). Correlations between synapses in pairs of neurons slow down dynamics in randomly connected neural networks. *Physical Review E*, 97(6):062314.

Massimini, M., Ferrarelli, F., Huber, R., Esser, S. K., Singh, H., and Tononi, G. (2005). Breakdown of cortical effective connectivity during sleep. *Science*, 309(5744):2228–2232.

May, R. (1972). Will a large complex system be stable? *Nature*, 238(5364):413–414.

May, R. (1973). *Stability and Complexity in Model Ecosystems*. Monographs in population biology. Princeton University Press.

May, R. M. (2013). Networks and webs in ecosystems and financial systems. *Philosophical Transactions of the Royal Society A: Mathematical, Physical and Engineering Sciences*, 371(1987):20120376.

Mccann, K. (2000). The diversity-stability debate. *Nature*, 405:228–33.

Mccann, K., Hastings, A., and R. Huxel, G. (1998). Weak trophic interactions and the balance of nature. *Nature*, 395:794–798.

Mehta, M. L. (1967). *Random matrices and the statistical theory of energy levels*. Academic Press, New York-London.

Metz, F. L. and Neri, I. (2020). Localization and universality of eigenvectors in directed random graphs. *arXiv preprint arXiv:2007.13672*.

Metz, F. L., Neri, I., and Bollé, D. (2010). Localization transition in symmetric random matrices. *Physical Review E*, 82(3):031135.

Metz, F. L., Neri, I., and Rogers, T. (2019). Spectral theory of sparse non-hermitian random matrices. *Journal of Physics A: Mathematical and Theoretical*, 52(43):434003.

Mézard, M. and Parisi, G. (2001). The Bethe lattice spin glass revisited. *The European Physical Journal B - Condensed Matter and Complex Systems*, 20(2):217–233.

Mézard, M., Parisi, G., and Virasoro, M. A. (1987). *Spin Glass Theory and Beyond*. Singapore: World Scientific.

Mirlin, A. D. and Fyodorov, Y. V. (1991). Universality of level correlation function of sparse random matrices. *Journal of Physics A: Mathematical and General*, 24(10):2273.

Molloy, M. and Reed, B. (1998). The size of the giant component of a random graph with a given degree sequence. *Combinatorics, Probability and Computing*, 7(3):295305.

Moore, J. and Hunt, W. H. (1988). Resource compartmentation and the stability of real ecosystems. *Nature*, 333:261–263.

Moran, J. and Bouchaud, J.-P. (2019). May's instability in large economies. *Phys. Rev. E*, 100:032307.

Nagao, T. and Tanaka, T. (2007). Spectral density of sparse sample covariance matrices. *Journal of Physics. A. Mathematical and Theoretical*, 40(19):4973–4987.

Nahmad-Achar, E. (2018). Differential forms and exterior calculus. In *Differential Topology and Geometry with Applications to Physics*, 2053-2563, pages 8–1 to 8–10. IOP Publishing.

Naumov, A. (2013). Elliptic law for real random matrices. *Moscow University Computational Mathematics and Cybernetics*, pages 31–38.

Neri, I. and Metz, F. L. (2012). Spectra of sparse non-hermitian random matrices: An analytical solution. *Physical Review Letters*, 109:030602.

Neri, I. and Metz, F. L. (2016). Eigenvalue outliers of non-hermitian random matrices with a local tree structure. *Physical review letters*, 117(22):224101.

Neri, I. and Metz, F. L. (2020). Linear stability analysis of large dynamical systems on random directed graphs. *Phys. Rev. Research*, 2:033313.

Newman, M. (2010). *Networks: an introduction*. Oxford university press.

Newman, M. (2018). *Networks*. Oxford university press.

Nguyen, H. H. and O'Rourke, S. (2015). The elliptic law. *International Mathematics Research Notices*, 2015(17):7620–7689.

Pan, G. and Zhou, W. (2010). Circular law, extreme singular values and potential theory. *J. Multivariate Anal.*, 101(3):645–656.

Pearl, J. (1988). *Probabilistic Reasoning in Intelligent Systems: Networks of Plausible Inference*. Morgan Kaufmann Publishers Inc., San Francisco, CA, USA.

Petersen, K. B. and Pedersen, M. S. (2012). The matrix cookbook. Version 20121115.

Pimm, S. (1984). The complexity and stability of ecosystems. *Nature*, 307:321–326.

Place, C. and Arrowsmit, D. (1992). *Dynamical Systems: Differential Equations, Maps, and Chaotic Behaviour*. CRC Press.

Reed, M., Simon, B., et al. (1980). *I: Functional analysis*, volume 1. Academic press.

Roberts, A. (1974). Stability of a feasible random ecosystem. *Nature*, 251:607–608.

Rodgers, G. J. and Bray, A. J. (1988). Density of states of a sparse random matrix. *Phys. Rev. B*, 37:3557–3562.

Rogasch, N. C. and Fitzgerald, P. B. (2013). Assessing cortical network properties using tms–eeg. *Human brain mapping*, 34(7):1652–1669.

Rogers, T. (2010a). *New Results on the Spectral Density of Random matrices*. PhD Thesis, Department of Mathematics, King's College London.

Rogers, T. (2010b). Universal sum and product rules for random matrices. *Journal of Mathematical Physics*, 51(9):093304.

Rogers, T., Castillo, I. P., Kühn, R., and Takeda, K. (2008). Cavity approach to the spectral density of sparse symmetric random matrices. *Phys. Rev. E*, 78:031116.

Rogers, T. and Pérez Castillo, I. (2009). Cavity approach to the spectral density of non-hermitian sparse matrices. *Phys. Rev. E*, 79:012101.

Rudin, W. (1987). *Real and Complex Analysis*. Mathematics series. McGraw-Hill.

Sandhu, R. S., Georgiou, T. T., and Tannenbaum, A. R. (2016). Ricci curvature: An economic indicator for market fragility and systemic risk. *Science Advances*, 2(5).

Sato, S. and Kobayashi, K. (1976). Asymptotic distribution of eigenvalues and degeneration of sparse random matrices. *Bull. Math. Statist.*, 17(3–4):83–99.

Semerjian, G. and Cugliandolo, L. F. (2002). Sparse random matrices: the eigenvalue spectrum revisited. *Journal of Physics A: Mathematical and General*, 35(23):4837.

Slanina, F. (2011). Equivalence of replica and cavity methods for computing spectra of sparse random matrices. *Physical Review E*, 83(1):011118.

Slanina, F. (2012). Localization of eigenvectors in random graphs. *The European Physical Journal B*, 85(11):361.

Sodin, S. (2009). The Tracy-Widom law for some sparse random matrices. *Journal of Statistical Physics*, 136(5):834–841.

Sommers, H. J., Crisanti, A., Sompolinsky, H., and Stein, Y. (1988). Spectrum of large random asymmetric matrices. *Phys. Rev. Lett.*, 60:1895–1898.

Sompolinsky, H., Crisanti, A., and Sommers, H. J. (1988). Chaos in random neural networks. *Physical Review Letters*, 61:259–262.

Sporns, O. (2010). *Networks of the Brain*. MIT press.

Stadler, P. F., Fontana, W., and Miller, J. H. (1993). Random catalytic reaction networks. *Physica D: Nonlinear Phenomena*, 63(3):378 – 392.

Susca, V. A., Vivo, P., and Kühn, R. (2019). Top eigenpair statistics for weighted sparse graphs. *Journal of Physics A: Mathematical and Theoretical*, 52(48):485002.

Tang, S., Pawar, S., and Allesina, S. (2014). Correlation between interaction strengths drives stability in large ecological networks. *Ecology Letters*, 17(9):1094–1100.

Tao, T. and Vu, V. (2008). Random matrices: the circular law. *Commun. Contemp. Math.*, 10(2):261–307.

Tao, T. and Vu, V. (2009). From the Littlewood-Offord problem to the circular law: universality of the spectral distribution of random matrices. *Bull. Amer. Math. Soc. (N.S.)*, 46(3):377–396.

Tao, T. and Vu, V. (2010). Random matrices: universality of ESDs and the circular law. *Ann. Probab.*, 38(5):2023–2065. With an appendix by Manjunath Krishnapur.

Tarnowski, W., Neri, I., and Vivo, P. (2020). Universal transient behavior in large dynamical systems on networks. *Physical Review Research*, 2(2):023333.

Tran, L., Vu, V., and Wang, K. (2010). Sparse random graphs: Eigenvalues and eigenvector. *arXiv:1011.6646 [math]*.

Trefethen, L., Embree, M., and Embree, M. (2005). *Spectra and Pseudospectra: The Behavior of Nonnormal Matrices and Operators*. Princeton University Press.

Vladimirov, V. (1979). *Generalized functions in mathematical physics*. Mir.

Wainrib, G. and Touboul, J. (2012). Topological and dynamical complexity of random neural networks. *Physical Review Letters*, 110.

Wigner, E. P. (1958). On the distribution of the roots of certain symmetric matrices. *Annals of Mathematics*, 67(2):325–327.

Williams, R. J. and Martinez, N. D. (2000). Simple rules yield complex food webs. *Nature*, 404(6774):180–183.

Wood, P. M. (2012). Universality and the circular law for sparse random matrices. *The Annals of Applied Probability*, 22(3):1266–1300.